

SUPRAMOLECULAR DESIGN OF NOVEL PHARMACEUTICAL SOLIDS AND THEIR PHYSICOCHEMICAL AND PHARMACOKINETIC PROPERTIES

A Thesis Submitted to the
University of Hyderabad in partial fulfillment of
the Award of PhD Degree in Chemistry

By

K. SURESH



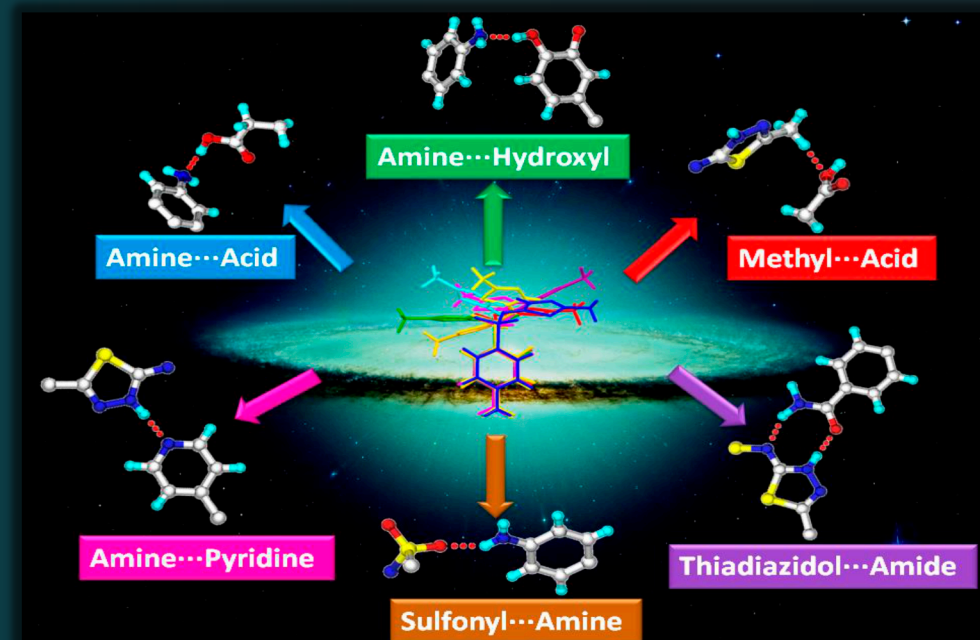
School of Chemistry
University of Hyderabad
Hyderabad 500 046, Telangana

India
May 2016

Ph.D. Thesis

SUPRAMOLECULAR DESIGN OF NOVEL PHARMACEUTICAL SOLIDS
AND THEIR PHYSICOCHEMICAL AND PHARMACOKINETIC PROPERTIES

K. SURESH



Six novel robust hetero synthons as well as weaker hydrogen bonds and chalcogen interactions in Sulfamethizole cocrystals



The first reported pharmaceutical alloy of Nitazoxanide exhibits higher pharmacokinetic profile than the cocrystals and pure drug

SUPRAMOLECULAR DESIGN OF NOVEL PHARMACEUTICAL SOLIDS AND THEIR PHYSICOCHEMICAL AND PHARMACOKINETIC PROPERTIES

A Thesis Submitted to the
University of Hyderabad in partial fulfillment of
the Award of PhD Degree in Chemistry

By

K. SURESH



School of Chemistry
University of Hyderabad
Hyderabad 500 046, Telangana

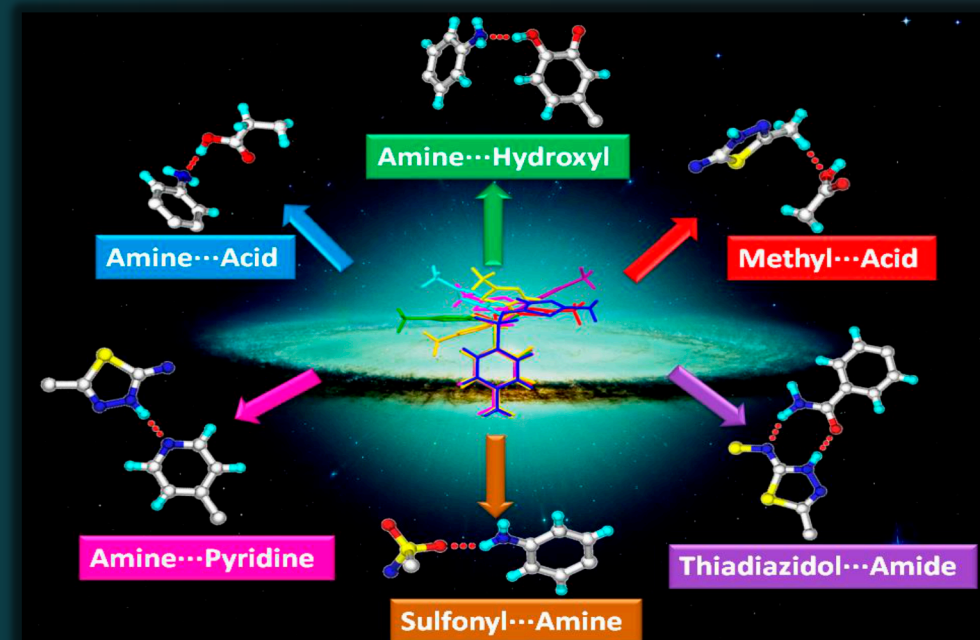
India

May 2016

Ph.D. Thesis

SUPRAMOLECULAR DESIGN OF NOVEL PHARMACEUTICAL SOLIDS
AND THEIR PHYSICOCHEMICAL AND PHARMACOKINETIC PROPERTIES

K. SURESH



Six novel robust hetero synthons as well as weaker hydrogen bonds and chalcogen interactions in Sulfamethizole cocrystals



The first reported pharmaceutical alloy of Nitazoxanide exhibits higher pharmacokinetic profile than the cocrystals and pure drug

SUPRAMOLECULAR DESIGN OF NOVEL PHARMACEUTICAL SOLIDS AND THEIR PHYSICOCHEMICAL AND PHARMACOKINETIC PROPERTIES

A Thesis Submitted to the
University of Hyderabad in partial fulfillment of
the Award of PhD Degree in Chemistry

By
K. SURESH



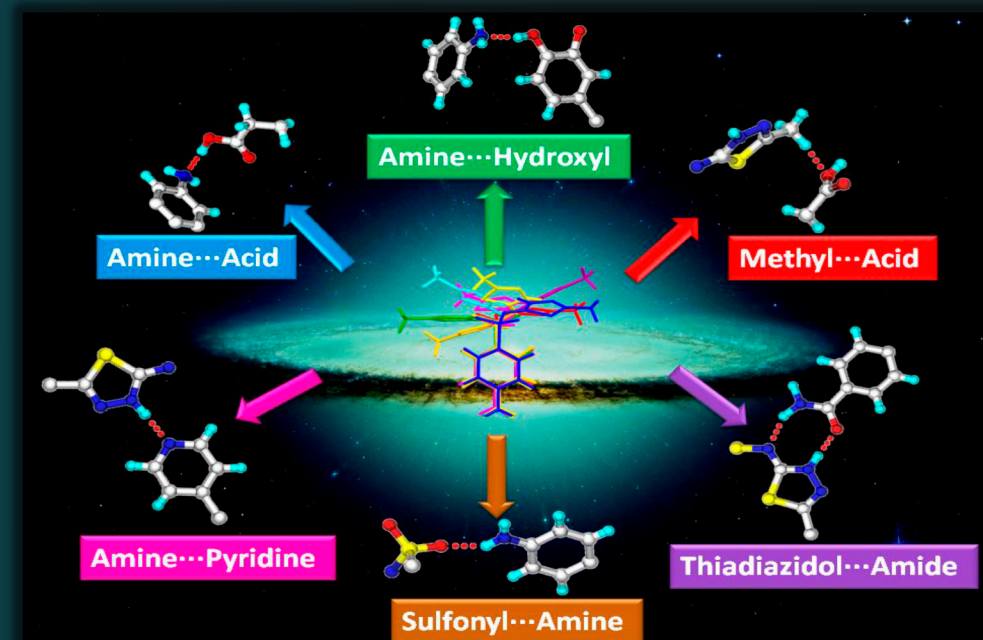
School of Chemistry
University of Hyderabad
Hyderabad 500 046, Telangana

India
May 2016

Ph.D. Thesis

SUPRAMOLECULAR DESIGN OF NOVEL PHARMACEUTICAL SOLIDS
AND THEIR PHYSICOCHEMICAL AND PHARMACOKINETIC PROPERTIES

K. SURESH



Six novel robust hetero synthons as well as weaker hydrogen bonds and chalcogen interactions in Sulfamethizole cocrystals



The first reported pharmaceutical alloy of Nitazoxanide exhibits higher pharmacokinetic profile than the cocrystals and pure drug

**Supramolecular Design and Synthesis of Novel
Pharmaceutical Solids and Their Physicochemical
and Pharmacokinetic Properties**

**A Thesis Submitted to the University of Hyderabad in partial
fulfillment of the Award of PhD Degree in Chemistry**

By

K Suresh



**School of Chemistry
University of Hyderabad
Hyderabad 500046, Telangana State, India
May 2016**

DEDICATION

To

Kuthuru Family



CERTIFICATE

This is to certify that the thesis entitled “**Supramolecular Design and Synthesis of Novel Pharmaceutical Solids and Their Physicochemical and Pharmacokinetic Properties**” submitted by **K Suresh** bearing Regd. No. **10CHPH26** in partial fulfillment of the requirements for the award of Doctor of Philosophy in Chemistry is a bonafide work carried out by him under my supervision. I hereby agree that my thesis can be deposited in Shodganga/INFLIBNET.

The thesis has not been submitted previously in part or in full to this or any other University or Institution for the award of any degree or diploma.

Prof. Ashwini Nangia

Thesis Supervisor (on lien)

Prof. Samar Kumar Das

(Supervisor I/c)

Dean

School of Chemistry

DECLARATION

I, **K Suresh** hereby declare that this thesis entitled “**Supramolecular Design and Synthesis of Novel Pharmaceutical Solids and Their Physicochemical and Pharmacokinetic Properties**” submitted by me under the supervision of **Professor Ashwini Nangia** is a bonafide research work. I also declare that it has not been submitted previously in part or in full to this University or any other University or Institution for the award of any degree or diploma.

Hyderabad

Signature:

Date:

Name: **K Suresh**

Regd. No. 10CHPH26

ACKNOWLEDGEMENTS

I express profound respect and a deep sense of gratitude to my supervisor, **Prof. Ashwini Nangia** for his encouragement, guidance, appreciation and freedom throughout my PhD tenure which made me complete the work in time. I have been able to learn a great deal in this fascinating field of research through his inspiring lectures and thoughtful discussions, and I consider my association with him a rewarding experience. I specially thank supervisor in-charge **Prof. Samar Kumar Das**. I take this opportunity to thank my doctoral committee members Prof. Tushar Jana and Dr. R. Chandrashekar for their constant encouragement and support during my PhD period.

I thank Prof. M. Durga Prasad, Dean, School of Chemistry, former Deans Prof. M.V. Rajasekharan and Prof. D. Basavaiah and faculty for their co-operation in providing facilities in the School.

It is my pleasure to Prof. Elena Boldyreva, Novosibirsk State University, Russia and Prof. Ivana Evans, Durham University, U.K. for their helpful discussions under collaboration work.

I am grateful to thank UGC for fellowship support. I would like to thank CSIR, DST and UOH-UPE for providing instrumentation and infrastructure facilities at the School of Chemistry. I thank to Department of Science and Technology-Russian Federation Basic Research (DST-RFBR) for funding visit to Novosibirsk State University, Russia, for a collaborative student exchange research programme. I also thank to Crystalin Research Pvt. Ltd. for collaborative studies on my thesis work.

I thank each and every non-teaching staff of the School of Chemistry, CIL, and an administrative section for their assistance on various occasions. I take this opportunity to thank Dr. P. Raghavaiah, Smt. Srilakshmi, and Mr. Ramana for their kind help in acquiring the Single crystal data on various occasions. I thank Mr. Satyanarayana, Smt. Vijayalakshmi, Mr. Turabuddin, and Mr. Durgesh for their help in recording NMR spectra. I thank Mr. Mallaya Shetty, Mr. Kumar, Mr. Vijay Bhaskar, Mr. Dilip, Mr. Sai, Mr. Gupta, Mr. Shetty, Mr. Aleem, Smt. Geeta, Mr. Naik and Mr. Venkat for their cooperation.

It gives me immense pleasure to thank my lab seniors Dr. Binoy K. Saha, Dr. Peddy Vishweshwar, Dr. Srinivasulu Aitipamula, Dr. Jagadeesh Babu, Dr. Bipul Sarma, Dr.

Ranjit Thakuria, Dr. Naba Kamal Nath, Dr. Palash Sanphui, Dr. Suryanarayan, Dr. Rajesh Goud, Dr. Maddileti, Dr. Sudalai Kumar and Dr. Geetha for their help and encouragement at various stages of my PhD. My sincere thanks to my labmates Swapna, Sudhir, Anil, Surya, Manish, Vishwanadh, Kranthi, Uday, Kiran, Ragavendra, Swarupa Sumanth, Srikanth, Divya, Dr. Ruchi, Dr. Daman, Dr. Abin, Dr. Soumendra. Chaitanya, Durgabhavani and Sudhir deserve special thanks for their help in carrying out Pharmacokinetic experiments and all project students, Santosh, Rajireddy, Swagath, Prashanth, Greeshma, Mamina, Savithri and Evelin for maintaining an innovative and friendly atmosphere in the lab.

I wish to record my thanks to Dr. Bhasker, Dr. Narayana, and Shiva for their help on various occasions. My stay on the campus has been pleasant with the association of many friends from different labs and to name a few, Edukondalu, Prasad, Shanmukh Raj, Raju, Sagar, Venkanna, Suresh, Krishna, Uday, Satyanarayana, Mohan, Anand, Ramesh, Harish.

I take this opportunity to express my gratitude to my school and college teachers Venkateshwara rao sir, Srinivas sir, Satyanarayana sir, Narasimha reddy sir and Mannan sir, B. Sc. Professors, Murthi sir, Prabhakar sir, Madushudan sir, and Vijjulatha madam, M. Sc. Lecturer Sathish sir and Althuf sir for their inspiration and guidance.

I would like to thank my friends, Jagan, Rajkumar, Suman, Anil, Ravi, Sridhar, Shiva, Ravindher, Srinivas, Dayakar, Shekar, Aruna, Supraja, Sharada, and Jahnvi for their support. I wish to record thanks to my best friend Nagesh and his family members Parvathamma, Pentaiah, Ramesh, Ramanilatha, Krishaniah, Sunitha and Anil for their ever willing support and encouragement. I would like to thank my Gurukulam friends, Kanakaiah, Javed, Srinivas, Goutham Raj, Ramudu, Ramulu, Raju, Bethaiah, Ratnaiah, and Srinivas for their wonderful friendship.

My heartfelt thanks to Nanamma and Ammamma for their blessings. I would like to take this opportunity to appreciate the support from my kuthuru family, Peddamma, Peddananna, Chinnamma, Chinnananna and my cousins Vijayalakshmi, Swapna, Srisha, and Sony.

The unconditional love of my Amma & Nanna and their blessings made me what I am today and I owe everything to them. The love and support I received from my brother Naresh & sister Swarnalatha are invaluable. Heartful thanks to late elder brother Ganesh who supported my education. Dedicating this thesis to kuthuru family is a minor recognition to their boundless love and affection.

–Suresh

SYNOPSIS

This thesis entitled “**Supramolecular Design and Synthesis of Novel Pharmaceutical Solids and Their Physicochemical and Pharmacokinetic Properties**” consists of eight chapters.

CHAPTER ONE

Introduction: Crystal Engineering and Pharmaceutical Solids

Supramolecular chemistry defined as “*chemistry beyond the molecule*”, and “*aims at developing highly complex chemical systems from components interacting by non-covalent intermolecular forces*”. The development requires an understanding of molecular chemistry (the chemistry of the covalent bond) together with noncovalent interactions for molecular self-assembly to tune the structure, properties and functionalities of the resulting products. The understanding and design of such noncovalent intermolecular interactions in the solid state is referred to as Crystal Engineering.

In crystal engineering, one uses different intermolecular interactions such as hydrogen bonding, π -stacking, halogen bonding, and van der Waals forces for the rational design of supramolecular structures in the broadest sense with the specific aim of tailoring their properties. In recent years, the design of novel pharmaceutical solids in both academic and pharmaceutical laboratories has become a popular research activity. The majority of currently marketed drugs are as solid forms which are administered orally (tablet, capsule, or lyophilized powder forms). About 40% of drugs in the market and emerging new chemical entities (NCEs) under research and development fall in the low solubility quadrant classified under the Biopharmaceutics Classification System (BCS) of Class II or IV. Some drugs are known to undergo degradation during the storage (ICH, International Conference Harmonisation) and handling, transport even under physiological conditions. The management of these challenges along with enhanced therapeutic efficacy for active pharmaceutical ingredients (APIs) is the prime objective for pharmaceutical scientists. Possible solutions to these issues in the solid formulation space are polymorphs, salts, amorphous, solvate/ hydrate, coamorphous solid blended with excipients (polymeric matrix), drug carriers, nanoparticles, etc. The

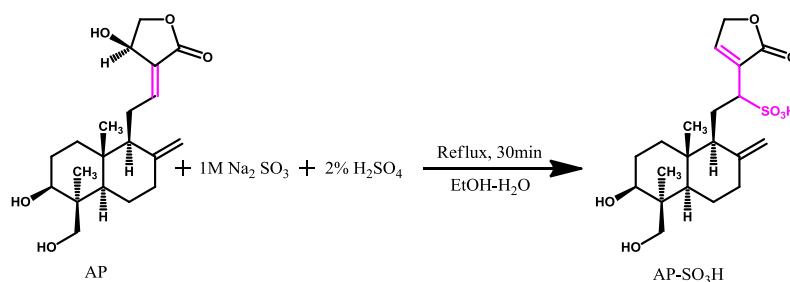
US-FDA regulatory guidelines and those of the European Medical Agency (EMA) are a time for formulation development of APIs for which the traditional routes are ineffective. By virtue of their hydrophilic/ hydrophobic nature, formulation solids can exhibit diverse physicochemical behavior which is possible to control with coformers, such as solubility, stability, permeability and bioavailability for improved shelf-life and drug-patient compatibility.

Solids are broadly classified as crystalline (having long-range order) and amorphous (with short-range order but no long-range periodicity) depending on the internal structure, length-scale of order, and degree of periodicity. A pharmaceutical solid may exist in a single or multicomponent system, either as crystalline or amorphous state. Different crystalline arrangements of the same chemical substance are polymorphs and those with multicomponent (two or more neutral chemical species) in a single crystalline lattice is referred to as a cocrystal. The ionized salt forms and which are interacting with another organic compound in crystal lattice are known as ionic cocrystals. The supramolecular family of multi-component solids therefore includes salts, hydrates, solvates, cocrystals, eutectics, solid solutions, alloys, etc. all of which may be assessed as pharmaceutical forms depending on the specific pharmaceutical properties required for a specific drug. A difference between cocrystal, eutectic and solid solution or alloy is that the stoichiometry is fixed in a cocrystal, eutectic, but can vary over a range (multiple stoichiometries) for an alloy or solid solution (namely multivariate stoichiometry cocrystals). These multicomponent crystalline solids can exhibit polymorphism, and now even polyamorphism cases have been reported. In coamorphous solids, the stoichiometric ratios of two or more solids which are held together through weak but discrete interactions in an aperiodic arrangement; the individual components are crystalline but the resulted adducts are characterized by X-ray diffraction amorphous (broad halo peak). The important point is that each of these solid forms can be advantageous for a specific application in different cases. Hence it is important to understand the nature and properties of diverse solid forms of drugs/ natural bioactive molecules from a pharmaceutical perspective. This thesis deals with the design and discovery of different solid forms of drugs and bioactive molecules and their physical behavior and physic-chemical properties, specifically solubility, stability and bioavailability.

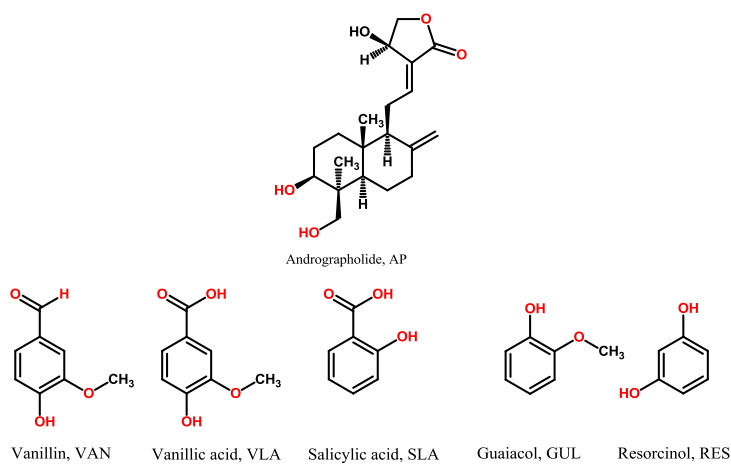
CHAPTER TWO

Andrographolide: Solving Chemical Instability and Poor Solubility By Means of Cocrystal

Cocrystallization is a well-established methodology in crystal engineering for the design of novel multicomponent crystalline solids. It has gained remarkable impetus from the last decade because of the potential implications of cocrystals as functional materials in pharmaceuticals. The principal advantage with cocrystals is improvement in the physical or chemical stability, hygroscopicity, tabletability, increasing the kinetic dissolution rate/thermodynamic solubility, and enhanced bioavailability etc. of Active Pharmaceutical Ingredients (APIs) or bioactive molecules. Hence with this background we selected Andrographolide (AP) naturally occurring molecule, explore the structural diversity of AP and to enhance the physicochemical properties. AP is a bioactive diterpenoid lactone used in traditional medicine in China, India and Southeast Asian countries. It is derived from the leaves of *Andrographis Paniculata*, a plant known as “King of Bitters”, in the acanthaceae family and the local plant name in India is Kalmegh. AP is known for diverse pharmacological activities, such as anti-viral, anti-inflammatory, anti-cancer, and anti-malarial. Despite being safe at high doses of 17 g/kg per day in humans, the efficacy of AP is limited in clinical application by poor aqueous solubility (46 mg/L) and oral bioavailability of 2.67% (reported in rats). A significant drop in the bioavailability of AP is due to an inactive metabolism and the four inactive metabolites isolated from humans and rats. Among these, three metabolites are isomers/diastereomers of 14-deoxy-12-sulfo-andrographolide, and the fourth product is the S-conjugate (sulfated derivative) of AP. Furthermore the main inactive metabolite of AP was identified as 14-deoxy-12-(*R*)-sulfo-andrographolide and Yao et al. developed an in vitro synthetic method that mimics the in vivo biochemical transformation of 14-deoxy-12-(*R*)-sulfo-andrographolide metabolite have been studied by mass spectroscopy. A schematic representation of the chemical transformation is shown below (Scheme 1). Additionally Cambridge Structural Database (CSD) search on AP, no polymorphs, solvates/hydrates, or cocrystals are disclosed, only one AP guest free from crystal structure is reported.



Scheme 1 Chemical transformation of AP to its main metabolite 14-deoxy-12-(*R*)-sulfoandrographolide, AP-SO₃H. The chemically reactive moiety is shown in color.



Scheme 2 Molecular structure of Andrographolide and coformers used in this study

Our objective was to study the pharmaceutical cocrystals of AP for improving its chemical stability and solubility. In an attempt of cocrystal screen AP by liquid assisted grinding technique with several GRAS phenols and acids as coformers to find the cocrystal having the chemical stability and high solubility. We obtained five cocrystals with Vanillin (VAN), Vanillic acid (VLA), Salicylic acid (SLA), Resorcinol (RES), and Guaiacol (GUL) (Scheme 2) cocrystals. All the cocrystals were characterized by X-ray diffraction (powder and single), thermal (DSC), spectroscopy (FT-IR, Raman, and ss-NMR) techniques. In the crystal structures of all these five cocrystals, AP and coformer associated via O–H···O (hydroxyl···hydroxyl) hydrogen bonds and those are isostructural to each other. The packing similarity (1D/2D/3D) of isostructural cocrystals is explained by the unit cell similarity index and XPac analysis.

Further in order to assess the chemical stability/instability for AP and its cocrystals performed chemical transformation experiments by applying the reported method at room temperature and the reaction was monitored by NMR. We demonstrate

that among all cocrystals, AP-VAN, AP-RES, and AP-GUL reacted slightly slower than pure AP but they are transformed into inactive metabolite. And this conversion was partial in the case of AP-VLA (43% by weight). Whereas AP-SLA cocrystal gave the best result in that no chemical transformation could be detected by NMR and HRMS. The inhibition of this conversion can be explained by the acidity of the coformer. The reason behind hypothesis is the acidity of the COOH group of SLA and VLA has a capable inhibitory effect on the chemical transformation of AP to AP-SO₃H. The reactive species in the aqueous ethanol medium is bisulfite anion (HSO₃⁻), where it reacts with the conjugated lactone of AP in a 1,4-nucleophilic addition. The carboxylic acid of the coformer in AP-SLA (and VLA) essentially titrates the HSO₃⁻ to H₂SO₃ and sodium salicylate, which will block the subsequent addition reaction. Since VLA is less effective in proton transfer to HSO₃⁻ being a weaker acid and this explains its intermediate inhibition. Additionally an added advantage with the chemically stable AP-SLA cocrystal is 12 folds enhanced solubility and dissolves 3 times faster than AP in 25% EtOH–water slurry medium.

The primary objective of this work was to improve the chemical instability and solubility of AP was achieved via cocrystallization with SLA coformer. This preliminary study also has scope the possibility of exploring *p*- and *m*-amino salicylic acids which are drugs on their own, as potential coformers with Andrographolide in novel drug–drug cocrystals.

CHAPTER THREE

Novel Synthons in Sulfamethizole Cocrystals: Structure–Property Relations and Solubility

This chapter emphasizes the non-covalent interactions and synthons preferences or competition and cooperation of Sulfamethizole (SMT) drug with respect coformers in the crystal lattice. Furthermore it is also discusses the preparation of less soluble forms of SMT by cocrystallization or salt approach. SMT is a sulfonamide class antibiotic that acts through the competitive inhibition of folate synthesis in microorganisms. It has good solubility (1.05 g/L at 37 °C in water) but it has a short half-life (2.1 h). Even though most of sulfonamide antibiotic class drugs exhibit moderate to high solubility but

bioavailability is limited. This is due to rapid metabolism and fast elimination under *in vivo* physiological conditions as a results marketed drug dosage was high to improve the bioavailability and maintain concentration for extended release. In literature to attempts, towards the extended release Remington et. al. has recognized that making of less soluble form of a high soluble drug is a facile procedure for producing extended release formulations. Besides on the SMT drug, extended release has been reported by making the Lipase-Sulfamethizole granule formulation in dogs. The concentration of SMT in blood level extended to 12 hours. A reason behind this improvement is rapid metabolism is reduced by a lipase enzyme which controls the digestion of glyceryl trilaurate and glyceryl tristearate and subsequent release of the embedded drug particles. Although in certain literature reports showed that the solubility of drug can be decreased by making cocrystals. The Zaworotko's group reported that cocrystals of Epigallocatechin gallate (EGCG) exhibited lower solubility compared to the parent drug resulting in significant increase of pharmacokinetic profile. The high solubility of sulfacetamide was controlled in pharmaceutical cocrystals with lower dissolution rates, reported by Goud et al. These results suggest that the cocrystal approach is adaptable to modulate the solubility towards higher or lower levels of rational selection of coformers. Encouraged in this context of literature, we explored structural landscape of SMT via pharmaceutical cocrystals would have the pertinent hydrogen bonding patterns to lowering the solubility. Cambridge structural Database search on SMT is given only one hit for SMT guest free form shows that the molecule exists as the imidine tautomer and there is a chance to exist as amidine tautomer. It has rich hydrogen bond functionalities (donors: amine NH_2 and imine NH ; acceptors: sulfonyl O , thiazolidine N and S , and imidine N) which makes it a functionally diverse molecule to form cocrystals. Using liquid assisted grinding and isothermal solution crystallization techniques, we obtained six cocrystals with *p*-aminobenzoic acid (PABA), vanillic acid (VLA), *p*-aminobenzamide (ABA), 4,4-bipyridine (BIP), suberic acid (SBA), adipic acid (ADP) and one salt with oxalic acid (OA). All of these cocrystals were characterized by thermal, spectroscopic and X-ray diffraction methods.

Intersignly in all cocrystal crystal structures, hydrogen bonds between the coformers and SMT are analyzed as six different synthons (Figure 1). Specifically synthon preferences/competition arises when acceptor is selected by the number of donors or vice versa during crystallization. Many literature reports were highlighted the hydrogen bond competition and hierarchy of hydrogen bonding in single and

multicomponent systems. The strong and directional O–H \cdots O, O–H \cdots N, N–H \cdots O, and N–H \cdots N are regularly used hydrogen bonds to construct the cocrystals. Additionally the weak C–H \cdots O, C–H \cdots N, π - π stacking, hetero atom bonding also have potential to steer the supramolecular assembly in cocrystals. Studies on the above non covalent interactions and its competition and cooperation will give a basic understanding of the functional materials property behaviour. Relatively synthon preferences/competition was observed in SMT cocrystals with respect coformer. Here in addition to strong N–H \cdots O and O–H \cdots N H-bonds, the cocrystal structures are also sustained by weak C–H \cdots O hydrogen bonds. The very rare and common chalcogen-chalcogen (S \cdots O) type II intermolecular interaction in SMT-ADP cocrystal and chalcogen-nicogen (S \cdots N) type II interaction in SMT-BIP cocrystal were observed. The products were characterized by vibrational spectroscopy to obtain information on the strengths of the intermolecular interactions.

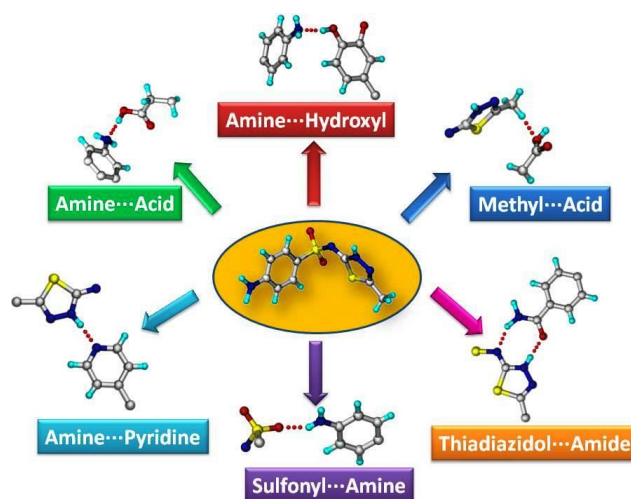


Figure 1 Different supramolecular synthons observed in SMT cocrystals in this study.

Solubility and dissolution experiments of SMT, SMT-ADP and SMT-SBA cocrystals, and SMT-OA salt were performed in 0.1 N HCl medium. All of these two cocrystals and salt showed a lower intrinsic dissolution rate (IDR) and equilibrium solubility compared to SMT in 0.1 N HCl medium, which is ascribed to stronger N–H \cdots O, N–H \cdots N, and O–H \cdots O hydrogen bonds and crystal packing. Furthermore, we observed that SMT-OA salt is formed spontaneously when the components were mixed in acidic medium (0.1 N HCl) whereas in neutral medium (phosphate buffer) no SMT-OA salt formation was observed. The decreased IDR and equilibrium solubility of

cocrystals and salt is useful in controlled/extended release of SMT to improve the therapeutic activity of the drug. Hence this study highlighted the importance of pharmaceutical cocrystallization/ salt strategy to make, the less soluble form of the API.

CHAPTER FOUR

Polymorphism, Isostructurality and Structure-Property Relations: Glibenclamide Salts

Polymorphism and Isostructurality are inversely related phenomena, and both displayed a great deal of impact in crystal engineering, material science. Polymorphism can be stated as *the ability of the chemical substance to exist different in crystalline packing arrangements in a crystal* and isostructurality can be defined as *identical or a nearly identical packing arrangements of chemically distinct/ or related substances in a crystal*. Polymorphism is important in pharmaceuticals and it is considered an important element in drug development. In the literature, numerous reports highlighted the importance of polymorphism in single component APIs; studies on the multicomponent systems such as pharmaceutical salts are relatively few, especially on sulfonyl urea salts. Sulfonyl urea/ Sulfonamide group consisting organic/drug molecules likely to exhibit polymorphism and these are second best candidates to display the polymorphism (frequency of >50% for more than one polymorph) and the top category is barbiturates at 70% as carboxamides. Nevertheless polymorphism in multicomponent systems of sulfonamide group compounds is rare and there is no report for sulfonylurea compounds. A sulfonyl urea class of organic/drug molecules are acting as weak acids and then can have a propensity to form salts with metals and organic bases. CSD search for molecules with sulfonylurea ($-\text{SO}_2-\text{N}-\text{CO}-\text{N}-$) skeleton showed 215 hits. Among them 169 single components and 46 multicomponent systems were present. In 46 multicomponent systems, only three salts were available (refcodes: BENVIP, KETNIH and PIJCUI) and there is no polymorphism of salts is disclosed and moreover no proper study of counter ion effect in crystal lattice (isostructurality) and property relations. Therefore it is important to understand the packing diversities in pharmaceutical salts of sulfonylurea ($-\text{SO}_2-\text{N}-\text{CO}-\text{N}-$) group compounds via polymorphism and isostructurality and its structure-property relations we have chosen the classical drug molecule Glibenclamide.

Glibenclamide (GBA) or Glyburide belongs to the class of sulfonylurea drugs and has been used to treat the type-II diabetes (non-insulin-dependent diabetes mellitus, NIDDM) to bring down the blood glucose levels by increasing the amount of insulin produced from beta cell located in the pancreas. GBA belongs to the Biopharmaceutical Classification System (BCS) class-II drug with high permeability and low aqueous solubility (~18mg/L at 37 °C). CSD search has given only one guest free form of GBA without any hydrogen's (disordered, Refcode: DUNXAL) along with synthesis and structural characterization by NMR and FT-IR of its metal complexes with magnesium, chromium, cobalt, nickel, zinc and cadmium. On subjecting, slurry technique and isothermal solution crystallization of the GBA with NaOH, KOH and NH₃ bases resulted three novel salts. In that, GBA-Na salt exists in dimorphic and one hydrate described as form I, II and III and GBA-K anhydrous and hydrate considered as form I and II. The products (except GBA-Na form II) were characterized by spectroscopic, thermal and diffraction techniques. Except GBA-K form II, crystal structures of all salts established by SXRD.

In crystal structures of GBA-Na salt forms, GBA-Na form I consist of central sodium ion that is coordinated by four O-bonded and one N-bonded ligands which comes from the GBA anion through Na–O and Na–N coordination bonds in square pyramid geometry (Figure 2a). In form II, central six coordinated sodium cation binds to five oxygen atoms and one nitrogen atom from different distinct ligands of GBA anion in the crystal lattice and displays the distorted octahedral geometry (Figure 2b). Whereas in form III, showed octahedral geometry of the central metal ion is coordinated by and one N- and four O-bonded ligands comes from the GBA anion and one water molecule in the crystal lattice through Na–O and Na–N coordination bonds. Form I and II, exhibit differences in their molecular packing and geometry of central metal ion. Therefore GBA-Na form I and II belong to both packing and geometry polymorphism. In addition to this GBA-K form I and GBA-NH₄ crystal structures were also described.

Interestingly GBA-Na form I : GBA-NH₄ and GBA-K form I : GBA-NH₄ are isostructural showing internal molecular packing and powder X-ray diffraction pattern similarity. In other system GBA-Na form II : GBA-K form I is isostructural according to Kàlmàn's equation but another methods such as XPac, packing and powder similarity analysis software are failing to explain the structural arrangement between them. It may due to larger atomic radii difference in Na⁺ and K⁺ metal ions.

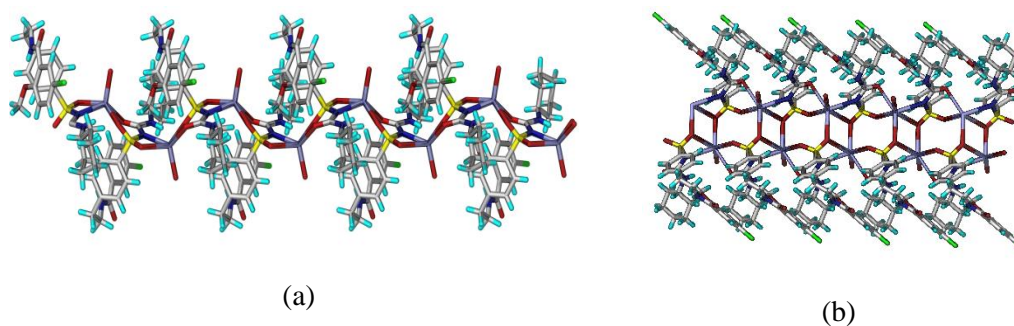


Figure 2: (a) Square pyramid geometry of GBA-Na form I 1D polymeric zig zag chain in crystal lattice (b) Distorted Octahedron geometry of GBA-Na form II complex 1D polymeric chain in crystal lattice.

Solubility studies shown that among five GBA salts GBA-K form I and II (77 folds in water and ~34 times in pH 7 buffer) exhibit more solubility than all salts and the parent drug (Figure 2) in water and pH 7 buffer media. Furthermore moisture uptake/release and phase stability of these five salts was established by DVS technique. All these forms absorb significant amounts of water (0.4 to 6.2% range for salts) during adsorption and while desorption cycle it loses the water. It indicates that the moisture behavior of all these five solid forms is reversible without any hysteresis. In summary we have shown the polymorphism and isostructurality behavior of sulfonyl urea class of GBA salts. Additionally discuss metal salts (K/Na) are isostructural with the ammonium salt. In contrast, the similarity in crystal structures has not translated into similarity in properties. With significant increases in solubility and stability, GBA-K form I is an optimum salt for pharmaceutical development.

CHAPTER FIVE

Crystal Structures, Conformations, and Solubility: Lornoxicam Salts

Salt formation is the first line method for improving the physicochemical properties of APIs, such as dissolution rate, bioavailability, and stability. The modification of an acidic or a basic API as a salt form gives the higher solubility and stability together with improved flowability, filterability, etc. The conversion of an acidic or basic or amphoteric API to a salt can also change its biological properties and offer novel patentable forms. In this chapter displays the advantages of molecular salts and

conformational flexibility of Lornoxicam. LXM is a non-steroidal anti-inflammatory drug (NSAID) with analgesic, anti-inflammatory, and antipyretic properties. It is an oxicam class drug in BCS II category with low solubility and high permeability (solubility of LXM in water 15 mg/L). It is currently marketed under the brand names Lorcam and Xafon and its solubility and bioavailability is used to be varying under physiological conditions. However, alternative solutions to improving the solubility of LXM were desirable. To improve the solubility and dissolution LXM cyclodextrin complexes and solid dispersions have been reported. In other reports, Polymorphs and cocrystals of LXM have been described and characterized by using powder X-ray diffraction. However there is no single crystal structure report on this molecule in CSD. In this work we explored structural landscape of LXM guest free form and its salts with acids and bases. Additionally we have studied the effect of counter ion on solubility, stability and conformation in the crystal structure (Figure 3).

LXM is an amphotropic molecule which exists as a zwitterion in the solid-state. The formation of two strong intramolecular $\text{N}^+-\text{H}\cdots\text{O}$ and $\text{N}-\text{H}\cdots\text{O}^-$ hydrogen bonds in a stable six-member ring geometry, $S(6)$, renders this flexible molecule in a rigid conformation (conformer *A*). LXM being an amphoteric molecule can form salts with both acids and bases. We obtained crystalline salts of LXM with hydrochloric acid (HCl), methanesulfonic acid (MSA), piperazine (PIP) and ammonia (AMM). The crystal structures of these salts exhibit different intramolecular hydrogen bonds and conformations of LXM in the acid and base salts (conformation *B* and *C*). The conformational variability of LXM in acidic and basic salts is explained by steric and hydrogen bonding factors. All the new salts bulk phase homogeneity was established by spectroscopic, thermal, powder X-ray diffraction techniques and they showed enhanced solubility in pH 7 buffer medium compared to the free drug.

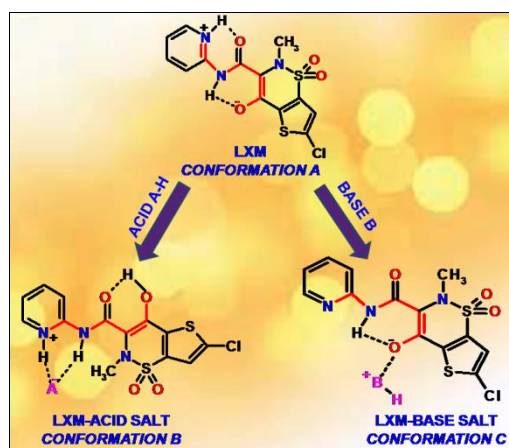


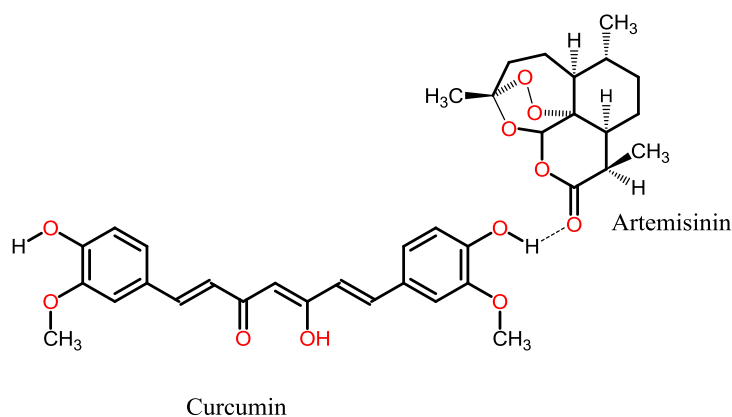
Figure 3 Different conformations of LXM and in salt structures

CHAPTER SIX

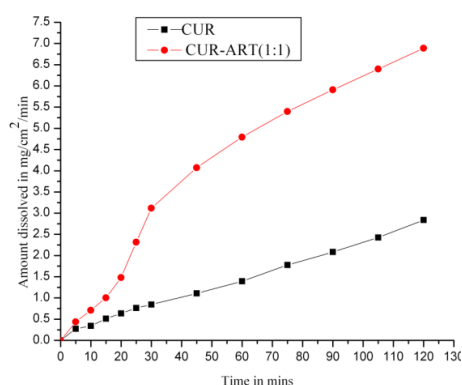
A Novel Curcumin-Artemisinin Coamorphous Solid: Physical Properties and Pharmacokinetic Profile

This chapter deals the binary system coamorphous solid advantages in pharmaceutics with improved solubility and pharmacokinetic profile of naturally occurring compounds of Curcumin and Artemisinin. Natural source compounds from traditional herbal medicines represent a prime source of potential therapeutic molecules to treat human diseases with minimal side effects. Major drawbacks of bioactive molecules are low aqueous solubility and poor bioavailability and also some of them have stability issues. For these reasons many bioactive molecules fail to reach the market as drugs, the prominent example being Curcumin. Curcumin (diferuloylmethane, CUR), a hydrophobic polyphenol derived from the rhizome of the herb *Curcuma longa* of the dietary Indian spice turmeric, has a plethora of pharmacological actions such as anti-inflammatory, anti-oxidant and anticancer. Despite high safety levels of CUR up to 12 g/day in humans, the efficacy of CUR as a drug is limited by low aqueous solubility (7.8 $\mu\text{g/L}$) and poor bioavailability (0.051 $\mu\text{g/mL}$), mainly due to its rapid metabolism and short half-life. In addition it has structural instability in pH 7 buffer medium. The enhanced stability and bioavailability of CUR has been reported by making nano particles and adjuvant like piperine. Our group discovered polymorphs, cocrystals and eutectics of curcumin which are shown enhanced solubility. Encouraged by these preliminary results and we performed cocrystallization with antimalarial drug

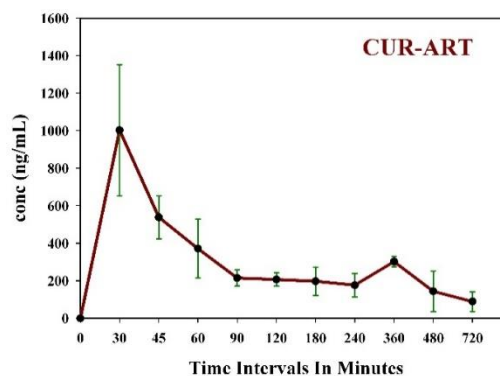
Artemisinin. Artemisinin (ART) is an antimalarial drug, first identified by Chinese researchers in the plant *Artemisia annua*. ART also independently exhibits anticancer activity by suppressing multiple signaling pathways and inhibits cell proliferation, invasion, metastasis and angiogenesis. In addition when ART is combined with CUR it exhibits better antimalarial activity compared to the individual drugs. With the intent of exploring a possible synergism between CUR and ART for both physical form and pharmaceutical property (they have phenol and lactone carbonyl complementary hydrogen bonding groups), we performed cocrystallization to obtain their solid combination product as a cocrystal or eutectic, mediated by O–H···O=C hydrogen bond (Scheme 3). Instead we obtained a 1:1 coamorphous solid form, CUR-ART. This new coamorphous solid was characterized by PXRD, DSC, ss-NMR and IR techniques. The intrinsic dissolution rate of CUR-ART (1:1) in 60% ethanol-water is 2.6 times faster than curcumin (Figure 4a). Bioavailability studies on coamorphous CUR-ART in Sprague Dawley rats showed higher curcumin concentration with $AUC_{0-12} = 2.59 \mu\text{g.h/mL}$ after administering 200 mg/kg dose, compared to pure CUR which could not be detected in blood plasma due to its poor solubility(Figure 4b). The primary objective, improved bioavailability of Curcumin was achieved by means of CUR-ART coamorphous solid.



Scheme 3 Molecular structure of curcumin (CUR)–Artemisinin (ART) and intermolecular O–H···O=C hydrogen bond.



(a)



(b)

Figure 4 (a) Intrinsic dissolution rate curves of CUR and CUR-ART in 60% EtOH–water. (b) Mean plasma concentration vs. time profile of the CUR-ART coamorphous form.

CHAPTER SEVEN

Cocrystals and Alloys of Nitazoxanide: Enhanced Pharmacokinetics

This chapter describes the novel pharmaceutical solid forms, isomorphous cocrystals and their alloys (solid solutions) of Nitazoxanide as improved medicines. Cocrystal alloy is a single phase about comprise mixtures of two or more isomorphous/isostructural cocrystals is also called as multivariate cocrystals (multiple stoichiometries). Nitazoxanide (NTZ) is a prodrug of nitrothiazolyl-salicylamide derivative used as an anti-protozoan agent and it's an active metabolite is Tizoxanide (TIZ). In the interesting of drug repositioning (as using drugs for new purpose is an attractive area in pharmaceuticals) Carl Nathan et. al. identified and studied nitazoxanide (NTZ) as a promising candidate for tuberculosis(TB) diseases caused by *Mycobacterium tuberculosis* bacteria. Currently the treatment of TB consists of four drugs namely isoniazid, ethambutol, rifampicin and pyrazinamide as a fixed dose combination (FDC). Although there is a serious stability issue with these FDC drugs because of high chemical reactivity between Rifampicin and Isoniazid drugs. There is a demanding need for new medication; hence the repurposing or repositioning of drugs to treat TB is progressively gaining favour. Even though NTZ has poor aqueous solubility (7.55×10^{-3} mg/mL in water) and less bioavailability (C_{\max} 258 ng/mL, 7.5 mg/kg dose in to rats) due maximum quantity of NTZ is glucuronidated in *in vivo*. To address these issues, the

cocrystallization approach was examined. Here we developed two isomorphous cocrystals with p-amino benzoic acid (PABA) and p-amino salicylic acid (PASA) and their alloys (NTZ-PABA : NTZ-PASA) of 0.67:0.33 (CA1) and 0.75:0.25 (CA2) compositions established by single crystal X-ray diffraction technique. In all these structures NTZ and coformer sustained by the robust heterodimer of amidothiazole-acid groups via N–H···O and O–H···N hydrogen bonds (Figure 5). The similarity in unit cell parameters, isostructurality index and XPac analysis confirmed the identity of the two cocrystal structures.

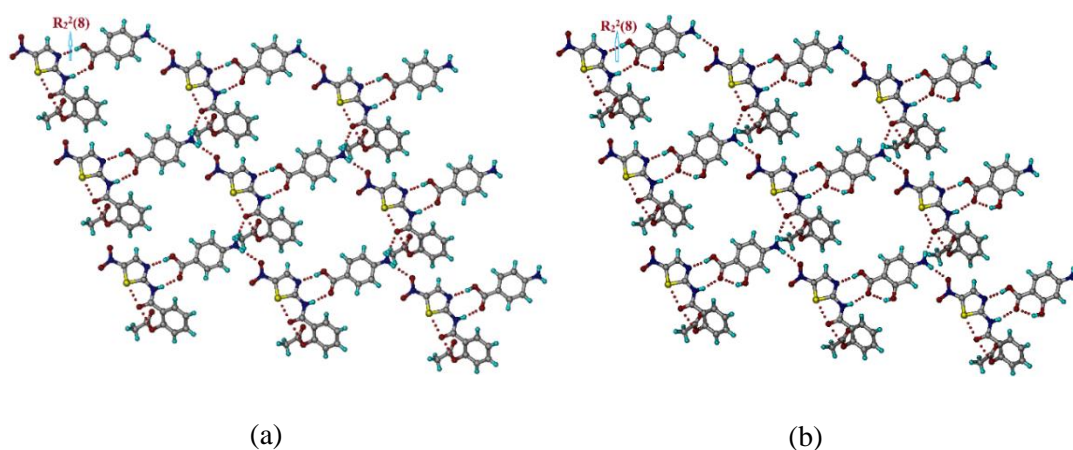


Figure 5 Sheet structures of NTZ-PABA and NTZ-PASA cocrystals is sustained by $R_2^2(8)$ dimer synthon between amidothiazole-acid groups via N–H···O and O–H···N hydrogen bonds.

Bulk phase purity of cocrystals and their alloys were confirmed by PXRD, DSC and FT-IR spectroscopy. The solubility advantage of these cocrystals and alloys was ascertained through dissolution studies in 3% CTAB (cetyltrimethyl ammonium bromide) phosphate buffer (pH 7) medium for 240 minutes. Interestingly, the cocrystals exhibit higher IDR than pure NTZ (which is common) but surprisingly the cocrystal alloys are even superior to the cocrystals (this is unexpected). The dissolution rate order is CA2 > CA1 > NTZ-PABA > NTZ-PASA (Figure 6a). Next the pharmacokinetics was measured by oral administration of NTZ cocrystals/ alloys (45 mg/kg active drug, equivalent to 500 mg human dosage) to Sprague Dwaley rats (Figure 6b). The C_{\max} and AUC of CA2 are far superior to those for CA1 and cocrystals. CA2 exhibits short T_{\max} (30 min) and highest C_{\max} 7.5 $\mu\text{g/mL}$ compared to the other 3 crystal forms. The $\text{AUC}_{(0-12)}$ (total drug

delivered in 12 h) is 24.2 $\mu\text{g.h/mL}$ for CA2 compared to 7.5 $\mu\text{g.h/mL}$ for NTZ. The present study shows that non-stoichiometric multi-component solid forms present yet another opportunity for oral drug bioavailability alongside the stoichiometric cocrystals and salts. The present results open opportunity for the repositioning of nitazoxanide as a multi-strain resistant anti TB drug.

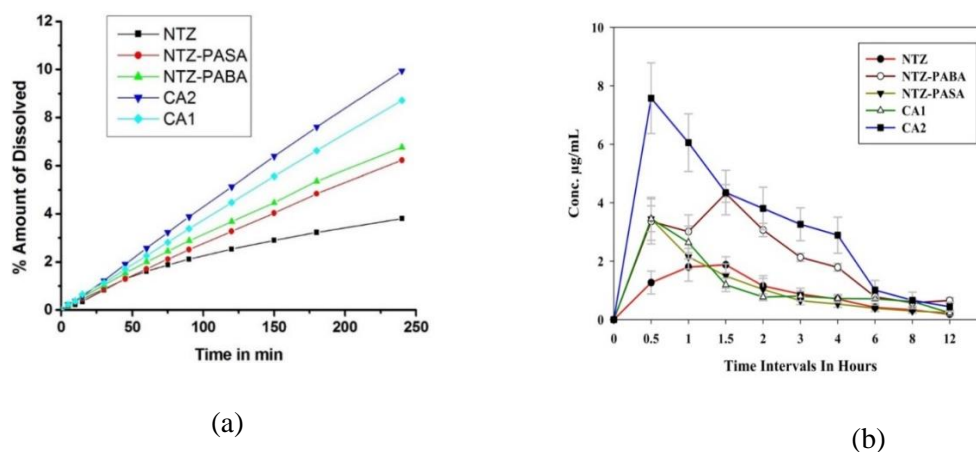


Figure 6 (a) IDR of NTZ cocrystals and alloys in 3% CTAB (pH 7) buffer. (b) Peak and mean plasma concentration of TIZ vs. Time profile for NTZ cocrystals and alloys. NTZ transforms to TIZ in vivo.

CHAPTER EIGHT

Conclusions and Future Prospects

From the studies of above seven chapters the following implications and conclusions can be drawn. Crystal engineering principles and hydrogen bonding rules with predictable and robust supramolecular synthons are the prime elements to design of diverse pharmaceutical solids strive to improve the physicochemical and pharmacokinetic properties of drugs/bioactive molecules. Comprehensive studies on various pharmaceutical solid forms such as polymorphs, amorphous and coamorphous, cocrystals, salts, ionic cocrystals, eutectics and alloys (solid solutions) of several APIs were carried out with the intent of understanding and addressing the problems associated with those APIs/bioactive agents. In chapter 2, the chemical instability and solubility was highlighted through novel andrographolide-salicylic acid cocrystal. Interestingly new isostructural cocrystal pairs were also described. In chapter 3 the solubility

modulating ability of cocrystals and salt were discussed. The ability of cocrystals may find application in developing better and optimized formulations of the parent drug. A study of the pharmaceutical utility of cocrystals is covered on both chapter 2 and 3. In the chapter, rare case of geometrical polymorphism, isostructurality between metallic salt with simple ammonium salt of Glibenclamide. Furthermore GBA-K form I and II exhibited higher solubility can be optimum solid for the formulation is studied in chapter 4. The counter ion effect on the conformation flexibility of lornoxicam and enhanced solubility studies were discussed in chapter 5. The importance of coamorphous multicomponent solid was highlighted in chapter 6 by making of the novel Curcumin-Artemisinin solid preparation through rotavaporization and its improved solubility and pharmacokinetics properties. In chapter 7, discuss the cocrystal alloys pharmaceutical utility and it can be explained with an example of isomorphous cocrystals of Nitazoxanide drug and this study determines importance of alloys opportunity for oral drug bioavailability alongside the stoichiometric cocrystals and salts. These results open opportunities for the repositioning of nitazoxanide as a multi-strain resistant anti-TB drug with improved bioavailability.

CONTENTS

Certificate	v
Declaration	vii
Acknowledgements	ix-x
Synopsis	xi-xxvii

Chapter One

Introduction: Crystal Engineering and Pharmaceutical Solids	1-52
1.1 Supramolecular Chemistry	2
1.2 Crystal Engineering	3
1.3 Hydrogen bonding	6
1.4 Molecular recognition: Supramolecular synthons	8
1.5 Hydrogen bond competition -Etter rules	9
1.6 Introduction to Pharmaceutical Solids	10
1.7 Classification of Pharmaceutical solids	12
1.7.1 Polymorphism	14
1.7.1.1 Classification of Polymorphs	15
1.7.1.2 Polymorph generation and Transformation	20
1.7.2 Solvates and Hydrates-Pseudopolymorphism	22
1.7.3 Pharmaceutical Salts	23
1.7.4 Pharmaceutical Cocrystals	24
1.7.4.1 Spring and Parachute model for solubility enhancement	32
1.7.4.2 Potential Energy diagram model for stability enhancement	33
1.7.5 Eutectic Compositions	35
1.7.6 Solid solutions/Alloys	37
1.7.7 Amorphous solids	39
1.7.8 Coamorphous solids	40
1.8 Conclusions	42
1.9 References	44

Chapter Two

Andrographolide: Solving Chemical Instability and Poor Solubility By Means of Cocrystal **53-91**

2.1	Introduction	54
2.2	Literature Reports on Andrographolide.....	57
2.3	Preparation of Andrographolide Cocrystals.....	58
2.4	Results and Discussion.....	59
2.4.1	Crystal Structure Description.....	61
2.4.2	XPac Comparison.....	65
2.4.3	Powder X-ray diffraction.....	69
2.4.4	Spectroscopic Characterization.....	71
2.4.5	Thermal Analysis.....	76
2.4.6	Stability of AP–SLA to Chemical Transformation.....	77
2.4.7	Solubility and Dissolution.....	79
2.5	Conclusions.....	81
2.6	Experimental Section.....	81
2.7	References.....	86

Chapter Three

Novel Synthons in Sulfamethizole Cocrystals: Structure-Property Relations and Solubility **93-127**

3.1	Introduction.....	94
3.2	Literature Reports on Sulfamethizole.....	96
3.3	Preparation of Sulfamethizole Cocrystals and Salt.....	97
3.4	Results and Discussion.....	98
3.4.1	Crystal Structure Analysis.....	102
3.4.2	Conformational Flexibility.....	109
3.4.3	FT-IR Spectroscopy.....	110
3.4.4	Powder X-ray Diffraction and Thermal analysis.....	114
3.4.5	Solubility and Dissolution.....	115
3.4.6	Phase Stability in Acidic and Neutral media.....	118
3.5	Conclusions.....	119
3.6	Experimental Section.....	120

3.7	References.....	124
-----	-----------------	-----

Chapter Four

Polymorphism, Isostructurality and Structure-property Relations: Glibenclamide Salts **129-161**

4.1	Introduction.....	130
4.2	Literature reports on Glibenclamide and CSD analysis of –SO ₂ – N–CO–N– group.....	130
4.3	Results and Discussion.....	131
4.3.1	Crystal Structure Analysis.....	134
4.3.2	Unit Similarity index equation and X-Pac analysis.....	140
4.3.3	Packing and Powder Pattern Similarity Analysis (Crystal packing in the Mercury software).....	142
4.3.4	Conformational Analysis.....	144
4.3.5	PXRD Analysis.....	145
4.3.6	FT-IR spectroscopy.....	146
4.3.7	Thermal Analysis.....	148
4.3.8	Solubility Studies.....	150
4.3.9	Stability study by Dynamic Vapor Sorption (DVS) Analysis.....	153
4.4	Conclusions.....	155
4.5	Experimental Section.....	156
4.6	References.....	161

Chapter Five

Lornoxicam Salts: Crystal structures, Conformations and Solubility **163-188**

5.1	Introduction.....	164
5.2	Lornoxicam-Literature Reports.....	165
5.3	Preparation of Lornoxicam salts.....	166
5.4	Results and Discussion.....	167
5.4.1	Crystal structures of LXM Acid salts.....	168
5.4.2	Crystal structures of LXM Base salts.....	170
5.4.3	PXRD Analysis.....	174
5.4.4	FT-IR Spectroscopic Analysis.....	174
5.4.5	ss-NMR Spectroscopic Analysis.....	176
5.4.6	Thermal Analysis.....	177
5.4.7	Solubility and Powder Dissolution.....	178

5.5	Conclusions.....	181
5.6	Experimental Section.....	182
5.7	References.....	185

Chapter Six

A Novel Curcumin-Artemisinin Coamorphous Solid: Physical Properties and Pharmacokinetic Profile 189-213

6.1	Introduction.....	190
6.2	Literature Reports on Curcumin and Artemisinin.....	192
6.3	Results and Discussion.....	193
6.3.1	PXRD analysis.....	195
6.3.2	Thermal Analysis.....	196
6.3.3	FT-IR Spectroscopy Analysis.....	197
6.3.4	Solid state NMR (ss-NMR) Spectroscopy.....	199
6.3.5	Stability of CUR-ART Coamorphous Solid.....	216
6.3.6	Solubility and Dissolution.....	201
6.3.7	Pharmacokinetics.....	202
6.3.8	FESEM Analysis.....	204
6.4	Conclusions.....	205
6.5	Experimental Section.....	206
6.6	References.....	210

Chapter Seven

Cocrystals and Alloys of Nitazoxanide: Enhanced Pharmacokinetics 215-240

7.1	Introduction.....	216
7.2	Literature Reports on Nitazoxanide.....	217
7.3	Preparation of Nitazoxanide cocrystals and their alloys.....	218
7.4	Results and Discussion.....	219
7.4.1	Crystal Structure Analysis.....	222
7.4.2	Conformational Analysis.....	225
7.4.3	PXRD Analysis.....	226
7.4.4	FT-IR spectroscopy.....	227
7.4.5	Thermal Analysis.....	229
7.4.6	Dissolution Studies.....	230
7.4.6	Pharmacokinetics.....	231
7.5	Conclusions.....	233

7.6	Experimental Section.....	233
7.7	References.....	237

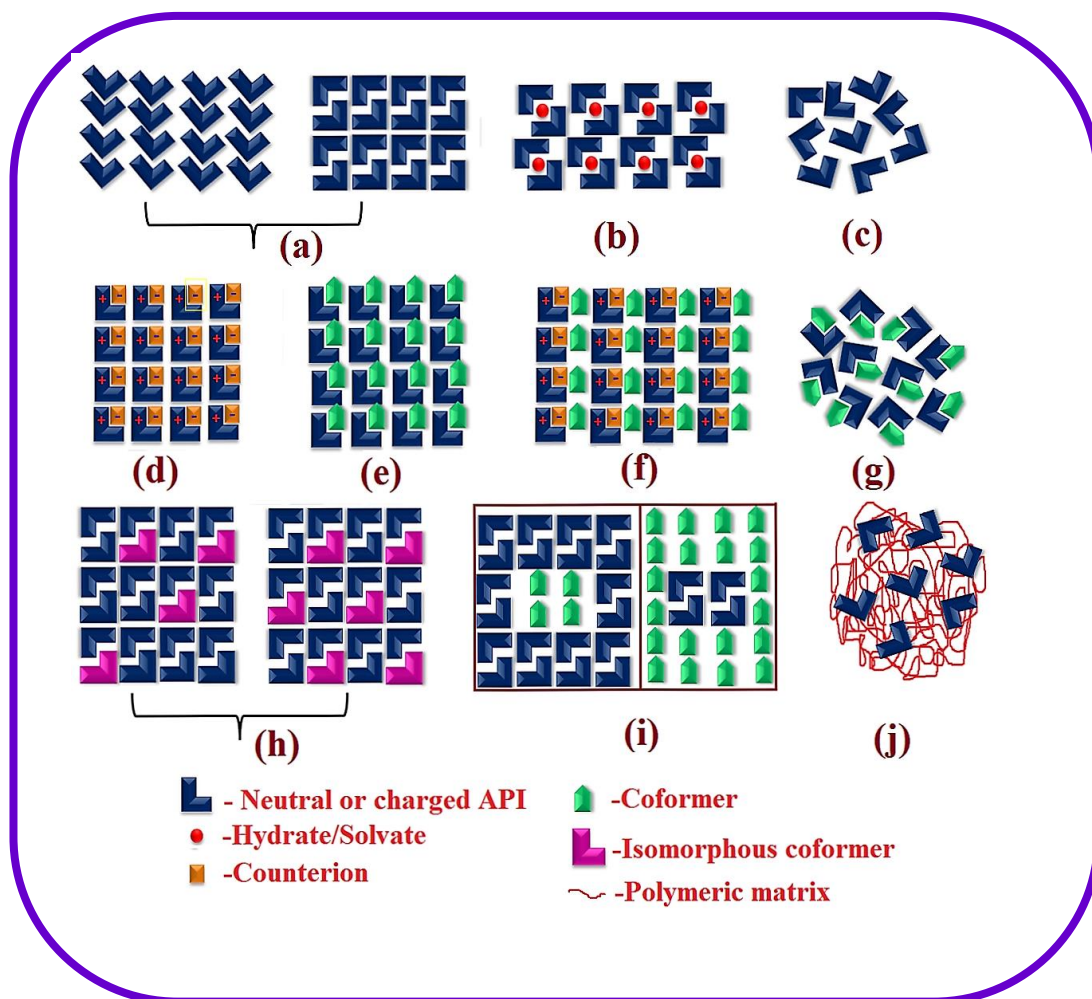
Chapter Eight

Conclusions and Future Prospects	241-245
---	----------------

About the Author.....	247
List of Publications.....	251
Participation in Symposia & Conferences.....	253

CHAPTER ONE

Introduction : Crystal engineering and Pharmaceutical Solids



Schematic representation of various solid forms, (a) Polymorphs (b) Solvate/hydrate (c) Amorphous (d) Salt (e) Neutral cocrystal (f) Ionic cocrystal (g) Coamorphous (h) Solid solution or alloy (i) Eutectic (j) Polymeric solid dispersion.

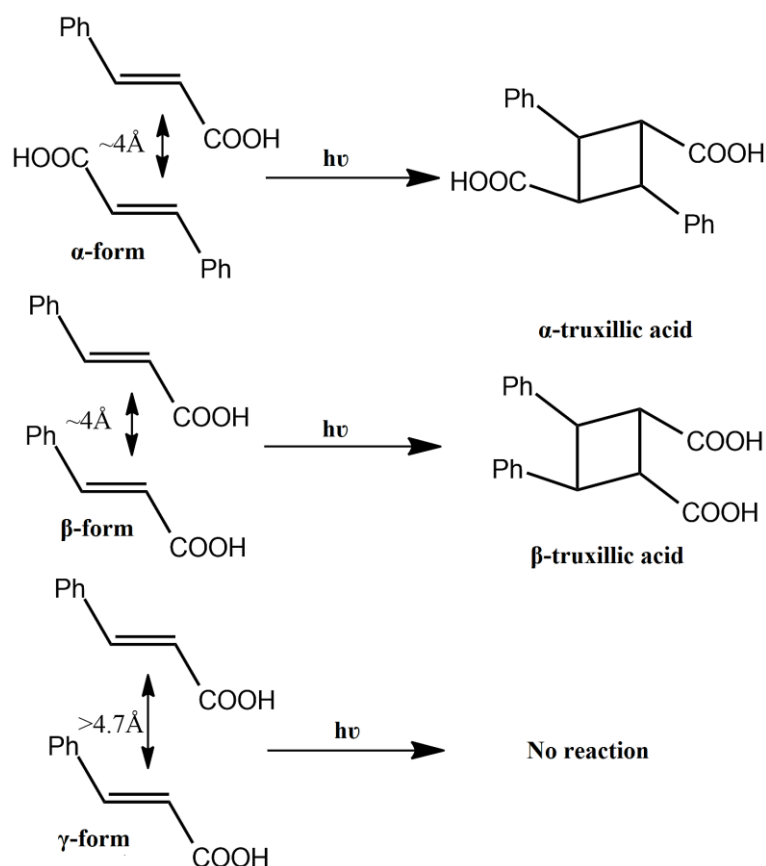
2 Chapter 1

1.1 Supramolecular Chemistry

Supramolecular chemistry¹ is one of the most popular and fastest growing progressive fields at the intersection ‘top down’ and ‘bottom up’ between physics, chemistry, biology, and materials science. It may be defined as “*chemistry beyond the molecule*”. The concept of supramolecular chemistry was first introduced by Lehn² in 1978 in the words: “*Just as there is field of molecular chemistry based on the covalent bond, there is a field of supramolecular chemistry, the chemistry of molecular assemblies and of the intermolecular bond*”. It is the study of high level aggregates (supermolecules) formed from the molecules via intermolecular interactions. The existence of intermolecular bonds/forces were postulated by Johannes Diderik van der Waals³ in 1873 and the rational design for supramolecular chemistry was initiated by Emil Fischer in the year 1894 the enzyme-substrate interactions to a lock and key mechanism.⁴ This model further explained by the fundamental principles of molecular recognition and host-guest chemistry. In the early 20th century, intermolecular interactions came to be understood in greater detail with hydrogen bond first described by Latimer and Rodebush^{5a} in 1920 and later by Linus Pauling.^{5b,c} The significance of supramolecular chemistry was recognized in the year 1987 with the Nobel Prize in chemistry conferred to Donald J. Cram, Jean-Marie Lehn and Charles J. Pederson for the design and synthesis of shape and size of ion receptors or host-guest complexes. Other pioneers Atwood, Vögtle, Gokel subsequently extended this concept into the synthetic receptors involving hydrogen bonding and other non-covalent interactions.⁶ In 2002, Jean-Marie Lehn gave the functional definition⁷: “*Supramolecular chemistry aims at developing highly complex chemical systems from components interacting by non-covalent intermolecular forces*”. Several books and reviews have been published on this fascinating field of supramolecular chemistry.⁸ The development of this field requires an understanding of molecular chemistry (the chemistry of the covalent bond) together with noncovalent interactions for molecular self-assembly to tune the structure, properties and functionalities of the resulting products. To define molecular self-assembly, it is broadly classified into two branches: 1) the study of solution dynamics in host guest complexes for recognition and binding and 2) understanding and design of such noncovalent intermolecular interactions in the solid state can be referred to as “Crystal Engineering”.

1.2 Crystal Engineering

The principal objective of crystal engineering⁹ is to tune physicochemical properties of crystalline solids via crystal design at the molecular level. It combines chemistry with crystallography provide a rationale for the understanding of molecular solids. The evolution of crystal engineering began in the year 1921 by Bragg's observation¹⁰ who noted that the unit cell parameters of two axial lengths were nearly same whilst third was 8.66 Å in naphthalene and 11.66 Å in anthracene. It defines the correlation between a crystal property and molecular property, between molecules and crystals, of both naphthalene and anthracene compounds. Subsequently Robertson,¹¹ student of W. H. Bragg made significant contributions on a large number of polynuclear aromatic hydrocarbons based on the molecular thickness and molecular area. In addition, Bernal proposed molecular structures phenanthrene related aromatic hydrocarbons from crystal unit cell parameters.¹² In 1955, Pepinsky introduced the term¹³ "Crystal Engineering" but it was conceptualized and elaborated by Schmidt and coworkers during the period of 1950-1970 in the context of organic solid state photochemical reactions in *trans*-cinnamic acids.^{14b,c} They comprehensively established a relationship between molecular structure and reactivity based on the 4 Å rule for photodimerization of alkenes via (2+2) cycloaddition reactions and this approach got much attention in photochemical solid state reactions. They crystallized α , β and γ forms of *trans*-cinnamic acids and irradiated them in the solid state where they found that α and β forms where the intermolecular distance is about 4 Å had undergone cycloaddition reaction and resulted in α/β -truxillic acids whereas the γ form with a longer intermolecular distance of >4.7 Å rendered it photo-stable (Scheme 1.1).



Scheme 1.1: Photo irradiation of α , β forms of trans-cinnamic acid with intermolecular distance of 4\AA has photodimerized to α - and β -truxillic acid respectively, whereas γ form with intermolecular distance of $> 4.7\text{\AA}$ was photo stable (Adapted from ref. 14).

Over the years the number of consecutive developments was brought into light by crystal engineering from the molecule to crystal. In these aspects a ‘crystal’ has been appreciated as an assembly of millions of molecules self-crafted by mutual recognition at an ‘amazing level of precision’ in an infinite and periodic arrangement. It is defined by Dunitz as ‘*supermolecule par excellence*’¹⁵ while Lehn termed it as ‘*a very large supermolecule indeed*’.¹ The intermolecular or non-covalent interactions that bind molecules in a crystal lattice are broadly classified into two types: the isotropic or non-directional medium range forces ($\text{C}\cdots\text{C}$, $\text{C}\cdots\text{H}$, $\text{H}\cdots\text{H}$ interactions) that influence the close packing based on the size and shape of molecules and anisotropic or directional long range forces ($\text{O}-\text{H}\cdots\text{O}$, $\text{N}-\text{H}\cdots\text{O}$, $\text{C}-\text{H}\cdots\text{O}$, $\text{C}-\text{H}\cdots\pi$, halogen \cdots halogen, nitrogen \cdots halogen, sulphur \cdots halogen etc.) which are electrostatic and include hydrogen bonds and heteroatom interactions.¹⁶ The importance of isotropic interactions is emphasized by A. I. Kitaigorodskii^{17a} who postulated the atom-atom potential method^{17b}

for intermolecular interactions in crystal structures. This model describes crystals as being derived from efficient utilization of space during their formation, hence it is also known as the principle of close packing. Among all the intermolecular interactions, hydrogen bonding is the most reliable directional interaction and it has a fundamental role in crystal engineering. The physicochemical properties of a crystalline solid are the result of molecular arrangement in the crystal lattice, which are controlled by intermolecular interactions. In 1989, a widely accepted broad definition of crystal engineering was proposed by Desiraju^{9a} as *“the understanding of the intermolecular interactions in the context of crystal packing and the utilization of such understanding in the design of new solids with desired physical and chemical properties”*. Even all types of interactions are drafted in crystal engineering, the most regularly used strategies are based on the hydrogen bonding (for organic solids) and coordination bonding (for metal-organic frameworks). In 1990 Etter described the hydrogen bonding rules¹⁸ (which is discussed later in section 1.5) and termed the hydrogen bonds are strong, directional and important to determine the crystal structures. Further the retrosynthetic analysis of crystal structures concerning the molecules and the intermolecular interactions, which connect them led to the supramolecular synthon concept. In 1995, Desiraju introduced the term supramolecular synthon¹⁹ to design the mixed or multicomponent molecular crystals (which is discussed later in section 1.4). Such a journey of crystal engineering field parallel with the advancement of X-ray diffraction technique as shown in Figure 1.2.

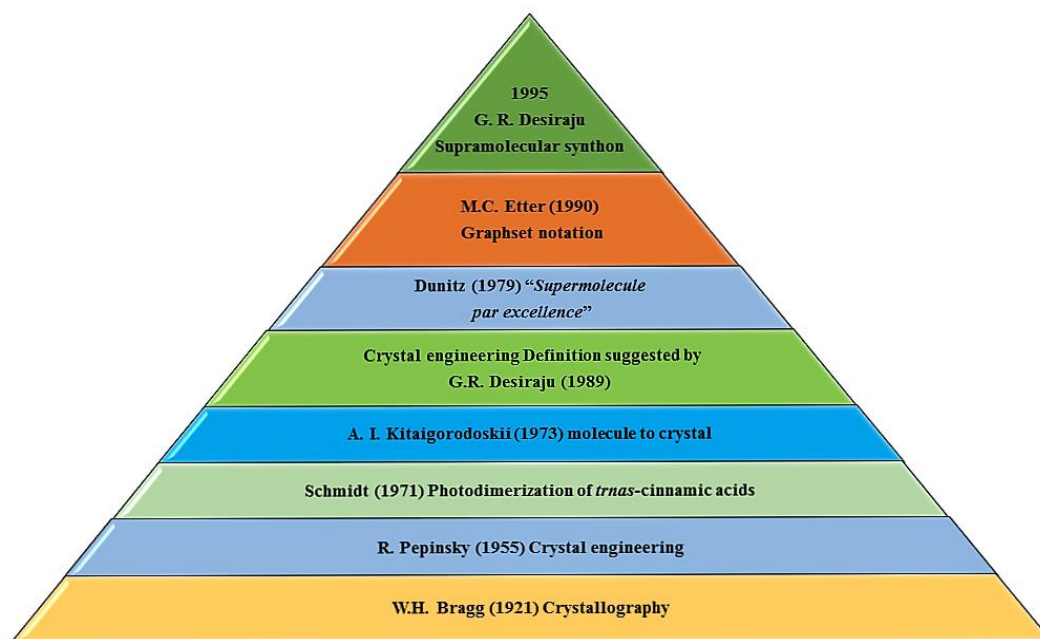


Figure 1.2: Crystal engineering journey from 1921 (Bragg) to present.

Additional contributions to this field included an article by Ermer²⁰ on the adamantane-1,3,5,7-tetracarboxylic acid crystal structure. He interpreted the crystal structure of this molecule concerning interpenetrated networks, which could be defined as a pioneering work for describing crystals using topological approach. Subsequently, in 1990 Robson²¹ explored interpenetrations in some coordination compounds which paved the way to the investigations on coordination polymers and metal-organic framework structures (MOFs). In brief, the initial interest in crystal engineering was to understand and design of a crystal with purpose. Today²², it is a mainstream interdisciplinary field influencing diverse areas like self-assembly in molecular crystals, metal-organic frameworks, coordination polymers, nanostructures etc. through hydrogen bonding, van der Waals interactions, electrostatic and metal-coordination bonding.

1.3 Hydrogen bonding

In the year 1939, Linus Pauling first defined the hydrogen bond as “*under certain conditions an atom of hydrogen is attracted by rather strong forces to two atoms instead of only one, so that it may be considered to be acting as a bond between them*”.^{5b,c} Later according to Pimentel and McClellan in the year 1960²³, a hydrogen bond is said to exist when (a) there is evidence of a bond, and (b) there is evidence that this bond specifically involves a hydrogen atom already bonded to another atom. Further Steiner and Saenger

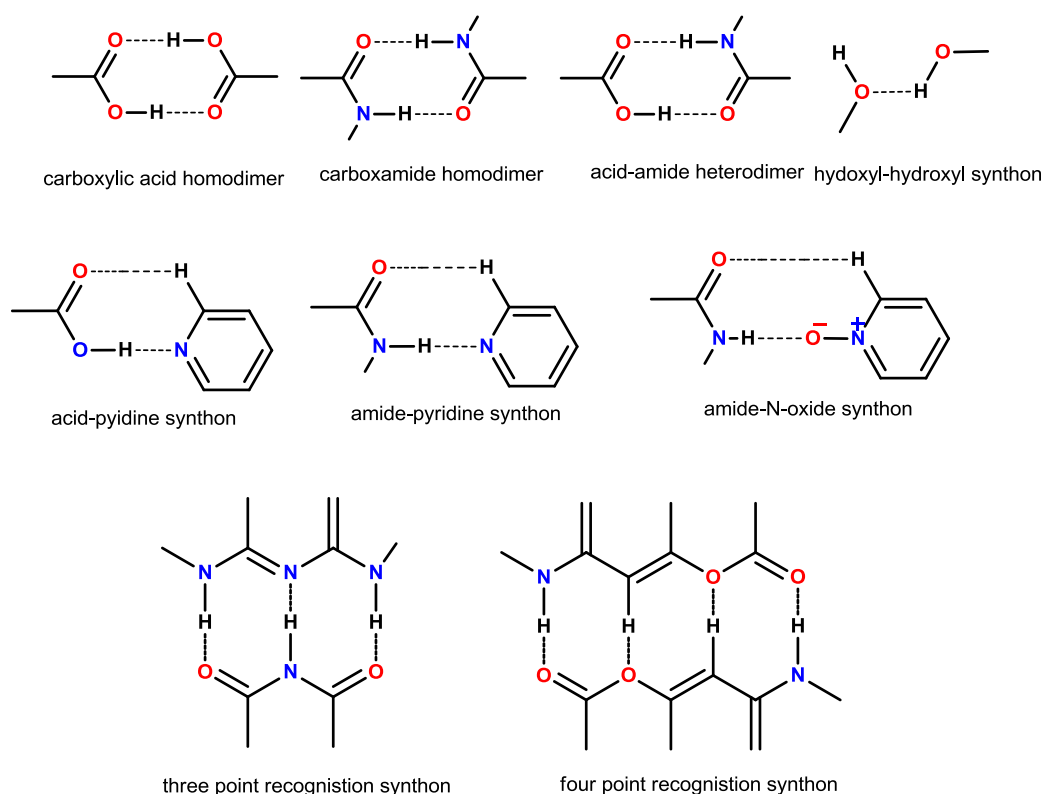
in 1993^{24a} and Desiraju and Steiner in 1999^{24b} also described the more general definition of hydrogen bond. In 2011 the International Union of Pure and Applied chemistry (IUPAC) stated^{24c} that “the hydrogen bond (designated as $D-H\cdots A$, where acceptor A and donor D are electronegative atoms) is an attractive interaction between a hydrogen atom from a fragment or molecule $D-H$ in which D is more electronegative than H , and an atom or a group of atoms A , in the same or different molecule where there is evidence of bond formation”. Hydrogen bond energy usually lies in the range of 0.5 to 40 kcal/mole and it depends on the nature of D and A . It has four chemical characteristics: polarization (hard/soft), electrostatics (acid/base), van der Waals (dispersion/repulsion), and covalency (charge transfer). It can be investigated by a variety of experimental techniques such as X-ray diffraction, neutron diffraction, NMR, FT-IR and Raman spectroscopy as well as high energy diffraction and light sources. Depending on the electronegativity of atoms to which it is bound either through covalent or non-covalent interactions; a hydrogen bond can exist with a continuum of strengths. Based on the strength (energy values) and directionality of hydrogen bonds, they can be classified into three categories as very strong, strong and weak (table 1.1).^{24b}

Table 1.1 Some properties of very strong, strong and weak hydrogen bonds

	Very strong	Strong	Weak
Bond Energy (Kcal/mol)	15-40	4-15	< 4
Examples	$[F-H\cdots F]$	$O-H\cdots O=C$	$C-H\cdots O$
IR vs relative shift	>25%	5-25%	< 5%
Bond lengths	$H-A \approx X-H$	$H\cdots A > X-H$	$H\cdots A \gg X-H$
Lengthening of $X-H$ (Å)	0.05–0.2	0.01–0.05	≤ 0.01
$D(X\cdots A)$ range (Å)	2.2–2.5	2.5–3.2	3.0–4.0
$d(H\cdots A)$ range (Å)	1.2–1.5	1.5–2.2	2.0–3.0
Bonds shorter than vDW	100%	Almost 100%	30-80%
$\theta(X-H\cdots A)$ range (°)	175–180	130–180	90–180
kT (at room temp.)	>25	7-25	<7
Effect on crystal packing	Strong	Distinctive	Variable
Covalency	Pronounced	Weak	Vanishing
Electrostatics	Significant	dominant	moderate

1.4 Molecular recognition: Supramolecular synthons

In the year 1967, E. J. Corey²⁵ introduced the term ‘synthon’ to simplify the synthesis of complex molecules and natural products in review article entitled “General Methods for Construction of complex molecules”. He specified synthon as “*Structural units within molecules which can be formed and/or assembled by known or conceivable synthetic operations*”. Right from its beginning, a synthon used to be considered as a part of the molecule which contains required information about the bond connectivity and/or stereochemical information.^{26a} Based on these synthon strategies, synthesis of a complex molecule are known as “Retrosynthesis”.^{26b} From these strategies, crystal engineering is the solid state equivalent of supramolecular synthesis, whereas Desiraju revived and modified the term as ‘Supramolecular synthon’¹⁹ and it is defined as “*structural units within supermolecules which can be formed and/or assembled by known or conceivable intermolecular interactions*”. The advantages of using the synthon strategy are that it offers a simplification in the understanding of crystal structures. Zaworotko²⁷ sub-classified synthons as homosynthons and heterosynthons based on the interacting functional groups. If supramolecular synthon is formed between the same functional group it is called a homosynthon, and between two different functional groups is called as heterosynthon. Heterosynthons acid–pyridine^{28a}, acid–amide^{28b}, phenol–amine^{28c}, phenol–pyridine^{28e}, aminopyridine–acid^{28f}, amide–pyridine-*N*-oxide^{28g} and sulfonamide–pyridine-*N*-oxide are well exploited in crystal engineering (Scheme 1.3).



Scheme 1.3 Strong hydrogen bond homo/hetero synthons report in literature.

1.5 Hydrogen bond competition -Etter rules

To synthesize a desired crystal structure, one must first identify the functionalities that will generate predictable intermolecular interactions or synthons. It becomes more difficult in multifunctional molecules because of competition between similar strength of acceptor/donor groups. To comprehend the hydrogen bonding and competition in organic compounds, Etter proposed hydrogen bond rules, a fundamental rule is “*all acidic hydrogens available in a molecule will be used in hydrogen bonding in the crystal structure of that compound.*”^{18a} A second rule, corresponding to the first one, is “*all good proton acceptors will be used in hydrogen bonding when there are available hydrogen-bond donors.*”^{18b} And the third rule is “*the best hydrogen-bond donor and the best hydrogen acceptor will preferentially form hydrogen bonds to one another.*”^{18c} If there is a possibility of forming a six-membered intramolecular hydrogen bond ring, it will form normally in preference to intermolecular hydrogen bonds. The methods to categorize solid-state hydrogen bond preferences are based on functional group competitions in

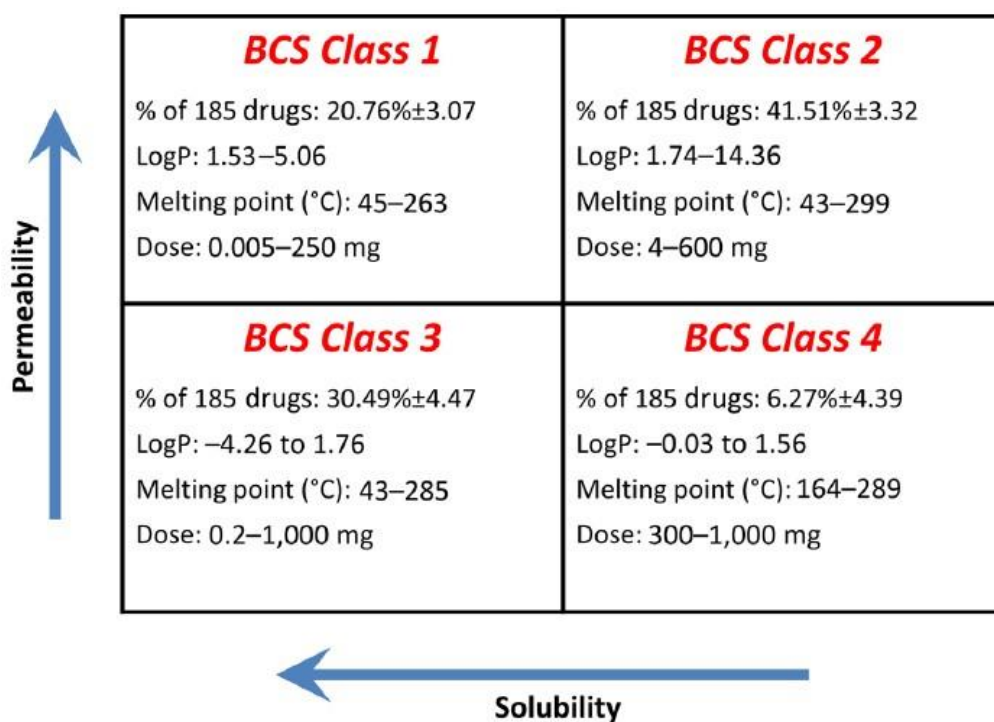
homomeric crystals or heteromeric cocrystals. The procedure involves analyzing which donors are selected by a limited number of acceptors or *vice versa* during crystallization.

1.6 Introduction to Pharmaceutical Solids

Active Pharmaceutical Ingredient (drug) is a chemical substance that is intended to explore physiological systems or pathological states in the form of a medicine that is used for diagnosis, prevention, treatment/cure of disease for the benefit of the recipient.²⁹ Drugs can initiate the pharmacological action only when they are absorbed and distributed all over, including sites of action, through the systemic circulation. Thus drug absorption is an important prerequisite step where the fraction of administered dose that gets absorbed. Most drugs can be administered by a variety of routes that depends upon the choice of appropriate route in a given situation. The route of administration is broadly divided into (a) local action (topical, deeper tissue, arterial supply), (b) systematic routes (oral, sublingual, rectal, cutaneous, inhalation, nasal, parenteral).³⁰ The most assessable, acceptable and affordable route of administration is the oral route. The main factors affecting the oral route absorption are physicochemical properties viz. water solubility, physical/chemical stability, permeability which influences bioavailability of a drug. The majority of the drugs are marketed as solid dosage formulations because of ease of manufacture, storage and convenience to patients which are in the form of tablet, capsule, or lyophilized powder forms.

Amidon et. al.^{31a} proposed and introduced the Biopharmaceutics Classification System (BCS) on the interpretation of the kinetics and dynamics of the drug, which were divided into BCS Class I,II,III and IV categories based on solubility and permeability³¹ (see Figure 1.4). Bioavailability of the drug is dependent on its solubility in the gastrointestinal tract and permeability across the cell membrane. About 40% of drugs (mainly BCS II and IV drugs) and emerging new chemical entities (NCEs) under research and development and some nutraceutical molecules exhibit poor aqueous solubility. Such drug candidates and nutraceutical molecules tend to be eliminated from the gastrointestinal tract before they get completely dissolved and absorbed into the blood circulation. This results in low bioavailability and less potency.³² In such cases, drug augmentation would be required to ensure therapeutic concentration in blood. However drug augmentation may lead to adverse/toxic effects on human body.³³ Thus, novel forms without doing any chemical modification of the drug for an optimal pharmaceutical solid formulation greatly reduces the risk, time and cost in drug

development. The conventional approaches in the solid space are polymorphic form/mixture, salt, amorphous, solvate/ hydrate, cocrystal, eutectic, solid solution/alloy and coamorphous solid blended with excipients (polymeric matrix) etc.³⁴ Broadly, each of these solid forms exhibit different physicochemical properties such as solubility, dissolution rate, flowability, compressibility and bioavailability, which finally governs the therapeutic efficacy of the drug. Thus the study of solid state chemistry of drugs has fundamental importance in the optimization of a drug solid form in pharmaceuticals. This process is decisive not only in research and development, but also for oral administration. Understanding the nature of solid forms in terms of their molecular packing, stability, and physicochemical properties will avoid pit-falls in drug development.



<p>BCS Class 1</p> <p>% of 185 drugs: 20.76%±3.07 LogP: 1.53–5.06 Melting point (°C): 45–263 Dose: 0.005–250 mg</p>	<p>BCS Class 2</p> <p>% of 185 drugs: 41.51%±3.32 LogP: 1.74–14.36 Melting point (°C): 43–299 Dose: 4–600 mg</p>
<p>BCS Class 3</p> <p>% of 185 drugs: 30.49%±4.47 LogP: –4.26 to 1.76 Melting point (°C): 43–285 Dose: 0.2–1,000 mg</p>	<p>BCS Class 4</p> <p>% of 185 drugs: 6.27%±4.39 LogP: –0.03 to 1.56 Melting point (°C): 164–289 Dose: 300–1,000 mg</p>

Figure 1.4 Biopharmaceutical Classification System (BCS) of drugs.

1.7 Classification of Pharmaceutical solids

Generally solids are broadly classified as crystalline (having long-range order) and amorphous (with short-range order, but no long-range periodicity) depending on the internal structure, length-scale of order, and degree of periodicity. A pharmaceutical solid may exist in a single or multicomponent system, either as crystalline or amorphous state. Different crystalline arrangements of the same chemical substance are polymorphs. And those with multicomponent (two or more neutral chemical species) in a single crystalline lattice are referred to as a cocrystal. The ionized salt forms and which are interacting with another organic compound in the crystal lattice are known as ionic cocrystals. The supramolecular family of multicomponent solids therefore includes salts, hydrates, solvates, cocrystals, eutectics, solid solutions, alloys, etc. all are assessed as pharmaceutical forms depending on the required specific pharmaceutical properties of a specific drug. A difference between cocrystal, eutectic and solid solution or alloy is, the stoichiometry is fixed in a cocrystal or eutectic, but can vary over a range (multiple stoichiometries) for an alloy or solid solution. Polymorphism is possible in multicomponent crystalline solids such as salts, cocrystals, solvates etc. In coamorphous solids, the stoichiometric ratios of two or more solids are held together through weak, but discrete interactions in an aperiodic arrangement; the individual components are crystalline but the resulted adducts are X-ray diffraction amorphous (broad halo peak). The classification of all pharmaceutical solids shown in Figure 1.5 and packing arrangement in crystal lattice of those solids is shown in scheme 1.6.

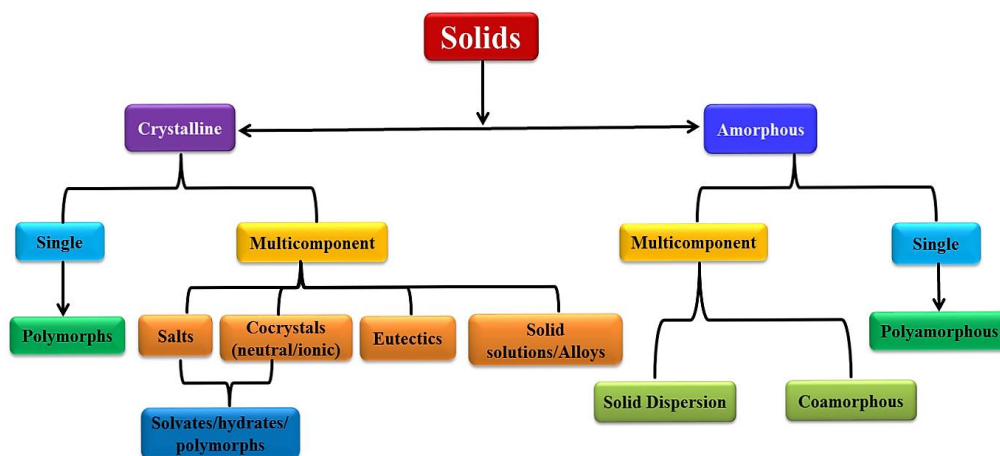
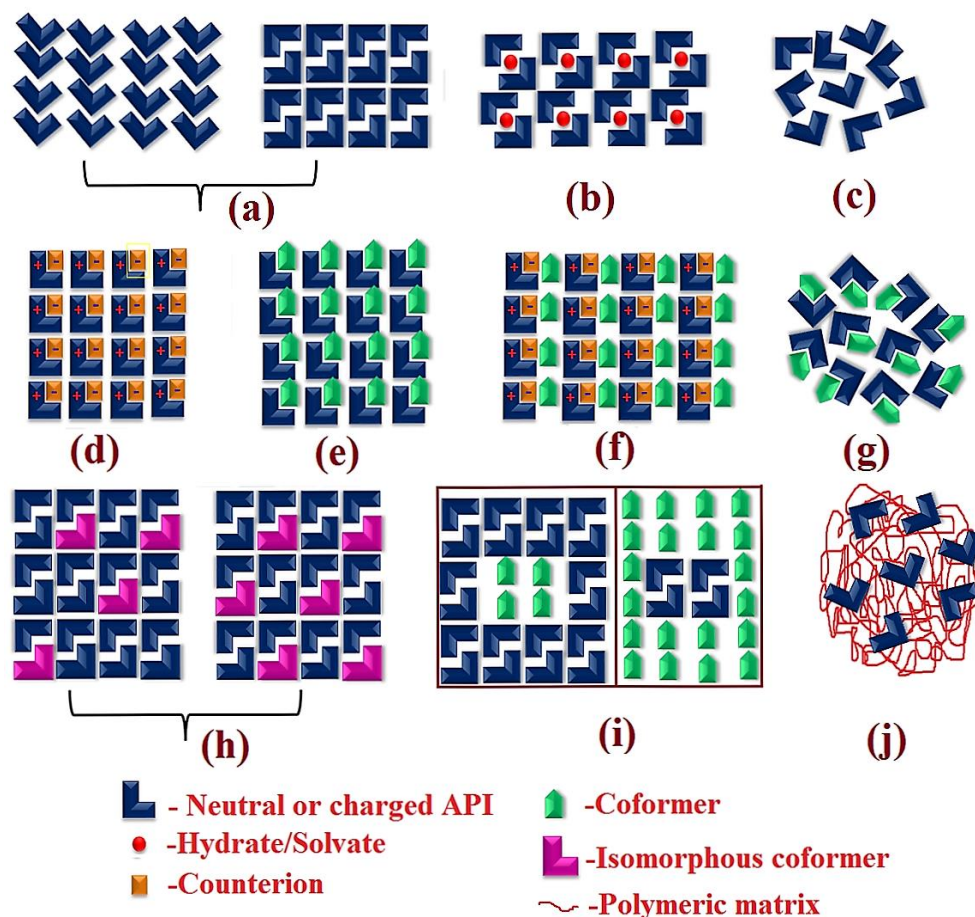


Figure 1.5 Classification of pharmaceutical solids based on the molecular packing in a crystal lattice into various solid state categories.



Scheme 1.6 Schematic representation of various pharmaceutical solid forms possible for a solid when combined with the same solid which can be polymorphic (a) and amorphous (c) or with a different material which can be solid or liquid (b). When different compounds combine where adhesive interactions dominate over cohesive interactions, a new compound with crystal structure different from that of the parent materials can form (e.g. salt (d), cocrystal (e) and ionic cocrystal, (f) compounds with similar size and crystal structures can form ‘continuous solid solutions’ (h) and the ones with mismatch and misfit can give rise to a ‘eutectic’ (i). A ‘eutectic’ is a ‘conglomerate of solid solutions’ wherein the solid solution domains are held by weak interactions. Solid solutions/eutectics resemble crystal structures of their individual components. Binary system existing in aperiodic lattice is called coamorphous (g). A drug is dispersed in polymeric matrix is called solid dispersion (j).

1.7.1 Polymorphism

The word polymorphism³⁵ is derived from Greek literature (*Poly* = many, *morph* = form) specifying the diversity in nature and is defined as the ability of a molecule to adopt more than one crystalline form in the solid state. Mitscherlich^{36a} (1822) first recognized the phenomenon of polymorphism and observed the different crystal forms of the same compound in a number of arsenate and phosphate salts ($\text{NaH}_2\text{AsO}_4 \cdot \text{H}_2\text{O}$ and $\text{NaH}_2\text{PO}_4 \cdot \text{H}_2\text{O}$). Berzelius^{36b} described the existence of different crystal structures of the same element as allotrope. Allotropes (element case) and polymorphs (molecule case) are closely related.^{35a} The significance of the polymorphism in the pharmaceuticals was brought to light by McCrone^{35b} who gave the widely accepted definition that “*a solid crystalline phase of a given compound resulting from possibility of at least two different arrangements of the molecules of the compound in a solid state*”. Later, Bernstein studied the stability relationship between polymorphs and their phase transformations.^{35b,37} The first observation of polymorphism in benzamide was made by Friedrich Wöhler and Justus von Liebig in the year 1832.^{38a} They found two polymorphs from a boiling benzamide solution which upon cooling initially crystallized in silky needles, but when standing these were slowly replaced by rhombic crystals. Similar to single components, cocrystals or salts also exhibit polymorphism and they can also serve to tune the physicochemical properties of the drug/materials.^{38b,c}

Polymorphism has received tremendous attention in the recent literature because of its importance in formulation³⁹ as the different properties of polymorphs make them commercial and patentable.⁴⁰ It gained immense interest to understand and control the polymorph production and stability in pharmaceuticals. If a generic pharmaceutical company discovers a novel crystal form of an existing marketed drug, it will gain an early access into the marketplace; therefore, the innovator must find out all possible polymorphs of the drug and patent them in order to extend their monopoly in pharmaceutical industry and protect their product. The well-known example is anti-ulcer drug Ranitidine hydrochloride polymorphs to show the importance in the context of polymorphism (Figure 1.7). Glaxo obtained a patent on the two polymorphs (I, followed by II) of Ranitidine hydrochloride.³⁵ In the mid-1990s, as the patent on the drug form I was approaching expiration, other companies began preparing to market a cheaper,

generic versions of form I. But the generic manufacturers were not able to crystallize form I exclusively as it was always crystallizing as a mixture of form I and form II. This kept the generic companies products off the market for several years and during that period Glaxo was making \$10 million in sales each day on this blockbuster drug. Ultimately Novopharm could find a method to prepare form I exclusively with non-detectable amounts of form II, and won the battle. Since then generic entry was made into the market. Other drugs cefadroxil, terazosin hydrochloride and aspartame are also well-known examples of patent issues surrounding polymorphism.^{35b}

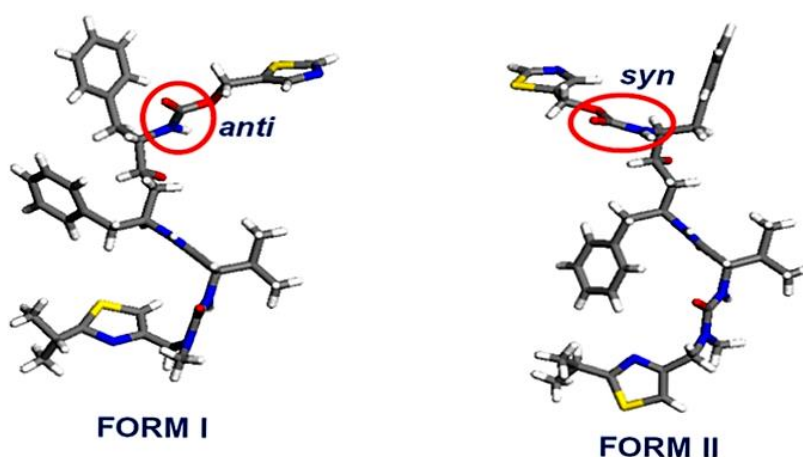


Figure 1.7 The *anti* and *syn* amide conformers of Ritonavir form I and II. (Adapted from Ref. 35).

1.7.1.1. Classification of polymorphs

In literature, polymorphs (single or multicomponent) synonymously are called as ‘forms’, ‘modifications’ or ‘phases’ and represented as numerals (Arabic: 1,2, 3 etc. and Roman: I, II, III etc.) or alphabets (Greek: α , β , γ etc. and English: A, B, C etc.).^{35a} Polymorphs can be broadly classified into three types⁴¹ i) Packing polymorphism^{41b} ii) Conformational polymorphism and iii) Synthons polymorphism (Figure 1.8). Conformational differences in molecular structure lead to different crystal structures of the same molecule, it is referred as ‘conformational polymorphism’ e.g. dimorphs of oligothiophene derivative^{42a} and N-acetyl cysteine (Figure 1.9).^{42b} When the non-covalent interactions or supramolecular synthons are different in different crystal structures of the same molecule it is stated as ‘synthon polymorphism’ e.g. Eparlestat (EPR) polymorphs.^{42c} When the arrangement of molecules varies in crystal structures it

is called as ‘packing polymorphism’. In a broader sense all the polymorphs can be classified under packing polymorphism because all the polymorphs differ in their packing by default. Though these classifications are subjective since overlapping is possible between them and more than one can coexist in a given system. For e.g. conformational synthon and synthon polymorphism of diuretic drug furosemide^{42d} (Figure 1.10) and anti-diabetic aldose reductase enzyme inhibitor eparlestat (Figure 1.11)^{42c} Eparlestat is also an example for color polymorphism. In addition polymorphism in each one of cocrystal and salt were discussed in Figure 1.12 and 1.13.

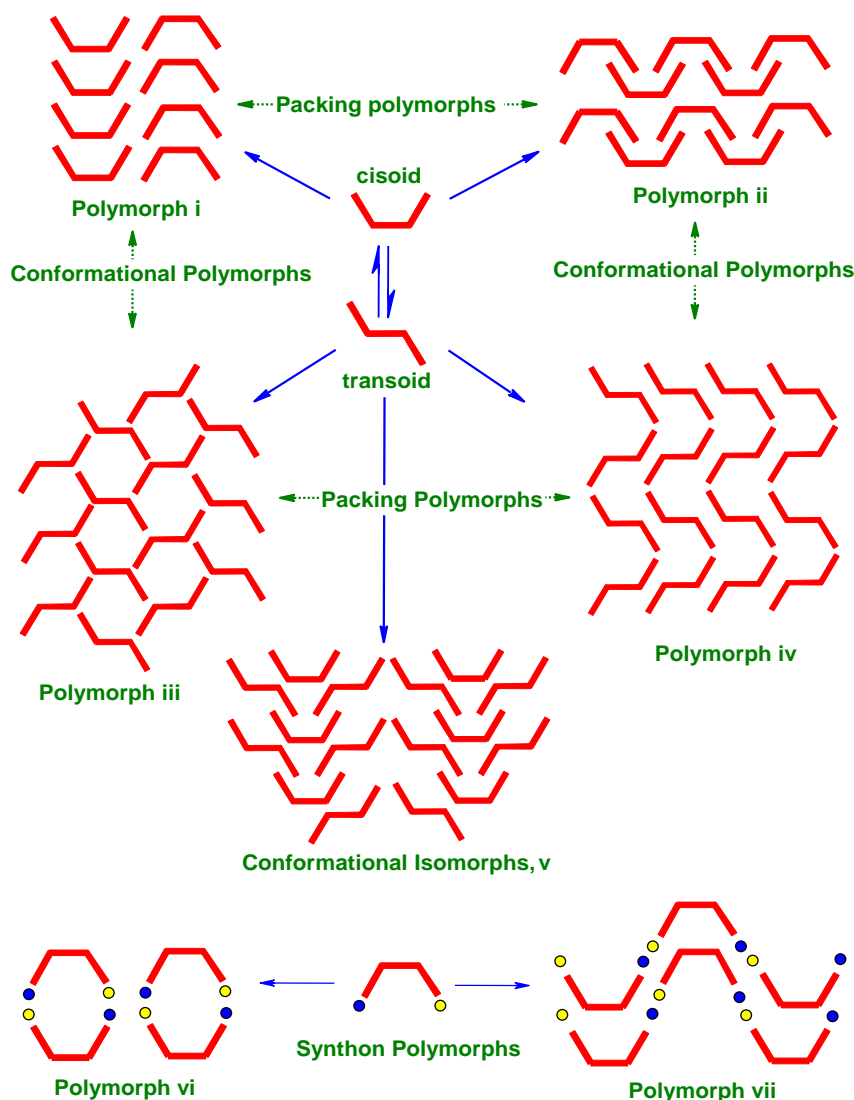


Figure 1.8 Schematic representation of different kind of polymorphs
(Adapted from ref. 41a)

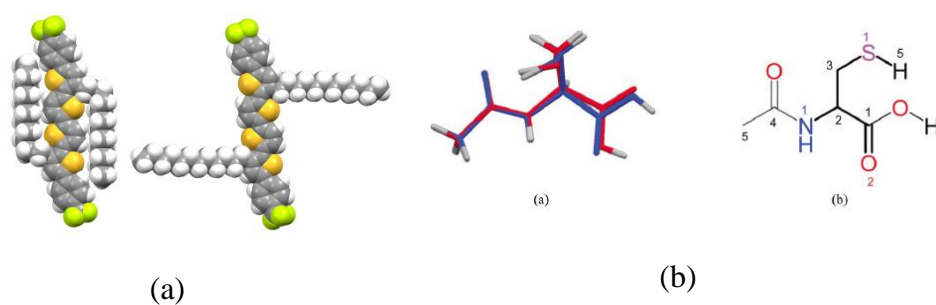


Figure 1.9 (a) Oligothiophene derivative of conformational polymorphism (Adapted from ref. 42a) (b) Overlay of molecular conformations (red form I and blue form II) and main conformational difference are highlighted in bold single bonds (Adapted from ref. 42b).

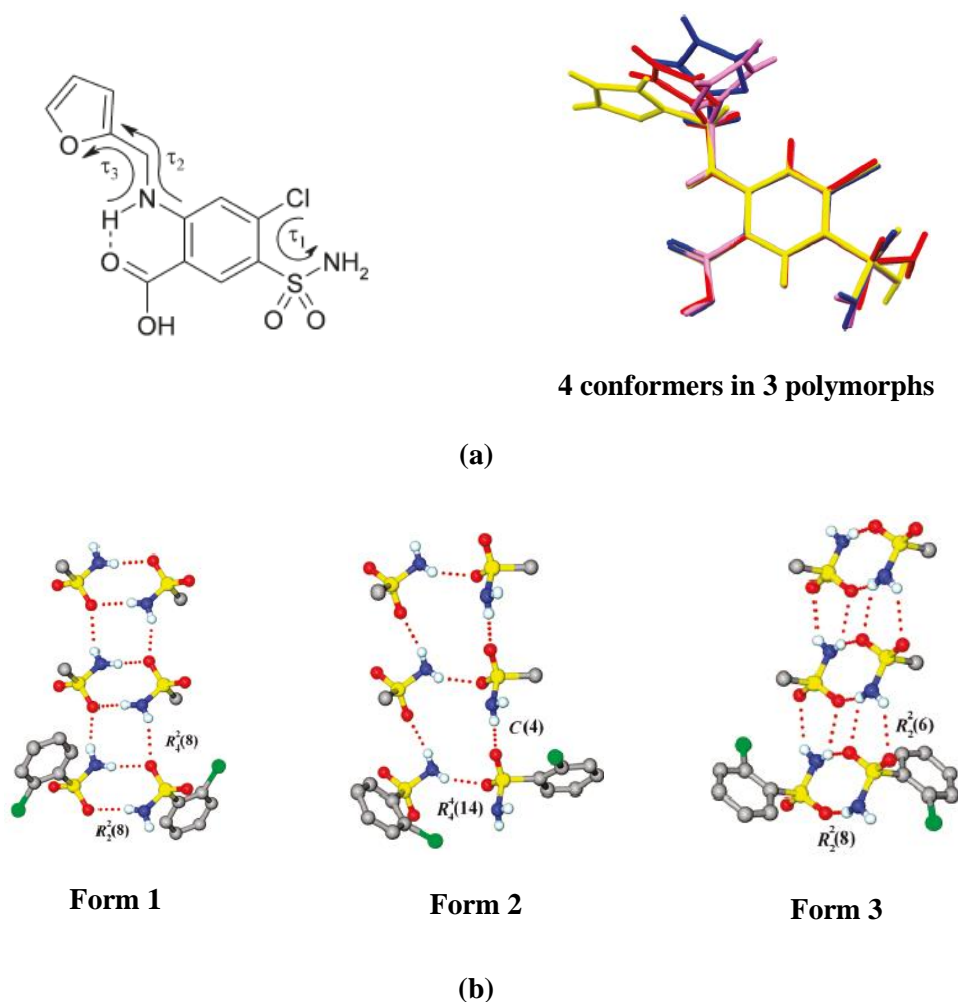


Figure 1.10 (a) Conformational polymorphism in Furosemide. The three torsion parameters in Furosemide: τ_1 =C-C-S-N, τ_2 =C-N-C-C, τ_3 =N-C-C-O. The anthranilic

acid moiety is conformationally locked by intramolecular hydrogen bond but conformational flexibility in the furan and sulfonamide moieties resulted in four conformers (red, blue, pink and yellow) manifested in three polymorphs. (b) Synthon polymorphism in Furosemide. $R_2^2(8)$ N-H \cdots O dimer and $R_4^2(8)$ motif in form 1, C(4) catemer and $R_4^4(14)$ tetramer motif in form 2, $R_2^2(8)$ N-H \cdots O motif and $R_2^2(6)$ rings in skewed dimer of form 3 (Adapted from ref. 42d).

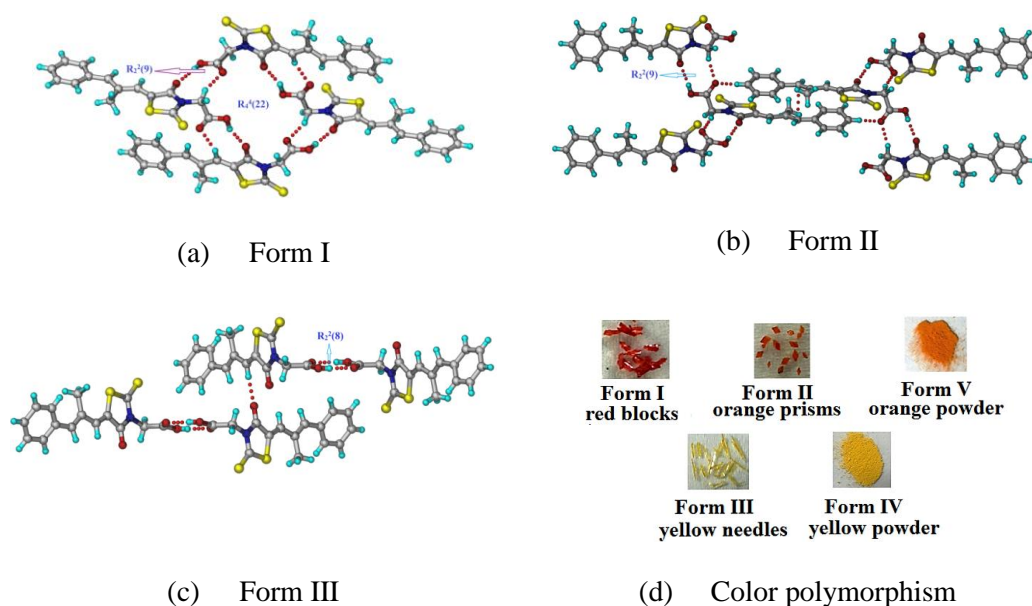


Figure 1.11 (a) $R_2^2(9)$ dimeric and $R_4^4(22)$ tetrameric assembly of EPR molecules via O-H \cdots O and C-H \cdots O hydrogen bonds (b) $R_2^2(9)$ dimeric motif in Form II, EPR together with π stacking and C-H \cdots O interactions (c) acid-acid dimer homosynthon ring motif between molecules connected through C-H \cdots O interactions in form III crystal structure (d) photographs of different colored EPR polymorphs and The archetype color polymorphism in ROY (red, orange, yellow colors) was ascribed to conformational differences between polymorphs (adapted from ref. 42c).

1.7.1.2 Polymorph generation and transformation

Solution crystallization is a traditional preferred method for polymorph generation. Solution crystallization conditions can be systematically varied by changing different solvents or mixtures of solvent, temperature, supersaturation, stirring, slurring, cooling rate, seeding, and use of antisolvent method.^{35c,38a} Recent approaches for polymorph generation include crystallization with structurally related additives^{43a}, melting^{43b}, epitaxial growth^{43c}, mechanical grinding^{43d}, sublimation^{43e}, using supercritical liquids^{43f} etc. Interestingly, many novel polymorphs of drug molecules and bioactive compounds were obtained serendipitously on cocrystallization⁴⁴. However polymorph interconversions are quite possible due to different energy levels on the free energy surface which therefore lead to the changes in properties of the bulk drug. Thus, it is essential to understand the properties to optimize the conditions for developing a desired polymorph for formulation.

Polymorphism outcomes from the interplay of thermodynamic functions (free energy, enthalpy and entropy) and kinetic factors (activation energy, temperature, supersaturation, rate of evaporation etc.) that guides the crystallization process.³⁵ The role of nucleation/crystallization guided by the Ostwald's law of stages is vital in predicting the nature of the polymorphic outcome of a molecule,⁴⁵ which states that *"when leaving an unstable state, a system does not seek out the most stable state, but rather the nearest metastable state which can be reached with least loss of free energy"* (Figure 1.14). Therefore number of intermediate forms manifesting during the process of transformation from the metastable form to the stable form is dependent on the free energy of activation, nucleation as well as time. Nevertheless, the polymorph obtained at the final stage is stable since its thermodynamic state has lowest in energy. If the same crystal structure is kinetically and thermodynamically favored, then polymorphism is less likely⁴⁶. At molecular level aspects, close packing and intermolecular interactions are the competent factors that determine the outcome of polymorph. Thermodynamic polymorph will be favored when close packing dominate the intermolecular interactions. Similarly, kinetic polymorph is preferred when the crystal nucleus is stabilized by intermolecular interactions. It is unlikely high to observe polymorphism in crystal systems where the preferred interactions are accompanied by the greatest packing. On the other hand, as the energy difference between the polymorphs is typically within a 5 kcal mol⁻¹ gap,^{36a} many polymorphs can crystallize simultaneously if their nucleation

rates are equal. This phenomenon is called ‘concomitant polymorphism’⁴⁷ wherein the polymorphs, both stable and metastable, crystallize under the same conditions in the same vessel. Concomitant polymorphs are generally ‘isoenergetic’ or ‘near-energetic’.⁴⁷

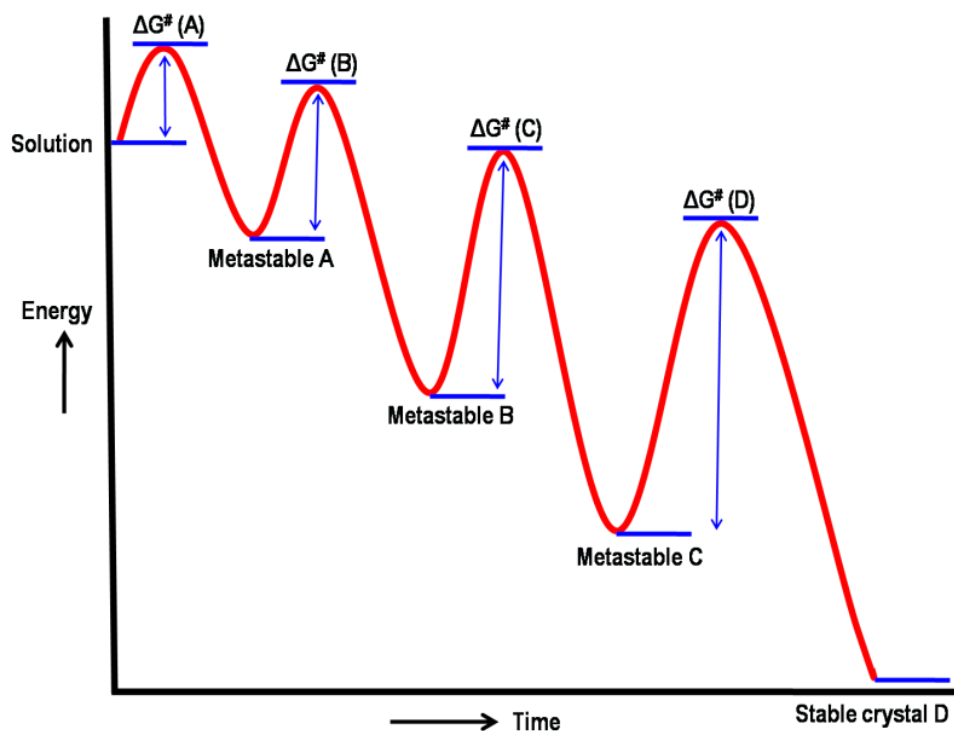


Figure 1.14 Ostwald's rule of stages to show the transformation of high energy (metastable) form to low energy (stable) form with time during crystallization. (Adapted from Ref. 45)

Polymorphic transformations can be thermodynamically reversible or irreversible. From this point of view polymorphic pairs can be divided as monotropic and enantiotropic systems.^{48,37b} Monotropic systems are defined as systems where single form is more stable regardless of temperature. Whereas in enantiotropic system are defined as a system where the relative stabilities of the two polymorphs invert at some temperatures. In another aspect if the free energy curves of two polymorphs cross below the melting point of the lower melting polymorph, they are said to be enantiotropically related and if the free energy curves do not cross below the lower melting polymorph, they are said to be monotropically related.^{37b}

1.7.2 Solvates and Hydrates – Pseudopolymorphism

Incorporation of solvent/water molecules into the lattice of crystalline solids results in solvate or hydrate formation. Inclusion of solvent or water changes the physicochemical properties of the molecular solid as are associated with polymorphs, and therefore the phenomenon is often called to as pseudopolymorphism.⁴⁰ Usually during crystallization, strong solute-solvent interactions result in the solvated crystals. In particular water molecule, though it has small size, has the ability to act as both a hydrogen bond donor and acceptor and capable of connecting drug molecules to form new crystal structures than any other solvent. It is found that approximately one third of active APIs can form crystalline hydrates.⁴⁹ Sometimes, a solid can incorporate different stoichiometric ratios of the same solvent for example, antibiotic drug norfloxacin forms a hydrated in 1.25 and 1.125 stoichiometric ratios in different crystal structures.^{49d} On the other hand different solvents can incorporate into the crystal lattice for example, antibacterial drug nitrofurantoin forms solvates with water, DMSO, DMF, methanol etc. Sometimes polymorphs of solvates are also observed e.g. nitrofurantoin monohydrate polymorphs I and II (Figure 1.15).^{50a} This phenomenon can also offer to tune the properties because solvates or hydrates exhibit different properties from their parent materials. The choice between solvated or unsolvated forms of a drug will depend on its pharmaceutical properties specifically stability under different conditions, shelf life, etc. Several drug molecules are currently marketed as solvates/hydrates, for example, Indinavir sulfate^{50b} is marketed as its ethanol solvate and Paroxetine hydrochloride^{50c} and Prantlukast^{50d} are marketed as their hemihydrates respectively. Additionally desolvation/dehydration can also results the new anhydrous polymorph of the parent material. In essence, hydrate/solvate formation can have diverse applications in pharmaceuticals.

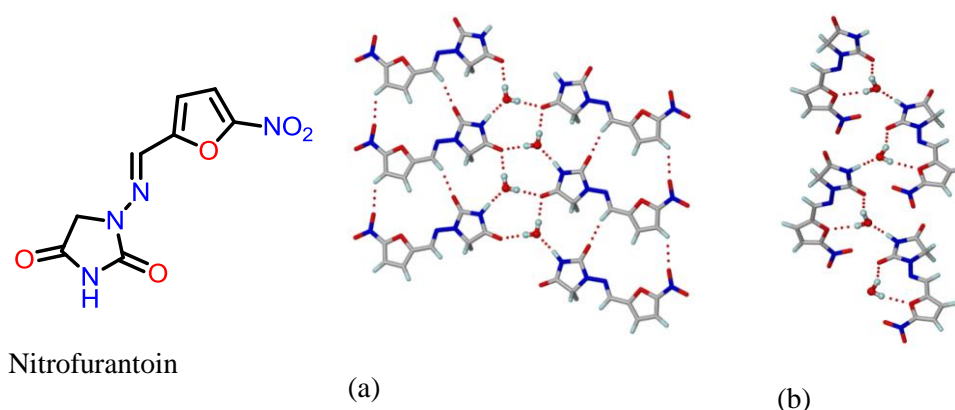


Figure 1.15 Pseudopolymorphs of Nitrofurantoin monohydrate. (a) In form I, tapes of translation related nitrofurantoin molecules are connected by water molecules through O–H···O and N– H···O hydrogen bonds. (b) In form II, discrete nitrofurantoin molecules form a zigzag tape through water molecules (Adapted from Ref. 50a).

1.7.3 Pharmaceutical Salts

Conventionally, acidic or basic drugs are formulated as their salt forms to attain higher solubility and stability.^{39a,51} Salts of their strong ionic interactions tend to be stable and in general exhibit higher melting points than their parent APIs. Ability of salts to form electrostatic interactions and charge-assisted hydrogen bonds with water in the biological media confers higher solubility to the API. Thus, salts offer the dual advantages of solubility and stability. The orange book database^{52a} lists the various drug products approved by the US-FDA, and the frequency of counter ions used for salt formation. In recent literature, Nangia et al.^{52b} improved the solubility and stability of the aceclofenac (BCS class II drug), a non-steroidal anti-inflammatory drug, by forming salt with L-lysine. They reported that it exhibits 135 times higher intrinsic dissolution rate and 127 folds higher solubility than pure aceclofenac (Figure 1.16). Rajput^{52c} reported the higher solubility of Haloperidol (BSC class II drug) by forming salt with methane sulfonic acid. Likewise, numerous papers and reviews on the pharmaceutical significance of salts have been published.

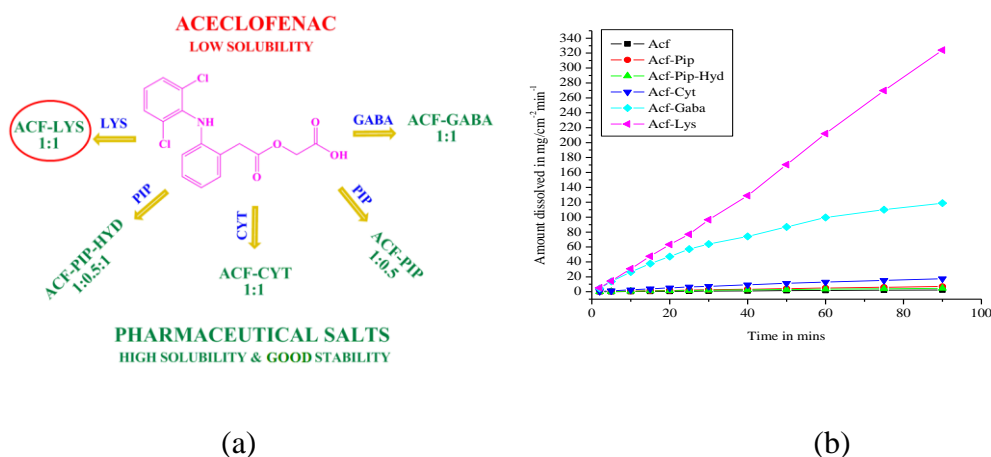


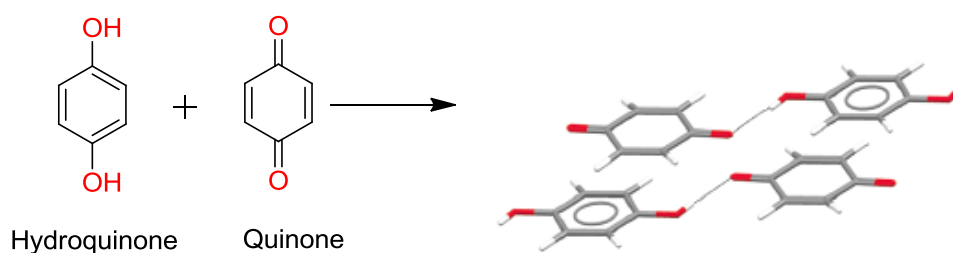
Figure 1.16 (a) aceclofenac salts (b) and its intrinsic dissolution rate curves of ACF salts in 25% EtOH–water (adapted from ref. 52c).

On the downside, salts tend to be more hygroscopic and restricted for ionizable functional groups.^{53a,b,c,d} The hygroscopic nature can cause loss of potency of drug, for instance the hygroscopicity of the anti-tuberculosis drug Ethambutol dihydrochloride salt is reported to cause instability of the fixed dose combination of anti-TB (FDC, Pyrazinamide, Isoniazid, Rifampicin and Ethambutol hydrochloride hydrate) drug, thus leads to less therapeutic activity and activity and therefore become useless for treatment.^{53e,f} Moreover, for neutral and weakly ionizable APIs, salts cannot be made. These issues warrant the need of novel solid forms that can circumvent these problems.

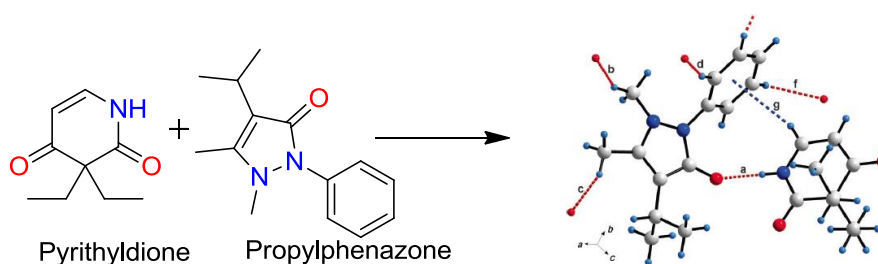
1.7.4 Cocrystals and Pharmaceutical Cocrystals

Crystal engineering principles are the rationale behind cocrystal design. Supramolecular synthon is a part of crystal engineering and plays the fundamental role to design and develop the cocrystals.^{9a,19,27,28} A cocrystal^{51d} may be defined as “a stoichiometric multi-component system where the individual components are held together by heteromeric interactions (adhesive) like hydrogen bonds, halogen bonds, stacking and are solids at room temperature”. Definition of cocrystals has been modified with time and evolved into a comprehensive one at the Indo-US meeting, 2011 and published in *Crystal Growth & Design*.⁵⁴ “Cocrystals are solids that are crystalline single phase materials composed of two or more different molecular and/or ionic compounds generally in a stoichiometric ratio which are neither solvates nor simple salts.” If at least one of the molecule is an API and other is Generally Recognized as Safe (GRAS)⁵⁵ substance then it is recognized

as ‘pharmaceutical cocrystal’.⁵⁶ Cocrystal classified into molecular and ionic cocrystals.⁵⁷ Two or more neutral molecular solids in a fixed stoichiometric ratio sustained by hydrogen bonding and/or halogen bonding is called as molecular cocrystal. Whereas ionic cocrystal where two or more molecular solids (ionic-neutral solids) sustained by charge assisted hydrogen bonds and/or coordination bonds. The first report of cocrystal between quinine and hydroquinone was reported by Friedrich Wöhler in 1844 (Figure 1.17a).⁵⁸ The first reported drug-drug cocrystal between pyrithyldione and propylphenazone was patented in 1937 and crystal structure reported in 2011 (Figure 1.17b).⁵⁹ Recently the first report on pharmaceutical cocrystal recognized between chloral hydrate and betaine (CHOBTN) and) has appeared in the US market well before in 1963 (Figure 1.17c).⁶⁰ Whilst cocrystals synthesis and their function came out in the form of pharmaceutical cocrystals in early 2000s.



(a)



(b)

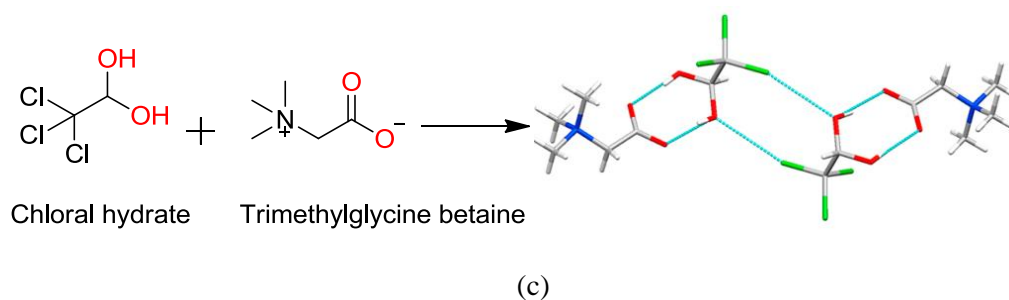


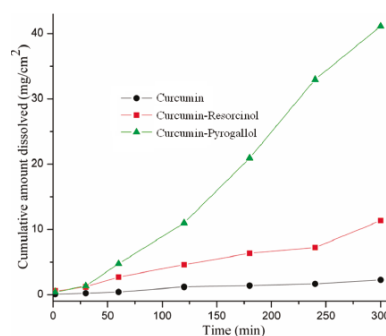
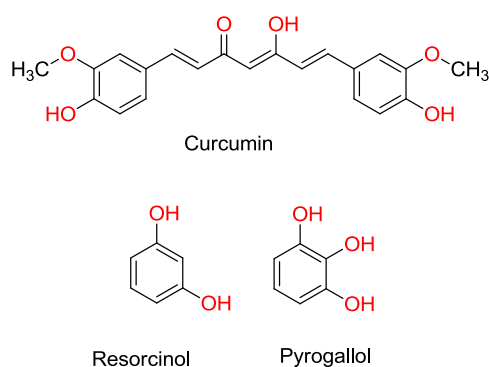
Figure 1.17 (a) molecular packing diagram of hydroquinone-quinone 1:1 cocrystal sustained by strong O–H···O synthon (b) drug-drug cocrystal of pyrithyldione-propylphenazone connect via N–H···O interaction (c) pharmaceutical cocrystal 1:1 of chloral hydrate and trimethylglycine betaine interact each other through dimeric O–H···O hydrogen bonds.

Different steps are involved for the pharmaceutical cocrystal design and synthesis. This includes selection of coformer guided by crystal engineering and hydrogen bonding principles followed by screening of cocrystal in different methods where the components are mixed together and subjected to solution crystallization, co-sublimation, co-melting, solid state grinding, liquid assisted grinding, slurry crystallization, reaction crystallization, spray drying etc.⁵⁶ Recently cocrystal preparation by inkjet printing^{56d} and crystallization at solvent-solvent interface^{56e} were proposed. In general cocrystals can be characterized by spectroscopic, thermal, and X-ray diffraction techniques. Specific applications of cocrystals can be extensively studied in pharmaceuticals to fine tune the physicochemical properties of an APIs or bioactive molecules without performing any chemical modification. Thus cocrystallization comes under the physical modification of drugs. Specifically coformer plays a vital role by influencing the physicochemical properties of a parent drug in the form of cocrystal. The development of this field can also be highlighted to synthesize the high energy materials, improve the conductivity, and tune the luminescence, phosphorescence and non-linear optics. All these applications of cocrystals are depicted in Figure 1.18.

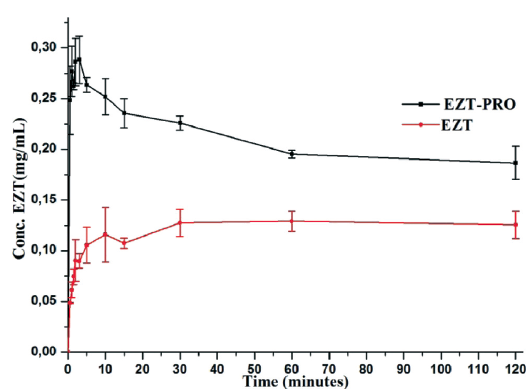
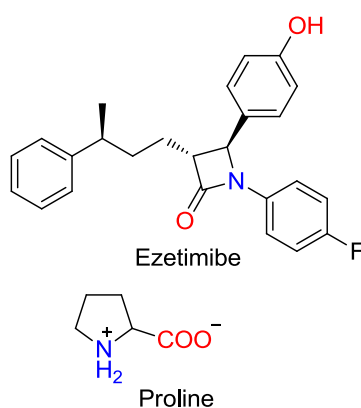


Figure 1.18 Several applications of cocrystals in drug chemistry and materials.

Classical examples from the literature are curcumin, is a natural polyphenol with diverse pharmacological actions. Though it exhibits poor aqueous solubility and limited bioavailability, the solubility enhancement was reported by making cocrystals with pyrogallol and resorcinol coformers. Among two cocrystals, curcumin-pyrogallol exhibits 11.7 times higher dissolution rate than pure curcumin (Figure 1.19a).^{61a} Another example ezetimibe is a hypocholesterolemic drug used in the treatment for reduction of cholesterol levels in plasma. It comes under BCS class II drug with poor aqueous solubility and it was reported that cocrystal with proline exhibits around 1.5 times higher dissolution rate than pure Ezetimibe (Figure 1.19b). In this way several papers and reviews are published on cocrystals for improving the solubility.^{61b} Few examples are listed in Table 1.1.



(a)



(b)

Figure 1.19 (a) Molecular structures of curcumin formed cocrystal formers and these two cocrystals exhibit higher intrinsic dissolution rate than curcumin (adapted from 61a). (b) Molecular structures of Ezetimibe and proline coformer and binary cocrystal of Ezetimibe-proline cocrystal shown greater intrinsic dissolution rate enhancement than pure Ezetimibe (adapted from 61b).

On the other hand API phase stability is an important phenomena to inhibit the phase conversion either in the form of solvate or hydrate or degradation product during storage, where cocrystal improves the ability to tune the API. Nangia et al.^{62a} reported the improved hydration stability of nitrofurantoin drug by forming cocrystal with p-aminobenzoic acid and Trask et al. showed the same for caffeine via cocrystallization with oxalic acid.^{62b} A well-known example, Qian et al. improved the thermal degradation of Adefovir dipivoxil (AD) drug (which is used the treatment of chronic hepatitis B) by forming cocrystal with saccharin (SAC).^{62c} They reported that during storage at 60 °C, for AD dramatically decreased to 48.5% on the 30th day and the remaining amount is corresponding to degraded products. Whereas AD-SAC cocrystal shown no degradation

during the whole course (Figure 1.20). In another report Nangia et.al.^{62d} also reported the hydrolytic stability of anticancer drug temozolomide (TMZ) by forming cocrystals. It is a BCS class I drug with high solubility and permeability but it has poor stability during storage. It is transformed to 5-aminoimidazole-4-carboxamide (AIC) and this makes the drug less effective. This issue was addressed by making cocrystal with succinic acid (SA) and showed that TMZ-SA is stable for over six months in accelerated stability conditions of 40°C and 75%RH and 30°C and 65%RH. Whereas pure TMZ transformed to AIC with two weeks and after six months only 30% of TMZ is left. Further bioavailability study of TMZ-SA cocrystal on sprague dwaley rats results shown that TMZ-SA is bioequivalent to TMZ (Figure 1.21). In this manner improved biopharmaceutical properties were reported with cocrystals in literature. Few examples were listed in Table 1.

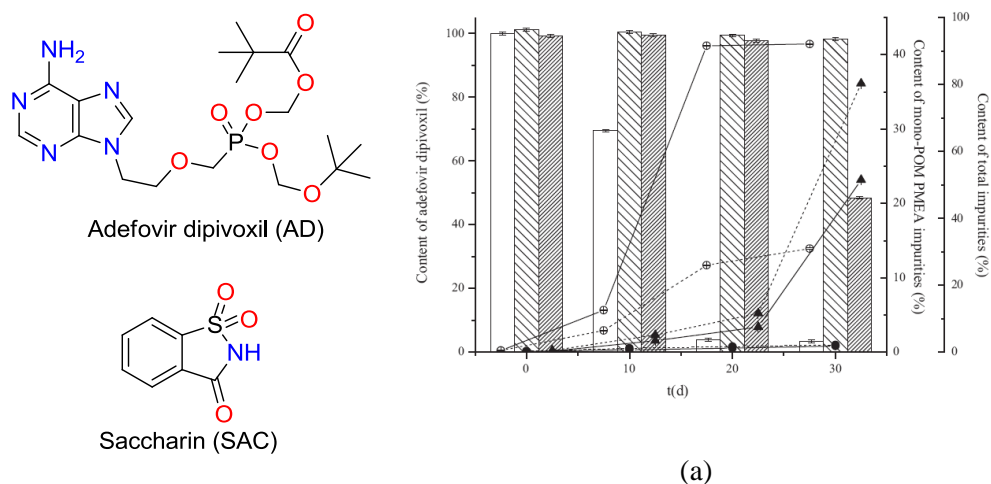
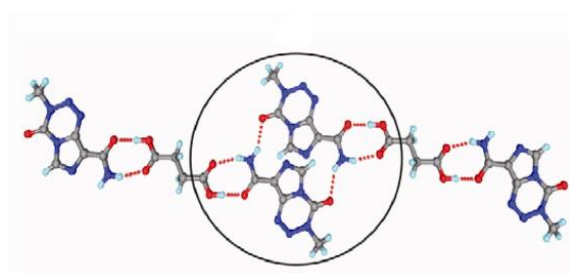
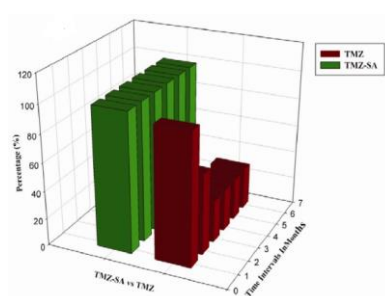


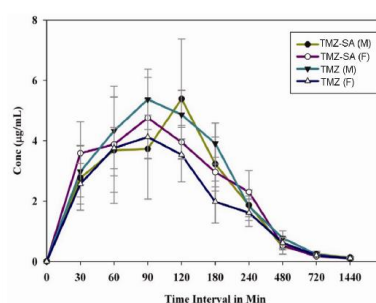
Figure 1.20 molecular structures of AD, SAC and content of AD (white column for AD, light gray for AD-NCT cocrystal and dark gray for AD-SAC cocrystal) at 60 °C storage (adapted from 62c).



(a)



(b)



(c)

Figure 1.21 (a) TMZ–succinic acid cocrystal sustained by acid-amide dimer interaction (b) chemical stability of pure TMZ and TMZ-SA cocrystal (for temozolomide) by HPLC analysis stored at accelerated conditions. TMZ showed degradation to 30% of the original purity in the 6-month period. TMZ-SA test cocrystal remained stable during the entire 6 months of study with final drug concentration of over 99%. (c) mean plasma concentration versus time profile of TMZ reference drug and TMZ-SA test cocrystal. (Adapted from ref. 62d).

Table 1.1 Literature survey of the cocrystal with tailor mode properties.

Modified property	Cocrystal (in medicine and materials chemistry)	References
Solubility and Dissolution rate	1. Itraconazole-L-malic acid cocrystal 2. Hexamethylene bisacetamide cocrystals 3. Curcumin cocrystals 4. Furosemide cocrystals 5. Ezetimibe-L-proline cocrystal 6. Melatonin-pimelic acid cocrystals 7. Carbamazepine-PABA(multiple stoichiometric ratios) cocrystals 8. Voriconazole cocrystals 9. Ethionamide cocrystals 10. Tegfur cocrystals	1. <i>J. Am. Chem. Soc.</i> , 2003, 125 , 8456. 2. <i>J. Am. Chem. Soc.</i> , 2009, 132 , 17048. 3. <i>Cryst.Growth Des.</i> , 2011, 11 , 4135. 4. <i>J. Pharm. Sci.</i> , 2012, 101 , 664. 5. <i>CrystEngComm</i> , 2014, 16 , 8984. 6. <i>CrystEngComm</i> , 2015, 17 , 612. 7. <i>Mol. Pharmaceutics</i> , 2016, 13 , 990. 8. <i>CrystEngComm</i> , 2014, 16 , 4722. 9. <i>Cryst. Growth Des.</i> , 2016, 16 , 1591. 10. <i>Cryst. Growth Des.</i> , 2014, 14 , 6557. 11. <i>Cryst. Growth Des.</i> , 2015, 15 , 3498. 12. <i>CrystEngComm</i> , 2014, 16 , 5859.

	11. Sulfamethizole cocrystals (discussed in chapter 3) 12. Sulfacetamide cocrystals	
chemical stability	1. Andrographolide cocrystals (discussed in chapter 2) 2. Temozolomide cocrystals 3. Vitamin K3 cocrystals 4. Vitamin D3 cocrystals 5. Tranilast cocrystals 6. Nitrofurantoin cocrystals	1. <i>Chem. Asian J.</i> , 2013, 8 , 3032. 2. <i>Chem. Asian J.</i> , 2012, 7 , 2274. 3. <i>Cryst. Growth Des.</i> , 2016, 16 , 483. 4. <i>Chem. Commun.</i> , 2014, 50 , 855. 5. <i>Cryst. Growth Des.</i> , 2013, 13 , 3546 6. <i>CrystEngComm</i> , 2011, 13 , 759.
Hydration stability	1. Etirocoxib cocrystals 2. Niclosamide cocrystals 3. Theophylline-oxalic acid cocrystal 4. Quercetin cocrystals 5. Nitrofurantoin cocrystals	1. <i>CrystEngComm</i> , 2016, 18 , 2825. 2. <i>Cryst. Growth Des.</i> , 2012, 12 , 4588. 3. <i>Int. J. Pharm.</i> , 2006, 320 , 114. 4. <i>Mol. Pharmaceutics</i> , 2011, 8 , 1867. 6. <i>J. Pharm. Sci.</i> , 2011, 100 , 3233.
Bioavailability	1. Nitazoxanide cocrystals (discussed in chapter seven) 2. Apixaban-oxalic acid cocrystal 3. Telmisartan cocrystals 4. Lithium ionic cocrystals 5. Ilperidone cocrystals 6. Zwitter ionic cocrystals of Flavonoids and Proline 7. Danazol cocrystals	1. <i>Chem. Commun.</i> , 2016, 52 , 4223. 2. <i>Cryst. Growth Des.</i> , 2016, 16 , 2923. 3. <i>CrystEngComm</i> , 2014, 16 , 8375. 4. <i>Mol. Pharmaceutics</i> , 2013 , 10, 4728. 5. <i>Inorg. Chem. Commun.</i> , 2014 , 39, 144. 6. <i>Cryst. Growth Des.</i> , 2016, 16 , 2348. 7. <i>Mol. Pharmaceutics</i> , 2013, 10 , 3112.
Permeability	1. Hydrochlorothiazide cocrystals 2. Theophylline cocrystals 3. Acyclovir cocrystals	1. <i>Mol. Pharmaceutics</i> , 2015, 12 , 1615 2. <i>Cryst. Growth Des.</i> , 2015, 15 , 5593 3. <i>CrystEngComm</i> , 2013, 15 , 6457.
Mechanical properties	1. Lamotrigine cocrystals 2. Nitazoxanide cocrystals 3. Voriconazole cocrystals 4. Ibuprofen and flurbiprofen cocrystals 5. Paracetamol cocrystals 6. Piroxicam-saccharin cocrystal	1. <i>Cryst. Growth Des.</i> , 2015, 15 , 5816. 2. <i>Cryst. Growth Des.</i> , 2014, 14 , 1086 3. <i>Mol. Pharmaceutics</i> , 2015, 12 , 889. 4. <i>Pharm. Res.</i> 2012, 29 , 1854. 5. <i>Adv. Mater.</i> , 2009, 21 , 3905 6. <i>Cryst. Growth Des.</i> , 2014, 14 , 3864.
Thermal stability	1. Propolol-isonicotinamide cocrystal 2. 3-Iodo-2-propynyl-N-butylcarbamate (IPBC, Preservative) cocrystals 3. Adefovir dipivoxil cocrystals	1. <i>Cryst. Growth Des.</i> , 2014, 14 , 2422. 2. <i>Mol. Pharmaceutics</i> , 2013, 10 , 1760 3. <i>Int. J. Pharm.</i> , 2012, 438 , 327.
Dyeing applications	1. Pyridine-2,4-dione based heterocyclic dye. 2. Colour-tuned fluorescein cocrystals	1. <i>CrystEngComm</i> , 2015, 17 , 2083. 2. <i>CrystEngComm</i> , 2013, 15 , 6289.
Conductivity	1. Phenazine:deuterated chloranillic acid	1. <i>J. Am. Chem. Soc.</i> 2005, 127 , 5010. 2. <i>J. Phys. Condens. Matter</i> 2007, 19 ,

improvement	2. Phenazine- chloranillic acid 3. Anilic acid-phenazine	226203. 3. <i>J. Mater. Chem.</i> 2009, 19 , 4421.
Non-linear optical properties	1. Nonlinear optical chalcone cocrystal and structure–property relationship 2. Nonlinear optical analyses of hexamine: phenol cocrystals	1. <i>Cryst. Growth Des.</i> , 2011, 11 , 5362. 2. <i>Spect. Acta Part A: Mol. and Biomol. Spect.</i> 2014, 120 , 14.

1.7.4.1 Spring and Parachute model for solubility enhancement

In the year 2011, Nangia et al.^{51b} proposed a model explaining the role of coformer in improving the solubility of cocrystals, based on ‘spring and parachute’ model of amorphous forms.⁶¹ In relation to the model, a cocrystal containing a high soluble coformer can facilitate the faster dissolution of a low soluble component. This happens via the fast release of high soluble coformer into aqueous medium that results in the dissociation of cocrystal, thereby leaving behind the low soluble component in an amorphous/randomized state, which understandably leads to an increase in the free energy of the system, ultimately leading to an improvement of solubility/dissolution of the low soluble component (Figure 1.8). This model confirms that high solubility coformer will give rise to high solubility cocrystal and *vice-versa*. If the coformer has low water solubility, it does not dissociate from the lattice easily and in effect can control the solubility/dissolution of the drug, for example, cocrystals of anti-lung cancer agent Hexamethylenebisacetamide^{56b} with sebacic acid and dodecanedioic acid. In some cases cocrystal packing also control the solubility independent of coformer solubility e.g. sulfacetamide-caffeine cocrystal since cocrystal packing and non-covalent interactions are stronger than sulfacetamide guest free form.⁶³ Thus cocrystal decreases the solubility of the sulfacetamide. Similar observation was observed in this thesis in chapter 3 on sulfamethizole cocrystals.

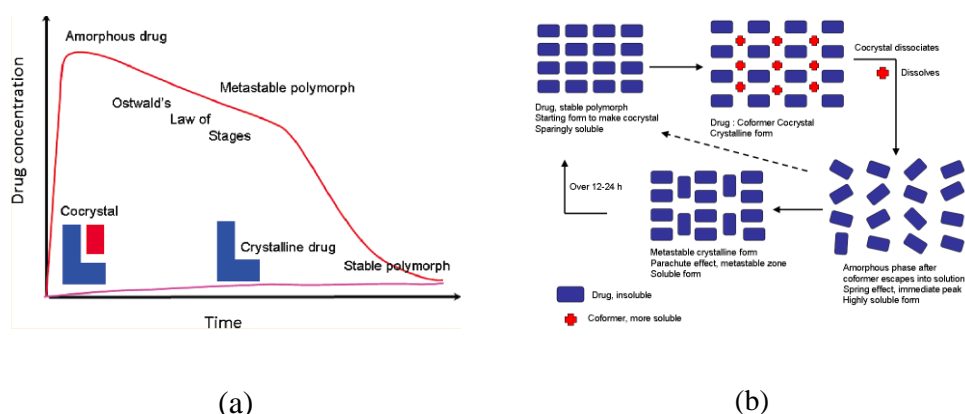
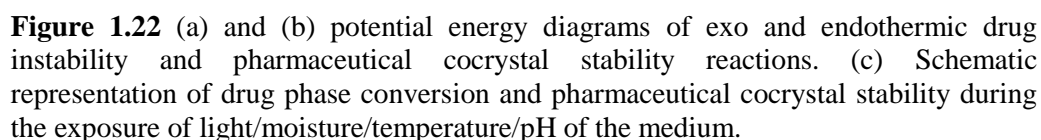


Figure 1.8 (a) The spring and parachute concept to achieve high apparent solubility for insoluble drugs. (1) The crystalline (stable) form has low solubility. (2) A short-lived metastable species (i.e., amorphous phase) shows peak solubility but quickly drops (within minutes to an hour) to the low solubility of the crystalline form. (3) Highly soluble drug forms manage to remain for a long enough time (usually hours) in the metastable zone. (b) Possible mechanisms of pharmaceutical cocrystals in dissolution medium (adapted from ref. 63).

1.7.4.2 Potential Energy diagram model for stability enhancement

The mechanism of drug phase stability improved by pharmaceutical cocrystals can be explained with the help of general potential energy diagram of chemical reaction kinetics and thermodynamics associated with exo- and endothermic chemical reactions. These reactions can occur because of the energy level differences and change in enthalpy (ΔH = sum of potential energy and kinetic energy). An exothermic reaction occurs where energy releases during the phase change reaction and this exhibits negative ΔH because enthalpy of product is lower. An endothermic reaction occurs absorbs the energy from the surroundings to complete the phase change reaction.⁶⁴ This has positive ΔH because, enthalpy of the product will be higher than the reactants. The activation energy requirement is more for endothermic reaction and less for exothermic reaction. We have interconnected the same endo and exothermic reactions potential energy diagram concept for drug stability during the storage/effect of the light/pH of medium/moisture/temperature. A drug may be less stable or more labile and more energetic during the above conditions. Therefore, it can be undergoing exo or endo reaction to form new phase. If the resultant new phase is low energetic than starting drug it is called as exothermic reaction and if the new phase has higher energy than drug is called as endothermic reaction. Eventually, it influences the drug efficacy or potentiality. However cocrystal tends to be a low energy system for this reason it cannot undergo



Conventionally, salts have been used to enhance solubility of drug molecules, but cocrystals have the ability to modulate the solubility of an API either way (increase or decrease). Numerous literature reports highlight the solubility enhancing ability of cocrystals. Recently polymorphism in cocrystals^{56e} has also been reviewed. Due to this property advantages, the US-FDA has published ‘Regulatory Classification of pharmaceutical cocrystals and newly, the EMA published a reflection paper on the use of

cocrystals that considers pharmaceutical cocrystals for edited applications. Cocrystals are given the status of ‘new active substances’ (NAS) if their safety and efficacy is proved.^{65,34} from the perspective of looking at them as intellectual property. To our knowledge, till date, APIs of Depakote (Sodium Valproate-Valproic acid) Cafcit (Caffeine-Citric acid), Lexapro (Escitalopram Oxalate) cocrystal forms are in the market. More recently In 2015 July Entresto (Monosodium Sacubitril and Disodium Valsartan) drug-drug cocrystal is approved following the cocrystal guidance by US-FDA for heart failure and it is a drug-drug ionic cocrystal.^{65a}

1.7.5 Eutectic Compositions

Eutectic⁶⁶ is a multicomponent system defined as “a fixed stoichiometric ratio of an intimate mixture of non-isomorphous components, which exhibit the lower melting point than any other compositions of constituents or individual components.” This formation is usually governed by the mismatch and misfit between interacting components and lacking of auxiliary interactions in the crystal lattice to result in predominantly cohesive interactions than adhesive interactions. Unlike cocrystals, where the internal arrangement is homogeneous, the complexes, heterogeneous arrangement in eutectics is comprised of domains of solid solutions held by weak inter phase interactions. Therefore, it is known as conglomerate of solid solutions or discontinuous solid solutions.⁶⁷ Differences in the molecular level interactions of eutectics lie in the short range order only and at the limit of X-ray diffraction to detect such changes. The latter microstructures are indistinguishable in the long range by Bragg reflections. This characterization and the phase establishment of eutectic phase is really a challenge task since depression in melting point by thermal methods is the only indicator of eutectic formation. Due to these poor characterizations, the microstructure of eutectic is still elusive as well as there is no clear rationale design for on selection of coformer for eutectic formation.

Hence it needs other techniques to analyze the local structure of eutectics. Recently, specific techniques like atomic pair distribution function (PDF) approach^{68a,b} and extended x-ray absorption fine-structure spectroscopy (EXAFS)^{68c,d} are used to analyze the local structure of materials. PDF is obtained from a total scattering powder diffraction pattern via a fourier transform. Because the total scattering is composed of Bragg as well as diffuse scattering contributions, it contains local, medium range and long range structural information. Similarly, EXAFS is used to determine the distances,

coordination number, and the nature of the neighbors of the absorbing atoms. Thus, these techniques may be helpful in dissecting the microstructure of an eutectic composition by analyzing the short range interactions comprising their inter phase boundaries which helps in the rational design and synthesis of eutectics. Usually they are prepared by fusion methods (Kofler method) and solvent-based co-precipitation.^{56,69}

Eutectics are known to have more applications in various fields such as pharmaceuticals, ceramic industry and metal industry. Particularly in pharmaceuticals it has more utility because of their high thermodynamic functions such as free energy, enthalpy, and entropy, which confer solubility and dissolution rate of poorly soluble drugs or bioactive molecules. The first pharmaceutical utility of eutectic compositions was reported in 1960s on drug eutectics of sulfathiazole-urea and chloramphenicol-urea by fusion method for dissolution and bioavailability improvement.^{70a,b} The first successful application of eutectic is a ternary mixture of cocaine hydrochloride, phenol and menthol (homogenous liquid at room temperature) for topical anesthesia.^{70c,d,e,f} Currently marketed a drug-drug eutectic composition is lidocaine-prilocaine (22°C) with enhanced local anesthetic and analgesic applications followed by rapid pharmacological action.^{70g} These drugs, when applied individually have a poor skin penetration because of their higher melting points (lidocaine, 68°C and prilocaine 38°C). Chiou and coworkers^{69a} have reported that a eutectic composition of antifungal drug Griseofulvin with succinic acid (55% w/w of Griseofulvin) have shown 6-7 times faster dissolution rate compared to pure Griseofulvin (Figure 1.23a). In another report, Nangia and coworkers^{66b} have reported the improved dissolution rate curcumin-nicotinamide (1:2) eutectic composition than curcumin (Figure 1.23b). And same group^{66a} described drug combination eutectic of pyrazinamide and isoniazid with succinic acid in a 1:1:1 fixed stoichiometric ratio exhibited higher dissolution rate than individual drugs and binary cocrystals (Figure 1.23c). Furthermore the same group also highlighted eutectic remedy for hygroscopic stability of ethambutol hydrochloride (EDH) by forming eutectic compositions with succinic acid (SA) and fumaric acid (FA). They reported that EDH-FA retain the solid state integrity for two months. Whereas pure EDH is turned to liquid like within a month (Figure 1.23d).⁶⁷

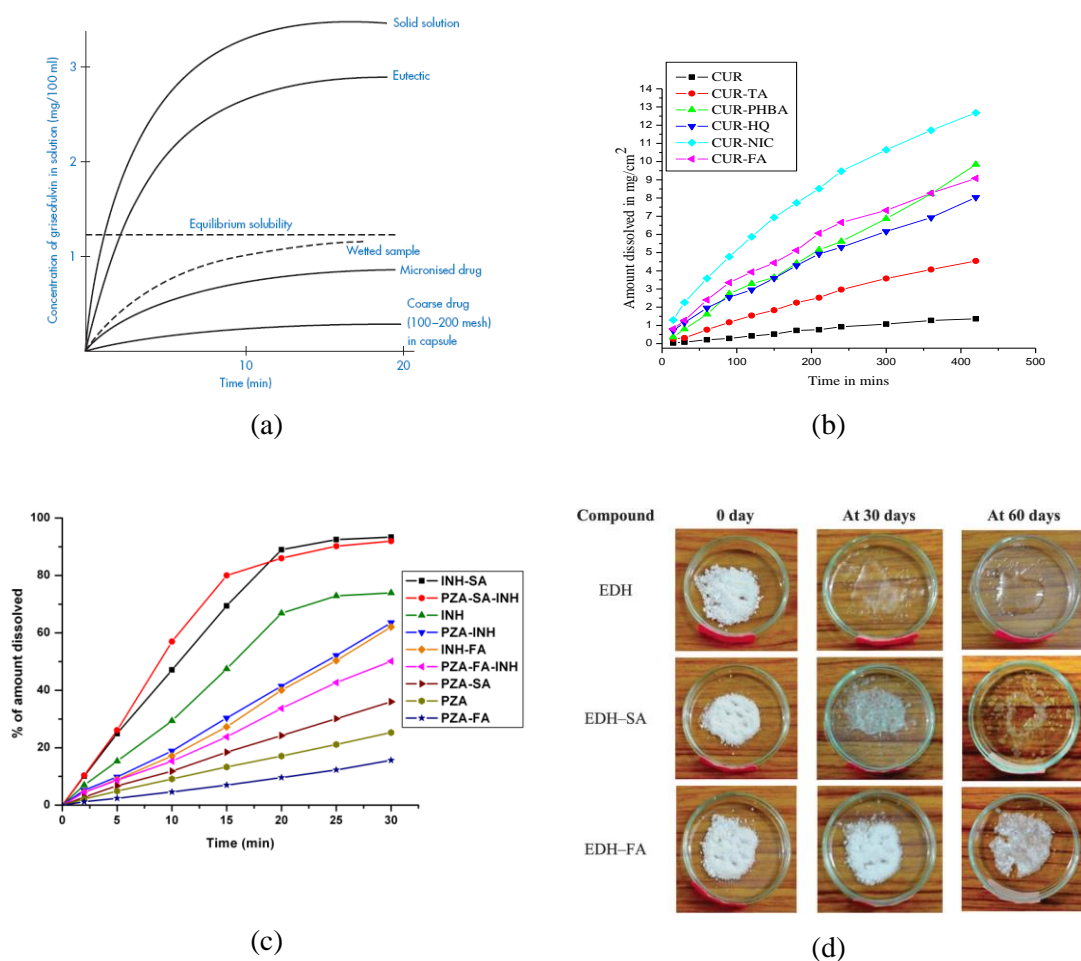


Figure 1.23 Rate of dissolution of Griseofulvin-succinic acid solid solution, eutectic mixture and crystalline material. The dissolution rate of Griseofulvin was improved by 6-7 times on forming eutectic (adapted from ref.72a) (b) intrinsic dissolution rate curves of curcumin binary eutectic compositions in 40% EtOH–water (c) dissolution curves of the compounds in pH 1.2 aq. HCl solution. (d) the physical state of EDH compounds to show their hygroscopic behavior at 40 °C and 75% RH as a function of time. Both the eutectics exhibit greater hygroscopic stability than EDH.

1.7.6 Solid solutions/Alloys

A solid solution defined as a single crystalline phase comprising a mixture of two or more isomorphous (same space group and unit cell dimensions) compounds is also referred as multivariate cocrystals.^{67,71} By virtue of structural similarities and unlimited solubility, they accommodate well (either substitutionally or interstitially) in the crystal without disturbing the parent lattice structure and thus form continuous solid solutions in all proportions (ranging from 1:99 to 99:1). Design and synthesis of alloys are common

for inorganic materials and minerals. Since inorganic metals have similar size and strong similar ionic bonding directional can enable the formation of substituted alloys. Conversely the diversity in shape and structural complexity in organic molecules makes the designing of organic solid solutions difficult. Usually they can be prepared by fusion methods and compositions of alloys can be established by single X-ray diffraction technique. Additionally alloys can also be characterized by DSC which exhibit melting point either low or in between starting isomorphous components. Application points of view, alloys have been used in the metal industry for a long time. Fabulous applications are Nickel-Chromium (Ni-Cr) and Nickel-Chromium-Iron (Ni-Cr-Fe) alloys have been used for high temperature heating elements. It also used in radio and electronic devices, aircraft controls and automotive applications. There are few reports on drugs, forming solid solutions/alloys and their thermal behavior. For example Row et. al.^{71d} have reported two solid solutions of ornidazole (ORL) cocrystals. ORL form cocrystals p-aminobenzoic acid (PABA) and p-hydroxybenzoic acid (PHBA) are isomorphous to each other. They reported two solid solutions between the cocrystals in different molar ratios (ORL-PABA: ORL-PHBA, 0.46:0.54 and 0.33:0.67, Figure 1.24). Oswald e. al.^{71e} reported different solid solution compositions of isomorphous (\pm)-4-methylmethcathinone hydrochloride and hydrobromide. They stated that different solid solution compositions alter the thermal behavior.

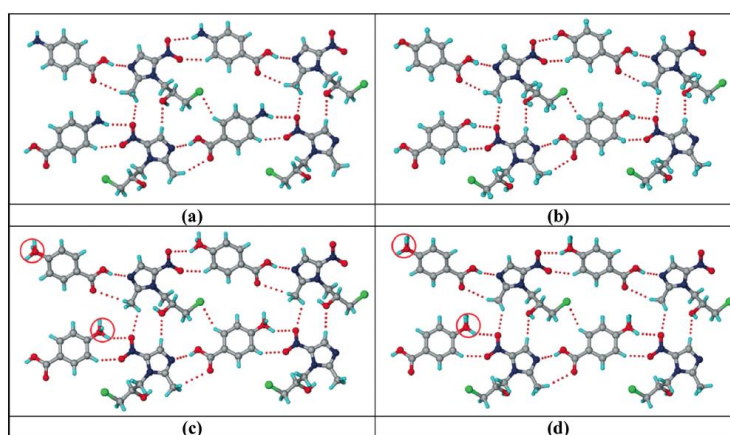


Figure 1.24 (a) ORL-PABA and (b) ORL-PHBA isomorphous cocrystals. Anti-parallel tapes of alternate PABA/PHBA and ORL molecules connected by the acid-imidazole and amine/hydroxyl-nitro interactions extend in corrugated sheets through

C–H...O and C–H...Cl interactions. (c) and (d) two solid solutions of ORL-PABA: ORL-PHBA in the respective 0.46:0.54 and 0.33:0.67 molar ratio. The amine and hydroxyl position is indicated by red circles.

1.7.7 Amorphous solids

Amorphous solids lack the long range order in the lattice space characteristic of a crystal.⁷² It occupies a prominent place in pharmaceuticals with their ability to improve solubility and dissolution rate APIs due to excess thermodynamic functions of amorphous phases. But when compared to crystalline phases, amorphous compounds do not show a regular diffraction pattern. These aperiodic solids can be produced by several techniques such as spray- and freeze-drying, melt quenching, milling, wet granulation^{31b} etc. and recently manual grinding^{72c} was shown to result in amorphous salts. They are characterized by thermal techniques with glass transition temperature (T_g). It is the temperature at which a glassy material (plastic) is converted to rubbery phase retaining some properties of the liquid^{72b}. Similar to their crystalline counterparts, amorphous forms are also known to exhibit polymorphism⁷³ which is termed as 'polyamorphism'. For example, polyamorphism in H₂O is extensively studied^{74a}, but the data interpretation remains controversial since the diffraction pattern does not show any Bragg lines. In another example, the evolution of acetaminophen polyamorphous phases I and II forms corresponding polymorphs I and II in different solvent systems was also studied by radial distribution functions derived from the pair distribution function (PDF).^{74b} On one hand the excess thermodynamic functions of amorphous phases confer solubility/dissolution advantage of the poorly soluble APIs. Therefore drugs Itraconazole, Lopinavir, Cefuroxime axetil, Quinapril hydrochloride etc., are marketed either as purely amorphous phases or in combination with other solid forms. But on the other hand, the higher entropy and enthalpy can be disadvantageous since they make the amorphous solid forms highly unstable. Several excipients such as methyl cellulose, alginic acid, polyvinyl pyrrolidone (PVP), polyethylene glycol (PEG) etc^{31b} have been developed to stabilize the amorphous forms.

1.7.8 Coamorphous solids

More recently the concept of “coamorphous” system was introduced by Norman Chieng et al. in the year 2009,⁷⁵ the formulation of binary amorphous mixture of ranitidine hydrochloride and γ -indomethacin in different stoichiometric (1:1, 1:2, and 2:1) ratios. Later Thomas Rades and his co-workers started to explore the coamorphous system as a formulation.⁷⁶ Coamorphous system has thus gained considerable interest in the pharmaceutical field because of their potential to improve the solubility and dissolution rate of poorly soluble drugs. It is a single homogenous phase mixture of two or more low molecular weight components or non-polymeric components which lacks periodic arrangement in the lattice and associated by weak and discrete intermolecular interactions between the components in the lattice. They can have short range ordering similar to amorphous solids of single component systems. In contrast to polymeric matrix solid dispersion, where API molecules are dispersed in high molecular weight polymeric matrix in non-stoichiometric ratio, a coamorphous solid in which a molecule of interest and a coformer interact with each other via non-covalent interactions in a fixed stoichiometry ratio and dispersed in lattice.⁷⁷ Similarly both polymeric solid dispersion and coamorphous solid can facilitate the high thermodynamic functions such as free energy, enthalpy and entropy, and confer solubility and dissolution advantage similar to amorphous solids. Additional Advantage gained coamorphous solid is stabilize the amorphous form due to non-covalent interaction among them. It contrasts with a cocrystal, salt or eutectic primarily by its amorphous nature in that it exhibits a broad hump (‘amorphous halo’) when subjected to powder X-ray diffraction.⁷⁸ The identity and integrity of the components of coamorphous systems can be established by FT-IR and Raman spectroscopic techniques and eventually coamorphous solids exhibit single glass transition temperature.^{76a} Together with the more well-known counterparts such as salts, eutectics and cocrystals, coamorphous solids are a new entry to pharmaceutical solid form space. However there is no clear information on the rational coformer selection to make the coamorphous form. There are few reports representing the amino acids repeatedly forming coamorphous forms during mixing with APIs.⁷⁸ Still the microstructure of coamorphous is elusive by pair distribution function. These solids can be produced by several techniques such as spray- and freeze-drying, melt quenching, milling, manual grinding and rotaevaporation.⁷⁶⁻⁷⁹

Till date coamorphous solids were extensively studied in pharmaceuticals specifically to improve the solubility, stability and bioavailability. Few examples are highlighted here. Recently Zhang et.al^{79a} has reported the improved solubility and stability of Lurasidone hydrochloride (LH) with saccharin in a 1:1 molar ratio. They stated the LH-SAC coamorphous solid stored at 25 °C/60% RH, is stable up to 60 days and it has higher stability than pure LH amorphous which showed only 7 days stability at same conditions (Figure 1.25a). Laitinen et.al^{79b} reported the drug-drug coamorphous of simvastatin (SVP) and glipizide (GPZ) in different stoichiometric ratios (1:1, 2:1 and 1:2). Cryo-milled 1:1 and 1:2 of the SVP-GPZ showed two months phase stability at 25 °C/65% RH (Figure 1.25b). Likewise, coamorphous system is gaining considerable attention in the academic and pharma industry because of their potential utility to improve drug dissolution rate, stability consequently oral bioavailability.⁸⁰ In chapter 6 we highlight the Curcumin-Artemisinin coamorphous solid utility in terms of oral bioavailability enhancement.

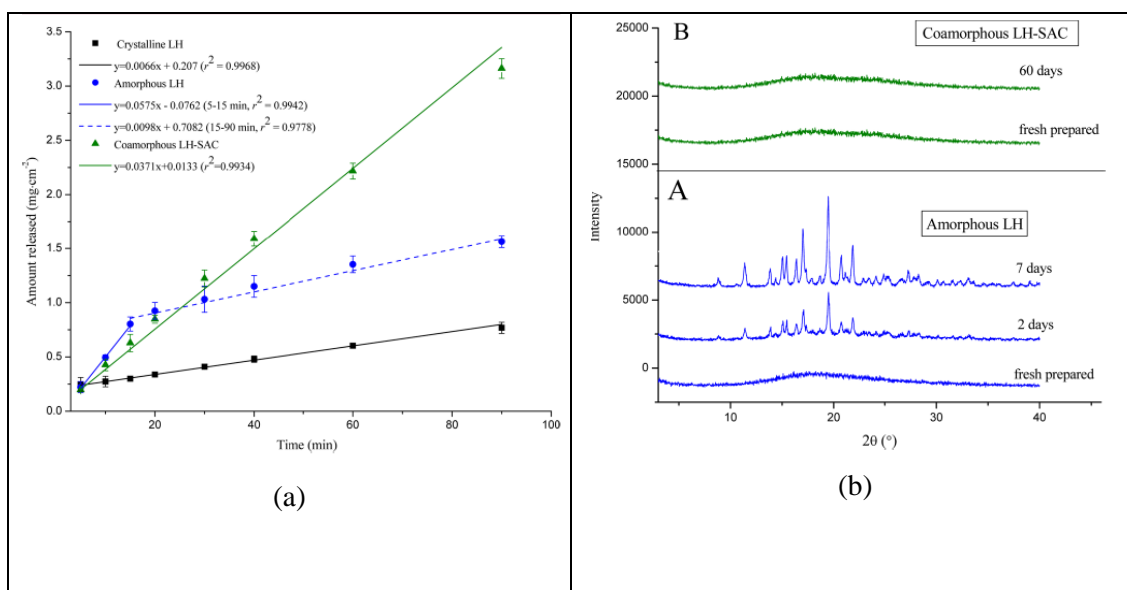


Figure 1.25 (a) Intrinsic dissolution rate profiles crystalline LH, amorphous LH, and coamorphous LH-SAC in 0.2M phosphate buffer solution (3.8, n=6). (b) PXRD patterns for amorphous LH (A), coamorphous LH-SAC (B) stored at 25 °C/60% RH over a specified period.

1.8 Conclusions

In this chapter, the origin and evolution of crystal engineering as a primary design element in developing pharmaceutical solid forms has been discussed. Alongside, intermolecular interactions and supramolecular synthons were emphasized and the importance of isotropic and anisotropic interactions in the evolution of complex supramolecular architectures was brought in. This understanding would be vibrant in the context of ‘pharmaceutical form development’ which allows the design of several solid forms with varying strengths of intermolecular interactions such as polymorphs, amorphous forms, salts, cocrystals and solid solutions/eutectics or coamorphous towards better therapeutic efficacy.

An API or a bioactive molecule can give rise to a multitude of crystal forms upon solid form screening. A review of all these solid forms was reviewed in various subdivisions of this chapter, which would focus the inherent differences in the structural aspects among these crystalline forms. By virtue of their uniqueness, these solid forms would result in varied physicochemical properties which are significant for best solid form selection and development. Since there is no single solution to the problems arising from the physicochemical behavior of various drug molecules, it is enormously essential to screen for all the possible solid forms (polymorphs, amorphs, salts, solvates, cocrystals, eutectics, solid solutions and coamorphs), which via their unique physicochemical properties would provide specific and desirable applications in different systems. A schematic representation of the drug to modified pharmaceutical solid and evolution is shown Figure 1.26.

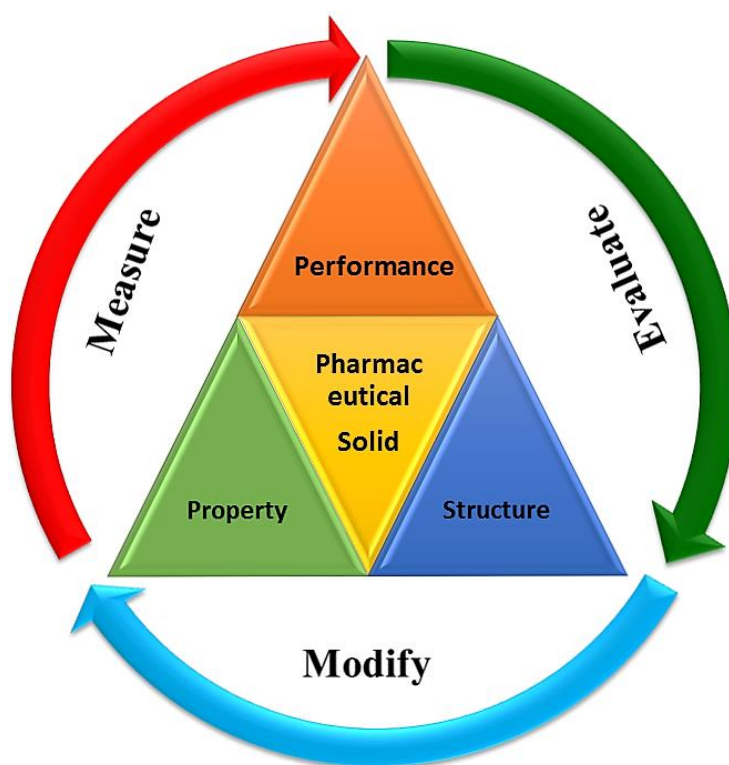


Figure 1.26 Pictorial presentations of pharmaceutical solid formulation stages.

In the following chapters, chapter 2 deals with solving chemical stability and high solubility of andrographolide by forming cocrystals with hydroxybenzoic acid coformers. Chapter 3 describes the modulating solubility ability of novel sulfamethizole cocrystals and chapter 4 explores polymorphism and isostructurality in Glibenclamide salts. Chapter 5 discusses the solubility enhancement of lornoxicam salts and conformational analysis and chapter 6 describes the solubility and bioavailability enhancement of curcumin-artemisinin coamorphous solid. Chapter 7 explores the pharmaceutical utility of alloys along with cocrystals of Nitazoxanide. In essence, this thesis deals with the application of crystal engineering principles in designing and discovering different solid forms of drugs or bioactive molecules and their application towards addressing their poor physicochemical properties.

1.9 References

1. (a) J. -M. Lehn, *Supramolecular Chemistry: Concepts and Perspectives*, VCH: Weinheim, 1995. (b) *The Crystal as a Supramolecular Entity; Perspectives in Supramolecular Chemistry*, Wiley: Chichester, 1996, Vol. 2.
2. J. -M. Lehn, *Pure Appl. Chem.*, 1978, **50**, 871.
3. J. D. V. D. Waals, Doctoral Dissertation, Over de continuïteit van den gas-en vloeistofoestand (Leiden, 1873; German ed., Leipzig, 1881; English ed., London, 1890; French ed., Paris, 1894).
4. E. Fischer, *Chem. Ber.*, 1894, **27**, 2985.
5. (a) W. M. Latimer, W. H. Rodebush, *J. Am. Chem. Soc.* 1920, **42**, 1419; (b) L. Pauling, *The Nature of the Chemical Bond*, Cornell University Press, 1939; (c) L. Pauling, *The Nature of the Chemical Bond and the Structure of Molecules and Crystals: An Introduction to Modern Structural Chemistry*, Third edition, Ithaca, NY, Cornell University Press, 1960.
6. (a) J. W. Steed, J. L. Atwood, *Supramolecular Chemistry*, Wiley, Chichester etc., 2000; (b) J. -M. Lehn, J. L. Atwood, J. E. D. Davies, D. D. MacNicol, D. D. MacNicol, F. Vögtle, *Comprehensive Supramolecular Chemistry*, Vol. 1-11; Ed.: Pergamon/Elsevier Oxford etc, 1996;
7. J. -M. Lehn, *Proc. Nat. Acad. Sci.*, 2002, **99**, 4763.
8. (a) T. Schrader, A. D. Hamilton, *Functional Synthetic Receptors* Hrgs.: Wiley-VCH, Weinheim, 2005; (b) J. W. Steed ; D. R. Turner ; K. J. Wallace, *Core concepts in Supramolecular Chemistry and Nanochemistry*, Chichester, Wiley, 2007; (c) A. Gavezzotti, *Molecular Aggregation structure analysis and molecular simulation of crystals and liquids*, Oxford University Press, Oxford, 2007.
9. (a) G. R. Desiraju, *Crystal Engineering: The Design of Organic Solids*, Elsevier, Amsterdam, 1989. (b) G. R. Desiraju, *J. Chem. Sci.*, 2010, **122**, 667; (c) G. R. Desiraju, J. J. Vittal and A. Ramanan, *Crystal Engineering. A Textbook*, World Scientific Publishing, Singapore, 2011.
10. W. H. Bragg, *Proc. Phys. Soc. London*, 1921, **34**, 33.

11. (a) J. M. Robertson, J. G. White, *J. Chem. Soc.* **1945**, 607; (b) J. M. Robertson, J. G. White, *J. Chem. Soc.* **1947**, 358; (c) J. M. Robertson, *Proc. R. Soc. London*, 1951, **A207**, 101.
12. J. D. Bernal, D. Crowfoot, *J. Chem. Soc.* **1935**, 93.
13. R. Pepinsky, *Phys. Rev.* **1955**, 100, 971.
14. (a) M. D. Cohen, G. M. J. Schmidt, *J. Chem. Soc.* **1964**, 1996; (b) G. M. Schmidt, *J. Pure Appl. Chem.* 1971, **27**, 647.
15. J. D. Dunitz, *Pure Appl. Chem.* 1991, **63**, 177.
16. (a) G. A. Jeffrey, *An Introduction to Hydrogen Bonding*, Oxford University Press, Oxford, 1997; (b) G. A. Jeffrey and W. Saenger, *Hydrogen Bonding in Biological Structures*, Springer, Berlin, 1991.
17. (a) A. I. Kitaigorodskii, *Molecular crystals and molecules*, Academic Press, New York, 1973; (b) A. J. Pertsin and A. I. Kitaigorodskii, *The Atom-Atom Potential Method*, Springer-Verlag, 1987.
18. (a) M. C. Etter, *J. Am. Chem. Soc.*, 1982, **104**, 1095; (b) M.C. Etter, *Acc. Chem. Res.*, 1990, **23**, 120; (c) M. C. Etter, *J. Phys. Chem.*, 1991, **95**, 4601.
19. G. R. Desiraju, *Angew. Chem. Int. Ed. Engl.* 1995, **34**, 2311.
20. O. Ermer, *J. Am. Chem. Soc.*, 1988, **110**, 3747.
21. (a) B. F. Hoskins and R. Robson, *J. Am. Chem. Soc.*, 1990, **112**, 1546; (b) B. F. Hoskins and R. Robson, *J. Am. Chem. Soc.*, 1989, **111**, 5962.
22. (a) D. Philip, J. F. Stoddart, *Angew. Chem. Int. Ed.*, 1996, **35**, 1154; (b) E. Weber (Ed.), *Design of Organic Solids*, Springer-Verlag, Berlin, 1998; (c) M. D. Hollingsworth, *Science*, 2002, **295**, 2410; (d) L. Brammer, *Chem. Soc. Rev.*, 2004, **33**, 476. (e) B. Moulton, M. J. Zaworotko, *Chem. Rev.*, 2001, **101**, 1629; (f) G. R. Desiraju (Ed.), *Crystal Design: Structure and Function, Perspectives in Supramolecular Chemistry*, Vol 7. Wiley & Sons, 2003; (g) E. R. T. Tiekink, J. J. Vittal and M. J. Zaworotko, *Organic Crystal Engineering: Frontiers in Crystal Engineering*, John Wiley & Sons, Ltd., West Sussex, 2010.
23. G. C. Pimentel, A. L. McClellan, *The Hydrogen Bond*. W. H. Freeman and Co., San Francisco, 1960.

24. (a) T. Steiner, W. Saenger, *J. Am. Chem.Soc.* 1993,**115**, 4540; (b) G. R. Desiraju, and T. Steiner, *The Weak Hydrogen Bond in Structural Chemistry and Biology*, 1999; (c) E. Arunan, G. R. Desiraju, R. A. Klein, J. Sadlej, S. Scheiner, I. Alkorta, D. C. Clary, R. H. Crabtree, J. J. Dannenberg, P. Hobza, H. G. Kjaergaard, A. C. Legon, B. Mennucci, D. J. Nesbitt, *Definition of the Hydrogen Bond (IUPAC Recommendations 2011)*. *Pure and Applied Chemistry*, 2011, 83(8).
25. E. J. Corey, *Pure Appl. Chem.* 1967, **14**, 19.
26. (a) E. J. Corey. *Chem. Soc. Rev.*, 1988, **17**, 111; (b) D. Seebach, *Angew Chem Int. Ed. Engl.*, 1990, **29**, 1320.
27. R. D. B. Walsh, M. W. Bradner, S. Fleishman, L. A. Morales, B. Moulton, N. Rodríguez-Hornedo, M. J. Zaworotko, *Chem Commun*, 2003, 186.
28. (a) B. R. Bhogala, S. Basavoju and A. Nangia, *Cryst. Growth Des.*, 2005, **5**, 1683; (b) L. S. Reddy, P. M. Bhatt, R. Banerjee, A. Nangia and G. J. Kruger, *Chem. Asian J.* 2007, **2**, 505; (c) L. S. Reddy, P. M. Bhatt, R. Banerjee, A. Nangia and G. J. Kruger, *Chem. Asian J.* 2007, **2**, 505; (d) V. R. Vangala, R. Mondal, C. K. Broder, J. A. K. Howard and G. R. Desiraju, *Cryst. Growth Des.*, 2005, **5**, 99; (e)) J. A. Bis and M. J. Zaworotko, *Cryst. Growth Des.*, 2005, **5**, 1169; (f) L. S. Reddy, N. J. Babu and A. Nangia, *Chem Commun*, 2006, 1369; (g) N. R. Goud, N. J. Babu and A. Nangia, *Cryst. Growth Des.*, 2011, **11**, 1930.
29. [Definition and classification of Drug or Pharmaceutical Regulatory aspects of drug approval](#) Accessed 30 December 2013.
30. F. Richard, C. Luigi, C. Michelle, *Lippencott's Illustrated Reviews: Pharmacology* 4th Edition. Lippencott Williams & Wilkins. 2009.
31. (a) G. L. Amidon, H. Lennernäs, V. P. Shah and J. R. Crison, *Pharm. Res.*, 1995, **12**, 413; (b) A. Dahan, J. M. Miller and G. L. Amidon, *AAPS Journal*, 2009, **11**, 740; (c) N. A. Kasim, M. Whitehouse, C. Ramachandran, M. Bermejo, H. Lennernäs, A. S. Hussain, H. E. Junginger, S. A. Stavchansky, K. K. Midha, V. P. Shah and G. L. Amidon, *Mol. Pharm.*, 2004, **1**, 85; (d) B. A. Hendriksen, M. V. S. Felix and M. B. Bolger, *AAPS PharmSci.*, 2003, **5**,1.

32. S. Yalkowsky, *Techniques of solubilisation of drugs*, Marcel Dekker New York, 1981.
33. Y. Kawabata, K. Wada, M. Nakatani, S. Yamada, S. Onoue. *Int. J. Pharm. Sci.* 2011, **420**, 1.
34. (a) N. Schultheiss and A. Newman, *Cryst. Growth Des.*, 2009, **9**, 2950; (b) N. K. Duggirala, M. L. Perry, Ö. Almarsson and M. J. Zaworotko, *Chem. Commun.*, 2016, **52**, 640; (c) G. Bolla and A. Nangia, *Chem. Commun.*, 2016, DOI: 10.1039/C6CC02943D.
35. (a) J. Bernstein, *Polymorphism in Molecular Crystals*; Clarendon, Oxford, U. K., 2002; (b) J. Halebian and W. McCrone, *J. Pharm. Sci.*, 1969, **58**, 911; (c) H. G. Brittain, *Polymorphism in Pharmaceutical Solids*, Informa Health Care, New York, 2009.
36. (a) E. Mitscherlich, *Abhl. Akad. Berlin*, 1822, 43; (b) J. Berzelius, *Jahresbericht*, 1844, **23**, 44. (c) R. Purohit and P. Venugopalan, *Resonance*, 2009, 882.
37. (a) G. P. Stahly *Crystal Growth Des.* 2007, **7**, 1007; (d) J. W. Steed, *Trends in Pharmacological Sciences*, 2013, **34**, 185; (b) D. Braga, F. Grepioni, *Chem. Commun.* 2005, 3635. (b) B. Rodriguez-Spong, C. P. Price, A. Jayasankar, A. J. Matzger, N. Rodríguez-Hornedo, *Adv. Drug Deliv. Rev.* 2004, **56**, 241; (d) Halebian, J.; McCrone, W. 1969, **58**, 911; (e) Borka, L. *Acta Pharma Jugosl*, 1990, **40**, 70.
38. (a) Wohler, F.; von Liebig, *J. Ann. Pharm.* 1832, **3**, 249; (b) D. Grillo, G. Polla, D. Vega, *J. Pharm. Sci.* 2012, **101**, 541; (b) W. W. Porter III, S. C. Elie and A. J. Matzger, *Cryst. Growth Des.*, 2008, **8**, 14; (c) J. Thun, L. Seyfarth, C. Butterhof, J. Senker, R. E. Dinnebier, J. Breu, *Angew. Chem. Int. Ed.* 2007, **46**, 6729.
39. (a) S. R. Byrn, R. R. Pfeiffer and J. G. Stowell, *Solid-State Chemistry of Drugs*; SSCI, West Lafayette, IN, 1999; (b) J. D. Mullins and T. J. Macek, *J. Pharm. Sci.*, 1960, **49**, 245; (c) <http://www.drugs.com/ppa/darunavir-ethanolate.html>
40. A. Nangia and G. R. Desiraju, *Chem Commun.*, 1999, 605-606.
41. (a) A. Nangia, *Acc. Chem. Res.*, 2008, **41**, 595; (b) D. E. Braun, T. Gelbrich, V. Kahlenberg, G. Laus, J. Wieser and U. J. Griesser, *New J Chem.*, 2008, **32**, 1677.
42. (a) A. Cruz-Cabeza, J. Bernstein, *Chem. Rev.* 2014, **114**, 2170; (b) S.S. Kumar and A. Nangia, *CrystEngComm*, 2013, **15**, 6498; (c) B. Swapna, K. Suresh and

- A. Nangia, *Chem. Commun.*, 2016, **52**, 4037; (d) N. J. Babu, S. Cherukuvada, R. Thakuria and A. Nangia *Cryst. Growth Des.*, 2010, **10**, 1979.
43. (a) P. K. Thallapally, R. K. R. Jetti, A. K. Katz, H. L. Carrell, K. Singh, K. Lahiri, S. Kotha, R. Boese and G. R. Desiraju, *Angew. Chem. Int. Ed.*, 2004, **43**, 1149; (b) D. Das and L. J. Barbour, *J. Am. Chem. Soc.*, 2008, **130**, 14032; (c) C. A. Mitchell, L. Yu and M. D. Ward, *J. Am. Chem. Soc.*, 2001, **123**, 10830; (d) A. V. Trask, N. Shan, W. D. S. Motherwell, W. Jones, S. Feng, R. B. H. Tan and K. J. Carpenter, *Chem. Commun.* 2005, 880; (e) N. K. Nath, H. Aggarwal and A. Nangia, *Cryst. Growth Des.*, 2011, **11**, 967; (f) A. Bouchard, N. Jovanović, G. W. Hofland, E. Mendes, D. J. A. Crommelin, W. Jiskoot and G. Witkamp, *Cryst. Growth Des.*, 2007, **7**, 1432.
44. (a) P. Sanphui, N. R. Goud, U. B. R. Khandavilli, S. Bhanoth and A. Nangia, *Chem Commun*, 2011, **47**, 5013; (b) L. H. Thomas, C. Wales and C. C. Wilson, *Chem Commun*, 2016. DOI: 10.1039/C6CC01027J.
45. W. F. Ostwald, *Z. Phys. Chem.*, 1897, **22**, 289.
46. (a) G. R. Desiraju, *Nature Materials*, 2002, **1**, 77; (b) D. Sisak, L. B. McCusker, G. Zandomenigi, B. H. Meier, D. Blaser, R. Boese, W. B. Schweizer, R. Gilmour and J. D. Dunitz, *Angew. Chem. Int. Ed.*, 2010, **45**, 4503.
47. (a) G. R. Desiraju (Ed.), *Crystal Design: Structure and Function, Perspectives in Supramolecular Chemistry*, Vol 7. Wiley & Sons, 2003; (b) E. Weber (Ed.), *Design of Organic Solids*, Springer-Verlag, Berlin, 1998; (c) M. D. Hollingsworth, *Science*, 2002, **295**, 2410; (d) B. Kratochvil, J. Novotny, M. Husak, J. Had, J. Stuchlik and A. Jogorov, *Collect. Czech. Chem. Commun.*, 1994, **59**, 149; (e) A. L. Bingham, D. S. Hughes, M. B. Hursthouse, R. W. Lancaster, S. Travenner and T. L. Threlfall, *Chem Commun.*, 2001, 603; (f) M. Suzuki and K. Kobayashi, *Cryst. Growth Des.*, 2011, **11**, 1814.
48. (b) J. Bernstein, R. J. Davey and J. -O. Henck, *Angew. Chem., Int. Ed.*, 1999, **38**, 3440; (b) S. Cherukuvada, R. Thakuria and A. Nangia, *Cryst. Growth Des.*, 2010, **10**, 3931.
49. (a) B. Kratochvil, J. Novotny, M. Husak, J. Had, J. Stuchlik and A. Jogorov, *Collect. Czech. Chem. Commun.*, 1994, **59**, 149; (b) A. L. Bingham, D. S. Hughes, M. B. Hursthouse, R. W. Lancaster, S. Travenner and T. L. Threlfall, *Chem Commun.*, 2001, 603. (c) M. Suzuki and K. Kobayashi, *Cryst. Growth*

- Des.*, 2011, **11**, 1814; (d) S. Roy, N. R. Goud, N. J. Babu, J. Iqbal, A. K. Kruthiventi, A. Nangia, *Cryst. Growth. Des.* 2008, **8**, 4343.
50. (a) M. R. Caira, E. W. Pienaar and A. P. Lötter, *Mol. Cryst. Liq. Cryst.*, 1996, **279**, 241. (b) J. Lin, D. Ostovic and J. Vacca, *Pharm. Biotechnol.*, 1998, **11**, 233-255; (c) http://www.gsk.com.au/resources.ashx/prescriptionmedicinesproductschilddatap/roinfo/1580/FileName/1FEC0F4C187D4D00DDE44D79CF7C72EA/Aropax_PI_007_approved.pdf (d) <https://newdrugapprovals.org/2014/10/21/pranlukast/>
51. (a) Y. Qiu; Y. Chen and G. G. Z. Zhang, Eds., *Developing Solid Oral Dosage Forms. Pharmaceutical Theory and Practice*, Academic Press, New York, 2009; (b) N. J. Babu and A. Nangia, *Cryst. Growth Des.*, 2011, **11**, 2662.
52. (a) G. S. Paulekuhn, J. B. Dressman and C. Saal, *J. Med. Chem.* 2007, **50**, 6665; (b) N. R. Goud, K. Suresh and A. Nangia, *Cryst. Growth Des.*, 2013, **13**, 1590; (c) L. Rajput *Cryst. Growth Des.* 2014, **14**, 5196.
53. (a) P. L. Gould, *Int. J. Pharm.*, 1986, **33**, 201; (b) T. Vasconcelos, B. Sarmento and P. Costa, *Drug Disc. Today*, 2007, **12**, 1068; (c) S. Janssens, C. Roberts, E. F. Smith and G. V. Mooter, *Int. J. Pharm.*, 2008, **355**, 100; (d) A. Fahr and X. Liu, *Expert Opin. Drug Deliv.*, 2007, **4**, 403; (e) H. Bhutani, S. Singh, K. C. Jindal and A. K. Chakraborti, *J. Pharm. Biomed. Anal.*, 2005, **39**, 892; (f) S. Singh and B. Mohan, *Int. J. Tuberc. Lung Dis.*, 2003, **7**, 298.
54. <http://www.fda.gov/Food/IngredientsPackagingLabeling/GRAS/> (accessed on 15/03/2015:
55. A. Srinivasulu *et. al.* *Cryst. Growth Des.* 2012, **12**, 2147.
56. (a) P. Vishweshwar, J. A. McMahon, J. A. Bis and M. J. Zaworotko, *J. Pharm. Sci.*, 2006, **95**, 499; (b) C. B. Aakeröy, S. Forbes and J. Desper, *J. Am. Chem. Soc.*, 2009, **132**, 17048; (c) A. Alhalaweh and S. P. Velaga, *Cryst. Growth Des.*, 2010, **10**, 3302. (d) A. B. M. Buanz, R. Telford, I. J. Scowen and S. Gaisford, *CrystEngComm*, 2013, **15**, 1031; (e) M. D. Eddleston, S. Sivachelvam and W. Jones, *CrystEngComm*, 2013, **15**, 175; (f) M. K. Stanton, R. C. Kelly, A. Colletti, Y.-H. Kiang, M. Langley, E. J. Munson, M. L. Peterson, J. Roberts and M. Wells, *J. Pharm. Sci.*, 2010, **99**, 3769.
57. (a) J. C. Krantz, J. M. Holbert, H. K. Iwamoto and C. J. Carr, *J. Am. Pharm. Assoc.*, 1947, **36**, 248; (b) S. L. Childs, L. J. Chyall, J. T. Dunlap, V. N.

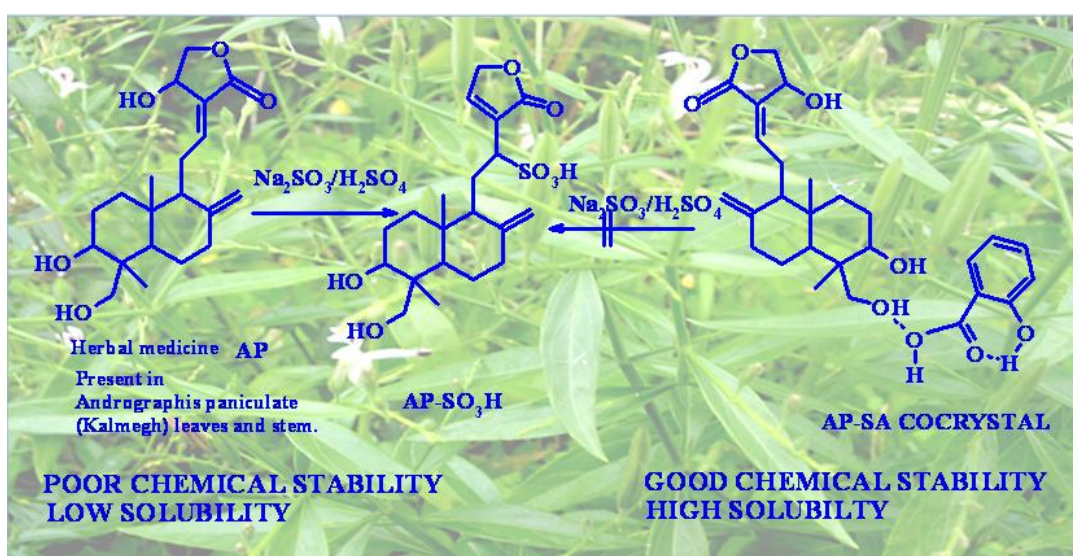
- Smolenskaya, B. C. Stahly and G. P. Stahly, *J. Am. Chem. Soc.*, 2004, **126**, 13335.
58. F. Wohler, *Annalen*, 1844, **51**, 145.
59. (a) F. H. Roche, Basel (Switzerland), CH 1878, **26**, 1937; (b) A. Lemmerer, J. Bernstein, U. J. Griesser, V. Kahlenberg, D. M. Tobbens, S. H. Lapidus, P. W. Stephens and C. Esterhuysen, *Chem.Eur. J.*, 2011, **17**, 13445.
60. (a) Mead, *J. Am. J. Nursing* 1963, **63**, 131; (b) D.O' Nolan, M.L. Perry, and M. J. Zaworotko, *Cryst. Growth Des.* 2016, **16**, 2211.
61. (a) P. Sanphui, N. R. Goud, U. B. R. Khandavilli, and A. Nangia, *Cryst. Growth Des.* 2011, **11**, 4135; (b) M. R. Shimpi, S. L. Childs, D. Boström and S. P. Velaga, *CrystEngComm*, 2014, **16**, 8984
62. (a) S. Cherukuvada and A. Nangia, *J. Pharm. Sci.*, 2011, **100**, 3233; (b) A. V. Trask, W. D. S. Motherwell, and W. Jones *Cryst. Growth Des.*, 2005, **5**, 1013; (c) Y. Gao, J. Gao, Z. Liu, H. Kan, H. Zu, W. Sun, J. Zhang, S. Qian, *Int. J. Pharm. Sci.*, 2012, **438**, 327; (d) N. J. Babu, P. Sanphui, A. Nangia, *Chem. Asian J.*, 2012, **7**, 2274; (e) E. Sravani, M. K. C. Mannava, D. Kaur, B. R. Annapurna, R. A. Khan, K. Suresh, S. Mittapalli, A. Nangia and B. D. Kumar, *Curr. Sci.*, 2015, **108**, 1097.
63. N. R. Goud, R. A. Khan and A. Nangia, *CrystEngComm*, 2014, **16**, 5859.
64. (a) P. Y. Bruice, *Organic Chemistry*, fourth edition, 2004; (b) Petrucci, Harwood, Herring, Madura. *General Chemistry Principles & Modern Applications*. Prentice Hall. New Jersey, 2007.
65. (a) <http://www.fda.gov/downloads/Drugs/.../Guidances/UCM281764.pdf>. Accessed 15-05-2016; (b) http://www.ema.europa.eu/docs/en_GB/document_library/Scientific_guideline/2015/07/WC500189927.pdf Accessed 15-05-2016.
66. (a) S, Cherukuvada and A. Nangia, *CrystEngComm*, 2012, **14**, 2579; (b) N. R. Goud, K. Suresh, P. Sanphui and A. Nangia, *Int. J. Pharm.*, 2012, **439**, 63; (c) D. R. Askeland and P. P. Fulay, *Essentials of Materials Science and Engineering*, 2nd ed., Cengage Learning, 2009; (d) W. D. Callister Jr., *Fundamentals of Materials Science and Engineering*, John Wiley & Sons, 2001; (e) D. M. Stefanescu, *Science and Engineering of Casting Solidification*, 2nd Ed., Springer, 2009.

67. S. Cherukuvada and A. Nangia, *Chem. Commun.*, 2014, **50**, 906
68. (a) T. Proffen, K. L. Page, S. E. McLain, B. Clausen, T. W. Darling, J. A. Tencate, S. Y. Lee, E. Ustundag, *Z. Kristallogr.* 2005, **220**, 1002; (b) V. Petkov, M. Gateshki, J. Choi, E. G. Gillan, Y. Ren, *J. Mater. Chem.*, 2005, **15**, 4654; (c) A. M. Beale and B. M. Weckhuysen, *Phys. Chem. Chem. Phys.*, 2010, **12**, 5562; (d) S. Cammelli, D. L. Hecht, C. Degueldre, J. Bertsch and R. Frahm, *J. Phys. Conf. Ser.*, 2009, **190**, 12027.
69. (a) M. Bi, S. -J. Hwang and K. R. Morris, *Ther. Acta*, 2003, **404**, 213; (b) W. L. Chiou and F. Niazi, *J. Pharm. Sci.*, 1976, **65**, 1212; (c) C. W. Park, H. M. Mansour, T. O. Oh, J. Y. Kim, J. M. Ha, B. J. Lee, S. C. Chi, Y. S. Rhee and E. S. Park, *Int. J. Pharm.*, 2012, **436**, 652-658.
70. (a) K. Sekiguchi and N. Obi, *Chem. Pharm. Bull.*, 1961, **9**, 866; (b) K. Sekiguchi and N. Obi, *Chem. Pharm. Bull.*, 1964, **12**, 134; (c) A. H. Goldberg, M. Gibaldi and J. L. Kanig, *J. Pharm. Sci.*, 1965, **54**, 1145; (d) T. J. Dr Bonain, an ENT surgeon with an ocean background. *B-ENT*. 2007, **3**, 217; (e) M. A Jyvakorpi., *Eur Arch Otorhinolaryngol.* 1996, **253**, 234; (f) U. Gala, M.C. Chuong, R. Varanasi, and H. Chauhan, *AAPS PharmSciTech*, 2015, **16**, 528; (g) B. F. J. Broberg and H. C. A. Evers, *US Pat.*, 4529601, 1985.
71. (a) S. P. Thomas, R. Sathishkumar and T. N. G. Row *Chem. Commun.*, 2015, **51**, 14255; (b) T. Friščić, A.V. Trask, W. Jones and W. D. S. Motherwell, *Angew. Chem. Int. Ed.*, 2006, **45**, 7546; (c) A. A. Bredikhin, Z. A. Bredikhina, D. V. Zakharychev, A. T. Gubaidullin and R. R. Fayzullin *CrystEngComm*, 2012, **14**, 648; (d) K. D. Prasad, S. Cherukuvada, L. D. Stephen and T.N. Guru Row. *CrystEngComm*, 2014, **16**, 9930. (e) A. Delori, P. Maclure, R. M. Bhardwaj, A. Johnston, A. J. Florence, O. B. Sutcliffe, and Iain D. H. Oswald, *CrystEngComm*, 2014, **16**, 5827 (f) T. Hasell, S. Y. Chong, M. Schmidtman, D.J. Adams, and A. I. Cooper, *Angew. Chem. Int. Ed.* 2012, **51**, 7154. (g) M. Dabros, P. R. Emery, and V. R. Thalladi. *Angew. Chem. Int. Ed.* 2007, **46**, 4132.
72. (a) L. R. Hilden and K. R. Morris, *J. Pharm. Sci.*, 2004, **93**, 3; (b) L. Yu, *Adv. Drug Deliv. Rev.*, 2001, **48**, 27; (c) R. Thakuria and A. Nangia, *CrystEngComm*, 2011, **13**, 1759; (d) J. F. Willart and M. Descamps, *Mol. Pharmaceutics*, 2008, **5**, 905.
73. (a) P. H. Poole, T. Grande, C. A. Angell and P. F. McMillan, *Science*, 1997, **275**, 322; (b) J. Kieffer, *J. Phys. Chem., B* 1999, **103**, 4153.

74. (a) D. Mishima, L. E. Calvert and E. Whalley, *Nature*, 1984, **310**, 393. (b) J. P. Johari, A. Hallbrucker and E. Mayer, *Nature*, 330, **1987**, 552; (b) T. Y. Nguyen, K. Rademann and F. Emmerling, *CrystEngComm*, 2015, **17**, 9029.
75. (a) N. Chieng, J. Aaltonen, D. Saville, T. Rades, *Eur. J. Pharm. and Biopharm.* 2009, **71**, 47; (b) M. Allesø, N. Chieng, S. Rehder, J. Rantanen, T. Rades, J. Aaltonen, *J. Cont. Rel.* 2009, 136, 45.
76. (a) K. Löbmann, R. Laitinen, H. Grohgan, C. J. Strachan, T. Rades, *Mol. Pharmaceutics*. 2011, **8**, 1919; (b) R. Laitinen, K. Löbmann, C. J. Strachan, H. Grohgan, T. Rades, *Int. J. Pharm. Sci.* 2013, **453**, 65.
77. L. R. Hilden and K. R. Morris, *J. Pharm. Sci.* 2004, **93**, 3.
78. (a) K. Löbmann, H. Grohgan, R. Laitinen, C. Strachan, T. Rades *Eur. J. Pharm. Biopharm.* 2013, **85**, 873; (b) K. Löbmann, R. Laitinen, C. Strachan, T. Rades, H. Grohgan, *Eur. J. Pharm. Biopharm.* 2013, **85**, 882; (c) K. T. Jensen, F. H. Larsen, C. Cornett, K. Löbmann, H. Grohgan, and T. Rades *Mol. Pharmaceutics*, 2015, **12**, 2484
79. (a) S. Qian, W. Heng, Y. Wei, J. Zhang, and Y. Gao, *Cryst. Growth Des.* 2015, **15**, 2920. (b) K. Löbmann, C. Strachan, H. Grohgan, T. Rades, O. Korhonen, R. Laitinen, *Eur. J. Pharm. Biopharm.* 2012, **81**, 159.
80. S. J. Dengale, H. Grohgan, T. Rades, K. Löbmann *Adv. Drug Deliv. Rev.* 2016, **100**, 116.

CHAPTER TWO

Andrographolide: Solving Chemical Instability and Poor Solubility By Means of Cocrystal



Andrographolide, the active principal of the Indian plant Kalmegh, is chemically stabilized in the cocrystal with salicylic acid and its solubility improved to make a bioavailable drug of the herbal ingredient used in traditional medicine. The inhibition of Andrographolide transformation to its inactive sulfate metabolite is ascribed to the lower pK_a of salicylic acid compared to the other coformers studied.

2.1 Introduction

Crystal engineering principles and hydrogen bonding rules are the primary design elements for the synthesis of cocrystals with predictable and robust supramolecular synthons.¹ Studies on cocrystals with tailor made properties find immediate applications in diverse areas such as pharmaceuticals,² optical materials,³ explosives,⁴ and synthetic chemistry⁵ while maintaining the chemical integrity of the chemical substance. The structural diversity of solids that can be generated from drug/organic molecule greatly increases through cocrystallization and the physicochemical properties of the cocrystals can vary depending on the characteristics of its constituent molecules in crystal lattice.⁶ Specifically pharmaceutical cocrystals (Drug + GRAS or nutraceutical coformer in crystal lattice) as improved medicines have created tremendous interest because of pharmaceutical relevant properties such as mechanical property, solubility, dissolution rate, physical/chemical stability, moisture uptake, permeability, and bioavailability etc. that can modulate/improve via cocrystallization.⁷ Categorically low solubility quadrant classified under the Biopharmaceutics Classification System (BCS) of Class II or IV and many bioactive molecules offers an ideal situation for the application cocrystallization methodology to improve the solubility and bioavailability. Extensively cocrystals provide the advantages of generating solid forms of API/bioactive molecules which lack ionizable functionalities.⁸ In the literature, pharmaceutical cocrystals more widely appreciated by the solubility improvement of poorly soluble drugs^{2f,6,7} and bioactive molecules.⁸ Similar to other solid forms of APIs, cocrystals not only provide a methodology for an improvement of physicochemical property, but also provide an opportunity to the intellectual property and patent protection.

J. F. Remenar and coworkers,^{7a} improved the solubility of itraconazole antifungal drug by forming cocrystals with GRAS 1,4 di-carboxylic acids. They showed that itraconazole-L-malic acid cocrystal exhibits 20 folds faster dissolution rate than itraconazole in 0.1N HCl (pH1.2) medium and comparable solubility as a crystalline phase to that of the marketed amorphous form (as solid dispersion itraconazole sporanox beads in capsule form). In another report, Aakeröy and coworkers shown that anticancer hexamethylenebisacetamide drug forming a cocrystal with succinic acid coformer shown higher equilibrium solubility in water.^{7b} Nangia and coworkers^{7c} enhanced the poor dissolution rate of furosemide (BCS class IV) by forming a cocrystal with nicotinamide,

which exhibited 2.6 times higher IDR compared to furosemide in 10% EtOH-water solution.

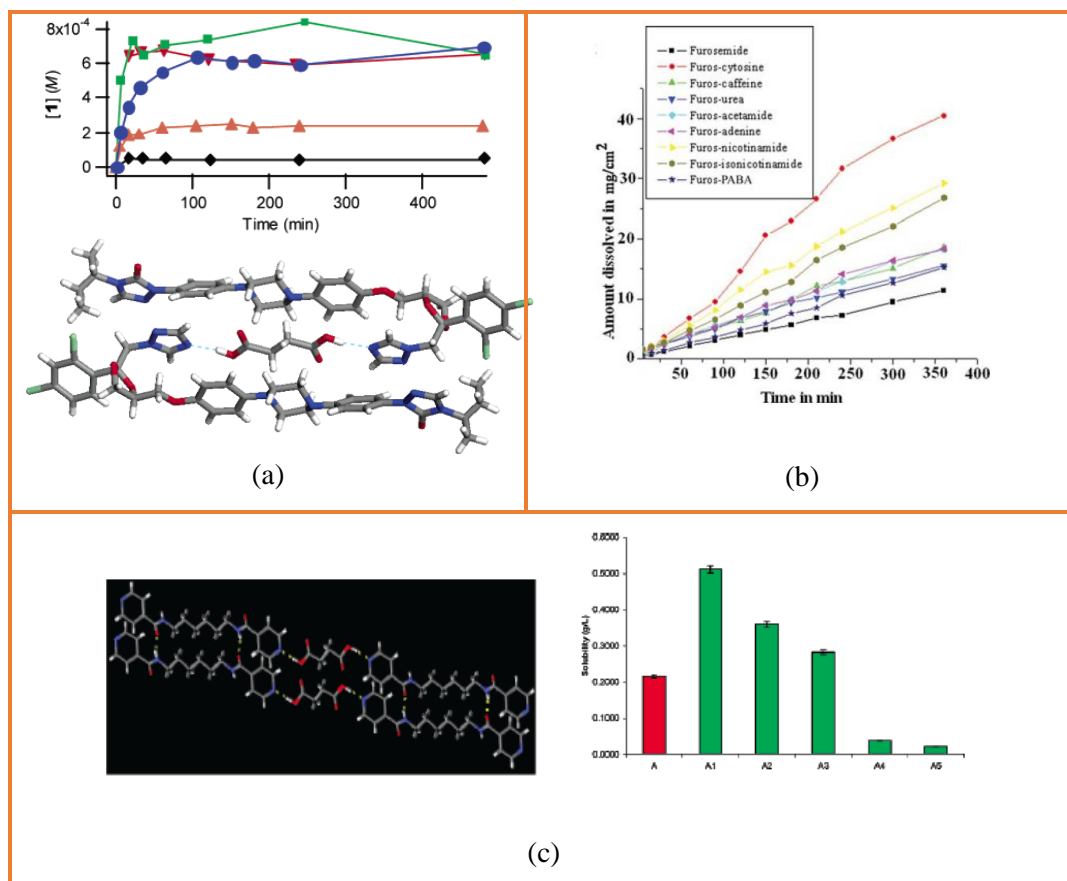


Figure 2.1 (a) Dissolution profiles into 0.1 N HCl medium at 25 °C for itraconazole cocrystals. Among these, itraconazole-L-malic acid cocrystal showed 20 times higher dissolution (green color) than crystalline itraconazole and in crystal structure both API and coformer sustained by $N \cdots H-O$ interaction. (b) dissolution curve of furosemide and its cocrystals for up to 6h and here furosemide-nicotinamide showed high dissolution rate (yellow color line). (c) 2D sheet in the crystal structure of hexamethylenebisacetamide-succinic acid cocrystal interacted through $O-H \cdots N$ and $N-H \cdots O$ hydrogen bonds and its equilibrium solubility in aqueous medium (green color A1).

Apart from the solubility and dissolution rate enhancement, other applications of pharmaceutical cocrystals are improvement in tableting behavior,⁹ color and photostability,¹⁰ and hydration control.¹¹ The antipyretic drug paracetamol has poor tableting property and to address this issue W. Jones and coworkers^{9a} have shown that cocrystallization of paracetamol with oxalic acid and theophylline coformers has significantly improved its tabletability. R.B.H Tan and coworkers^{10a} have been reported

the remarkable improvement of physical and photo stability of nitrofurantoin drug by forming a cocrystal with 4-hydroxybenzoic acid coformer. They showed that nitrofurantoin transformed to hydrate within in a week during the stability studies at 40 °C and 75% RH (relative humidity) of accelerated ICH (International Conference harmonization) conditions and while in its cocrystal no phase change or dissociation was observed during 13 weeks of storage analyzed by PXRD technique. In addition, this cocrystal also showed superior photo stability than nitrofurantoin. Nangia and coworkers^{11a} improved the hydrolytic stability of temozolomide drug by forming cocrystals with oxalic acid and succinic acid. They highlighted that, temozolomide was degraded within a week during stability studies at accelerated ICH conditions of 40°C and 75% RH; its cocrystals were intact for 28 weeks. Furthermore hydration problem of caffeine was addressed by Trask et. al^{11d} via cocrystallization with oxalic acid. With these literature reports, in this chapter we highlight, cocrystallization methodology is a viable platform where salt formation is not an option due to lack of ionizable functionalities of andrographolide (AP) herbal molecule for improving the chemical stability and solubility.

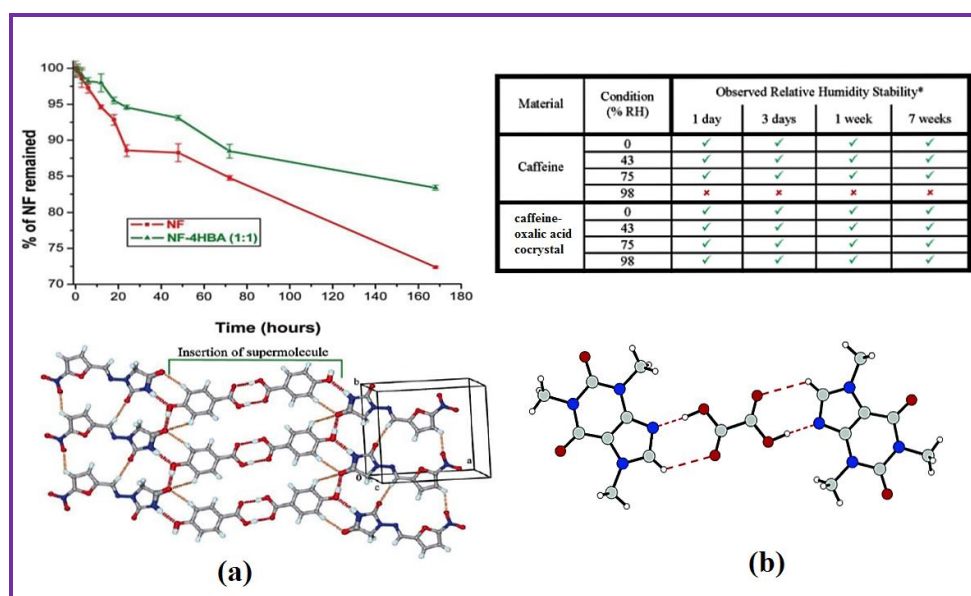
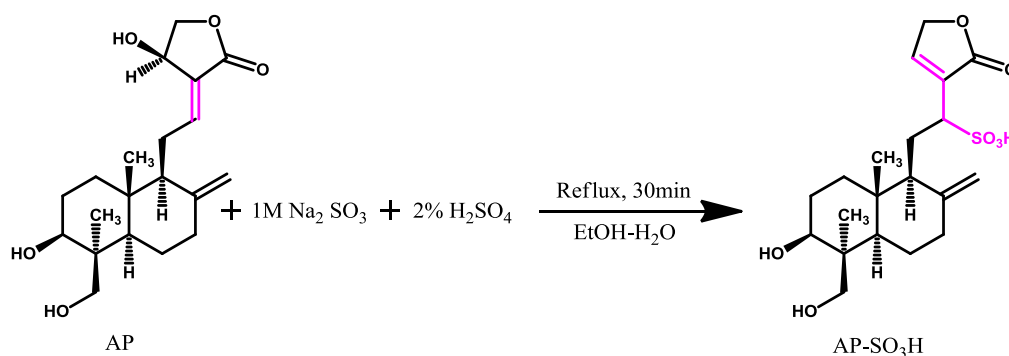


Figure 2.2 (a) nitrofurantoin and 4-hydroxybenzoic acid together through N–H···O and C–H···O hydrogen bonds and it is shown good photo stability than nitrofurantoin. (b) in cocrystal, caffeine and oxalic acid associated via N–H···O and C–H···O hydrogen bonds and it is shown greater hydration stability than pure caffeine.

2.2 Literature reports on andrographolide

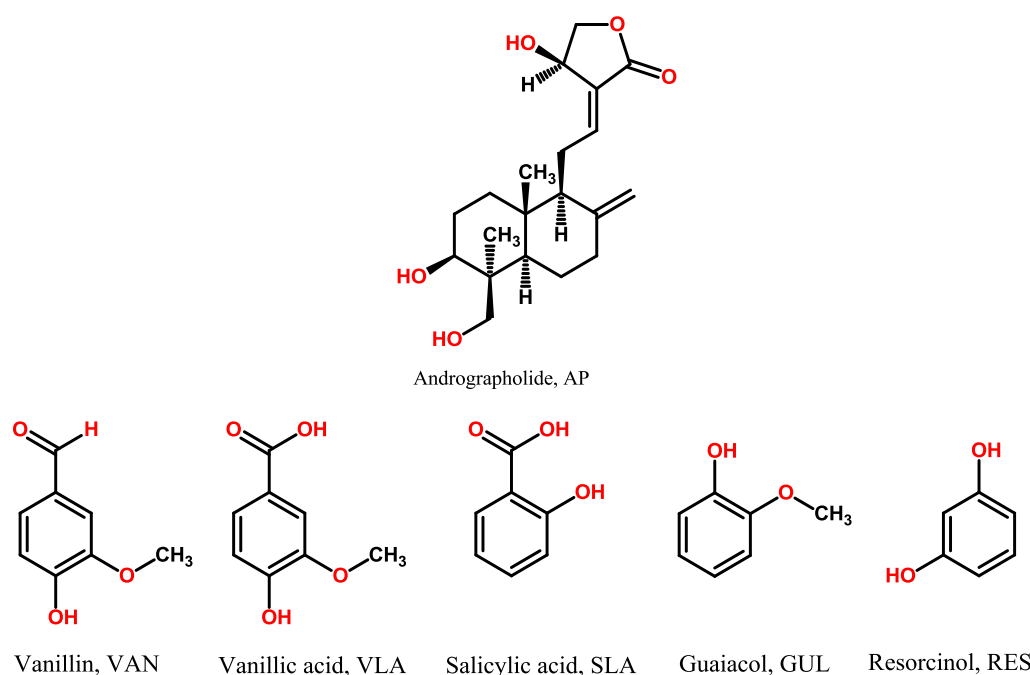
Andrographolide (AP) is a bioactive diterpenoid lactone used in traditional medicine in China, India and Southeast Asian countries.¹² It is derived from the leaves of *Andrographis Paniculata*, a plant known as “King of Bitters”, in the acanthaceae family and the local plant name in India is Kalmegh. AP is known for its diverse pharmacological activities, such as anti-viral, anti-inflammatory, anti-cancer, and anti-malarial.¹³ Despite being safe at high doses of 17 g/kg per day in humans, the efficacy of AP is limited in clinical application by poor aqueous solubility (46 mg/L) and oral bioavailability of 2.67% (reported in rats).¹⁴ A significant drop in the bioavailability of AP is due to an inactive metabolism, as a result four inactive metabolites isolated from humans and rats. Three of the AP metabolites are isomers/diastereomers of 14-deoxy-12-sulfo-andrographolide, and the fourth product is the S-conjugate (sulfated derivative) of AP.^{15a} Among these, the main inactive metabolite of AP was identified as 14-deoxy-12-(*R*)-sulfo-andrographolide and Yao et al. developed an in vitro synthetic method that mimics the in vivo biotransformation and isolated the main metabolite 14-deoxy-12-(*R*)-sulfo-andrographolide (Scheme 2.3) have been studied by NMR spectroscopy and mass spectrometry.^{15b} Cambridge Structural Database (CSD) search on AP, no polymorphs, solvates/hydrates, or cocrystals are disclosed, only one crystal structure is reported.^{16a,b}



Scheme 2.3 Chemical transformation of AP to its main metabolite 14-deoxy-12-(*R*)-sulfo-andrographolide, AP-SO₃H. The chemically reactive moiety is shown in color (magenta).

2.3 Preparation of andrographolide cocrystals

In order to inhibit the above chemical transformation (scheme 2.3) and improves the solubility of AP, we have explored the structural landscape via cocrystallization methodology with an idea that the resulting pharmaceutical cocrystals would have the appropriate hydrogen bonding patterns for improving the chemical stability and solubility of the AP which is leading to better therapeutic efficacy. Using liquid assisted grinding (LAG)¹⁷ and isothermal crystallization techniques we have screened AP with various GRAS coformers of phenols and carboxylic acids, which resulted in cocrystals with Vanillin (VAN), Vanillic acid (VLA), Salicylic acid (SLA), Resorcinol (RES), and Guaiacol (GUL) (Scheme 2.4). These cocrystals were characterized by various thermal, spectroscopic and diffraction methods. The implications of cocrystal formation on the chemical stability and solubility of AP are discussed in this chapter.



Scheme 2.4 Andrographolide and coformers discussed in this study. Compound abbreviations are used throughout the paper.

2.4 Results and Discussion

The selection of coformers for the supramolecular design cocrystals of an API/bioactive agent is primarily based on the functional groups, so as to maximize the strong and robust heterosynthons. AP has three hydroxyl groups and in literature coformers containing C=O, COOH and OH functional groups were chosen to form synthons with hydroxyl group containing molecule. Therefore, in order to obtain cocrystals, we combined AP with coformers containing above functional groups are complementary to give strong O–H...O hydrogen bonds in the cocrystal. A complete list of all the coformers used to form cocrystals is shown in the experimental section (Table 2.10). Liquid-assisted grinding¹⁷ of AP with Vanillin (VAN), Vanillic acid (VLA), Salicylic acid (SLA), Resorcinol (RES), and Guaiacol (GUL) gave a unique powder pattern as confirmed by PXRD. Upon dissolving this material in different solvents or mixture of solvents and standing the solution for slow evaporation resulted in single crystals of 1:1 stoichiometry cocrystal in each case. Crystallographic parameters are listed in Table 2.1 and hydrogen bond distances in Table 2.2.

Table 2.1 Crystallographic parameters of AP cocrystals

	AP–VAN	AP–VLA	AP–SLA	AP–GUL	AP–RES
Emp. form.	C ₂₈ H ₃₈ O ₈	C ₂₈ H ₃₈ O ₉	C ₂₇ H ₃₆ O ₇	C ₂₇ H ₃₈ O ₇	C ₂₆ H ₃₆ O ₇
Form. wt	502.58	518.58	488.56	474.57	460.55
Cryst. syst.	Monoclinic	Monoclinic	Monoclinic	Monoclinic	Monoclinic
Sp. Gr.	<i>P</i> 2 ₁	<i>P</i> 2 ₁	<i>P</i> 2 ₁	<i>P</i> 2 ₁	<i>P</i> 2 ₁
<i>T</i> (K)	100(2)	298(2)	298(2)	298(2)	298(2)
<i>a</i> (Å)	10.2515(18)	10.3343(4)	10.576(6)	10.4954(6)	10.3340(11)
<i>b</i> (Å)	12.468(2)	12.6800(4)	12.923(6)	12.8025(7)	11.6243(11)
<i>c</i> (Å)	11.0827(19)	11.3675(5)	10.544(7)	10.7318(7)	10.5375(10)
α (°)	90	90	90	90	90
β (°)	114.246(2)	113.201(5)	114.99(7)	117.962(8)	108.050(11)
γ (°)	90	90	90	90	90
<i>Z</i>	2	2	2	2	2
<i>V</i> (Å ³)	1291.6(4)	1369.11(9)	1306.1(13)	1273.65(13)	1203.5(2)
Rflns. Collect.	13278	5577	4567	5303	4300
Unique. Rflns.	5061	3946	3390	3937	3110
Obsd. Rflns.	4882	2779	1352	2938	1386
Parameters	356	342	330	325	303
<i>R</i> ₁	0.0397	0.0401	0.0651	0.0361	0.0823
w <i>R</i> ₂	0.0985	0.0795	0.1026	0.0800	0.0860
GOF	1.035	0.892	0.863	0.923	0.872
Diffractionmeter	Bruker Smart Apex	Oxford Xcalibur Gemini	Oxford Xcalibur Gemini	Oxford Xcalibur Gemini	Oxford Xcalibur Gemini

Table 2.2 Normalized hydrogen bond distances and angles in AP cocrystals (neutron-normalized O–H and C–H distance).

D–H...A	D...A (Å)	H...A (Å)	D–H...A (°)	Symmetry code
AP–VAN				
O1–H1...O3	2.719(2)	1.85	171	–1+x,y,z
O2–H2C...O1	2.6067(19)	1.87	147	--- ^a
O3–H3C...O5	2.755(2)	1.99	147	3–x,1/2+y,2–z
O8–H8C...O7	2.670(2)	2.27	111	--- ^a
O8–H8C...O2	2.635(2)	1.89	154	–x,–1/2+y,1–z
C15–H15A...O5	3.199(6)	2.51	127	3–x,1/2+y,2–z
C18–H18B...O6	3.431(2)	2.58	144	x,y,–1+z
C19–H19C...O1	2.940(7)	2.52	106	--- ^a
C25–H25...O5	3.524(1)	2.60	165	–2+x,y,z
C27–H27...O2	3.280(7)	2.43	148	x,y,1+z
AP–VLA				
O1–H1C...O3	2.738(3)	1.94	163	1+x,y,z
O2–H2C...O1	2.591(2)	1.91	140	--- ^a
O3–H3C...O5	2.778(3)	1.97	170	–1–x,–1/2+y,–z
O7–H7C...O2	2.676(3)	1.89	159	1–x,–1/2+y,2–z
O9–H9C...O2	2.722(3)	2.01	146	–1+x,y,z
O9–H9C...O8	2.666(3)	2.22	114'	--- ^a
C19–H19A...O1	2.933(3)	2.53	105	--- ^a
C26–H26...O7	2.710(4)	2.40	100	--- ^a
AP–SLA				
O1–H1C...O2	2.595(7)	1.96	133	--- ^a
O2–H2C...O3	2.807(8)	2.03	157	1+x,y,z
O3–H3C...O5	2.803(8)	2.24	127	–1–x,1/2+y,–z
O7–H7C...O1	2.579(10)	1.75	171(5)	1–x,–1/2+y,1–z
O8–H8C...O6	2.582(10)	1.86	147	--- ^a
C14–H14...O7	3.334(11)	2.52	140	–x,1/2+y,–z
C15–H15A...O8	3.364(12)	2.45	158	–1–x,1/2+y,1–z
C19–H19C...O	2.895(10)	2.53	103	--- ^a
C24–H24...O6	3.236(3)	2.66	120	x–1, +y, +z
C24–H24...O1	3.460(3)	2.70	138	–x, +y+1/2, –z+2
AP–GUL				
O1–H1C...O3	2.796(2)	1.98	173	1+x,y,z
O2–H2C...O1	2.662(2)	1.91	145	--- ^a
O3–H3C...O5	2.789(2)	2.01	158	–1–x,–1/2+y,–z
O6–H6C...O7	2.646(3)	2.20	115	--- ^a
O6–H6C...O2	2.728(3)	1.98	152	2–x,1/2+y,1–z
C14–H14...O6	3.290(3)	2.56	131	1–x, –1/2+y, –z
C15–H15A...O6	3.330(3)	2.60	133	1–x, –1/2+y, –z
C19–H19A...O1	2.904(3)	2.49	106	--- ^a
AP–RES				
O3–H3C...O4	3.138(5)	2.47	139	–1–x,1/2+y, –z
O3–H3C...O5	3.020(4)	2.28	150	–1–x,1/2+y, –z

O24–H24···O23	2.735(4)	2.07	165	1+x,y,z
O2–H2C···O1	2.617(7)	2.00	132	--- ^a
O6–H6···O2	2.644(5)	1.95	142	1–x, –1/2+y, 1–z
O7–H7C···O6	2.859(4)	2.09	156	–x, 1/2+y, –z
C15–H15B···O7	3.214(9)	2.51	130	--- ^a
C19–H19C···O2	2.819(2)	2.48	101	--- ^a
O32–H32···O25	2.644(5)	1.95	142	1–x, –1/2+y, 1–z
O33–H33···O32	2.859(4)	2.09	156	–x, 1/2+y, –z
C5–H5B···O33	3.214(9)	2.51	130	--- ^a
C20–H20C···O25	2.819(2)	2.48	101	--- ^a

^a = Intramolecular hydrogen bond

2.4.1 Crystal Structure Description

Andrographolide-Vanillin (AP-VAN) cocrystal: Single crystals of AP–VAN cocrystal were obtained by dissolving the ground material in methanol-water solvent mixture followed by slow evaporation of this solution. The X-ray crystal structure was solved and refined in the monoclinic space group $P2_1$. AP molecules are connected along the screw axis through bifurcated O–H···O (O3–H3C···O5, 1.99 Å, 147°) and C–H···O (C15–H15A···O5, 2.51 Å, 127°) hydrogen bonds. Such linear chains are bridged by VAN molecules through O8–H8C···O2 hydrogen bond on one side (1.89 Å, 154°) and a C–H···O ring motif of $R^2_2(6)$ graph set^{1,18} (C18–H18B···O6, 2.58 Å, 144°; C27–H27···O2, 2.43 Å, 148°) on the other (Figure 2.5).

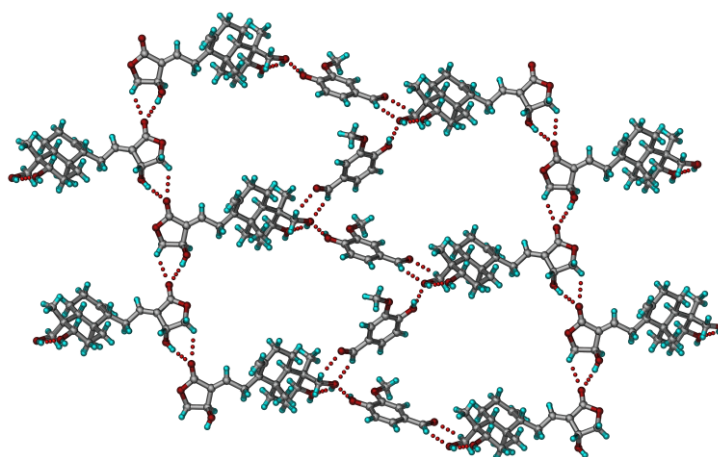


Figure 2.5 A layered section of the AP–VAN cocrystal connected by O–H···O and C–H···O H-bonds.

Andrographolide–Vanillic acid (AP–VLA) cocrystal: Single crystals of AP–VLA cocrystal (1:1, in $P2_1$ space group) were obtained by slow evaporation from methanol–water. AP molecules are arranged along the 2_1 screw axis, similar to the previous structure, but now the hydroxyl lactone moiety of adjacent AP molecules is connected via single point strong $O-H\cdots O$ ($O5\cdots O3$, 1.97 Å, 170°) hydrogen bond. VLA molecules connect these 1D tapes through $O-H\cdots O$ H-bonds on both sides ($O7-H7C\cdots O2$, 1.89 Å, 159° and $O9-H9C\cdots O8$, 2.22 Å, 114°) (Figure 2.6). Unlike the previous case there are no $C-H\cdots O$ interactions in this cocrystal structure.

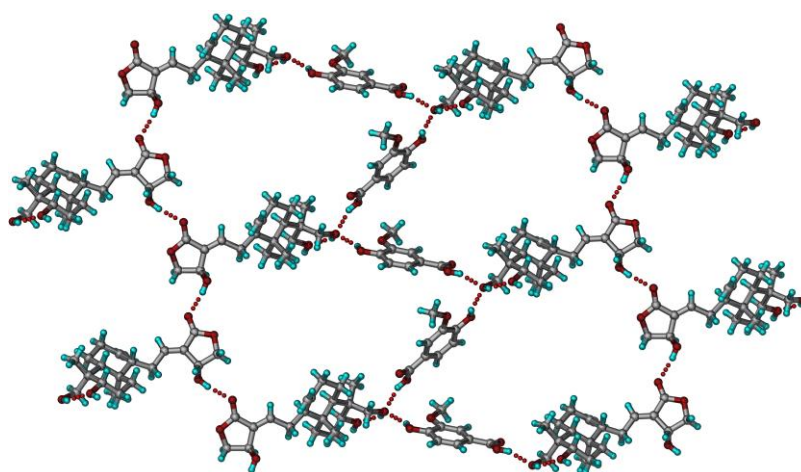


Figure 2.6 A layered section of the AP–VLA cocrystal connected by $O-H\cdots O$ and $C-H\cdots O$ H-bonds. The only difference compared to AP–VAN is that the AP-coformer $O-H\cdots O$ hydrogen bonds are now with the COOH and OH groups of VLA.

Andrographolide–Salicylic acid (AG–SLA) cocrystal: 1:1 stoichiometric AP–SLA cocrystal was obtained from ethyl formate–MeOH by slow evaporation. The 1D tapes of screw axis related AP molecules are connected through $O3-H3C\cdots O5$ hydrogen bond (2.24 Å, 127°). SLA molecules bridge the molecular chains through $O-H\cdots O$ H-bond on one side ($O8-H8C\cdots O6$, 1.86 Å, 147°) and $C-H\cdots O$ interactions on the other ($C24-H24\cdots O6$, 2.66 Å, 120° and $C28-H24\cdots O1$, 2.70 Å, 138°). An intramolecular $O-H\cdots O$ hydrogen bond ($O8-H8C\cdots O6$, 1.85 Å, 146°) persists in the SLA coformer (Figure 2.7).

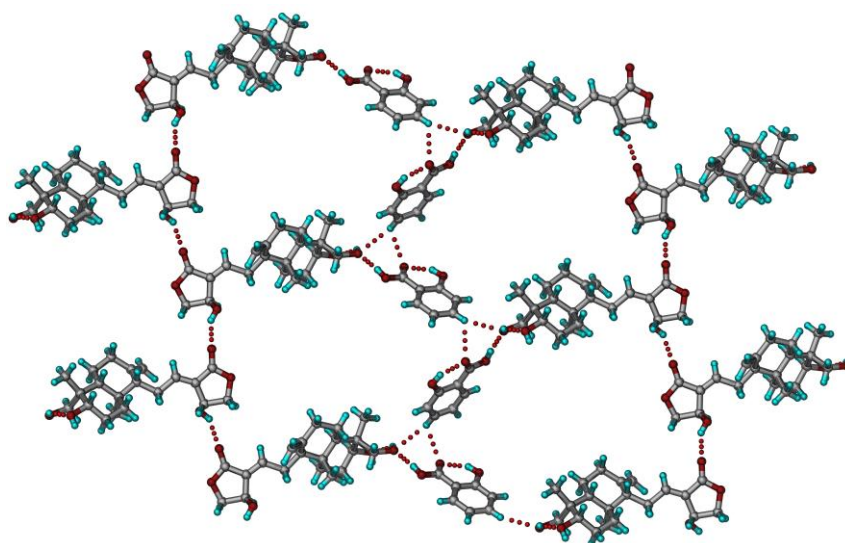


Figure 2.7 A layered section of AP–SLA cocrystal connected by O–H \cdots O H bonds and C–H \cdots O interactions.

Andrographolide–Guaiacol (AP–GUL) cocrystal: single crystal of 1:1 ($P2_1$) stoichiometry was obtained from EtOH–H₂O by slow evaporation. Similar to the AP–VAN cocrystal, the 2_1 related AP molecules are connected through a bifurcated O–H \cdots O and C–H \cdots O hydrogen bonds to the carbonyl acceptor of a lactone group (O3–H3C \cdots O5, 2.01 Å, 158°; C15–H15B \cdots O5, 2.64 Å, 123°). The GUL molecules intersperse between the AP tapes connected via O–H \cdots O (O6–H6 \cdots O2, 1.98 Å, 152°) hydrogen bond (Figure 2.8).

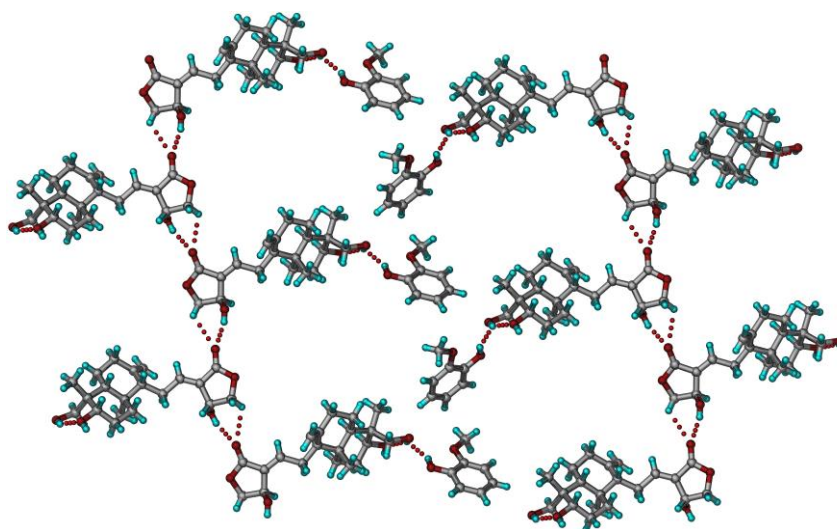


Figure 2.8 A layered section of the AP–GUL cocrystal connected by O–H···O interactions. The interaction on the other side of the coformer is missing (because there is no OH/COOH group) but the molecular placement in the crystal lattice is similar.

Andrographolide–Resorcinol (AP–RES) cocrystal: 1:1 cocrystal ($P2_1$) was obtained from ethyl acetate. The linear arrangement of 2_1 related AP molecules via bifurcated O–H···O hydrogen bonds to the lactone acceptor (O3–H3C···O4, 2.47 Å, 139°, O3–H3C···O5, 2.28, 150°) is recurring. Such linear tapes are bridged through RES molecules via O–H···O hydrogen bonds (O6–H6···O2, 1.95 Å, 142°, and O7–H7C···O6, 2.09 Å, 156°). There are no C–H···O interactions in the crystal structure (Figure 2.9).

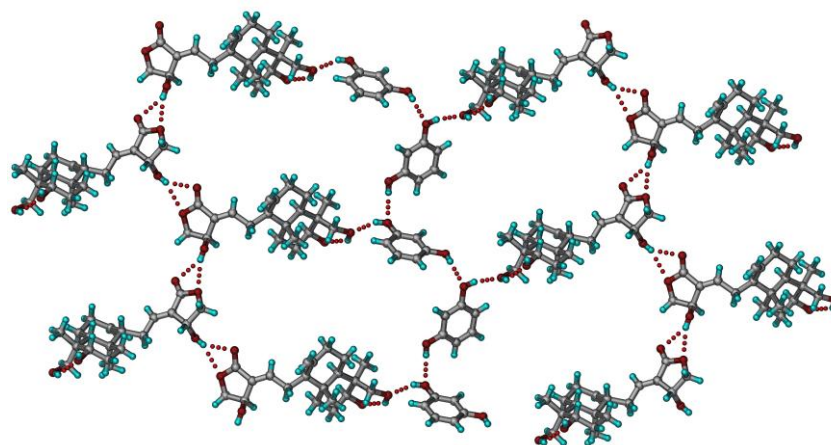


Figure 2.9 A layered section of the AP–RES cocrystal connected by O–H···O H-bonds.

The above cocrystals of AP are isostructural to the change of coformer. The O–H···O chain of AP molecules is identical in all structures and there are only minor changes in the H-bonding of the coformer to the drug. The unit cell similarity index,¹⁹ Π is close to zero for these isostructural crystals (Table 2.3).

Table 2.3 Unit Cell similarity index Π of AP cocrystals.

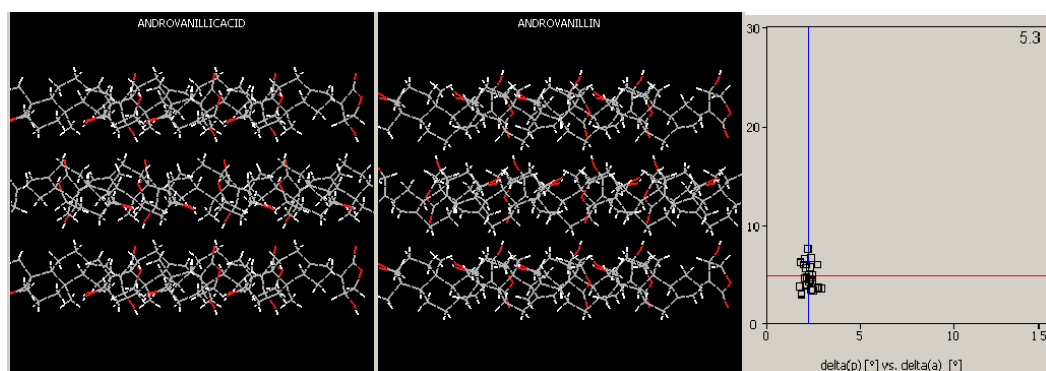
$$\Pi = \left| \frac{a+b+c}{a'+b'+c'} \right| - 1$$

$\Pi \approx 0$ for isostructural crystal pairs

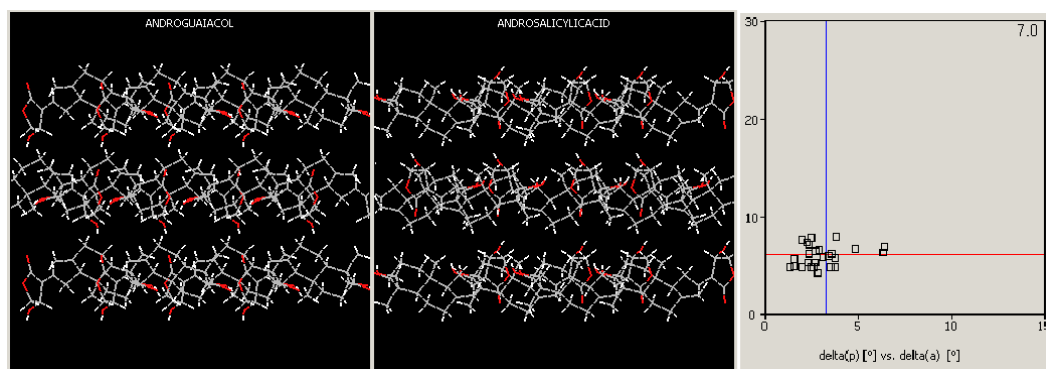
Cocrystal pairs	Unit cell similarity index, Π
AP-VAN & AP-VLA	0.017
AP-VAN & AP-SLA	0.0071
AP-VAN & AP-GUL	0.0067
AP-VAN & AP-RES	0.04
AP-VLA & AP-SLA	0.0009
AP-VLA & AP-GUL	0.01
AP-VLA & AP-RES	0.058
AP-SLA & AP-GUL	0.0003
AP-SLA & AP-RES	0.047
AP-GUL & AP-RES	0.047

2.4.2 XPac Comparison

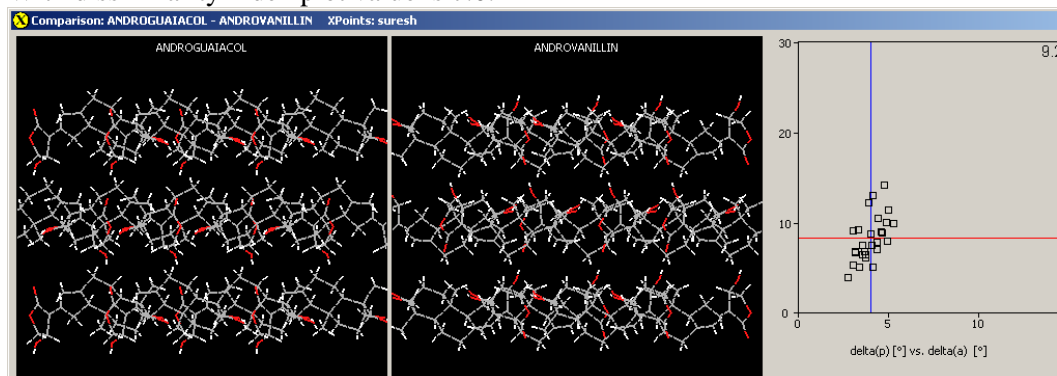
In addition to the Π parameter which gives identity of the crystallographic unit cell, the internal molecular arrangement was compared by the XPac method.²⁰ The analysis of the two structures is based on comparing the angular, planar and distance relationships between the coordination spheres of 14 neighboring molecules around a central molecule in each structure. Depending on the number of matches, the dimensionality and similarity of the structures are derived. Application of XPac to AP cocrystals showed 3D supramolecular constructs (3D similarity is at the highest level of comparison) between all combinations of AP-VAN, AP-VLA, AP-SLA and AP-GUL except for AP-RES, which is a 1D supramolecular construct. The 3D/1D or dissimilarity supramolecular constructs of AP-cocrystals pairs along with their dissimilarity index plots are shown in Figure 2.10 and Table 2.4. The not so good match of AP-RES is also suggested by the slightly higher value of Π compared to the other structures (Table 2.3). AP-VAN, AP-VLA, and AP-GUL cocrystals have a common 2-methoxy phenol skeleton moiety and they are related by a 3D supramolecular construct, which means that CHO/COOH/H in VAN, VLA, and GUL respectively can be interchanged and yet retain cocrystal isostructurality. Furthermore AP-SLA and AP-GUL similarity emphasize COOH/OCH₃ exchange. These isostructural exchanges vastly expand the group of coformers and functional groups which may be attempted in a cocrystal screen for modulating a given property within an isostructural series. These novel isostructural pairs could also lead to solid solutions for new applications.²¹ Jones^{19a} has advocated that structural equivalence in isostructural pairs could be a strong guiding principle in the property directed crystal engineering of multicomponent solids.



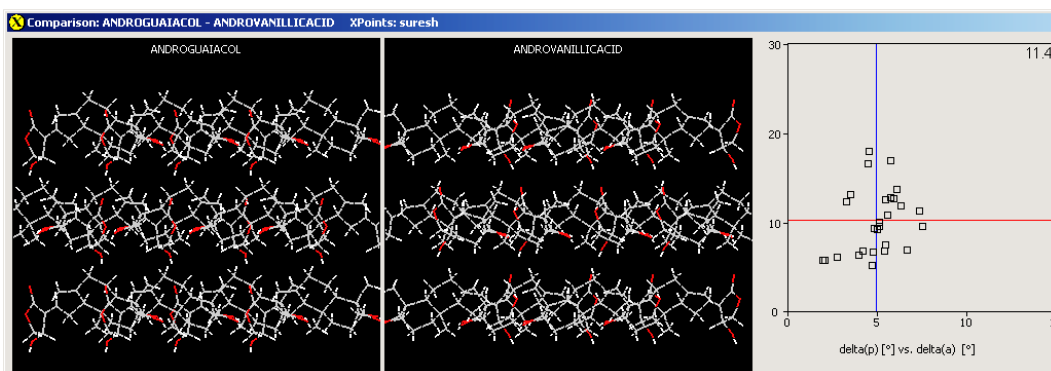
(a) 3D supramolecular construct identified by XPac analysis of AP-VLA and AP-VAN. With dissimilarity index plot value is 5.3.



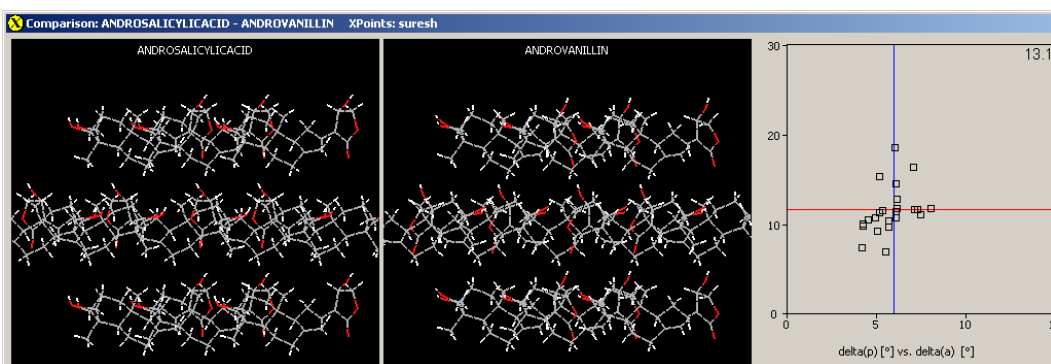
(b) 3D supramolecular construct identified by XPac analysis of AP-GUL and AP-SLA. With dissimilarity index plot value is 7.0.



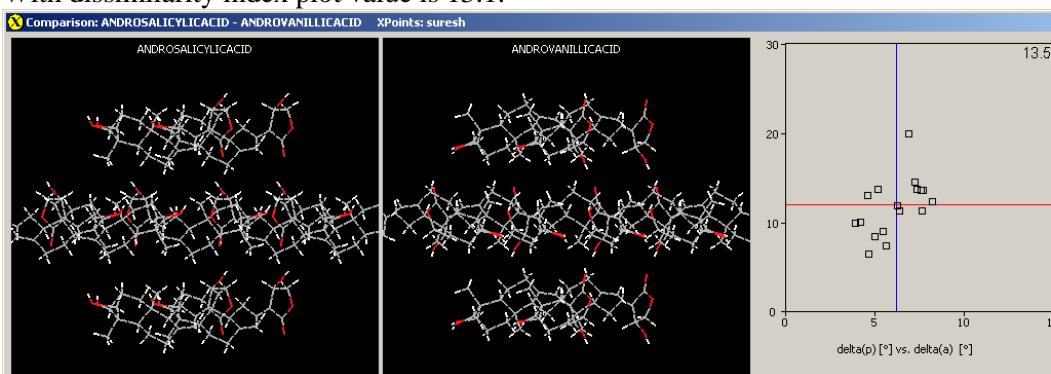
(c) 3D supramolecular construct identified by XPac analysis of AP-GUL and AP-VAN. With dissimilarity index plot value is 9.2.



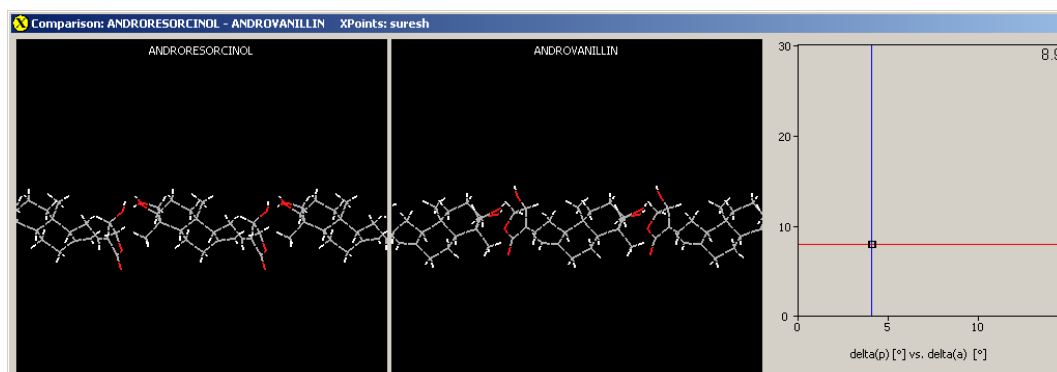
(d) 3D supramolecular construct identified by XPac analysis of AP-GUL and AP-VLA. With dissimilarity index plot value is 11.4.



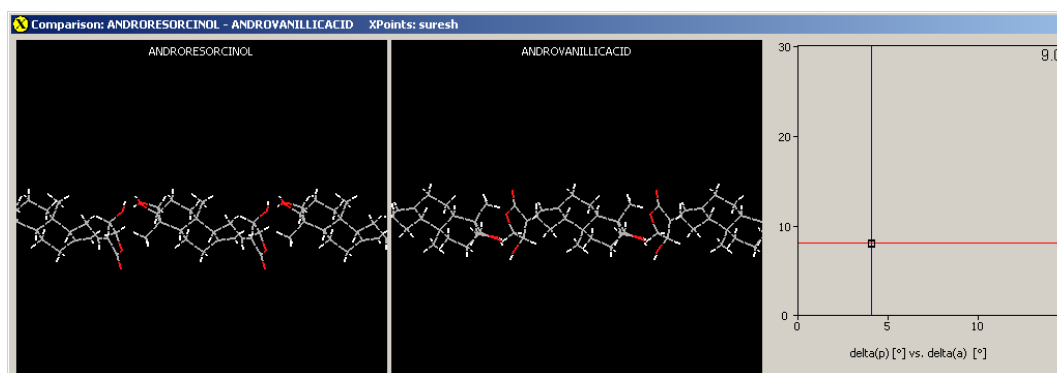
(e) 3D supramolecular construct identified by XPac analysis of AP-SLA and AP-VAN. With dissimilarity index plot value is 13.1.



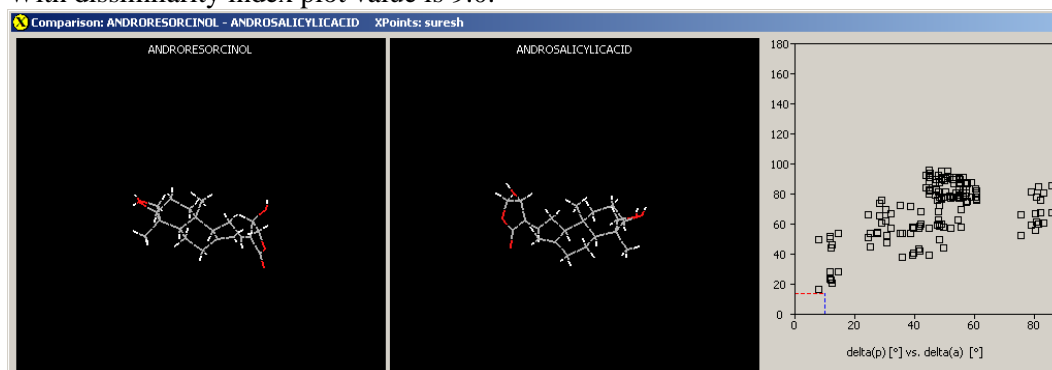
(f) 3D supramolecular construct identified by XPac analysis of AP-SLA and AP-VLA. With dissimilarity index plot value is 13.5.



(g) 1D supramolecular construct identified by XPac analysis of AP-RES and AP-VAN. With dissimilarity index plot value is 8.9.



(h) 3D supramolecular construct identified by XPac analysis of AP-VLA and AP-VLA. With dissimilarity index plot value is 9.0.



(i) No supramolecular construct identified by XPac analysis of AP-RES and AP-SLA.

Figure 2.10a-i Supramolecular construct identified by XPac analysis of all possible combinations of AP cocrystals.

Table 2.4 Dissimilarity indices of AP cocrystals obtained from XPac analysis

Cocrystal pairs	Dissimilarity index from XPac analysis
AP-VAN & AP-VLA	5.3
AP-VAN & AP-SLA	13.1
AP-VAN & AP-GUL	9.2
AP-VAN & AP-RES	8.9
AP-VLA & AP-SLA	13.5
AP-VLA & AP-GUL	11.4
AP-VLA & AP-RES	9.0
AP-SLA & AP-GUL	7.0
AP-SLA & AP-RES	--- no similarity
AP-GUL & AP-RES	13.5

2.4.3 Powder X-ray diffraction

Powder diffraction technique is a reliable technique to establish the novelty and bulk phase purity of diverse solid forms through their unique diffraction patterns and also amorphous content in a crystalline solid.^{22a} It entitles easy distinction of the modified solid from their starting components. This technique becomes more important in those cases where single crystals are not available for solids and get the structure solution of a crystalline material from its powder diffraction for structural analysis.²² In this work PXRD was used to establish the bulk purity of AP cocrystals. The powder diffraction lines of the five cocrystals exhibited an excellent overlay of the experimental PXRD pattern with the calculated lines from the X-ray crystal structure (Figure 2.11). All these cocrystal have similar PXRD lines this is a common observation for isostructural cocrystals.

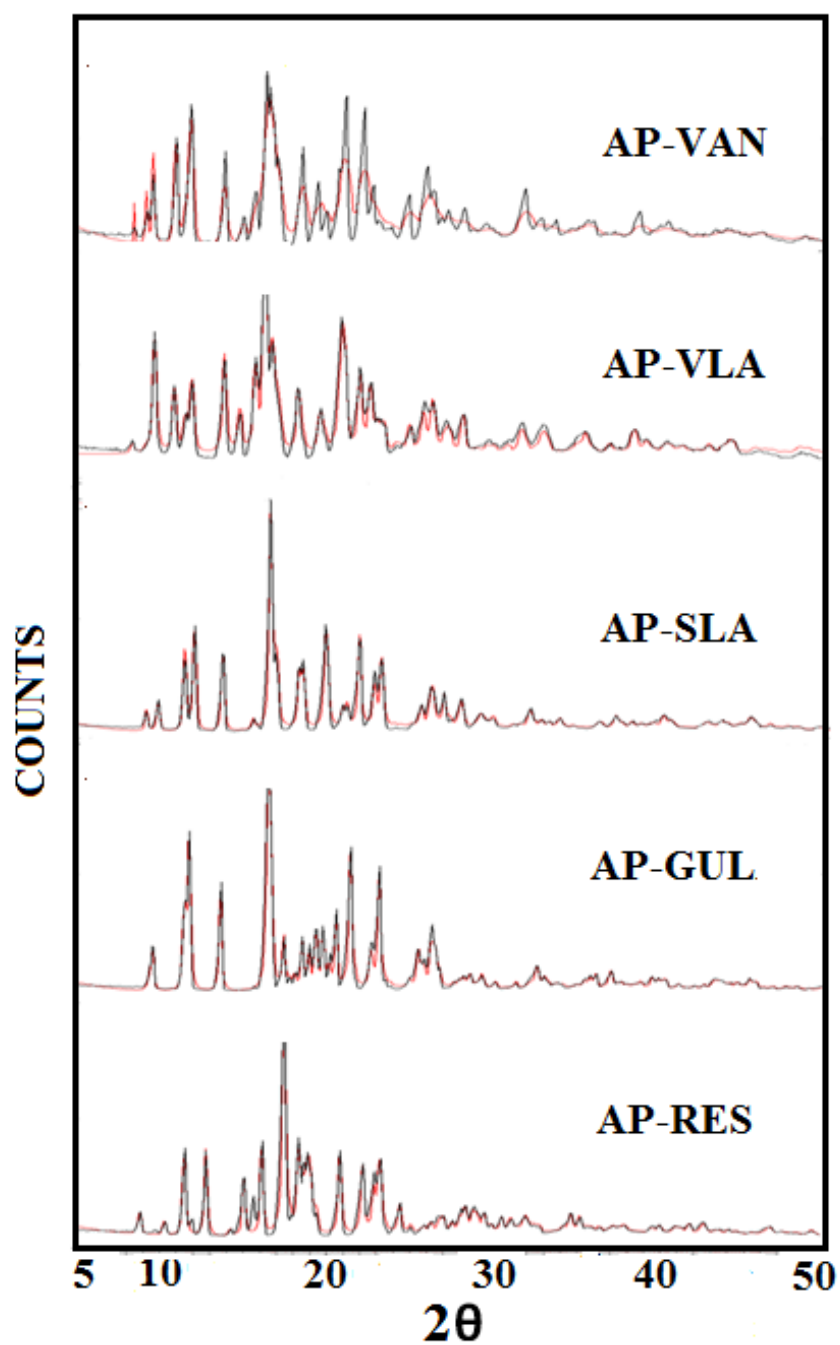


Figure 2.11 Overlay of the experimental PXRD (black) of AP cocrystals with the calculated lines from the X-ray crystal structure (red) confirm the bulk purity and homogeneity of each phase.

2.4.4. Spectroscopic Characterization

Infrared and Raman techniques provide information about the bonding interactions and molecular arrangement.²³ Changes in the bonding interactions between molecules or intramolecular changes in vibration modes of various covalent bonds can be inferred using these techniques.^{23a} Changes in the bonding patterns hint at the functional groups involved and efficiently complement the diffraction methods in characterizing various solid forms.^{23b,c,d} In the FT-IR spectra of AP, the hydroxyl OH stretching frequency appears as a broad peak at 3397 cm⁻¹. In addition to this ester carbonyl and olefin –CH stretching frequencies appear at 1727 cm⁻¹ and 1674 cm⁻¹ respectively. The bands due to C–O stretch and O–H bend appears at 1074 cm⁻¹ and 1454 cm⁻¹. On forming cocrystals, these functional groups showed significant changes in their hydrogen bond patterns (Figure 2.12). Raman peak intensities which are complementary to IR vibrational modes showed similar changes in the product phases compared to the starting components (Figure 2.13).^{23b} Representative IR and Raman values are shown in Table 2.5.

Table 2.5 List of major IR and Raman stretching frequencies in the cocrystals and their individual components (in cm⁻¹).

INFRARED					
	O-H stretch	C=O stretch	C=C stretch	C-O stretch	O-H bend
AP	3397	1727	1674	1074	1454
AP-VAN	3362	1729	1673,1596	1052,1032	1436,1466
VAN	3184	1665	1588	1028	1465
AP-VLA	3326	1723,1680	1673,1595	1051,1028	1430,1464
VLA	3483	1684	1597	1028	1465
AP-SLA	3376,3473	1730,1668	1642,1484	1055,1036	1450,1468
SLA	3238	1658	1483	1031	1465
AP-GUL	3400	1728	1673,1596	1078,1030	1445,1468
GUL	3496	---	1596	1039	1469
AP-RES	3400	1727	1674,1607	1055	1465,1488
RES	3261	---	1608	---	1489
RAMAN					
	C=O stretch	C=C stretch	C-O stretch		
AP	1724	1675,1649	1035		
AP-VAN	1730	1678,1642,1595	1029		
VAN	1669	1594	1032		
AP-VLA	1707, 1680	1645,1609	1014		
VLA	--	1641	--		
AP-SLA	1733, 1669	1645	1033		
SLA	--	1634	--		

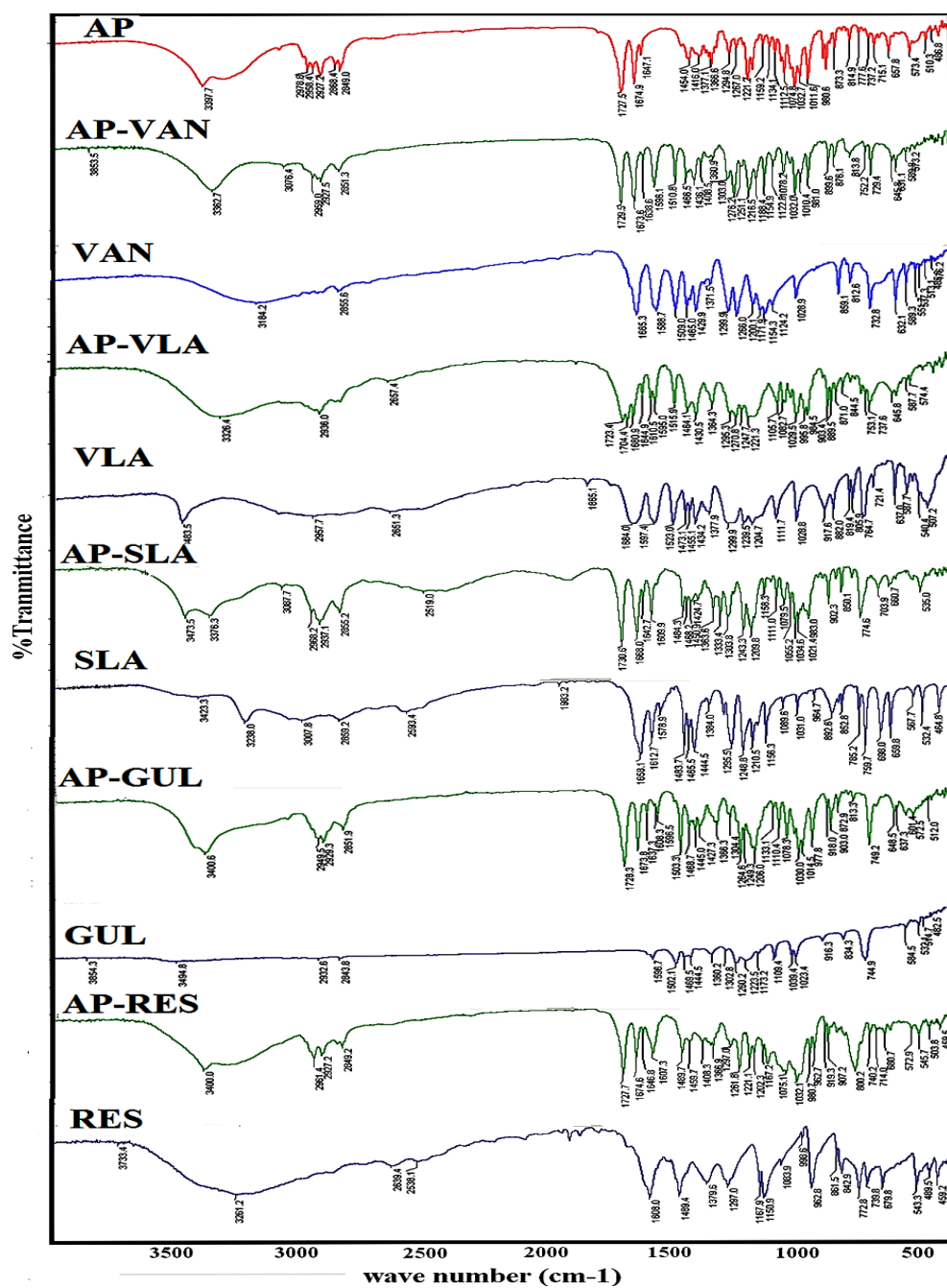


Figure 2.12 Overlay of IR spectra of AP cocrystals in comparison to their individual components.

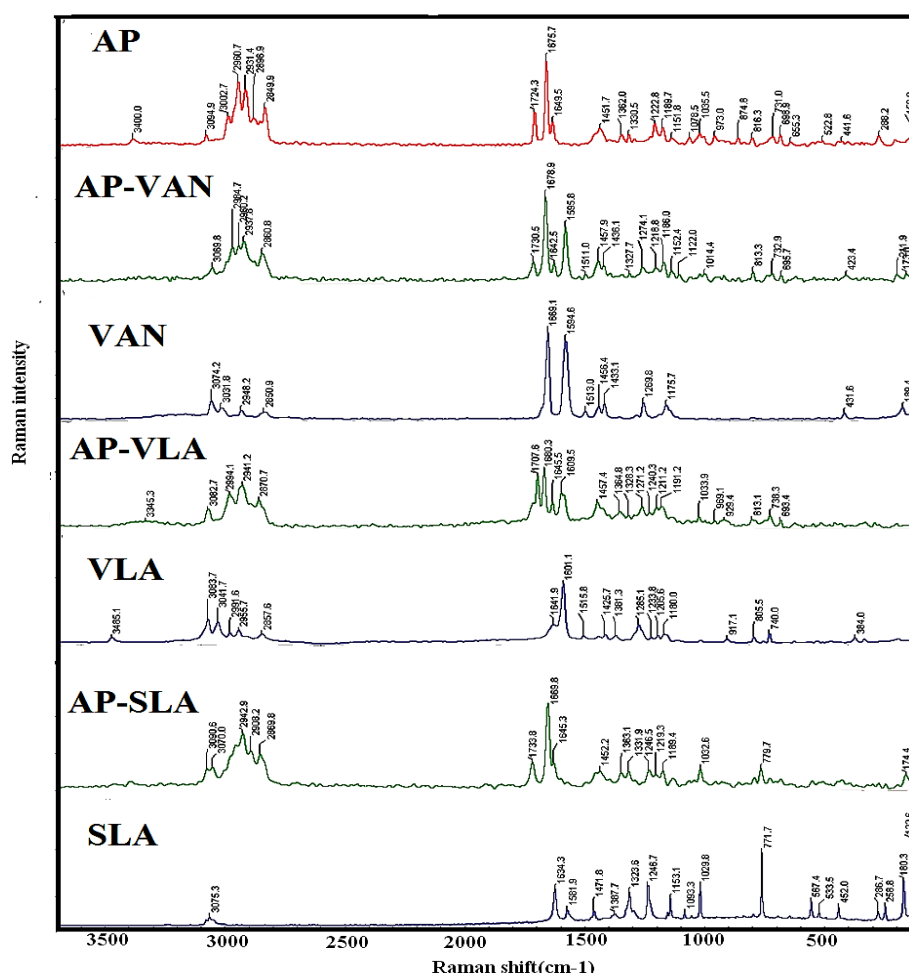


Figure 2.13 Overlay of Raman spectra of novel cocrystals with comparison to their individual components. Raman spectra of AP-GUL and AP-RES could not be obtained due to burning of the samples on exposure to laser light.

Solid-state ^{13}C NMR spectroscopy is a non-destructive analysis of solid samples which can provide ample information about differences in bonding patterns, molecular conformations, and molecular mobility.^{23a, 24} Significant changes in the chemical shifts of AP cocrystals in comparison to their starting components were observed during ss-NMR (Figure 2.14 and Table 2.6) analysis, thus ably complementing diffraction, thermal and spectroscopic techniques in establishing the unique nature of AP cocrystal.

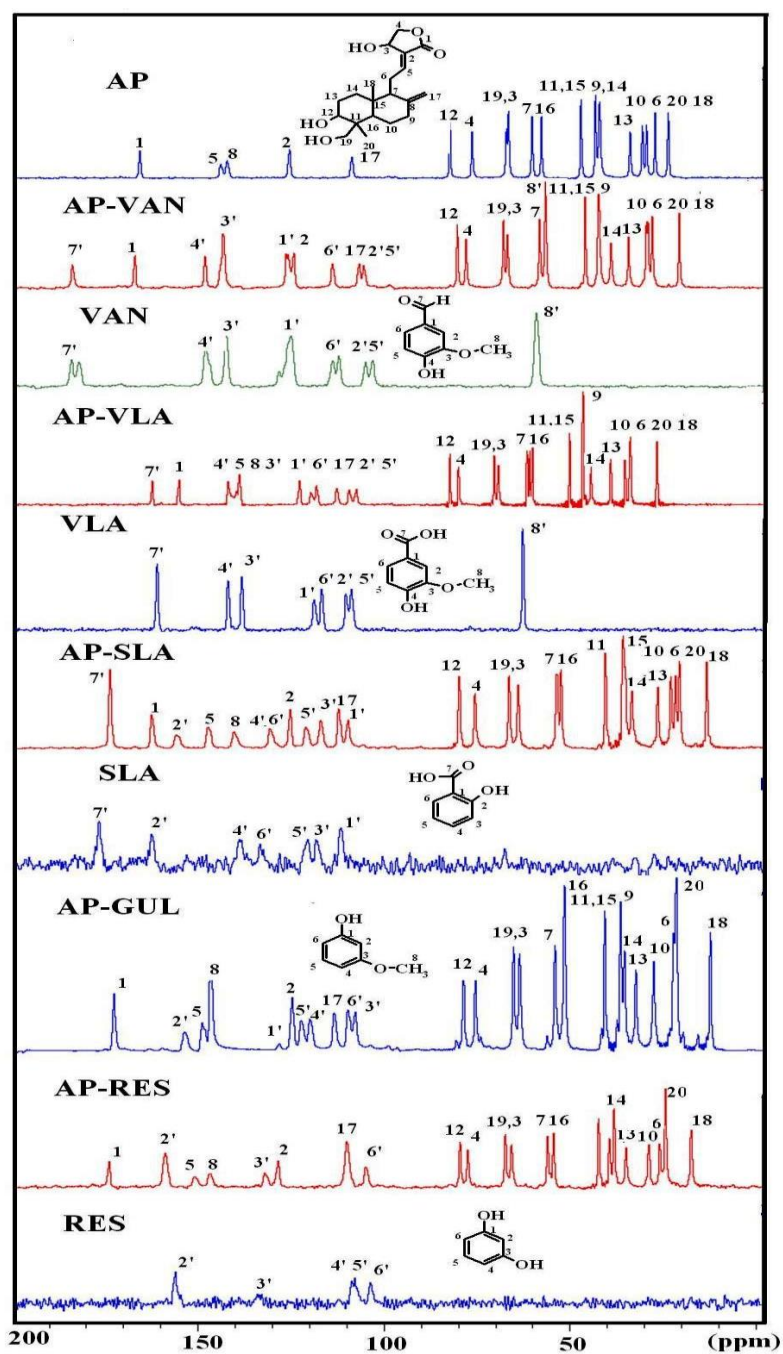


Figure 2.14 ss-NMR spectra of AP cocrystals (δ , ppm).

Table 2.6 ss-NMR ^{13}C chemical shifts (δ , ppm) of AP cocrystals

Carbon	AP	VAN	AP_VAN	VLA	AP-VLA	SLA	AP-SLA	RES	AP-RES	AP-GUL
1	172.6	-	174.1	-	174.1	-	173.4	173.1	-	173.6
5	148.9	-	153.5	-	148.7	-	147.4	149.7	-	150.7
8	147.0	-	148.1	-	147.6	-	147.4	147.5	-	146.5
2	128.7	-	128.7	-	129.2	-	125.5	125.7	-	128.1
17	110.2	-	129.1	-	110.9	-	110.2	109.0	--	109.8
12	84.5	-	79.3	-	82.5	-	80.7	80.7	-	79.3
4	75.0	-	76.3	-	75.5	-	76.5	77.1	-	77.3
19	64.9	-	65.8	-	66.9	-	67.4	66.9	-	67.1
3	64.2	-	64.6	-	64.8	-	65.0	65.4	-	65.5
7	57.4	-	55.2	-	57.9	-	54.7	56.0	-	55.8
16	57.3	-	53.4	-	57.9	-	53.7	53.5	-	54.3
11,15	43.0	-	41.8	-	43.5	-	41.9	42.7	-	42.1
9	38.7	-	37.7	-	39.2	-	37.2	38.5	-	39.3
14	37.4	-	34.2	-	38.0	-	36.7	37.4	-	34.0
13	28.5	-	29.1	-	29.0	-	28.0	29.7	-	28.6
10	24.9	-	23.8	-	25.5	-	24.5	24.3	-	25.7
6	23.7	-	23.4	-	24.3	-	23.2	23.7	-	24.2
20	21.2	-	22.1	-	21.7	-	22.3	21.8	-	24.2
18	17.0	-	14.1	-	17.9	-	14.9	14.6	-	17.3
7'	-	192.7	192.5	173.4	173.2	177.3	173.4	57.3	-	-
4'	-	152.4	153.5	150.8	148.7	139.1	140.6	121.1	107.7	109.8
3'	-	147.3	148.1	146.4	145.2	118.7	117.5	111.0	133.3	131.8
1'	-	128.4	129.7	123.3	121.7	112.1	112.7	129.4	155.8	158.5
6'	-	116.0	116.1	120.9	115.8	133.6	130.9	114.6	103.4	104.7
2'	-	106.3	108.2	113.2	112.1	162.4	162.4	154.4	108.4	109.8
5'	-	104.3	106.9	111.4	110.9	120.9	121.4	123.4	155.8	158.5
8'	-	56.1	55.2	56.7	55.3	-	-	-	-	-

2.4.5 Thermal Analysis

Differential scanning calorimetry (DSC)) was used to characterize the thermal behavior of AP cocrystals.^{25,2d} The cocrystals exhibited a sharp melting endotherm in DSC heating curves at a temperature in between that of AP and the coformer, except AP-VLA which is lower (Figure 2.15 and Table 2.7). The melting point of the cocrystal correlated, in general, with the melting point of the coformer, except VAN cocrystal. The DSC of AP-GUL cocrystal shows two endotherms, first being the vaporization of GUL (a liquid coformer) and the second for the melting of AP.

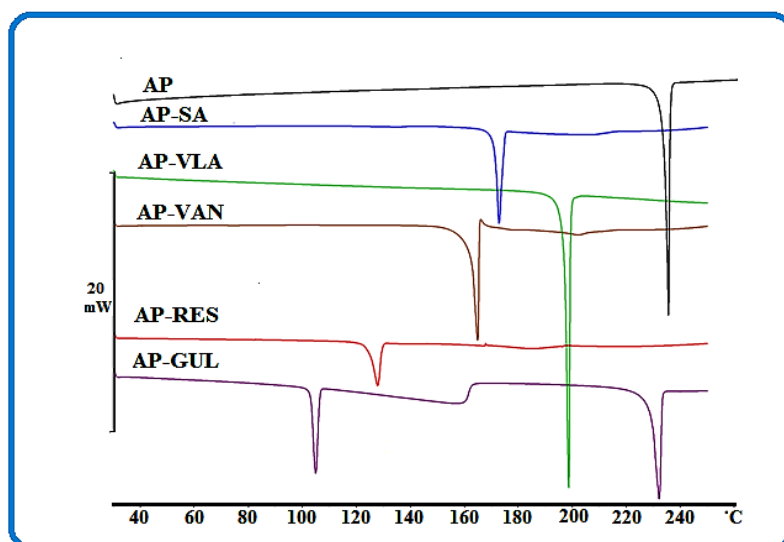


Figure 2.15 DSC heating curves of AP cocrystals. The sharp endotherm is at the melting point of the cocrystal, except for AP-GUL (see text).

Table 2.7 Melting points of AP cocrystals and their coformers.

S.No	SACT cocrystal/salt	Melting Point (°C)	Coformer	Melting Point (°C)
1	AP-VAN	163–164	Vanillin	82–83
2	AP-VLA	195–196	Vanillic acid	210–213
3	AP-SLA	168–170	Salicylic acid	155–157
4	AP-RES	124–127	Resorcinol	110–113
5	AP-GUL	106–107	Guaiacol	27–28

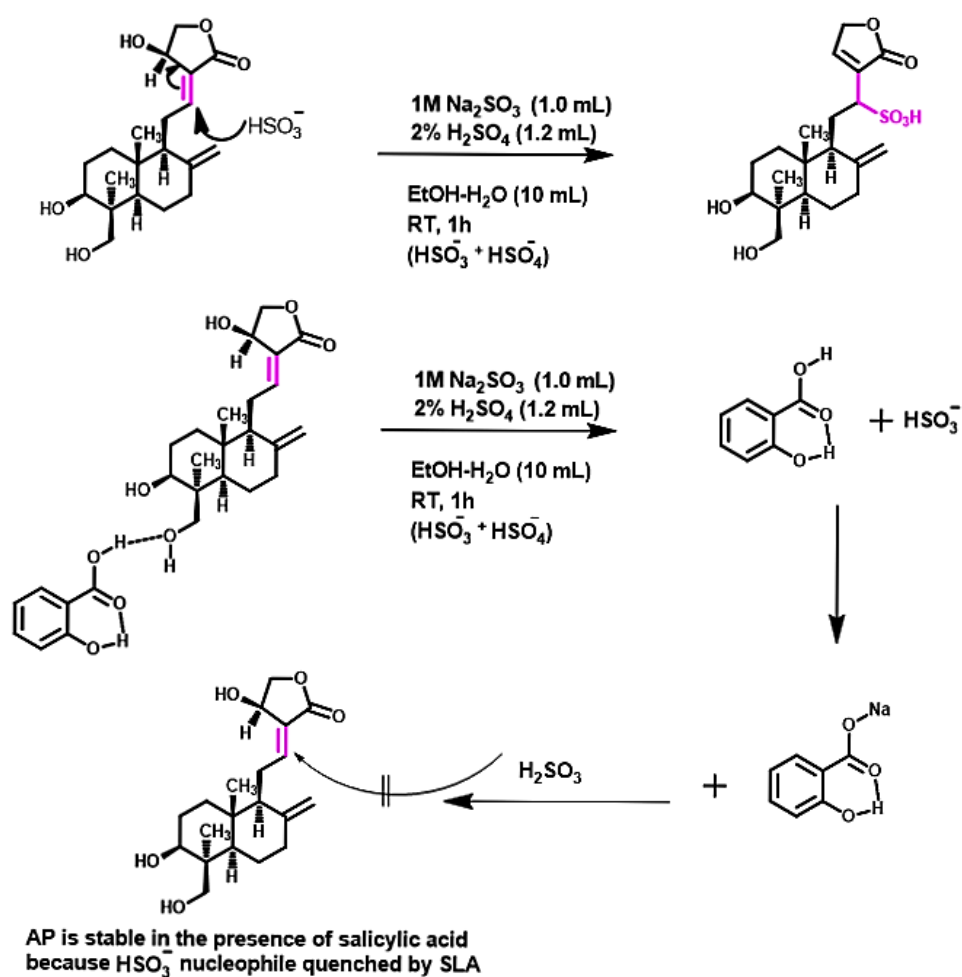
Melting point of AP 233 °C

2.4.6 Stability of AP–SLA to Chemical transformation

The biochemical transformation of AP to AP-SO₃H (Scheme 2.1), which limits the bioavailability of the active metabolite, was carried out in vitro.^{14d} Accordingly AP was treated with HSO₃[−] (in the presence of HSO₄[−] and excess Na₂SO₃) to generate the sulfated product by the nucleophilic attack of HSO₃[−] ion at the β position (C12-carbon) of the α,β unsaturated lactone moiety in AP to isolate the primary sulfonate metabolite, 14-deoxy-12(*R*)-sulfo andrographolide (Scheme 2.14, see Experimental Section for details). The reaction was complete in 30 min and the product was characterized as AP-SO₃H by its reported ¹H and ¹³C NMR spectra and the M+1 peak at m/z 415.1786 (C₂₀H₃₀O₇S, calcd. M+1 415.1790) in the HRMS of the sulfate product.^{14d} Next, each of the AP cocrystals was subjected to the same reaction conditions (same molar equivalent of AP, concentration, room temperature) to study the chemical stability of AP as a hydrogen-bonded cocrystal. AP cocrystals with VAN, RES, and GUL reacted slightly slower than pure AP in that a mixture of AP, AP-SO₃H inactive product and dissociated coformer were detected by NMR at 30 min. The conversion to the inactive sulfonate metabolite was partial in the case of AP–VLA (43% by weight). AP–SLA cocrystal gave the best result that no transformation to AP-SO₃H could be detected by NMR and HR-MS.

We reason that the acidity of the COOH group of SLA and VLA has an inhibitory effect on the chemical transformation of AP to AP-SO₃H (*pK_a*'s of the relevant species are listed in Table 2.8). The reactive species in the aqueous ethanol medium is bisulfite anion (HSO₃[−]), which reacts with the conjugated lactone of AP in a 1,4-nucleophilic addition. The carboxylic acid of the coformer in AP–SLA (and VLA) is able to titrate the HSO₃[−] to H₂SO₃ and sodium salicylate, which will stop/inhibit the subsequent addition reaction. The *o*-hydroxy acid (SLA) is stronger than the *p*-hydroxy acid (VLA) by almost 2.5 *pK_a* units and consequently much more reactive in protonating the HSO₃[−] ion. Sodium salicylate then reacts with H₂SO₃ to give salicylic acid and HSO₃[−]Na⁺. There will be equilibrium between the acid–conjugate base pairs of SLA and H₂SO₃ because their acid strengths are within 2 *pK_a* units. Vanillic acid is less effective in proton transfer to HSO₃[−] being a weaker acid, and this explains its intermediate inhibition. VAN, RES and GUL are phenolic and unable to participate in the acid-base protonation-deprotonation chemistry of Scheme 2.16, and these cocrystals are ineffective to make

any change to the HSO_3^- reactivity. The complete inhibition of the undesired pathway for AP–SLA cocrystal is due to the higher acidity of SLA, the so called ortho effect.²⁶ The peak at δ 7.5, which is indicative of the sulfated carbon, is absent in the NMR spectrum of post-reaction product for AP–SLA. These results and the mechanistic explanations mean that it is the acidity of SLA in the AP–SLA cocrystal that stops the chemical transformation of AP in the flask. Given its chemical stability, the solubility profile of AP–SLA cocrystal (discussed next) was examined.



Scheme 2.16 (a) Transformation of AP to AP-SO₃H (b) A plausible mechanism for the inhibition of the reaction by AP–SLA cocrystal.

Table 2.8 pK_a of active species in water.

Acid	pK _a (water)	Literature source
Salicylic acid	2.97	www.drugbank.ca/drugs/DB00936 accessed on 20-05-13
Vanillic acid	4.45	www.chemicaldictionary.org/dic/V/Vanillic-acid_1030.html accessed on 20-05-13
H ₂ SO ₃	1.90	evans.harvard.edu/pdf/evans_pka_table.pdf accessed on 20-05-13
HSO ₃ ⁻	7.21	evans.harvard.edu/pdf/evans_pka_table.pdf accessed on 20-05-13

2.4.7 Solubility and Dissolution

Having improved the stability of Andrographolide in AP–SLA cocrystal, we next compared its solubility and dissolution. Good solubility is essential for better pharmacokinetics and higher therapeutic efficacy. Solubility improvement is a major challenge for improving drug bioavailability.²⁷ Solubility studies were performed on AP–SLA only in 25% EtOH-water medium, the solvent being chosen such that the less soluble AP is sufficiently soluble to make the Conc. vs. Intensity calibration curves by UV-Vis spectroscopy (using the λ_{max} of pure AP at 225 nm and AP–SLA at λ_{max} 227 nm). Solubility was measured at the end of 24 h. The solubility of AP–SLA (4.55 g/L) is 12 times higher than that of AP (0.38 g/L, Table 5). Both AP and AP–SLA cocrystal forms are stable under the solubility conditions. (By PXRD match of the residue at the end of the experiment are shown Figure 2.18a and b).

The dissolution rate is a kinetic phenomenon which gives the peak concentration of the solute and the amount of drug dissolved in a short time period (30 min to a few hours). The dissolution method is particularly useful to estimate drug release, and it is the suitable parameter for those drugs which undergo phase transformation/dissociation in solution. IDR experiments on AP and AP–SLA cocrystal was performed in 25% EtOH-water for 6 h by the rotating disk intrinsic dissolution rate (DIDR) method²⁸ at 37 °C. AP–SLA exhibited 3 fold higher IDR than AP (Figure 2.17, dissolution rates and AUC₀₋₆ are listed in Table 2.9). Thus in vitro experiments show that the inactivation of andrographolide by biochemical sulfation is completely inhibited in the AP–SLA cocrystal, and together with solubility improvement of 12 fold, set the stage for preclinical studies on AP–SLA. At the end dissolution rate and equilibrium solubility experiments undissolved was characterized by PXRD. AP and AP-SLA matches very well with their calculated pattern indicating phase stability.

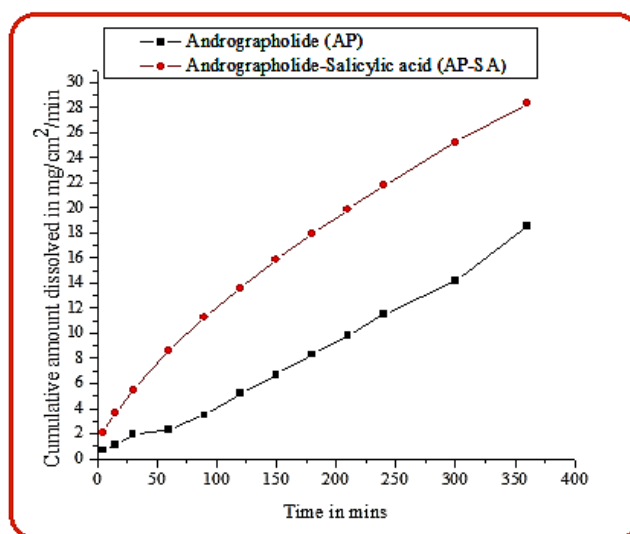


Figure 2.17 Intrinsic dissolution rate curves of AP and AP-SA cocrystal in 25% EtOH-water.

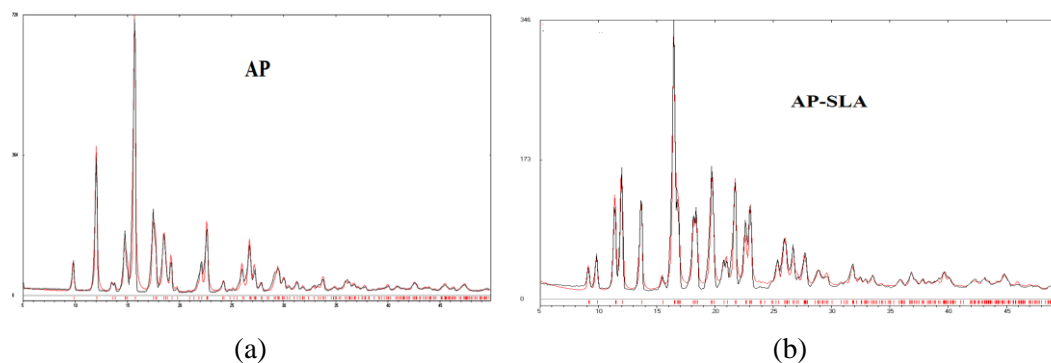


Figure 2.18 a-b. Representative PXRD pattern of AP and AP-SLA at the end of equilibrium solubility and dissolution experiments matches very well with their calculated pattern indicating phase stability.

Table 2.9 Intrinsic dissolution rates of AP and AP-SA cocrystal along with their molar extinction coefficient (ϵ), and equilibrium solubility. The number of times enhancement of IDR and AUC with respect to AP is given in parentheses.

Compound	Molar extinction coefficient, ϵ /mM cm	Equilibrium Solubility (g/L)	Intrinsic dissolution rate, IDR (mg/cm ²)/min ($\times 10^{-3}$)	Area under the curve, AUC _{0-6h} (mg.h)/L
AP	13.02	0.378	0.090	3025.95
AP-SA	21.33	4.555 (x 12.04)	0.277 (x 3.01)	6137.74 (x 2.03)

2.5 Conclusions

Liquid-assisted grinding of AP with GRAS (generally regarded as safe) coformers in a fixed stoichiometry resulted in cocrystals with vanillin (1:1), vanillic acid (1:1), salicylic acid (1:1), resorcinol (1:1), and guaiacol (1:1). All the crystalline products were characterized by thermal, spectroscopic and diffraction methods. Interestingly, even though the cocrystals are isostructural, their physico-chemical properties are quite different. The biotransformation process of AP to AP-SO₃H was studied in vitro by NMR spectroscopy. Among the novel cocrystals of AP synthesized and characterized with the objective to inhibit/stop the undesired transformation of sulfation which reduces the activity of AP as a drug, AP-SLA cocrystal showed the best result and there are no secondary chemical reactions. The acidic nature of the ortho-hydroxy acid in SLA and lower pK_a were reasoned as the cause for this inhibitory effect. The 12 fold improvement in solubility and 3 times faster dissolution rate of AP-SLA is an added benefit for oral formulation. This preliminary study also opens the possibility of exploring *p*- and *m*-amino salicylic acids,²⁹ which are drugs on their own, as potential coformers with Andrographolide in novel drug–drug cocrystals.

2.6 Experimental Section

Andrographolide was obtained from Mesochem Import & Export Co. Ltd., China. All coformers (purity > 99.8%) were purchased from Sigma-Aldrich (Hyderabad, India). Solvents (purity > 99%) were purchased from Hychem Laboratories (Hyderabad, India). Water filtered through a double deionized purification system (Aqua DM, Bhanu, Hyderabad, India) was used for all experiments.

Table 2.10 List of all the compounds used to form cocrystals with AP

2,6 di-hydroxybenzoic acid	Suberic acid
3,4 di-hydroxybenzoic acid	Hydroquinone
4-aminobenzoic acid	Apocyanin
Benzoic acid	Catechol
Maleic acid	3-methoxyoxybenzoic acid
Fumaric acid	Guaiacol
Oxalic acid	Resorcinol
Salicylic acid	Phloroglucinol
Adipic acid	2- methoxy benzoic acid
Succinic acid	glucose

2,5 di-hydroxybenzoic acid	Vanillyl alcohol
<i>P</i> -Hydroxy benzoic acid	4- methoxy benzoic acid
L-Tartaric acid	Vanillic acid
Ethyl vanillin	Hydroquinone
Vanillin	Caffeic acid
Ferulic acid	2,4-dihydroxybenzoic acid

Apart from vanillin, vanillic acid, salicylic acid, guaiacol and resorcinol all the other coformers were unsuccessful in making cocrystals with AP. Preparation methods for the successful candidates are shown below.

Preparation of AP solid forms

AP-VAN cocrystal: The cocrystal was obtained by grinding AP and VAN in 1:1 stoichiometry with a few drops of CH₃CN added in a liquid-assisted method for 30 min. Single crystals were obtained when 40 mg of the ground product was dissolved in MeOH-H₂O (5:1 v/v, 6 mL) and left for slow evaporation for 4-5 days.

AP-VLA cocrystal: This cocrystal was obtained by grinding AP and VLA in 1:1 stoichiometry with a few drops of CH₃CN added in a liquid-assisted method for 30 min. Single crystals were obtained when 40 mg of the ground product was dissolved in MeOH-H₂O (1:2 v/v, 6 mL) and left for slow evaporation for 4-5 days.

AP-SLA cocrystal: The cocrystal was obtained by grinding AP and SLA in 1:1 stoichiometry with a few drops of water added in a liquid-assisted method for 30 min. Single crystals were obtained when 40 mg of the ground product was dissolved in ethyl formate-MeOH mixture (4:1 v/v, 6 mL) and left for slow evaporation for 4-5 days.

AP-RES cocrystal: The cocrystal was obtained by grinding AP and RES in 1:1 stoichiometry with a few drops of water added in a liquid-assisted method for 30 min. Single crystals were obtained when 40 mg of the ground product was dissolved in 6 mL of ethyl acetate and left for slow evaporation for 4-5 days.

AP-GUL cocrystal: The cocrystal with GUL (a liquid) was obtained by grinding AP with guaiacol (used in excess as a solvent for 30 min). A single crystal of 1:1 stoichiometry was obtained when the ground mixture was dissolved in EtOH-H₂O (1:2 v/v, 6 mL) and left for slow evaporation for 4-5 days.

Sulfation of AP reaction procedure:

To a solution of AP (250 mg) in 6 mL ethanol, a mixture of 1 mL of 1M Na₂SO₃, 1.2 mL H₂SO₄ and 2 mL water were added.^{14d} The reaction mixture was stirred at room temperature for one hour. After completion of the reaction, the pH value of the reaction mixture was adjusted to neutral by adding 2% H₂SO₄ and evaporated to dryness. The residue was dissolved in 8 mL water and extracted with 20 mL chloroform. Both the organic and aqueous layers were evaporated to dryness in a rotary evaporator. The water layer residue was dissolved in 10 mL methanol and filtered to remove inorganic salt Na₂SO₄. The filtrate was evaporated to dryness to obtain 227 mg of andrographolide sulfonate (AP-SO₃H) in 77% yield.

The above procedure was repeated for each cocrystal by keeping the amount of AP constant (250 mg, 0.71 mmol). Except AP-VLA and AP-SLA, the other cocrystals AP-VAN, AP-RES, AP-GUL reacted in the same way to give AP-SO₃H product in 70-80% yield. AP-VLA gave 43% AP-SO₃H by-product and 57% unreacted AP by NMR analysis. AP-SLA cocrystal did not result in any side product formation (AP-SO₃H) and pure AP was isolated in 75% yield.

Solution NMR spectra were recorded on Bruker Avance 400 MHz spectrometer (Bruker-Biospin, Karlsruhe, Germany).

AP: ¹H NMR (DMSO-d₆, δ, ppm): 0.62 (s, 3H), 1.06 (s, 3H), 1.18 (d, J 7.6, 1H), 1.32 (d, J 7.6, 1H), 1.60-1.80 (m, 4H), 1.80-2.00 (m, 2H), 2.32 (d, J 7.6, 1H), 2.52 (d, J 7.6, 2H), 3.21 (br s, 2H), 3.80-3.90 (m, 2H), 4.03 (d, 7.2, 1H), 4.28 (s, 1H), 4.38 (d, J 7.2, 1H), 4.58 (s, 1H), 4.78 (s, 1H), 4.89 (s, 1H), 5.24 (s, 1H), 5.82 (d, J 5.6, 1H), 6.61 (s, 1H). ¹³C NMR (DMSO-d₆, δ, ppm): 15.16, 23.39, 24.31, 28.21, 36.85, 37.67, 42.62, 54.70, 55.87, 63.71, 64.95, 74.84, 78.95, 108.73, 129.23, 147.11, 147.99, 170.61. Two peaks are buried under the solvent peak at 39-40 ppm.

AP-SO₃H: ¹H NMR (DMSO-d₆, δ, ppm): 0.58 (s, 3H), 0.80-0.90 (m, 1H), 1.01 (s, 3H), 0.98-1.05 (m, 1H), 1.14-1.30 (m, 2H), 1.56 (br s, 2H), 1.60-1.85 (m, 4H), 2.10 (br t, J 7.4, 1H), 2.23 (d, J 7.2, 1H), 3.10-3.20 (m, 1H), 3.18 (d, J 7.2, 1H), 3.46 (d, J 7.2, 1H), 4.78 (d, J 12.3, 2H), 4.89 (d, J 12.3, 2H), 7.50 (s, 1H). One proton (SO₃H) exchanged with solvent and 3 protons are buried under the solvent peak at δ 3.8-4.0 ppm. ¹³C NMR

(DMSO- d_6 , δ , ppm): 15.22, 23.33, 24.32, 27.00, 28.17, 36.73, 38.27, 42.62, 53.04, 53.96, 54.82, 63.13, 71.06, 78.86, 107.89, 131.24, 147.61, 148.72, 174.66. One peak is buried under the solvent peak at 39-40 ppm.

Vibrational spectroscopy

Thermo-Nicolet 6700 FT-IR-NIR spectrometer with NXR FT-Raman module (Thermo Scientific, Waltham, MA) was used to record IR and Raman spectra. IR spectra were recorded on samples dispersed in KBr pellets. Raman spectra were recorded on samples contained in standard NMR diameter tubes or on compressed samples contained in a gold-coated sample holder. Data were analyzed using the Omnic software (Thermo Scientific, Waltham, MA).

Solid-state NMR spectroscopy

Solid-state ^{13}C NMR spectra were recorded on Bruker Avance 400 MHz spectrometer (Bruker- Biospin, Karlsruhe, Germany). ss-NMR measurements were carried out on Bruker 4-mm double resonance CP-MAS probe in zirconia rotors with a Kel-F cap at 5.0-kHz spinning rate with a cross-polarization contact time of 2.5 ms and a delay of 8 s. ^{13}C NMR spectra were recorded at 100 MHz and referenced to the methylene carbon of glycine, and then recalibrated to the TMS scale ($\delta_{\text{glycine}} = 43.3$ ppm).

Thermal analysis

Differential scanning calorimetry was performed on Mettler-Toledo DSC 822e module, (Mettler-Toledo, Columbus, OH). Samples were placed in crimped but vented aluminum pans for DSC experiments. The typical sample size is 3-5 mg for DSC. The temperature range for the heating curves was 30-300°C, and the sample was heated at a rate of 5 °C/min. Samples were purged in a stream of dry nitrogen flowing at 80 mL/min.

Powder X-ray diffraction

Powder X-ray diffraction was recorded on Bruker D8 Advance diffractometer (Bruker-AXS, Karlsruhe, Germany) using Cu-K α X-radiation ($\lambda = 1.5406$ Å) at 40 kV and 30 mA power. X-ray diffraction patterns were collected over the 2θ range 5–50° at a scan

rate of 5°/min. Powder Cell 2.4³⁰ (Federal Institute of Materials Research and Testing, Berlin, Germany) was used for Rietveld refinement of experimental PXRD and calculated lines from the x-ray crystal structure.

X-ray crystallography

X-ray reflections were collected on Oxford CCD X-ray diffractometer (Yarnton, Oxford, UK) equipped with Mo-K α radiation ($\lambda = 0.71073 \text{ \AA}$) source. Data reduction was performed using CrysAlisPro 171.33.55 software.^{30a} Crystal structures were solved and refined using Olex2-1.0 with anisotropic displacement parameters for non-H atoms.^{30b} Hydrogen atoms were experimentally located through the Fourier difference electron density maps in all crystal structures. All O–H, and C–H atoms were geometrically fixed using HFIX command in SHELX-TL program of Bruker-AXS. X-ray reflections on AP–VAN cocrystal were collected on Bruker SMART-APEX CCD diffractometer (Bruker-AXS, Karlsruhe, Germany). Mo-K α X-radiation ($\lambda = 0.71073 \text{ \AA}$) was used to collect X-ray reflections on the single crystal at 100K. Data reduction was performed using the Bruker SAINT software.^{31a} Intensities for absorption were corrected using SADABS,^{31b} the Siemens area detector absorption correction program (Bruker-AXS). Crystal structures were solved and refined using SHELX-97^{31c} with anisotropic displacement parameters for non-H atoms. Hydrogen atoms on O experimentally located in difference electron density maps. All C–H atoms were fixed geometrically using HFIX command in SHELX-TL (Bruker-AXS). A check of the final CIF file using PLATON^{31d,e} did not show any missed symmetry. Hydrogen bond distances shown in Table 2 are neutron normalized to fix the D–H distance to its accurate neutron value in the X-ray crystal structures (O–H 0.983 \AA , N–H 1.009 \AA , and C–H 1.083 \AA). X-Seed^{31f,g} was used to prepare packing diagrams. Crystallographic .cif files (CCDC Nos. 947292 – 947296) are available at www.ccdc.cam.ac.uk/data or as part of Supporting Information.

Dissolution and solubility

The solubility curve of AP and AP–SLA was measured using the Higuchi and Connor method³² in 25% ethanol-water medium at 30 °C. First, the absorbance of a known concentration of the pure compound was measured at the given λ_{max} (AP 225 nm, AP–SLA 227 nm) in 25% ethanol-water on a Thermo Scientific Evolution 300 UV-vis spectrometer (Thermo Scientific, Waltham, MA). These absorbance values were plotted

against several known concentrations to prepare the concentration vs. intensity calibration curve. From the slope of the calibration curves, molar extinction coefficients for AP and AP-SLA were calculated. An excess amount of the sample was added to 6 mL of 25% ethanol-water. The supersaturated solution was stirred at 300 rpm using a magnetic stirrer at 30 °C. After 24 h, the suspension was filtered through Whatman's filter paper No. 1. The filtered aliquots were diluted sufficiently, and the absorbance was measured at the given λ_{max} . IDR experiments were carried out on USP-certified Electrolab TDT-08L dissolution tester type II (paddle) (Mumbai, India). Dissolution experiments were performed for 6 h in 25% ethanol-water at 37 °C. Prior to IDR estimation, standard curves for all the compounds were obtained spectrophotometrically at their respective λ_{max} . The calculated molar extinction coefficients were used to determine the IDR values. For IDR measurements, 200 mg of the compound was taken in the intrinsic attachment and compressed to 0.5 cm² disk using a hydraulic press 4.0 ton/ in² pressure for 5 min. The intrinsic attachment was placed in a jar of 500 mL medium preheated to 37 °C and rotated at 150 rpm. 5 mL of the aliquot was collected at specific time intervals, and the concentration of the aliquots was determined with appropriate dilutions from the predetermined standard curves of the respective compounds. The IDR of the compound was calculated in the linear region of the dissolution curve (which is the slope of the curve or amount of drug dissolved/surface area of the disk) per unit time. The identity of the undissolved material at the end of dissolution/ solubility experiment was confirmed by PXRD. The nature of the solid samples after disk compression and solubility/dissolution measurements was verified by PXRD (to ascertain any phase changes, hydration, etc.).

2.7 References:

1. (a) G. R. Desiraju, J. J. Vittal, A. Ramanan, *Crystal Engineering. A Textbook*, World Scientific Publishing, Singapore, 2011; (b) G. R. Desiraju, *Crystal Engineering. The Design of Organic Solids*. Elsevier, 1989; (c) G. R. Desiraju, *Angew. Chem., Int. Ed. Engl.* 1995, **34**, 2311.
2. (a) N. Blagden, M. de Matas, P. T. Gavan and P. York, *Adv. Drug Deliv. Rev.*, 2007, **59**, 617; (b) A. V. Trask, *Mol. Pharmaceutics*, 2007, **4**, 301; (c) E. Lu, N. Rodríguez-Hornedo and R. Suryanarayanan, *CrystEngComm*, 2008, **10**, 665; (d) N. Schultheiss and A. Newman, *Cryst. Growth Des.*, 2009, **9**, 2950; (e) M. K.

- Stanton, R. C. Kelly, A. Colletti, Y.-H. Kiang, M. Langley, E. J. Munson, M. L. Peterson, J. Roberts and M. Wells, *J. Pharm. Sci.*, 2010, **99**, 3769; (f) N. J. Babu and A. Nangia, *Cryst. Growth Des.*, 2011, **11**, 2662; (g) N. K. Duggirala, M.L. Perry, Ö. Almarsson and M. J. Zaworotko *Chem. Commun.*, 2016, **52**, 640.
3. a) T. Friščić, D. B. Varshney, E. Elacqua, J. C. Sumrak, A. N. Sokolov, L. R. MacGillivray, in *Molecular Self-Assembly: Advances and Application* (Ed. A. L. Dequan) Pan Stanford Publishing, 2013, 223; (b) E. D. D'Silva, G. K. Podagatlapalli, S. V. Rao, D. N. Rao, S. M. Dharmaparakash, *Cryst. Growth Des.*, 2011, **11**, 5362; (c) D. P. Yan, A. Delori, G. O. Lloyd, T. Friščić, G. M. Day, W. Jones, J. Lu, M. Wei, D. G. Evans, X. Duan, *Angew. Chem. Int. Ed.*, 2011, **50**, 12483.
 4. (a) J. P. Shen, X. H. Duan, Q. P. Luo, Y. Zhou, Q. Bao, Y. J. Ma, C. H. Pei, *Cryst. Growth Des.*, 2011, **11**, 1759; (b) O. Bolton, L. R. Simke, P. F. Pagoria, A. J. Matzger, *Cryst. Growth Des.* 2012, **12**, 4311; (c) K. B. Landenberger, O. Bolton, A. J. Matzger, *Angew. Chem. Int. Ed.*, 2013, **52**, 6468.
 5. (a) T. Kawasaki, K. Jo, H. Igarashi, I. Sato, M. Nagano, H. Koshima, K. Soai, *Angew. Chem., Int. Ed.*, 2005, **44**, 2774. (b) H. Zhang, C. Guo, X. Wang, J. Xu, X. He, Y. Liu, X. Liu, H. Huang, and J. Sun. *Cryst. Growth Des.*, 2013, **13**, 679.
 6. (a) H. G. Brittain, *Physical Characterization of Pharmaceutical Solids*, Marcel Dekker Inc. NY, 1995; (b) S. R. Byrn, R. R. Pfeiffer and G. G. Stowell, *Solid-State Chemistry of Drugs*, SSCI, West Lafayette, IN, 1999; (c) Y. Qiu, Y. Chen and G.G.Z. Zhang, *Developing Solid Oral Dosage Forms: Pharmaceutical Theory and Practice*, First ed. Academic Press, NY, 2009. (d) M. K. Stanton, A. Bak *Cryst. Growth Des.*, 2008, **8**, 3856.
 7. (a) J. F. Remenar, S. L. Morissette, M. L. Peterson, B. Moulton, J. M. MacPhee, H. R. Guzmán, Ö. Almarsson, *J. Am. Chem. Soc.*, 2003, **125**, 8456; (b) C. B. Aakeröy, S. Forbes and J. Desper, *J. Am. Chem. Soc.*, 2009, **132**, 17048; (c) N. R. Goud, S. Gangavaram, K. Suresh, S. Pal, S. G. Manjunatha, S. Nambiar, A. Nangia, *J. Pharm. Sci.*, 2012, **101**, 664; (d) M. R. Cheney, N. Shan, E. R. Healey, M. Hanna, L. Wojtas, M. J. Zaworotko, V. Sava, S. Song, J. R. Sanchez-Ramos, *Cryst. Growth Des.*, 2010, **10**, 394.
 8. (a) J. F. Remenar, M. L. Peterson, P. W. Stephens, Z. Zhang, Y. Zimenkov, and M.B. Hickey. *Mol. Pharm.*, 2007, **4**, 386; (b) M. L. Cheney D. R. Weyna, N. Shan, M. Hanna, L. Wojtas, M. J. Zaworotko. *J. Pharm. Sci.*, 2011, **100**, 2172;

- (c) P. Sanphui, N. R. Goud, U. B. R. Khandavilli and A. Nangia. *Cryst. Growth Des.*, 2011, **11**, 4135; (d) A. J. Smith, P. Kavuru, L. Wojtas, M. J. Zawarotko and R. D. Shytle. *Mol. Pharm.*, 2011, **8**, 1867; (e) S. Aitipamula, A. B. H. Wong, P. S. Chow and R. B. H. Tan. *CrystEngComm*, 2012, **14**, 8515.
9. (a) A. V. Trask, W. D. S. Motherwell, W. Jones, *Cryst. Growth Des.*, **2005**, **5**, 1013; (b) S. Karki, T. Friščić, L. Fábián, P. R. Laity, G. M. Day, W. Jones, *Adv. Mater.*, 2009, **21**, 3905; (c) P. M. Bag, M. Chen, C. Calvin, C. M. Reddy, *CrystEngComm*, 2012, **14**, 3856; (d) R. Thipparaboina, D. Kumar, S. Mittapalli, S. Balasubramanian, A. Nangia and N. R. Shastri. *Cryst. Growth Des.*, **2015**, **15**, 5816.
 10. (a) V. R. Vangala, P. S. Chow, R. B. H. Tan, *CrystEngComm*, 2011, **13**, 759. (b) N. Geng, J-M. Chen, Z-J. Li, L. Jiang and T-B. Lu. *Cryst. Growth Des.*, 2013, **13**, 3546; (c) J-R. Wang, C Zhou, X. Yu and X. Mei. *Chem. Commun.*, 2014, **50**, 855-858; (d) B. Zhu, J-R Wang, Q. Zhang and X. Mei. *Cryst. Growth Des.*, 2016, **16**, 483.
 11. (a) N. J. Babu, P. Sanphui, A. Nangia, *Chem. Asian J.*, 2012, **7**, 2274; (b) Z-Z. Wang, J-M. Chen, and T-B. Lu *Cryst. Growth Des.*, 2012, **12**, 4562; (c) S. Cherukuvada, N. J. Babu, A. Nangia, *J. Pharm. Sci.*, 2011, **100**, 3233; (d) A. V. Trask, W. D. S. Motherwell, and W. Jones *Cryst. Growth Des.*, 2005, **5**, 1013
 12. (a) R. P. Samy, M. M. Thwin, P. Gopalakrishnakone, *Nat. Prod. Commun.*, 2007, **2**, 607; (b) P. K. Singha, S. Roy, S. Dey, *J. Ethnopharmacol.*, 2007, **111**, 13.
 13. (a) A. Y. Woo, M. M. Waye, S. K. Tsui, S. T. Yeung, C. H. Cheng, *J. Pharmacol. Exp. Ther.*, 2008, **325**, 226; (b) F. Zhao, E. Q. He, L. Wang, K. Liu, *J. Asian Nat. Prod. Res.*, 2008, **10**, 467; (c) A. P. Raina, A. Kumar, S. K. Pareek, *Ind. J. Pharm. Sci.*, 2007, **69**, 473; (d) K. Mishra, A.P. Dash, N. Dey, *J. Trop. Med.*, 2011, 1.
 14. (a) L. Ye, T. Wang, L. Tang, W. Liu, Z. Yang, J. Zhou, Z. Zheng, Z. Cai, M. Hu, Z. Liu, *J. Pharm. Sci.*, 2011, **100**, 5007; (b) M. Chen, C. Xie, L. Liu, *J. Chem. Eng. Data.*, 2010, **55**, 5297.
 15. (a) L. Cui, F. Qiu, N. Wang, X. Yao, *Chem Pharm Bull.*, 2004, **52**, 772; (b) H.-Y. Zhao, H. Hu, Y.-T. Wang, *Rapid. Commun. Mass Spectrom.*, 2013, **27**, 1385;

- (c) Z. M. Meng, *Acta Pharmaceutica Sinica*, 1981, **16**, 571; (d) X. He, J. Li, H. Gao, F. Qiu, K. Hu, X. Cui, X. Yao, *Drug Metab. Dispos.*, 2003, **31**, 983.
16. (a) A. B. Smith, B. H. Toder, P. J. Corroli, J. Dononohue. *J. Crystallogr. Spectrosc. Res.*, 1982, **12**, 309; (b) S. Pramanick, S. Banerjee, B. Achari, B. Das, A. K. Sen, S. Mukhopadhyay, A. Neuman, T. Prangé, *J. Nat. Prod.*, 2006, **69**, 403.
17. (a) T. Friščić, W. Jones, *Cryst. Growth Des.* 2009, **9**, 1621; (b) A. V. Trask and W. Jones, *Top Cur. Chem.*, 2005, **254**, 41; (c) N. Shan, F. Toda and W. Jones, *Chem Commun.*, 2002, **20**, 2372.
18. (a) G. R. Desiraju, *Angew. Chem., Int. Ed. Engl.*, 1995, **34**, 2311.
19. (a) D. Cinčić, T. Friščić, W. Jones, *New J. Chem.*, 2008, **32**, 1776; (b) S. Ebenezer, P. T. Muthiah, R. J. Butcher, *Cryst. Growth Des.*, 2011, **11**, 3579; (c) N. K. Nath, B. K. Saha, A. Nangia. *New J. Chem.*, 2008, **32**, 1693; (d) A. Kálmán, L. Párkányi, G. Argay, *Acta Crystallogr.*, 1993, **B49**, 1039.
20. (a) T. Gelbrich, T. L. Threlfall, M. B. Hursthouse, *CrystEngComm*, 2012, **14**, 5454; (b) T. Gelbrich, M. B. Hursthouse, *CrystEngComm*, 2006, **8**, 448; (c) T. Gelbrich, M. B. Hursthouse, *CrystEngComm*, 2005, **7**, 324.
21. M. Dabros, P. R. Emery, V. R. Thalladi, *Angew. Chem., Int. Ed.* 2007, **46**, 4132.
22. (a) K. D. M. Harris, M. Tremayne and B. M. Kariuki, *Angew. Chem. Int. Ed.*, 2001, **40**, 1626; (b) K. D. Harris, M. Tremayne, P. Lightfoot and P. G. Bruce, *J. Am. Chem. Soc.*, 1994, **116**, 3543; (c) E. Y. Cheung, S. J. Kitchin, K. D. M. Harris, Y. Imai, N. Tajima and R. Kuroda, *J. Am. Chem. Soc.*, 2003, **125**, 14658; (c) T. Ueto, N. Takata, N. Muroyama, A. Nedu, A. Sasaki, S. Tanida, and K. Terada. *Cryst. Growth Des.*, 2012, **12**, 485.
23. (a) R. M. Silverstein, F. X. Webster and D. J. Kiemle, *Spectrometric Identification of Organic Compounds*, John Wiley & Sons, NJ, 2005; (b) E. Smith and G. Dent, *Modern Raman Spectroscopy, A Practical Approach*, John Wiley: New York, 2005; (c) S. L. Childs, G. P. Stahly and A. Park, *Mol. Pharm.*, 2007, **4**, 323; (d) Z. J. Li, Y. Abramov, J. Bordner, J. Leonard, A. Medek and A. V. Trask, *J. Am. Chem. Soc.*, 2006, **128**, 8199; (e) F. G. Vogt, J. S. Clawson, M. Strohmeier, A. J. Edwards, T. N. Pham and S. A. Watson, *Cryst. Growth Des.*, 2009, **9**, 921.
24. (a) D. Braga, L. Maini, G. de Sanctis, K. Rubini, F. Grepioni, M. R. Chierotti and R. Gobetto, *Chem – Eur. J.*, 2003, **9**, 5538. (b) Z. J. Li, Y. Abramov, J.

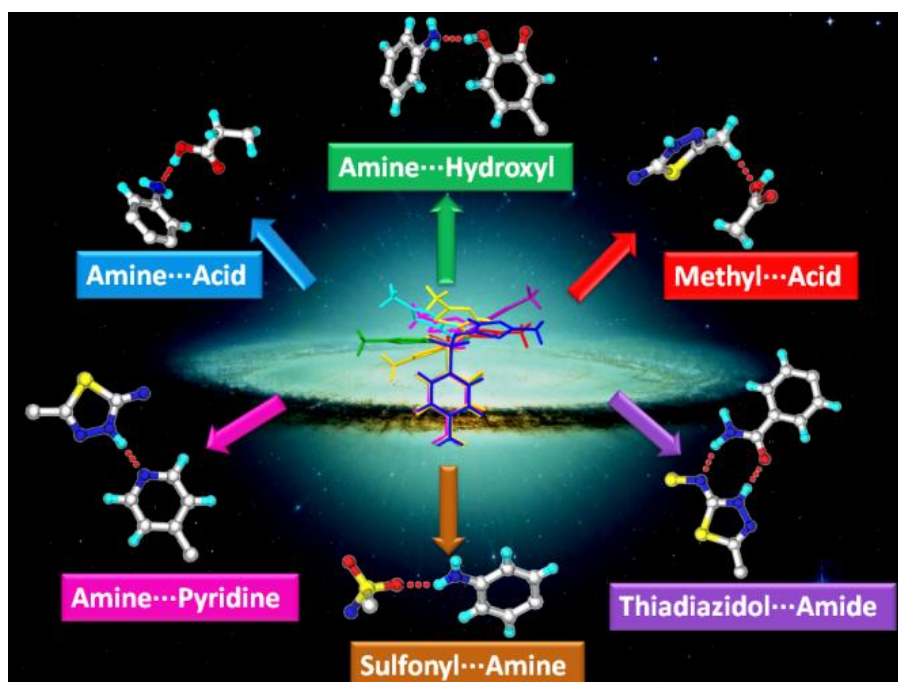
- Bordner, J. Leonard, A. Medek and A. V. Trask, *J. Am. Chem. Soc.*, 2006, **128**, 8199.
25. (a) W. Jones, W. D. S. Motherwell and A. V. Trask, *MRS Bull.*, 2006, **31**, 875; (b) M. K. Stanton and A. Bak, *Cryst. Growth Des.*, 2008, **8**, 3856; (c) M. K. Stanton, S. Tufekcic, C. Morgan and A. Bak, *Cryst. Growth Des.*, 2009, **9**, 1344.
26. (a) M. Charton, *Can. J. Chem.*, 1960, **38**, 2493; (b) K. Bowden, G. E. Manser, *Can. J. Chem.*, 1968, **46**, 2941; (c) U. Berg, R. Gallo, G. Klatte, J. Metzger, *J. Chem. Soc., Perkin Trans. 2*, 1980, 1350; (d) M. H. Aslam, A. G. Burden, N. B. Chapman, J. Shorter, M. Charton, *J. Chem. Soc., Perkin Trans. 2*, 1981, 500; (e) S. Böhm, P. Fiedler, O. Exner, *New J. Chem.*, 2004, **28**, 67.
27. (a) T. Takagi, C. Ramachandran, M. Bermejo, S. Yamashita, X. L. Yu, G. L. Amidon, *Mol. Pharm.*, 2006, **3**, 631; (b) C. A. Lipinski, in *Pharmaceutical profiling in Drug Discovery for Lead Selection*, Eds: R. T. Borchardt, E. H. Kerns, C. A. Lipinski, D. R. Thakker, B. Wang; AAPS Press, Arlington, VA, 2004, 93.
28. J. B. Dressman, G. L. Amidon, C. Reppas, V. P. Shah, *Pharm. Res.*, 1998, **15**, 11.
29. S. Cherukuvada, G. Bolla, K. Sikligar, A. Nangia, *Cryst. Growth Des.*, 2013, **13**, 1551.
30. Powder Cell, a program for structure visualization, powder pattern calculation and profile fitting. <http://www.ccp14.ac.uk/tutorial/powdcell/>.
31. (a) CrysAlis CCD and CrysAlis RED, Versions 1.171.33.55, Oxford Diffraction, Oxford, 2008; (b) O. V. Dolomanov, L. J. Bourhis, R. J. Gildea, J. A. K. Howard, H. Puschmann, *J. Appl. Crystallogr.*, 2009, **42**, 339.
32. (a) SAINT-Plus, Ver. 6.45; Bruker AXS, Madison, WI, 2003; (b) G. M. Sheldrick, SADABS, *Program for Empirical Absorption Correction of Area Detector Data*; University of Göttingen, Göttingen, Germany, 1997; (c) G. M. Sheldrick, SHELX-97, *Program for the Solution and Refinement of Crystal Structures*, University of Göttingen: Göttingen, Germany, 1997; (d) A. L. Spek, PLATON: *A Multipurpose Crystallographic Tool*; Utrecht University, Utrecht, The Netherlands, 2002; (e) A. L. Spek, *J. Appl. Crystallogr.*, 2003, **36**, 7; (f) L. J. Barbour, *Supramol. Chem.* 2001, **1**, 189; (g) L. J. Barbour, *X-Seed, Graphical*

Interface to SHELX-97 and POV-Ray; University of Missouri-Columbia, Columbus, MO, 1999.

33. T. Higuchi, K. A. Connors, *Adv. Anal. Chem. Instrum.*, 1965, **4**, 117.

CHAPTER THREE

Novel Synthons in Sulfamethizole Cocrystals: Structure–Property Relations and Solubility



Sulfamethizole is a conformationally flexible drug molecule with multiple hydrogen bond functionalities (donors: amine NH_2 and imine NH ; acceptors: sulfonyl O atoms, thiazolidine N and S , and imidine N). Six novel $\text{N-H}\cdots\text{O}$ and $\text{O-H}\cdots\text{N}$ synthons as well as weaker hydrogen bonds and chalcogen interactions are analyzed in cocrystals of this drug. The SMT cocrystals and salt with low solubility and good stability may be suitable candidates for making an extended release formulation of SMT to improve its therapeutic efficacy.

3.1 Introduction

Crystal engineering is emerged and an important tool in the supramolecular chemistry which support in the invention of new molecular structures having desired properties with a target supramolecular assembly that enacts the network approach between molecular and supramolecular structure on the basis of intermolecular interactions.¹ Thus the prime tenet of crystal engineering being “*making crystal with purpose*”. Cocrystals are *multicomponent system assembled via non covalent interactions in crystal lattice* and which are designed via supramolecular synthon strategies.^{1,2,3} Specifically cocrystallization methodology furnishes opportunities for the Active Pharmaceutical Ingredients (APIs) to fine tune their properties.⁴ Cocrystals of APIs with GRAS or nutraceutical cofomer are termed as pharmaceutical cocrystals have gained increased importance and popularity in academic and pharmaceuticals. Especially cocrystals are amenable to modify crystal arrangements of non-ionizable APIs.⁵ Cocrystals can modify the physicochemical properties and they can be easily synthesized by various methods such as limited or no use of solvent grinding.⁶ The proliferation of this cocrystallization strategy is illustrated by many examples in the literature including patents.^{4,5,6} The application of cocrystals is widely appreciated by solubility and stability enhancement of poorly soluble drugs (40% in the market) in pharmaceuticals.^{4,7} However, in the present market about 60% drug molecules have moderate to high solubility. Even though higher solubility of a drug is essential to maintain the drug concentration in blood for therapeutic efficacy, but sometimes it creates limited bioavailability due to short half-life and rapid metabolism resulting in faster elimination. This requires frequent administration of dosage or high dosage at a time to improve the bioavailability and maintain optimum drug concentration in blood leading to drug-patient incompatibility.⁸ Therefore in order to address this issue, modified, extended release formulations were developed for high soluble drugs.⁹ Various methods such as hot melt extrusion, polymer assisted matrix tablets compression coated matrix tablets and lipase-enzyme coated tablets etc. are commonly used to prepare extended release formulations.¹⁰ This type of formulations allow the steady release of the drug molecule for extended release to maintain the drug concentration in blood leading to better therapeutic efficacy. Augmentin XR (combination of amoxicillin and clavulanate potassium)^{11a} and Ecosprin (aspirin)^{11b} are early examples of this choice. Recently Remington et. al. has also recognized that making of less soluble form of a high/moderate soluble drug is a facile

procedure for producing extended release formulations.¹² Literature reports showed that in the process of cocrystallization, self-assembly of hydrogen bonding patterns of high soluble drug molecules can be modified with pertinent coformer to lower their solubility.¹³ For instance the natural bioflavonoid molecule Epigallocatechin-3-gallate (EGCg) extensively studied to improve the bioavailability by cocrystallization. It is a highly soluble (20 mg/mL) molecule, but it has poor bioavailability because of rapid metabolism and faster elimination, due to this reason it is not yet approved as a drug. Smith et. al.^{13a,b} proposed to study the cocrystallization effect by reducing the solubility on EGCg and improves the pharmacokinetic profile. They designed cocrystals with isonicotinamide (INM) and isonicotinic acid (INA) cofomers and shown that EGCg cocrystals exhibited lower aqueous solubility than pure EGCg and subsequently bioavailability of the EGCg is improved. Especially the relative bioavailability of EGCg-INA.3H₂O and EGCg-INA is 1.53 and 1.18 folds higher compared to EGCg (Figure 3.1). Thus they showed that the bioavailability of the EGCg is improved by lowering its solubility via cocrystallization. In another article, the high solubility of sulfacetamide (SACT, sulfonamide class drug) is controlled in pharmaceutical cocrystals with lower dissolution rates, reported by Goud et al.^{13c} they have shown that SACT-theophylline, SACT-caffeine and SACT-isonicotinic acid cocrystals exhibited lowering dissolution rates than SACT. Among three, SACT-Caffeine cocrystal showed lower solubility and good stability in the dissolution and equilibrium solubility experiments (Figure 3.2).

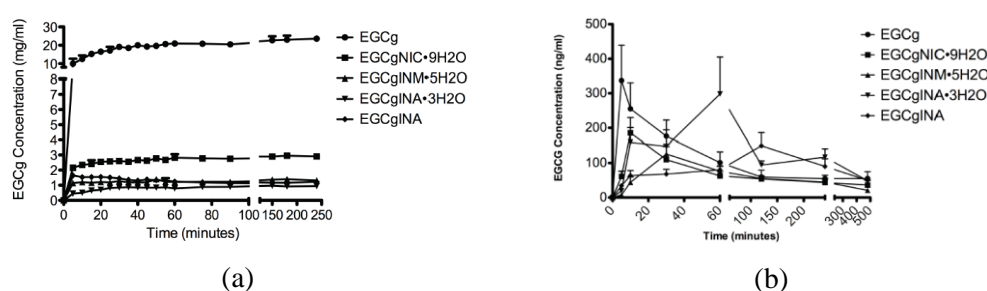
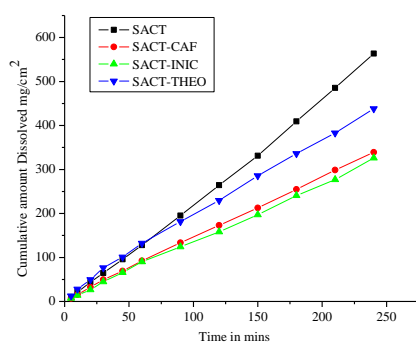
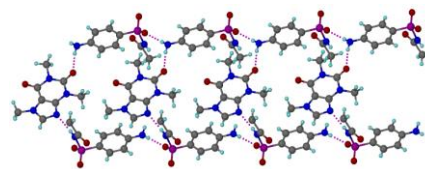


Figure 3.1 (a) Dissolution profile of EGCg and its cocrystals in water. The graph indicates that all the cocrystals have far lower dissolution rate compared to the parent molecule (Adapted from ref. 13b). (b) Pharmacokinetic profile of EGCg and its cocrystals. The relative bioavailability of EGCgINA.3H₂O and EGCgINA cocrystals are 1.53 and 1.18 times higher compared to EGCg (Adapted from ref. 13b).



(c)



(d)

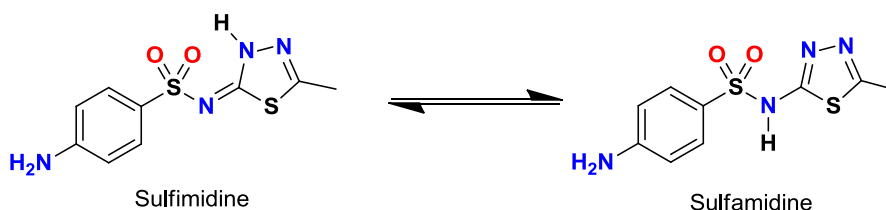
Figure 3.2 (a) Intrinsic dissolution rate curves of SACT and its cocrystals in pH 7 Buffer. (b) Linear chains of SACT molecules bridged through CAF coformer molecules. (Only one layer of CAF molecules are shown for clarity).^{13c}

Apart from the studies of Smith et.al on EGCg and Goud et. al. on SACT, there are limited literature reports showed that the solubility of drug/natural molecules can be lowered by making cocrystal.¹⁴ However these results suggest that the cocrystal approach is adaptable to modulate the solubility towards higher or lower levels by rational selection of coformers to addressing the poor bioavailability of highly soluble drugs/bioactive molecules. Hence with this background of the study in this chapter we highlight the solubility lowering ability of cocrystals and salt. Moreover we also discussed different synthons preferences/competition with same/different functionalities of coformers in SMT cocrystals.

3.2 Literature reports on Sulfamethizole

Sulfamethizole (SMT) is a sulfonamide class antibiotic drug that acts through the competitive inhibition of folate synthesis in microorganisms.¹⁵ SMT has better solubility (1.05 g/L at 37 °C in water)¹⁶ even though it has a short half-life (2.1 h) due to rapid metabolism leads to fast elimination.¹⁷ Most of sulfonamide class drugs exhibit moderate to high solubility but bioavailability is limited due to rapid metabolism and fast elimination. As a result the dosage strength of sulfonamide drugs has to be higher. To improve the concentration of SMT in blood level, an extended release of Lipase-SMT granule system is reported,¹⁸ in dogs. The concentration of SMT in blood level extended to 12 hours. A reason behind this improvement is rapid metabolism is reduced by a lipase enzyme which controls the digestion of glyceryl trilaurate and glyceryl tristearate and subsequent release of the embedded drug particles. Cambridge Structural Database

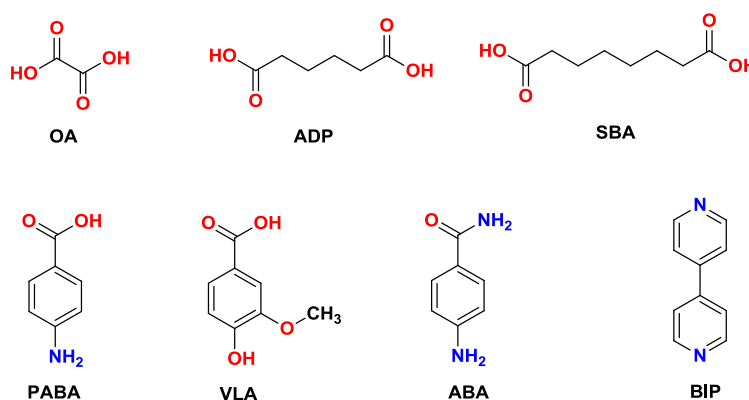
(CSD) search on SMT, no polymorphs, solvates/hydrates, or cocrystals/salts are disclosed, only one crystal structure is reported.¹⁹ The crystal structure of SMT (reported in 1987) represents that the molecule exists as the sulfimidine tautomer and there is a chance to exist as sulfamidine tautomer (Scheme 3.3).



Scheme 3.3 Schematic representation of tautomerism in sulfamethizole

3.3 Preparation of Sulfamethizole Cocrystals and Salt

The cocrystals were produced by co-grinding²⁰ as a first choice method. The bulk phase composition of adducts was tested by powder X-ray diffraction, DSC and IR. The powder samples were used as seeds in evaporative crystallization (see Experimental Section)²¹ to obtain single crystals for X-ray diffraction. Cocrystals with adipic acid (ADP), *p*-aminobenzoic acid (PABA), vanillic acid (VLA), *p*-aminobenzamide (ABA), suberic acid (SBA), 4,4'-bipyridine (BIP), and a salt with oxalic acid (OA) was crystallized. The crystal structures were solved and refined. Relatively synthon preferences/competition in SMT cocrystals with respect coformer and implications of such cocrystals/salt formation on the solubility and dissolution of SMT are discussed in this chapter.



Scheme 3.4 Chemical structures of cofomers successful in forming cocrystals with SMT. Abbreviations are used entire chapter.

3.4 Results and Discussion

SMT drug has rich and strong hydrogen bonding functionalities (two donors: amine NH_2 and imine NH ; five acceptors: two sulfonyl O atoms, thiazolidine N and S, and imidine N) makes it capable of forming cocrystals with cofomer partners. Therefore GRAS and model non GRAS cofomers containing COOH , NH_2 , pyridine and CONH_2 functional group were chosen to form complementary synthons with rich functionalities of SMT in a cocrystal. Cocrystals with ADP, PABA, VLA, ABA, SBA, BIP, and a salt with OA cofomers was crystallized. The crystal structures were solved and refined. Selected crystal data, data collection and refinement parameters are summarized in Table 3.1 and 3.2.

Table 3.1 Summary of crystal structure parameters.

	SMT-ADP	SMT-PABA	SMT-VLA	SMT-ABA	SMT-BIP	SMT-SBA	SMT-OA
Chemical formula	(C ₉ H ₁₀ N ₄ O ₂ S ₂). 0.5 (C ₆ H ₁₀ O ₄)	(C ₉ H ₁₀ N ₄ O ₂ S ₂). (C ₇ H ₇ N O ₂)	(C ₉ H ₁₀ N ₄ O ₂ S ₂). (C ₈ H ₈ O ₄)	(C ₉ H ₁₀ N ₄ O ₂ S ₂). (C ₇ H ₈ N ₂ O)	(C ₉ H ₁₀ N ₄ O ₂ S ₂). (C ₁₀ H ₈ N ₂)	2(C ₉ H ₁₀ N ₄ O ₂ S ₂). (C ₈ H ₁₄ O ₄)	(C ₉ H ₁₁ N ₄ O ₂ S ₂). (C ₂ H O ₄)
Formula weight	343.40	407.47	490.61	406.48	426.51	714.85	360.37
Crystal system	Monoclinic	Monoclinic	Monoclinic	Triclinic	Monoclinic	Orthorhombic	Monoclinic
Space group	$P2_1/c$	$P2_1/n$	$P2_1/c$	$P\bar{1}$	$P2_1/n$	$Pc a 2_1$	$P2_1/c$
T [K]	100(2)	100(2)	100(2)	100(2)	100(2)	100(2)	100(2)
a [Å]	7.9915(4)	9.2097(3)	8.1263(5)	13.5102(6)	8.1754(7)	10.4481(3)	8.0559(3) Å
b [Å]	21.6918(8)	10.8241(5)	19.7763(7)	15.2418(6)	18.6120(10)	19.2259(5)	20.6543(6)
c [Å]	8.5756(4)	18.2910(7)	12.0584(7)	18.3238(7)	13.1690(11)	16.5666(7)	8.5539(4)
α [°]	90	90	90	99.534(3)	90	90	90
β [°]	95.737(4)	101.645(3)	109.396(4)	98.720(3)	93.048(7)	90	99.903(3)
γ [°]	90	90	90	90.086(3)	90	90	90
Z	4	4	4	8	4	4	4
V [Å ³]	1479.13(11)	1785.84(12)	1827.90	3676.7(3)	2001.0(3)	3327.80(19)	1402.07(9)
D_{calc} [g cm ⁻³]	1.542	1.516	1.593	1.469	1.416	1.427	1.707
Reflns. collected	17542	21883	27232	59096	12415	26795	12515
Unique reflns.	3665	4427	4527	16205	3412	7643	3479
R_1 [I>2(I)]	0.0291	0.0294	0.0292	0.0943	0.0560	0.0440	0.0324
wR_2 (all)	0.0714	0.0748	0.0707	0.2399	0.1160	0.0865	0.0789
Goodness-of-fit	1.016	1.022	1.059	1.116	1.047	1.040	1.034
Diffractionmeter	STOE	STOE	STOE	STOE	STOE	STOE	STOE
CCDC No.	1060516	1060513	1060511	1060517	1060515	1060512	1060514

Table 3.2 Selected geometric parameters characterizing hydrogen bonds in SMT cocrystals and salt.

D–H...A	D...A (Å)	H...A (Å)	D–H...A (°)	symmetry code
SMT-ADP				
N1–H1A...N2	3.306(17)	2.48	160	-1+x,y,z
N1–H1B...O1	2.930(17)	2.29	130	-1+x,1/2-y,-1/2+z
N3–H3A...O3	2.748(16)	1.96	173	x,y,-1+z
O4–H4A...N1	2.705(16)	1.76	168	1+x,y,1+z
C2–H2...O2	2.928(16)	2.57	102	intramolecular
C3–H3...N2	3.451(17)	2.61	147	-1+x,y,z
SMT-PABA				
N1–H1B...N5	3.393(2)	2.52	175	3/2-x,1/2+y,1/2-z
N3–H3A...N2	2.895(15)	2.00	173	2-x,1-y,1-z
O3–H3B...O4	2.616(14)	1.80	173	1-x,1-y,1-z
N5–H5A...O2	2.968(15)	2.41	122	-1+x,-1+y,z
N5–H5B...O1	3.115(16)	2.29	162	1/2-x,-1/2+y,1/2-z
C11–H1...O3	2.743(16)	2.37	102	Intramolecular
SMT-VLA				
N1–H1A...O1	3.247(3)	2.52	146	-1+x,1/2-y,-1/2+z
N3–H3A...O5	2.769(5)	2.18	130	x,1/2-y,1/2+z
N3–H3A...O6	3.155(4)	2.38	161	x,1/2-y,1/2+z
O4–H4A...O3	2.621(2)	1.80	177	-x,-y,1-z
O5–H5A...N1	2.760(1)	1.91	166	-x,-y,-z
C9–H9B...O1	3.337(9)	2.44	155	1-x,1/2+y,1/2-z
SMT-BIP				
N1–H1A...O2	2.971(4)	2.17	159	1/2+x,1/2-y,-1/2+z
N1–H2A...O1	3.025(4)	2.12	165	1+x,y,z
N1–H3A...N6	2.739(4)	1.84	170	-3/2+x,1/2-y,-1/2+z
C3–H3...O2	3.320(4)	2.56	136	1/2+x,1/2-y,-1/2+z
C6–H6...O2	2.919(4)	2.51	107	Intramolecular
C13–H13...O1	3.447(5)	2.53	151	1+x,y,z
C19–H19...O1	3.447(4)	2.41	177	1+x,y,z
SMT-SBA				
N1–H1A...O1	2.937(4)	2.05	164	-3/2-x,y,-1/2+z
N1–H1B...O2	2.894(4)	2.07	166	1-x,-y,-1/2+z
N3–H3A...N6	2.851(3)	1.94	174	x,y,z
N5–H5A...O3	2.961(3)	2.00	164	1/2-x,y,-1/2+z
N5–H5B...O4	2.888(3)	2.08	150	1-x,1-y,-1/2+z
O6–H6A...O7	2.640(3)	1.81	172	1+x,y,z
N7–H7A...N2	2.845(3)	2.02	167	x,y,z
O8–H8A...O5	2.670(3)	1.88	167	-1+x,y,z
C9–H9B...O2	3.400(4)	2.60	139	-1/2+x,-y,z
C18–H18A...N4	3.489(4)	2.56	158	1+x,y,z
C9–H9A...O6	3.321(4)	2.65	126	1/2-x,y,-1/2+z
SMT-OA				
N1–H1A...N2	2.9837(19)	2.08	173	-1+x,y,z

N1–H1B...O1	2.7853(19)	2.25	116	-1+x,1/2-y,-1/2+z
N1–H1B...O5	3.1302(19)	2.40	137	-1+x,1/2-y,-1/2+z
N1–H1C...O4	2.8815(19)	2.35	118	-1+x,y,-1+z
N1–H1C...O5	2.8360(18)	2.00	154	-1+x,y,-1+z
N3–H3A...O4	2.6642(17)	1.78	166	x,y,-1+z
O6–H6A...O3	2.6658(17)	2.13	118	Intramolecular
O6–H6A...O3	2.7017(17)	1.96	139	2-x,-y,1-z
C2–H2...O2	2.9307(19)	2.59	102	Intramolecular
C3–H3...O6	3.0872(18)	2.55	114	-1+x,y,z
C6–H6...O1	2.9470(2)	2.55	103	Intramolecular

SMT-ABA

N1–H1A...N14	3.277(8)	2.27	154	1-x,-y,-z
N1–H1B...O14	2.926(7)	1.89	160	-1+x,y,z
N3–H3A...O4	2.967(7)	1.95	156	1+x,y,z
N4–H4A...N11	3.068(8)	2.08	150	x,y,z
N4–H4B...N21	3.070(8)	2.22	134	x,y,z
N5–H5A...N24	3.033(8)	2.03	153	-1+x,y,z
N5–H5B...N12	3.061(8)	2.19	136	x,y,z
N6–H6A...O2	2.971(7)	2.01	146	x,y,z
N6–H6B...N23	3.335(8)	2.26	173	1-x,1-y,-z
N8–H8B...O13	2.973(7)	1.93	160	x,y,z
N10–H10...O2	2.654(6)	1.77	177	x,y,z
N12–H12A...O8	3.546(7)	2.51	161	-1+x,y,z
N12–H12B...O9	3.030(7)	1.96	169	x,y,z
N13–H13A...O8	3.030(7)	2.07	146	x,y,z
N13–H13B...O9	3.440(7)	2.50	145	1+x,y,z
N15–H15...O13	2.710(6)	1.83	175	x,y,z
N18–H18...O14	2.668(7)	1.79	177	-1+x,y,z
N20–H20A...O5	3.448(7)	2.41	161	x,y,z
N20–H20B...O11	3.039(7)	1.98	166	x,-1+y,z
N21–H21B...O5	3.030(7)	1.96	170	x,1+y,z
N22–H22...O4	2.667(6)	1.79	179	1+x,y,z
N25–H25A...N16	2.964(7)	1.96	153	x,y,z
N25–H25B...N20	3.066(8)	2.17	139	x,y,z
N26–H26A...N19	2.991(6)	2.00	151	1+x,y,z
N26–H26B...N13	3.057(7)	2.18	137	x,y,z
C31–H31...O12	3.395(7)	2.46	168	x,-1+y,z
C34–H34...O7	3.276(8)	2.57	131	x,y,z
C40–H40...O6	3.316(7)	2.58	134	-1+x,1+y,z
C43–H43...O10	3.413(8)	2.47	171	x,y,z
C49–H49...O7	3.397(7)	2.46	167	x,y,z
C52–H52...O12	3.285(7)	2.57	132	1+x,-1+y,z
C61–H61...O10	3.304(7)	2.57	134	x,y,z
C64–H64...O6	3.413(8)	2.47	170	x,1+y,z

3.4.1 Crystal Structure Analysis

In the X-ray crystal structure of SMT¹⁹ the conformationally flexible molecule exists as the imidine tautomer (Scheme 3.3). The sulfimidine nitrogen and amine nitrogen atoms form a dimeric N–H···N (N1–H1···N3 2.42 Å, 148.6°) hydrogen bond synthon in a $R_2^2(8)$ ring motif (Figure 3.5). These dimeric motifs are associated through bifurcated type II inter chalcogen-chalcogen S···O (S1···O2, 3.22 Å, 157°) interactions of $R_2^2(10)$ rings as a 1D chain, which are in turn connected via N–H···N (N1–H1A···O 2.19 Å, 163°) hydrogen bonds.

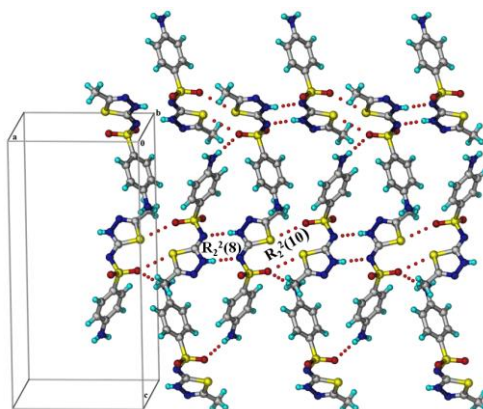
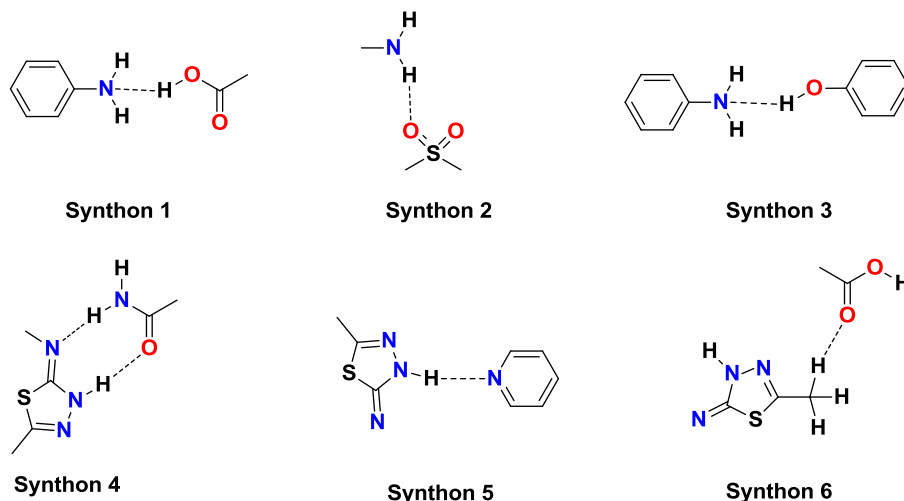


Figure 3.5 Linear chains of SMT molecule are bridged by N–H···N (N4–H9···N2 2.26 Å, 163.2°) hydrogen bond interaction in 2D network¹⁹ (CSD refcode FOLHAP).

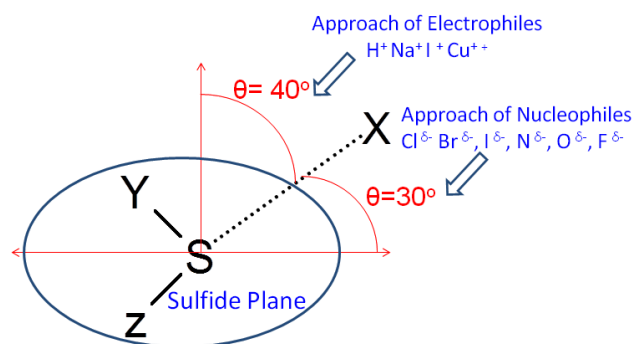
Intersignly in all cocrystal crystal structures, the hydrogen bond motifs of Figure 3.5 are replaced by new synthons (Scheme 3.6). Specifically synthon preferences/competition arises when acceptor is selected by the number of donors or *vice versa* during crystallization. Many literature reports were highlighted the hydrogen bond competition and hierarchy of hydrogen bonding in single and multicomponent systems. The strong and directional O–H···O, O–H···N, N–H···O, and N–H···N are regularly used hydrogen bonds to construct the cocrystals. Additionally the weak C–H···O, C–H···N, π - π stacking, hetero atom bonding also have potential to steer the supramolecular assembly in cocrystals. Studies on the above non covalent interactions and its competition and cooperation will give a basic understanding of the functional materials property behaviour. Relatively synthon preferences/competition was observed in SMT cocrystals with respect to coformer. Here, in addition to strong N–H···O and O–H···N H-bonds, the cocrystal structures are also sustained by weak C–H···O hydrogen bonds. The very rare and uncommon chalcogen-chalcogen (S···O) type II intermolecular interaction in SMT-

ADP cocrystal and chalcogen-nitrogen ($S\cdots N$) type II interaction in SMT-BIP cocrystal were observed.



Scheme 3.6 Schematic representations of supramolecular synthons in SMT cocrystals observed in this study.

Generally, sulfur is an ambivalent atom and acts either as an electrophile or a nucleophile, depending on the partner heteroatom. While coordinating to metal complexes ($X = H^+, Na^+, Cu^+$), S acts as a nucleophile and approaches them along the lone pair direction, while non-bonded interactions with halogens or electronegative atoms (Cl, Br, I, N, O, F, X^-), when S acts as an electrophile, the approach is in the Y–S–Z plane (Figure 3.7). The two main types of non-bonded contacts of divalent sulfur are defined as Type I and Type II. In Type I interactions, $S\cdots X$ directionality is $<40^\circ$ from the perpendicular to the Y–S–Z plane ($0 < [\theta] \leq 40^\circ$), whereas in Type II interactions $S\cdots X$ directionality is $<30^\circ$ from the perpendicular to the Y–S–Z plane ($60 < [\theta] \leq 90^\circ$).²²



If $0 < [\theta] \leq 40^\circ$, Type I

If $60 < [\theta] \leq 90^\circ$, Type II

Figure 3.7 Type I and Type II geometry of Sulfur...Heteroatom ($S \cdots X$) nonbonded interactions classified based on the $S \cdots X$ directional preference to the $Y-S-Z$ plane.⁴¹

The heteroatom interactions in pure SMT are of Type II. In the structures of SMT-ADP and SMT-BIP, the S atom acts as an electrophile ($S^{\delta+}$) to the oxygen ($O^{\delta-}$) and nitrogen ($N^{\delta-}$) acceptor atoms, and the interaction may be termed as Type II.

Sulfamethizole-Adipic acid (SMT-ADP, 1:0.5) cocrystal: ADP binds to two SMT molecules through single amine-acid H bond (synthon 1, Scheme 3.6) ($O4-H4A \cdots N1$, 1.76 Å, 168°). The acid group of ADP binds to the lone pair of NH_2 group of SMT. The sinusoidal wave is extended in a 1D motif through type II chalcogen-oxygen $S \cdots O$ ($S2 \cdots O4$, 3.176 Å, 164°) intermolecular interaction between the thiazolidine S and sulfonyl O of SMT molecules (Figure 3.8). The more electronegative oxygen acts as a nucleophile ($O^{\delta-}$) and the sulfur acts as an electrophile ($S^{\delta+}$) in a $R_2^2(10)$ ring motif. The nonbonded heteroatom interactions $S \cdots O$ and $Se \cdots O$ electrostatic interactions have been studied computationally.²³ The molecular chains are sustained by strong $N-H \cdots O=S$ ($N3-H3A \cdots O3$ 1.96 Å, 173°) hydrogen bonds in a 2D network.

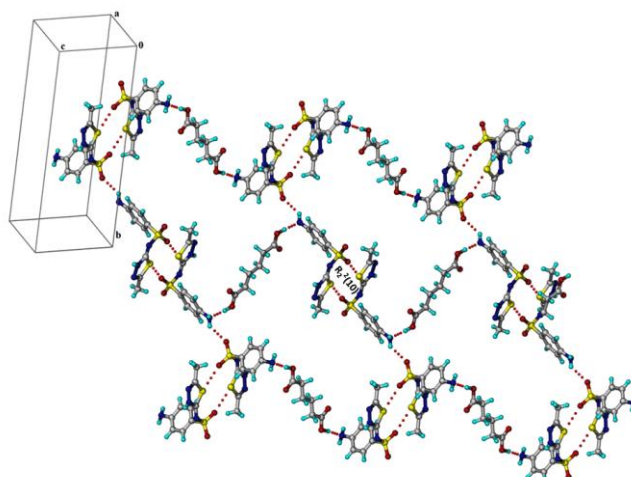


Figure 3.8 Zigzag chains of SMT-ADP molecules linked through type II S...O interactions; the chains are sustained by strong N-H...O=S bonds in a 2D structure.

Sulfamethizole- *p*-aminobenzoic acid (SMT-PABA, 1:1) cocrystal: PABA interacts with SMT through amine-sulfonyl synthon (synthon 2, Scheme 3.6) (N5-H5A...O2: 2.41 Å, 122°). The N-H...N dimer $R_2^2(10)$ ring motif of SMT (N3-H3A...N2 2.00 Å, 170°) and acid dimer $R_2^2(10)$ ring motif of PABA present in the structures of pure components were preserved also in cocrystal (Figure 3.9). Cocrystal extend into a linear chain through N-H...O=S interaction.

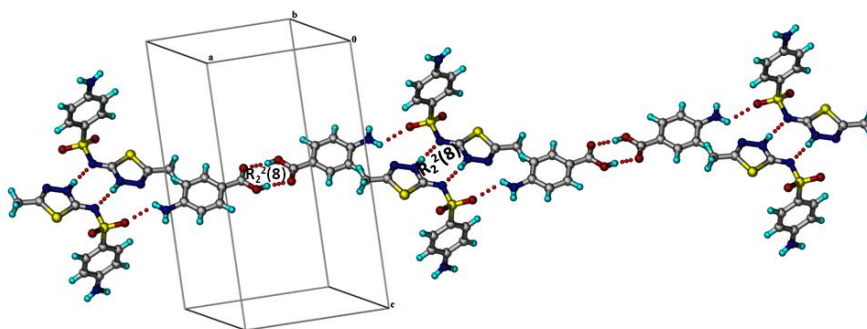


Figure 3.9 N-H...N and carboxylic acid dimers of SMT and PABA extend into linear chains through N-H...O=S in SMT-PABA cocrystal.

Sulfamethizole-Vanillic acid (SMT-VLA, 1:1) cocrystal: VLA binds to SMT through hydroxyl-amine (O5...H5A-N1:1.91 Å, 166°) single point hydrogen bonding interaction (synthon 3, Scheme 3.6). SMT and VLA molecules are aligned along the 2_1 screw axis through bifurcated N-H...O hydrogen bonds and such screw-axis related helices are associated by acid dimer $R_2^2(8)$ ring motif. These hydrogen bonds link SMT and VLA in

a 2D hexagonal network (Figure 3.10). This cocrystal is an example of honeycomb (6, 3) nets connected by a Hopf link.²⁴

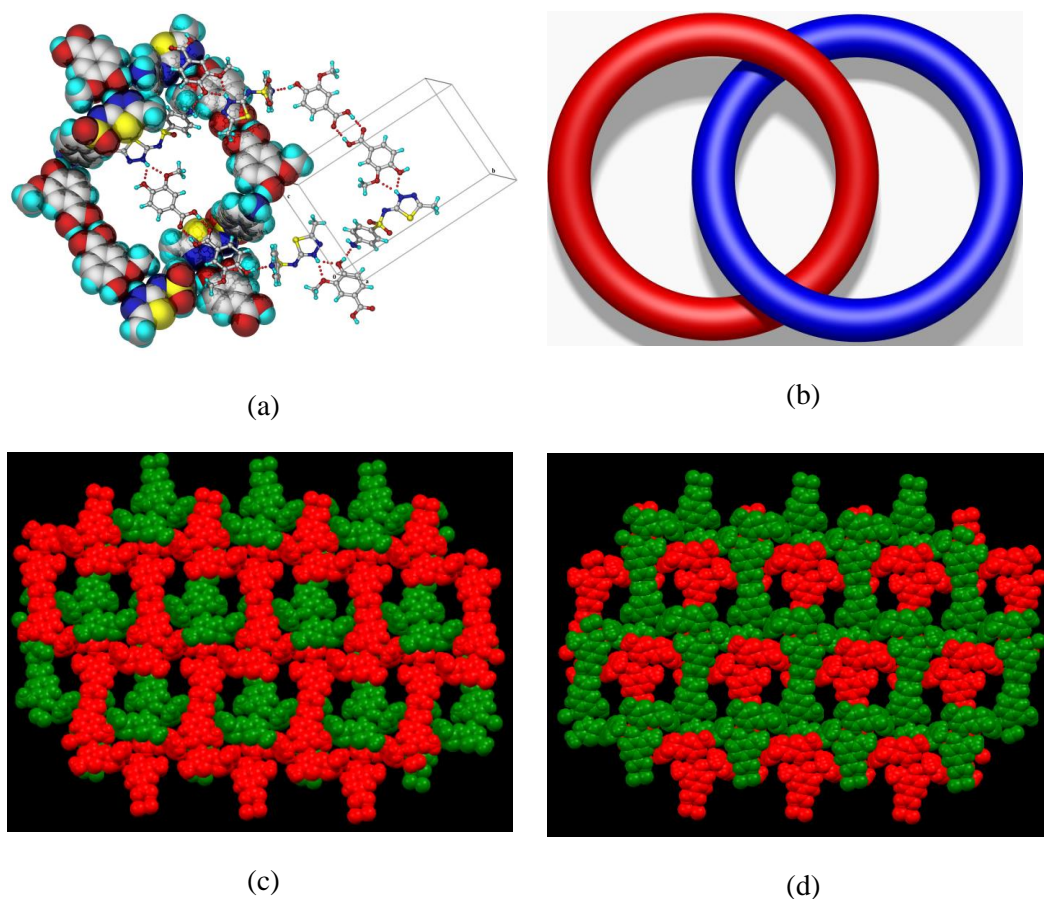


Figure 3.10 (a) 2D honeycomb (6, 3) net formed by screw-axis related SMT and VLA molecules bridged by acid–acid dimer $R_2^2(8)$ ring motifs in the cocrystal, (b) Hopf link, (c) and (d) 2D \rightarrow 2D two-fold interpretation of Hopf links in the cocrystal structure.

Sulfamethizole- *p*-aminobenzamide (1:1) cocrystal: ABA is bound to SMT through the two-point hydrogen bonds of amide-thiadiazidole groups (synthon 4, Scheme 3.6), through $N-H\cdots O$ and $N-H\cdots N$ in a $R_2^2(8)$ ring motif. The amide-thiadiazidol synthon H bonds four different molecules in the asymmetric unit ($N4-H4A\cdots N11$: 2.08 Å, 150° and $N10-H10\cdots O2$: 1.77 Å, 177°; $N5-H5A\cdots N24$: 2.03 Å, 153° and $N22-H22\cdots O4$: 1.79 Å, 177°; $N25-H25A\cdots N16$: 1.96 Å, 153° and $N15-H15\cdots O13$: 1.83 Å, 175°; $N26-H26A\cdots N19$: 2.00 Å, 151° and $N18-H18\cdots O14$: 1.79 Å, 177°). The zigzag chain of SMT-ABA structure extends through $N-H\cdots O$ (3.03 Å, 146°) hydrogen bonds in a chain motif (Figure 3.11).

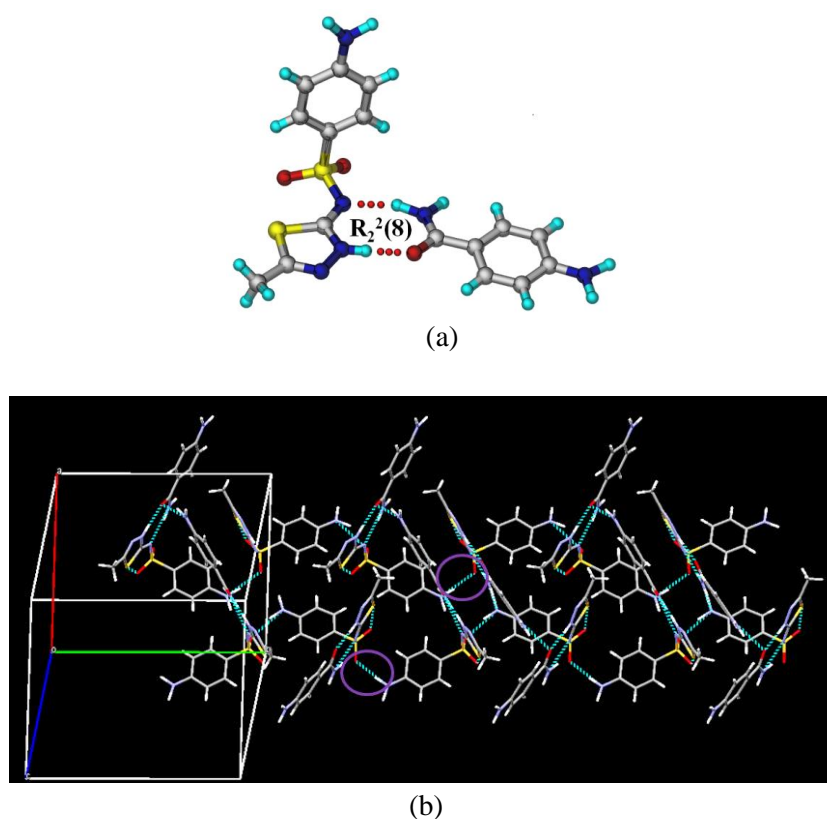


Figure 3.11 (a) SMT-ABA cocrystal is assembled via two-point hydrogen bond synthon between amide-thiadiazidol groups through N–H...O and N–H...N H-bonds in a $R_2^2(8)$ ring motif. (b) Zigzag chain of SMT-ABA cocrystal is extended through N–H...O (highlighted with violet color circle) hydrogen bonds in a 1D chain.

Sulfamethizole-4,4'-bipyridine (SMT-BIP, 1:1) cocrystal: BIP interacts with SMT through N–H...N interaction (2.73 Å, 170°) (synthon 5, Scheme 3.6). The linear chain of SMT-BIP molecules is formed by Type II chalcogen-nitrogen S...N interactions²⁵ (N5...S1: 2.99 Å, 171°; the sum of the van der Waals radii = 1.55 + 1.80 = 3.35 Å). The strongly electronegative N^{δ-} acts as a nucleophilic partner to S^{δ+} electrophilic part of the atom. The sheets of SMT-BIP structure are sustained by C–H...O interactions (C13–H13...O1: 2.53 Å, 151°; C19–H19...O1: 2.41 Å, 171°) (Figure 3.12).

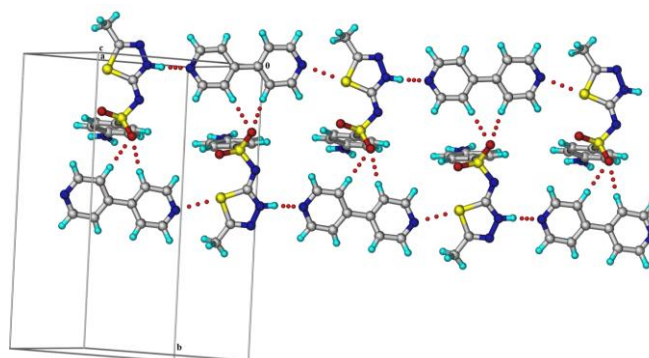


Figure 3.12 SMT-BIP cocrystal structure extends through Type II chalcogen⋯nitrogen interactions and the sheet structure is sustained by C–H⋯O interactions.

Sulfamethizole-Suberic acid (SMT-SBA, 1:0.5) cocrystal: SMT and SBA molecules are linked via C–H⋯O hydrogen bonds (C9–H9A⋯O6: 2.60 Å, 126°).²⁶ Sheets of SMT molecules aggregate via N–H⋯N dimer motif (N3–H3A⋯N6: 1.94 Å, 174°; N7–H7A⋯N2: 2.02 Å, 167°) between the sulfamidine and imine groups of SMT. The sheets are sustained by N–H⋯O (2.00 Å, 164°; 2.05 Å, 164°) hydrogen bond with cavities that accommodate SBA cofomers bonded through C–H⋯O interactions (2.60 Å, 126°) (synthon 6, Scheme 3.6). In the crystal structure, homomeric interactions are replaced by heterosynthons (Figure 3.13).

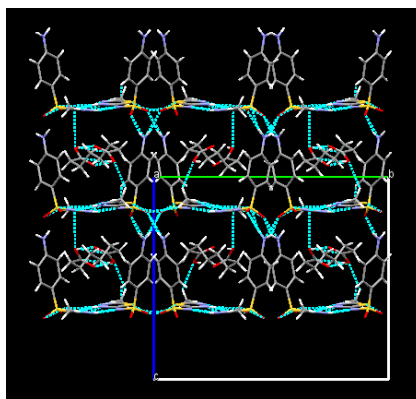


Figure 3.13 Molecules in the SMT-SBA cocrystal are linked into chains by weak C–H⋯O hydrogen bonds and further via N–H⋯N bonds into 2D sheets. The channels in the SMT host are filled with suberic acid molecules through additional N–H⋯O bonds.

Sulfamethizole-Oxalate (SMT-OA 1:1) salt: This structure is an ionic salt, in contrast to cocrystals discussed previously. The mono-oxalate anion interacts with ammonium cation of SMT through N–H⋯O ionic hydrogen bonds (2.35 Å, 118°; 2.00 Å, 154°) in a

bifurcated $R_1^2(5)$ ring motif. Inversion related SMT-OA dimers are bridged through O—H \cdots O hydrogen bond $R_2^2(10)$ ring motif (1.96 Å, 139°) (Figure 3.14).

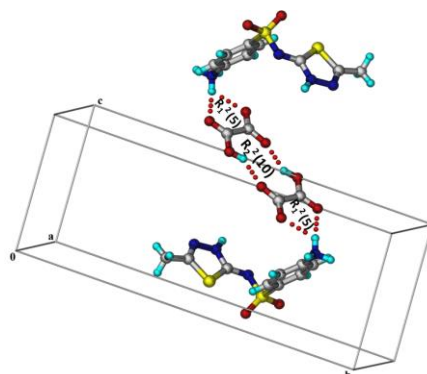


Figure 3.14 Inversion related SMT-OA dimers connected by strong O—H \cdots O interactions in SMT-OA salt. The ammonium \cdots oxalate $R_1^2(5)$ ring motif sustains a stable salt structure.

3.4.2 Conformational Flexibility

Generally hydrogen bonding with the coformer changes the conformation of the drug in the crystal structure due to systemic effects.²⁷ The presence of sulfonamide group in SMT suggests that this molecule can potentially adopt different orientations, conformations and tautomers in the cocrystal structure because of strong hydrogen bonding with the coformer and due to flexible rotation of the sulfonamide group. In fact, different conformations of SMT were observed in its multi-component crystals are shown Figure 3.15, torsion angles are listed in Table 3.3.

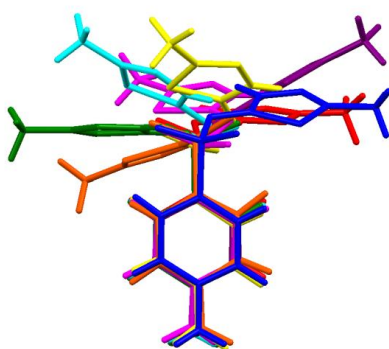
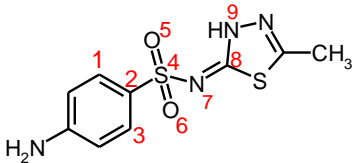


Figure 3.15 Overlay of SMT molecules extracted from crystal structures. SMT: Purple, SMT-ADP: Green, SMT-VLA: Cyan, SMT-BIP: Magenta, SMT-OA: Blue, SMT-PABA: Red, SMT-SBA: Orange, SMT-ABA: Yellow.

Table 3.3 Torsion angles in SMT molecule in different crystal structures.

 <p>τ_1 C1-C2-S4-O5, τ_2 C3-C2-S4-O6, τ_3 O5-S4-N7-C8, τ_4 O6-S4-N7-O8, τ_5 S4-N7-C8-N9</p>					
	τ_1	τ_2	τ_3	τ_4	τ_5
SMT	9.47	129.40	0.35	176.1	-42.03
SMT-ADP	29.5	158.04	28.71	177.54	-24.65
SMT-PABA	25.29	158.09	29.27	173.01	-30.40
SMT-VLA	31.04	135.20	5.03	176.68	-22.76
SMT-ABA	-44.65	-154.40	-26.38	-168.41	5.97
SMT-BIP	-58.36	-169.43	-41.47	-170.31	-1.76
SMT-SBA	-34.28	-169.03	-40.93	-176.36	21.29
SMT-OA	25.29	158.09	29.27	173.01	-30.40

3.4.3 FT-IR Spectroscopy

Additional information on the hydrogen bonding in the structure was obtained by FT-IR spectroscopy²⁸ and correlated functional groups band changes in FT-IR with hydrogen bonding interaction in crystal lattice of all cocrystals and salt. In the spectrum thiamidine NH stretching vibrations of SMT appear as a broad peak at 3255 cm^{-1} , and the symmetric and asymmetric NH_2 stretching bands at 3358 cm^{-1} and 3445 cm^{-1} . The sulfonyl $\text{SO}_{2(\text{sym})}$ and $\text{SO}_{2(\text{asym})}$ peaks are at 1081 cm^{-1} and 1129 cm^{-1} . The amine and hydroxyl stretching bands were significantly shifted compared to the starting materials (Table 3.4 and Figure 3.16). IR spectra were further recorded in ATR mode (attenuated total reflection spectra in Figure 3.17) so as to exclude possibility of phase transformation during sample grinding and compression with KBr to make the pellet. Generally peak shifts of $10\text{--}15\text{ cm}^{-1}$ are indicative of changes in hydrogen bonding for salt/cocrystal.

According to $\Delta\text{p}K_a$ rule,²⁹ the difference in $\text{p}K_a$ of SMT-ADP and SMT-SBA cocrystals is <3 and in the grey zone, which means that adduct can be either a cocrystal or a salt ($\text{p}K_a$ values are listed in Table 3.5). The $\Delta\text{p}K_a$ is actually very small (<1) for oxalic acid, but this is a salt which is contrary to the rule because the difference must be large (>3) for salt formation. The formation of a carboxylate anion for OA further stabilized by the proximal $\text{C}=\text{O}$ group seems to favor deprotonation despite the $\text{p}K_a$'s of acid and base being so close. Thus the bifurcated ammonium \cdots diketo hydrogen bond motif in SMT-OA structure appears to drive deprotonation even though the $\Delta\text{p}K_a$ is negligible. This

point that the special positioning of functional groups will favor salt formation has been discussed by Sarma et. al.³⁰ The ammonium...oxalate $R_1^2(5)$ ring motif present on SMT-OA salt (Figure 3.14) is quite frequent, being observed in 68 crystal structures out of 87 which contain a primary amine and oxalic acid functional groups (data extracted from the Cambridge Structure Database). The carbonyl stretching bands in FT-IR are consistent with a free carboxylic acid group in SMT-ADP, SMT-SBA (about 1740 cm^{-1}) and a carboxylate for SMT-OA (1550 cm^{-1} , Table 3.4).

Table 3.4 IR stretching frequencies of SMT NH groups in the crystalline forms (Figure 3.16, spectra).

Solid form	amine $\nu_{(\text{NH}_2)_{\text{asym}}}$ (cm^{-1})	amine $\nu_{(\text{NH}_2)_{\text{asym}}}$ (cm^{-1})	Imidine ν_{NH} (cm^{-1})	COOH/CONH ₂ / COO- $\nu_{\text{C=O}}$ (cm^{-1}) in cocrystal/salt	COOH/CONH ₂ / $\nu_{\text{C=O}}$ (cm^{-1}) in coformer
SMT	3445	3358	3255	---	---
SMT-ADP	3312	3388	3156	1698	1693
SMT-PABA	3376	3479	---	1661	1662
SMT-VLA	3332	3408	3237	1670	1684
SMT-ABA	3342	3441	3232	1644	1650
SMT-BIP	3357	3459	3246	---	---
SMT-SBA	3376	3462	3246	1704	1682
SMT-OA	3432	---	3202	1658, 1742	1666

Table 3.5 ΔpK_a values of dicarboxylic acid coformers and SMT drug.

	1 st , 2 nd pK_a in water	ΔpK_a	Molecular complex
SMT	1.95 for aromatic amine ^a	---	---
OA	1.36, 4.11	0.59, 2.16	1:1 salt
ADP	4.70, 3.92	2.75, 1.97	1:0.5 cocrystal
SBA	4.90, 4.15	2.95, 2.20	1:0.5 cocrystal

^a The pK_a (1.95) of SMT NH_2 group is much less basic (almost acidic) compared to aniline (pK_a 4.63). The reduced basicity by almost 3 log units is due to the electron withdrawing sulfonyl group at the para position.²⁹

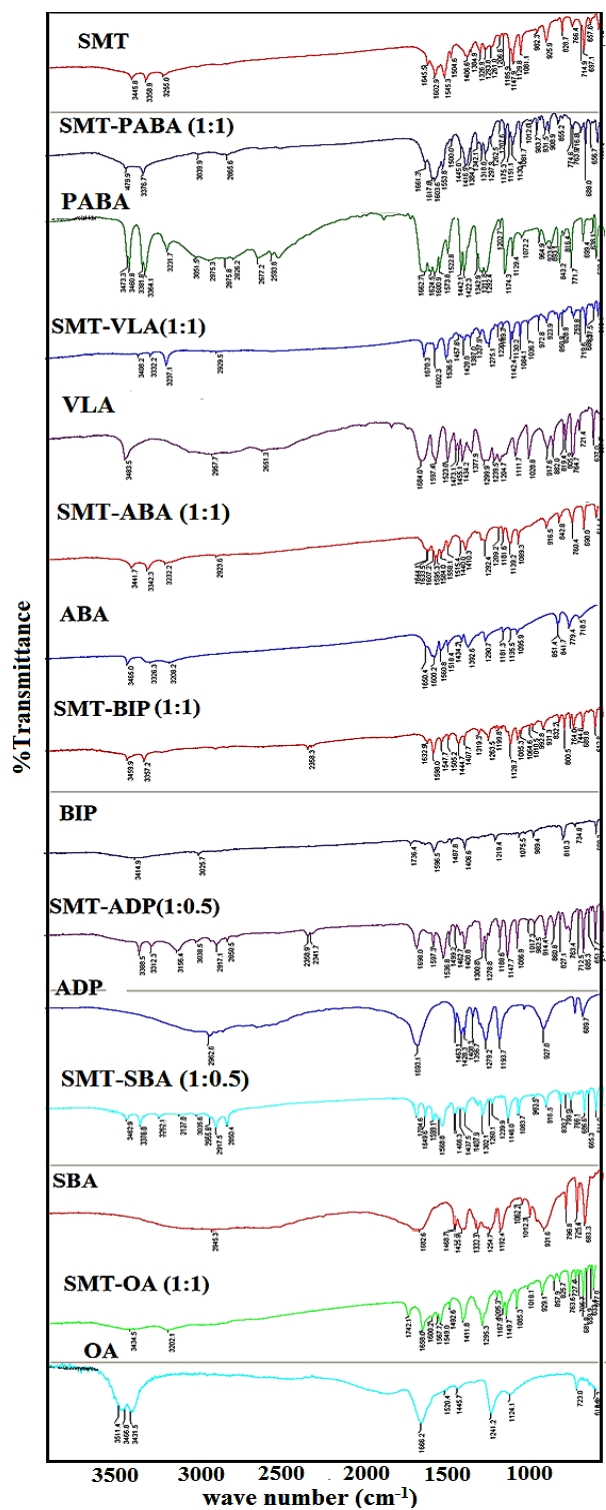


Figure 3.16 Overlay of FT-IR spectra of SMT cocrystals and salt with starting materials

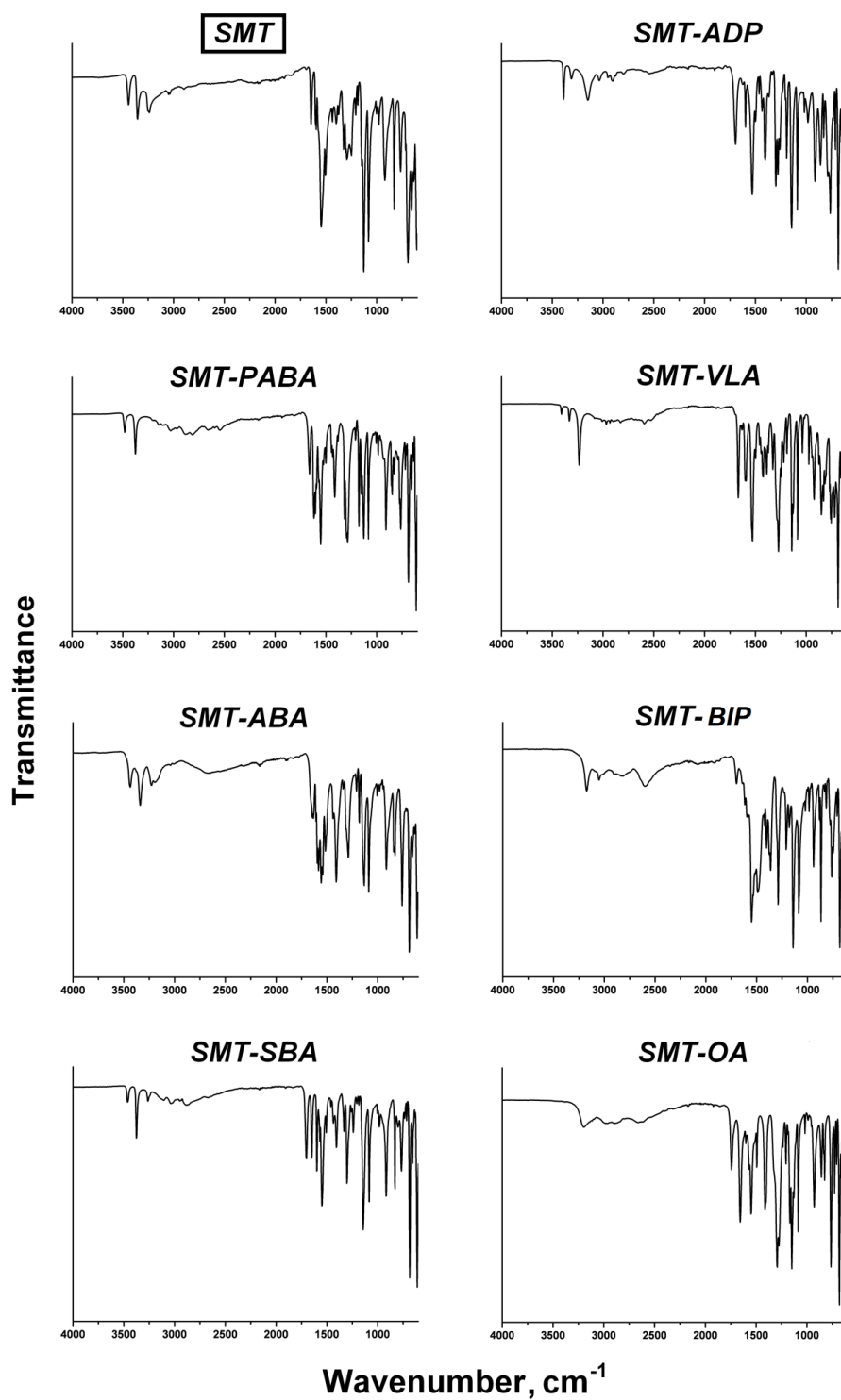


Figure 3.17: ATR mode FT-IR spectra SMT and its cocrystals and salt (exclude possibility of phase transformation during sample grinding and compression with KBr to make the pellet). Here we observed that there is no much significance difference with KBr FT-IR spectra.

3.4.4 Powder X-ray Diffraction and Thermal analysis

Powder X-ray diffraction is a reliable characterization tool to establish the new solid forms and phase purity. It can unambiguously distinguish the products obtained from its starting components through unique diffraction line pattern. The PXRD lines of the all cocrystals and one salt prepared in this work confirm the bulk phase purity and homogeneity of each solid form exhibited excellent match of the experimental PXRD with the calculated lines from the X-ray crystal structure (Figure 3.18). Differential Scanning Calorimetry (DSC) measurements can confirm the purity and monitor phase transformations.³¹ The melting point of the cocrystals was found to be lower than that of SMT except that for SMT-OA, which is higher because it is a salt (Figure 3.19 Table 3.6). Aromatic acids and amide group containing coformers, e.g. SMT-PABA, SMT-VLA and SMT-ABA gave lower melting endotherm compared to the starting materials. Cocrystals with aliphatic acids and aromatic bipyridine, such as SMT-ADP, SMT-SBA, and SMT-BIP, have an intermediate temperature melting endotherm.

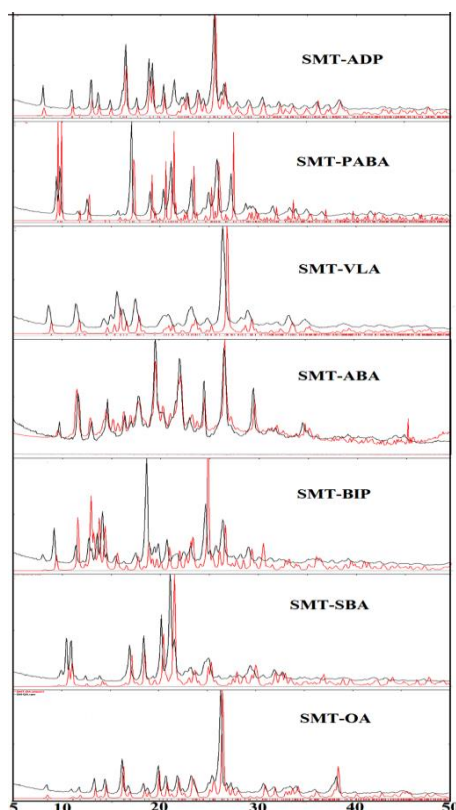


Figure 3.18 Overlay of experimental PXRD lines of cocrystals and salt showed good match with their calculated lines from X-ray crystal structures indicating bulk phase purity and homogeneity.

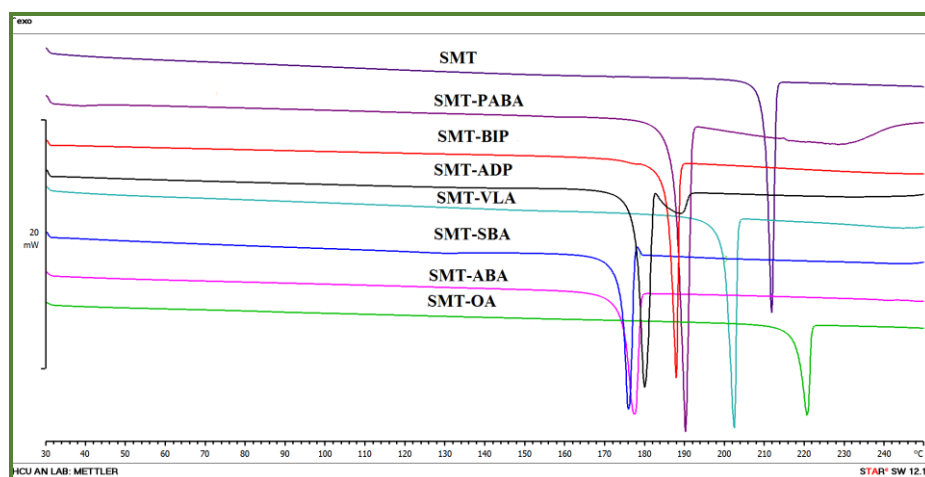


Figure 3.19 DSC plots measured of SMT cocrystals and salts.

Table 3.6 Melting point of SMT cocrystals/salt and conformers.

S. No.	Cocrystal/Salt	m.p. (°C)	Coformer	m.p. (°C)
1	SMT-ABA	174-176	ABA	181-183
2	SMT-BIP	185-187	BIP	109-112
3	SMT-PABA	187-189	PABA	187-189
4	SMT-VLA	199-201	VLA	210-213
5	SMT-SBA	173-175	SBA	141-144
6	SMT-ADP	177-179	ADP	151-154
7	SMT-OA	217-220	OA	102-104

Melting point of SMT 209-210 °C

3.4.5 Solubility and dissolution

Solubility is a measure of “how much” the drug is soluble in the medium while dissolution rate is “how fast” the drug reaches that equilibrium value. The former is a thermodynamic quantity while the latter is influenced by kinetic factor which gives an idea of the peak concentration and amount of drug dissolved in a short time. Solubility and dissolution were determined mainly by two factors: strength of crystal lattice, and solvation of components in cocrystals. These two factors can modulate (increase/decrease) the cocrystal solubility. The prime objective of present SMT cocrystals is to address the extended release by decreasing solubility of SMT to avoid the rapid absorption rate of *in vivo* kinetic profile. This decreasing solubility profile would be altered through hydrogen bonding interactions of SMT as cocrystals via strong homomeric and heteromeric N–H...N and N–H...O interactions. In this regard, the present IDR and equilibrium solubility experiments on SMT, SMT-ADP, SMT-SBA and SMT-OA were carried out in 0.1 N HCl (pH 1.2) medium. The IDR measurements were

performed for 4 h by rotating disk intrinsic dissolution rate (IDR) method³² at 37 °C. However it is not possible to measure IDR and solubility for SMT-VLA and SMT-PABA cocrystals (aromatic ring present) due to coformer absorption band and SMT absorption UV-Vis bands occurring in the same wavelength region. The IDR and equilibrium solubility of cocrystals and salt found to be less dissolution rate and solubility than SMT reference drug. The IDR decreases in order is SMT > SMT-ADP > SMT-OA > SMT-SBA, where as in case of equilibrium solubility, SMT > SMT-ADP > SMT-SBA > SMT-OA. Decrease the both solubility and IDR in cocrystals due to the close packing via strong homomeric and heteromeric N–H···N and N–H···O interactions in crystal lattice. Interestingly in SMT-OA salt case, even it is ionic compound and in addition OA is high soluble coformer, results in decreasing both IDR and equilibrium solubility. The reason behind SMT-OA crystal structure consist of one carboxyl group is deprotonated and another carboxyl group is contributing to close packing of salt through O–H···O hydrogen bond $R_2^2(10)$ ring motif with carboxylate anion in crystal lattice and also with high density of SMT-OA. Furthermore when correlating with melting point of SMT cocrystals and salt, the high melting of SMT-OA(x0.81 folds) showed least solubility than less melting point of cocrystals (SMT-SBA and SMT-ADP) not followed in IDR. Intrinsic dissolution rate curves are displayed in Figure 3.20, and dissolution rates, equilibrium solubility and molar extinction coefficient are listed in Table 3.6. All solids forms were stable during dissolution and equilibrium solubility experiments were confirmed by PXRD (Figure 3.21). By making the cocrystals and salt of SMT we achieved the extended release of SMT drug.

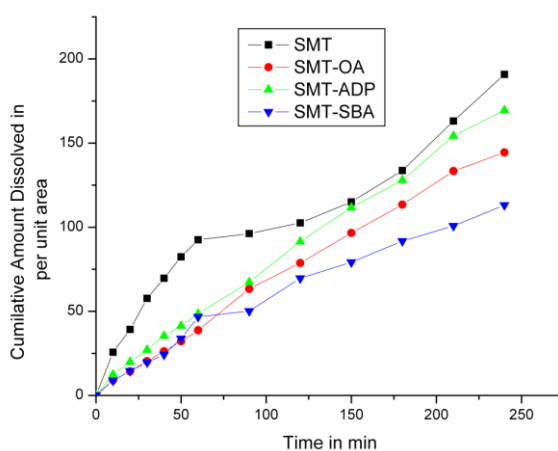


Figure 3.20 Intrinsic dissolution rate curves of SMT, SMT-ADP, SMT-SBA and SMT-OA in pH 1.2 HCl medium.

Table 3.7 Intrinsic dissolution rates of SMT and its cocrystal and salt systems

Compound	Coformer Solubility in (mg/mL)	Molar Extinction coefficient ($\text{mM}^{-1} \text{cm}^{-1}$)	Equilibrium Solubility in pH 1.2, 0.1N HCl medium (mg/mL)	Intrinsic dissolution rate, IDR ($\text{mg}/\text{cm}^2/\text{min}$)	Cumulative amount dissolved per unit area (mg/500 mL)
SMT	10.5	14.2	3.7	1.36	190.8
SMT-ADP	23.0	15.5	3.5(x0.94)	0.83(x0.61)	169.5(x0.86)
SMT-SBA	11.9	13.7	3.4(x0.91)	0.62(x0.45)	113.1(x0.59)
SMT-OA	143.0	14.6	3.0(x0.81)	0.67(x0.49)	144.4(x0.75)

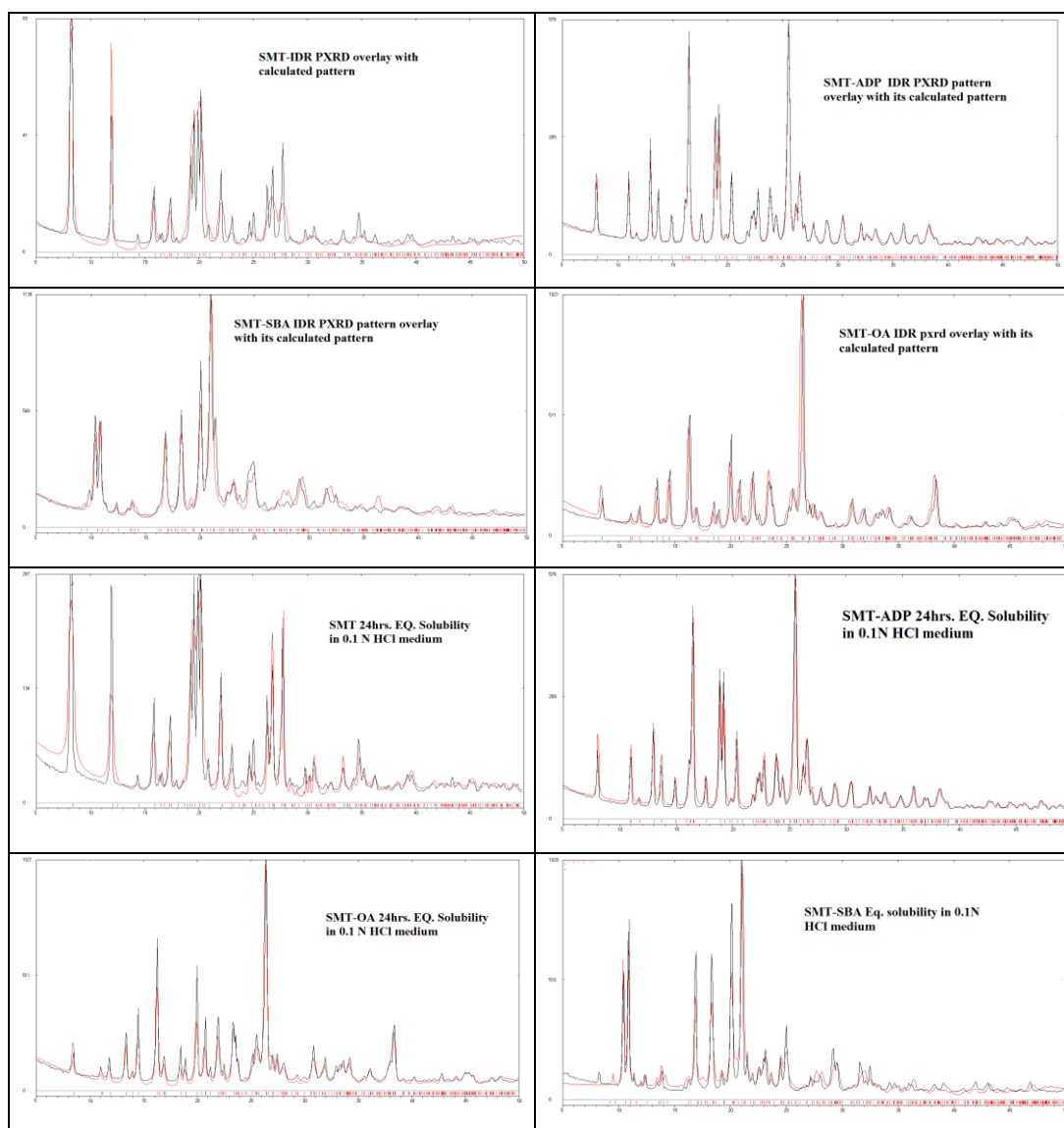


Figure 3.21 PXRD plots of SMT and its cocrystals and salt at the end of IDR and equilibrium solubility experiment in pH 7 buffer medium. All the solid forms were found to be stable in both experiments.

3.4.6 Phase stability in acidic and neutral media

Next we studied the cocrystal/ salt phase formation in acidic and neutral media by dissolving the parent components in 1:1 molar ratio in 5 mL of the medium for SMT-ADP, SMT-SBA and SMT-OA. Generally salt formation is driven by the acidity and basicity of the components.³³ Here we observed that there is no cocrystal formation in the slurry medium (both acidic and neutral) after 24 h for SMT-SBA and SMT-ADP. In the case of SMT and OA, the physical mixture mixed in acidic slurry medium (0.1 N HCl) gave SMT-OA salt after one hour by PXRD of the precipitate residue (Figure 3.22). In neutral medium (phosphate buffer) however the components remained as separate species. The formation of SMT-OA salt in strongly acidic medium is driven by the HSAB principle. Accordingly the HSAB rule,³⁴ the preferred hard acid-hard base and soft acid-soft base pairing will give SMT-OA salt. In acidic media, the weak base SMT will form a salt with OA due to soft acid-soft base interaction. The strength of multi-point ammonium...oxalate $R_1^2(5)$ ring motif is another factor to favor SMT-OA salt formation over SMT-HCl which will have a single hydrogen bond. In neutral media there is no support to increase the strength of acid-base pairing and hence no salt formation was observed. For cocrystals, no adduct formation was noted in either acidic or neutral medium because of the solubility mismatch of coformer and SMT.

A phase stability study was performed for 24 h in slurry media. The cocrystals and salt were stable for up to 24 h in acidic medium whereas in neutral medium SMT-OA and SMT-ADP partially converted to the parent components and SMT-SBA was completely dissociated.

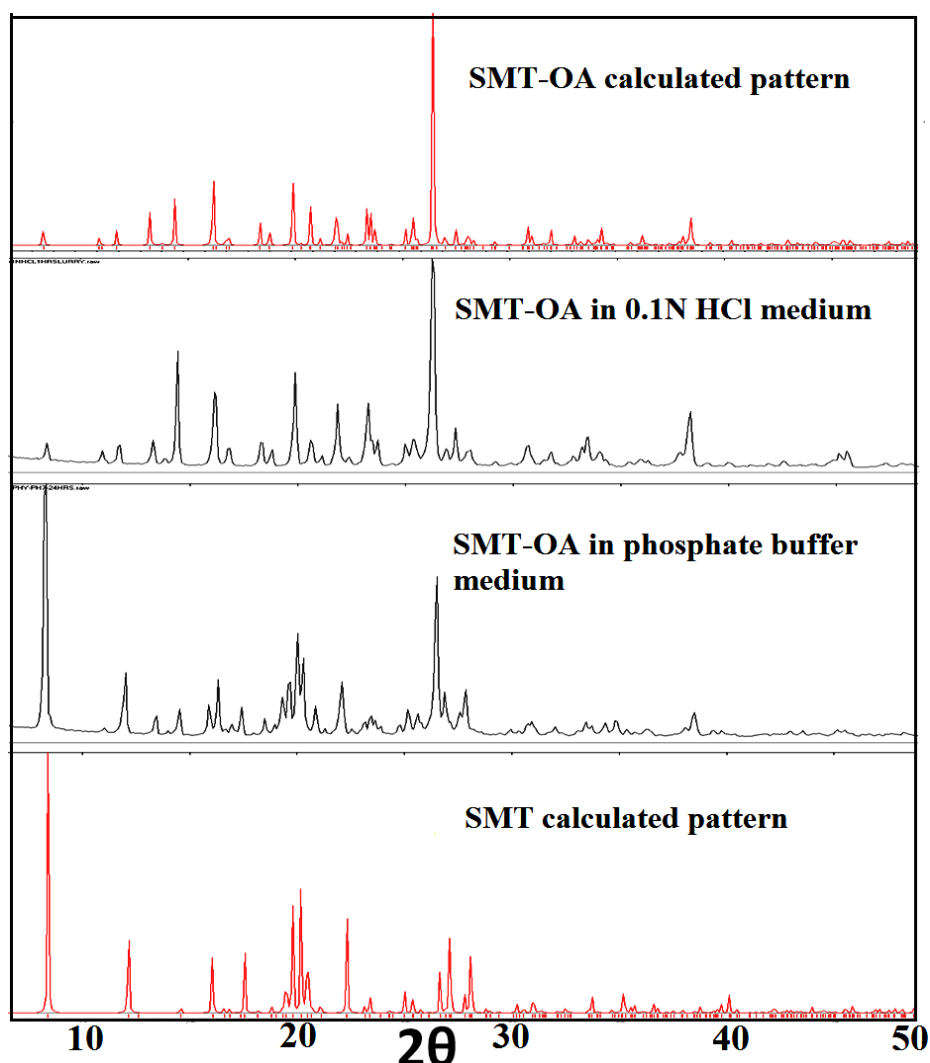


Figure 3.22 Equimolar SMT and OA physical mixture kept in slurry for 1 h gave SMT-OA salt in acidic medium (0.1 N HCl) but the components are separate in neutral medium (phosphate buffer) (by PXRD pattern analysis).

3.5 Conclusions

A solid form screening of SMT for binary solids afforded six cocrystals and one salt. In the crystal structures, three aliphatic dicarboxylic acids coformers interact with SMT via different hydrogen bonding synthons. SMT-ADP has strong acid-amine synthon, SMT-SBA cocrystal has weak C–H \cdots O hydrogen bonds together with homomeric interactions, and in SMT-OA structure the proton is transformed from OA to SMT. The uncommon chalcogen-oxygen (S \cdots O) interaction was observed in SMT-ADP S \cdots N interaction in SMT-BIP. These chalcogenic interactions are important in the tubular structures of peptides and in superconducting tetrathiafulvalene (TTF) and

tetracyanoquinodimethane (TCNQ).³⁵ Furthermore, *in vitro* solubility and dissolution experiments for SMT-ADP, SMT-SBA and SMT-OA showed that the IDR and equilibrium solubility of adducts were reduced compared to SMT, which is ascribed to efficient molecular packing and stronger interactions through strong homomeric and heteromeric N–H...N and N–H...O interactions in the crystal lattice of salt/cocrystal. Thus SMT cocrystals and salt were useful in controlled/extended release of drug to improve its poor residence time by reducing the absorption rate in improved crystal forms. Interestingly, we noted salt formation of SMT-OA in acidic medium due to the soft acid-soft base rule. Phase stability studies in neutral and acidic media showed that SMT-ADP, SMT-SBA and SMT-OA are stable in acidic medium whereas in neutral medium these solid forms dissociated to the components. Our structural and solubility and stability studies on SMT give novel and practical leads for further improvements on the physicochemical properties of sulfonamide drug.

3.6 Experimental Section

SMT and coformers (purity > 99.8%) were purchased from Sigma-Aldrich (Hyderabad, India). Solvents (purity > 99%) were purchased from Hychem Laboratories (Hyderabad, India). Water and solvents (HPLC grade) were purchased from Merck chemicals (Bangalore, India) for solubility and dissolution experiments.

Preparation of SMT solid forms

SMT-ADP cocrystal: The cocrystal was obtained by grinding SMT (270.3mg) and ADP (73.0 mg) in 1:0.5 molar ratios with a few drops of CH₃CN added in a liquid-assisted method for 30 min. Single crystals were obtained when 40 mg of the ground product was dissolved in CH₃CN (5 mL) and left for slow evaporation for 4-5 days at ambient conditions.

SMT-PABA cocrystal: This cocrystal was obtained by grinding SMT (270.3mg) and PABA (137.1mg) in 1:1 molar ratios with a few drops of CH₃CN added in a liquid-assisted method for 30 min. Single crystals were obtained when 40 mg of the ground product was dissolved in CH₃CN (5 mL) and left for slow evaporation for 4-5 days at ambient conditions.

SMT–VLA cocrystal: The cocrystal was obtained by grinding SMT (270.3mg) and VLA (168.1 mg) in 1:1 molar ratios with a few drops of CH₃CN added in a liquid-assisted method for 30 min. Single crystals were obtained when 40 mg of the ground product was dissolved in MeOH (5 mL) and left for slow evaporation for 4-5 days at ambient conditions.

SMT–ABA cocrystal: The cocrystal was obtained by grinding SMT (270.3mg) and VLA (136.1 mg) in 1:1 molar ratios with a few drops of CH₃CN added in a liquid-assisted method for 30 min. Single crystals were obtained when 40 mg of the ground product was dissolved in acetone (5 mL) and left for slow evaporation for 4-5 days at ambient conditions.

SMT–BIP cocrystal: The cocrystal was obtained by grinding SMT (270.3mg) and BIP (156.1 mg) in 1:1 molar ratios with a few drops of CH₃CN added in a liquid-assisted method for 30 min. Single crystals were obtained when 40 mg of the ground product was dissolved in CH₃CN (5 mL) and left for slow evaporation for 4-5 days at ambient conditions.

SMT–SBA cocrystal: The cocrystal was obtained by grinding SMT (270.3mg) and SBA (87.0 mg) in 1:0.5 molar ratios with a few drops of CH₃CN added in a liquid-assisted method for 30 min. Single crystals were obtained when 40 mg of the ground product was dissolved in CH₃CN (5 mL) and left for slow evaporation for 4-5 days at ambient conditions.

SMT–OA salt: The cocrystal was obtained by grinding SMT (270.3mg) and OA (90.0 mg) in 1:1 molar ratios with a few drops of CH₃CN added in a liquid-assisted method for 30 min. Single crystals were obtained when 40 mg of the ground product was dissolved in acetone (5 mL) and left for slow evaporation for 4-5 days at ambient conditions.

FT-IR spectroscopy

Thermo-Nicolet 6700 Fourier transform infrared spectrophotometer with NXR-Fourier transform Raman module (Thermo Scientific, Waltham, Massachusetts) was used to record IR spectra. FT-IR was recorded on sample dispersed in KBr pellet. Data were analyzed using the Omnic software (Thermo Scientific, Waltham, Massachusetts). ATR IR spectra (attenuated total reflection mode) were recorded on a Digilab Excalibur 3100

spectrometer equipped with MIRacle ATR (Pike) accessory in the frequency range 4500 to 600 cm^{-1} and a resolution of 2 cm^{-1} . The sample was prepared without any grinding to avoid possible phase transformations during sample preparation grinding.

Differential scanning calorimetry

DSC was performed on Mettler Toledo DSC 822e module (Mettler Toledo, Columbus, Ohio). Samples were placed in crimped but vented aluminum sample pans. The typical sample size is 4-6 mg; temperature range was 30-250 °C @ 5 °C/min. Samples were purged by a stream of nitrogen flowing at 150 mL/min.

Powder X-ray diffraction

Powder X-ray diffraction was recorded on a Bruker D8 Advance diffractometer (Bruker-AXS, Karlsruhe, Germany) using Cu-K α radiation ($\lambda = 1.5406 \text{ \AA}$) at 40 kV and 30 mA power. X-ray diffraction patterns were collected over the 2θ range 5–50° at a scan rate of 5°/min.

Single crystal X-ray diffraction

Single crystal X-ray diffraction experiments were carried out using a Stoe IPDS-II diffractometer (STOE, Darmstadt, Germany) equipped with a molybdenum X-ray tube ($\lambda = 0.71073 \text{ \AA}$), an image plate detector, a flat graphite monochromatic and an Oxford Cryostream cooling device (stability of gas flow temperature is $\pm 0.1 \text{ K}$). All single-crystal X-ray diffraction experiments were performed at 100 K. All crystals were covered by low viscosity CryoOil (MiTeGen) to protect them additionally from environment during data collection. The data collection, indexing and integration of the reflections were performed using Stoe X-Area software package, data reduction was performed using Stoe X-Red software,^{36a} and the structures were refined using SHELXL^{36bcd} implemented in the X-Step32 shell.^{36e} Hydrogen atoms were experimentally located through the Fourier difference electron density maps in all crystal structures. All H atoms were found in a difference Fourier map and their positions were refined freely, with $\text{Uiso(H)} = 1.5\text{Ueq(C)}$ for terminal methyl H atoms and 1.2 Ueq(parent atom) for internal chain atoms. The parameters characterizing data collection and refinement are summarized in Table 3. The structural data for different Sulfamethizole cocrystals are deposited as CIFs at the Cambridge Crystallographic

Database (CCDC Nos.: 1060511-1060517), and can be downloaded freely from <http://www.ccdc.cam.ac.uk>.

Dissolution and solubility

The solubility curves of SMT, two cocrystals and one salt were measured using the Higuchi and Connor method³⁷ in pH1.2 HCl medium at 30 °C. First, the absorbance of a known concentration of the all these forms was measured at the given λ_{max} 268 nm in pH1.2 HCl medium on Thermo Scientific Evolution 300 UV-vis spectrometer (Thermo Scientific, Waltham, MA). These absorbance values were plotted against several known concentrations to prepare the concentration vs. intensity calibration curve. From the slope of the calibration curves, molar extinction coefficients for SMT, SMT-ADP, SMT-SBA, and SMT-OA were calculated. These respective molar extinction coefficients were used to determine the IDR values and equilibrium solubility values. An excess amount of the sample was added to 5 mL of pH1.2 HCl medium. The supersaturated solution was stirred at 800 rpm using a magnetic stirrer at 30 °C. After 24 h, the suspension was filtered through Whatmann 0.45 μm syringe filter. Intrinsic dissolution rate experiments were carried out on a USP certified Electrolab TDT-08L Dissolution Tester (Electrolab, Mumbai, MH). Dissolution experiments were performed for 240 min in pH1.2 0.1N HCl medium at 37 °C. For IDR measurements, 250 mg of the compound was taken in the intrinsic attachment and compressed to a 0.5 cm^2 disc using a hydraulic press at pressure of 4.0 ton/inch^2 for 5 min. The intrinsic attachment was placed in a jar of 500 mL pH1.2 0.1N HCl medium preheated to 37 °C and rotated at 100 rpm. 5 mL aliquots were collected at specific time intervals and concentration of the aliquots were determined with appropriate dilutions from the predetermined standard curves of the respective compounds. The identity of the undissolved material after the dissolution experiment was ascertained by PXRD (Figure S5 and Figure S6). The stability of the solid samples upon disc compression and solubility conditions was confirmed by powder X-ray diffraction.

3.7 References

1. (a) G. R. Desiraju, *Crystal Engineering: The Design of Organic Solids*, Elsevier, Amsterdam, 1989; (b) G. R. Desiraju, T. Steiner, *The Weak Hydrogen Bond in Structural Chemistry and Biology*, IUCr Monographs in Crystallography, 1999; (c) G. R. Desiraju, *J. Chem. Sci.*, 2010, **122**, 667; (d) G. R. Desiraju, J. J. Vittal and A. Ramanan, *Crystal Engineering. A Textbook*, World Scientific Publishing, Singapore, 2011.
2. (a) G. R. Desiraju, *Angew. Chem. Int. Ed. Engl.*, 1995, **34**, 2311; (b) C. B. Aakeröy, *Acta Crystallogr. Sect. B*, 1997, **53**, 569; (c) B. Moulton and M. Zaworotko, *Chem. Rev.*, 2001, **101**, 1629.
3. (a) T. Steiner, *Acta Crystallogr. Sect. B*, 2001, **57**, 103; (b) P. Vishweshwar, A. Nangia and V. M. Lynch, *J. Org. Chem.*, 2002, **67**, 556; (c) T. R. Shattock, K. K. Arora, P. Vishweshwar and M. J. Zaworotko, *Cryst. Growth Des.* 2008, **8**, 4533; (d) R. Santra, N. Ghosh and K. Biradha, *New J. Chem.*, 2008, **32**, 1673; (e) C. B. Aakeröy and D. J. Salmon, *CrystEngComm*, 2005, **7**, 439; (f) C. B. Aakeröy, A. M. Beatty and B. A. Helfrich, *J. Am. Chem. Soc.*, 2002, **124**, 14425; (g) C. B. Aakeröy, A. M. Beatty and B. A. Helfrich, *Angew. Chem., Int. Ed.*, 2001, **40**, 3240.
4. (a) N. J. Babu, P. Sanphui and A. Nangia, *Chem. Asian J.*, 2012, **10**, 2274; (b) M. B. Hickey, M. L. Peterson, L. A. Scoppettuolo, S. L. Morrisette, A. Vetter, H. Guzman, J. F. Remenar, Z. Zhang, M. D. Tawa, S. Haley, M. J. Zaworotko and O. Almarsson, *Eur. J. Pharm. Biopharm.*, 2007, **67**, 112; (c) S. Ghosh and C. M. Reddy, *Angew. Chem. Int. Ed.*, 2012, **51**, 10319; (d) M. Khan, V. Enkelmann and G. Brunklaus, *J. Am. Chem. Soc.*, 2010, **132**, 5254; (e) D. Yan, A. Delori, G. O. Lloyd, T. Friscic, G. M. Day, W. Jones, J. Lu, M. Wei, D. G. Evans and X. Duan, *Angew. Chem. Int. Ed.*, 2011, **50**, 12483; (f) X. Pang, H. Wang, X. R. Zhao and W. J. Jin, *CrystEngComm*, 2013, **15**, 2722-2730;; (g) S. Karki, T. Friščić, L. Fábián, P. R. Laity, G. M. Day and W. Jones, *Adv. Mater.*, 2009, **21**, 3905.
5. (a) J. F. Remenar, M. L. Peterson, P. W. Stephens, Z. Zhang, Y. Zimenkov, and M.B. Hickey. *Mol. Pharm.*, 2007, **4**, 386; (b) M. L. Cheney D. R. Weyna, N. Shan, M. Hanna, L. Wojtas, M. J. Zaworotko. *J. Pharm. Sci.*, 2011, **100**, 2172; (c) P. Sanphui, N. R. Goud, U. B. R. Khandavilli and A. Nangia. *Cryst. Growth Des.*, 2011, **11**, 4135; (d) A. J. Smith, P. Kavuru, L. Wojtas, M. J. Zawarotko and

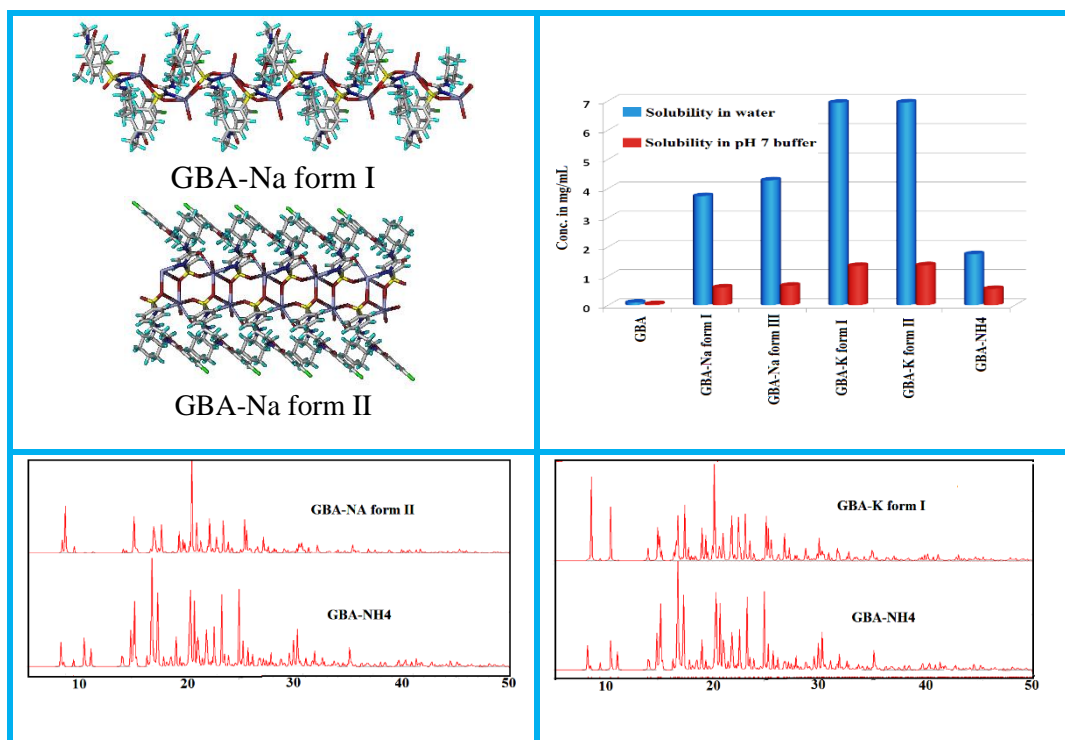
- R. D. Shytle. *Mol. Pharm.*, 2011, **8**, 1867; (e) S. Aitipamula, A. B. H. Wong, P. S. Chow and R. B. H. Tan. *CrystEngComm*, 2012, **14**, 8515.
6. (a) P. Vishweshwar, J. A. McMahon, J. A. Bis and M. J. Zaworotko, *J. Pharm. Sci.*, 2006, **95**, 499; (b) C. B. Aakeröy, S. Forbes and J. Desper, *J. Am. Chem. Soc.*, 2009, **132**, 17048; (c) A. Alhalaweh and S. P. Velaga, *Cryst. Growth Des.*, 2010, **10**, 3302; (d) A. B. M. Buanz, R. Telford, I. J. Scowen and S. Gaisford, *CrystEngComm*, 2013, **15**, 1031; (e) M. D. Eddleston, S. Sivachelvam and W. Jones, *CrystEngComm*, 2013, **15**, 175; (f) M. K. Stanton, R. C. Kelly, A. Colletti, Y.-H. Kiang, M. Langley, E. J. Munson, M. L. Peterson, J. Roberts and M. Wells, *J. Pharm. Sci.*, 2010, **99**, 3769.
7. A. M. Thayer, *Chem. Eng. News*, 2010, **88**, 13.
8. Y. Kawabata, K. Wada, M. Nakatani, S. Yamada, S. Onoue. *Int. J. Pharm. Sci.* 2011, **420**, 1.
9. (a) X. Chen, H. Wen and K. Park, in *Oral Controlled Release Formulation Design and Drug Delivery: Theory and Practice*, Eds., John Wiley and Sons, Inc., 2010; (b) P. De Haan and C. F. Lerk, *Pharmaceutisch Weekblad*, 1984, **6**, 57.
10. (a) D. Patel, B. Patel, H. Patel and C. Patel, *J. Young Pharm.*, 2011, **3**, 176; (b) A. Almeida, L. Brabant, F. Siepmann, T. De Beer, W. Bouquet, L. Van Hoorebeke, J. Siepmann, J. P. Remon and C. Vervaet, *Eur. J. Pharm. Biopharm.*, 2012, **82**, 526; (c) B. K. Nanjwade, S. R. Mhase and F. V. Manvi, *Trop. J. Pharm. Res.*, 2011, **10**, 375.
11. (a) N. G. Das and S. K. Das, *Formulation Fill and Finish*, 2003, 10; (b) P. M. Brooks, M. S. Roberts and B. Patel, *Br. J. Clin. Pharmacol.*, 1978, **5**, 337.
12. A. R. Gennaro, *Remington: The Science and Practice of Pharmacy*, 20th Ed., Lippincott Williams and Wilkins, NY, 2000.
13. A. J. Smith, *Modulating the Pharmacokinetics of Bioflavonoids*, Ph.D Thesis, University of South Florida page 67; (b) A. J. Smith, P. Kavuru, K. Arora, S. Kesani, J. Tan, M. J. Zaworotko, and R. D. Shytle. *Mol. Pharm.* 2013, **10**, 2948; (c) N. R. Goud, R. A. Khan, and A. Nangia, *CrystEngComm.*, 2014, **16**, 5859.
14. (a) S. L. Childs, L. J. Chyall, J. T. Dunlap, V. N. Smolenskaya, B. C. Stahly and G. P. Stahly, *J. Am. Chem. Soc.*, 2004, **126**, 13335; (b) C. B. Aakeroy, S. Forbes

- and J. Desper, *J. Am. Chem. Soc.*, 2009, **131**, 17048; (c) R. Thakuria, S. Cherukuvada, and A. Nangia, *Cryst. Growth Des.*, 2012, **12**, 3944.
15. M. B. Kern, N. Frimodt-Møller, F. Espersen, *Antimicrob. Agents Chemother.* 2003, **47**, 1002.
 16. Sulfamethizole solubility <http://www.drugbank.ca/drugs/DB01015>.
 17. N. H. Shear, S. P. Spielberg, D. M. Grant, B. K. Tang, W. Kalow, *Ann Intern. Med.* 1986, **105**, 179.
 18. K.A. Javaid, C.W. Hartman, *J. Pharm. Sci.*, 1972, **61**, 900.
 19. (a) V. Fuglp, A. Kalman, *J. Mol. Struct.*, 1987, **159**, 303; (b) P. S. Thomas, S. P. K. P. Veccham, L. J. Farrugia, T. N. G. Row, *Cryst. Growth Des.* 2015, **15**, 2110.
 20. (a) S. A. Myz, T. P. Shakhtshneider, K. Fucke, A. P. Fedotov,; E. V. Boldyreva, V. V. Boldyrev, N. I. Kuleshova, *Mendeleev Communications* 2009, **19**, 272; (b) K. Fucke, S. A. Myz, T. P. Shakhtshneider, E. V. Boldyreva, U. J. Griesser *New J. Chem.*, 2012, **36**, 1969; (c) N. A. Tumanov, S. A. Myz, T. P. Shakhtshneider, E. V. Boldyreva, *CrystEngComm* 2012, **14**, 305.
 21. (a) D. A. Rychkov, S. G. Arkhipov, E. V. Boldyreva, *J. App. Cryst.* **2014**, 47, 14351; (b) S. G. Arkhipov, E. V. Boldyrev, *Zh. Struktur. Himii.* 2014, **55**, 778.
 22. (a) R. E. R. Jr, R. Parthasarathy, J. D. Dunitz, *J. Am. Chem. Soc.* 1977, **99**, 4860; (b) J. P. Glusker, E. Weber Directional Aspects of Intermolecular Interactions (Design of Organic Solids), *Top. Curr. Chem.* 1998, **198**, 1.
 23. (a) F. T. Burling , B. M. Goldstein, *J. Am. Chem. Soc.* 1992, **114**, 2313; (b) M. Iwaoka, N. Isozumi, *Molecules* 2012, **17**, 7266.
 24. (a) J. P. Sauvage, *Acc. Chem. Res.*, 1998, **31**, 611; (b) S. T. Caldwell, G. Cooke, B. Fitzpatrick, D. L. Long, G. Rabania, V. M. Rotello, *Chem. Commun.*, 2008, 5912; (c) J-Q. Liu, Y-Y. Wang, L-F Ma, G-L. Wen, Q-Z. Shi, S. R. Batten, D. M. Proserpio, *CrystEngComm*, 2008, **10**, 1123; (d) R. Thakuria, B. Sarma, A. Nangia, *New J. Chem.*, 2010, **34**, 623.
 25. A. K. Singh, N. Singh, S. Sharma, K. Shin, M. Takase, P. Kaur, A. Srinivasan, P. Singh, *Biophysical*, **2009**, **96**, 646.
 26. (a) B. J. Tickle, C. K. Prout, *J. Chem. Soc., Perkin II*, 1973, **20**, 724; (b) H. Chen, F. Gao, E. Yao, Q. Chen, Y. Ma, *CrystEngComm*, 2013, **15**, 4413; (c) T. Steiner, *New J. Chem.* 1998, 1099. (d) G. R. Desiraju, *J. Chem. Soc., Chem. Comm.*, **1989**, 179.

27. (a) K. Suresh, A. Nangia, *Cryst. Growth Des.* 2014, **14**, 2945; (b) B. Swapna, D. Maddileti, A. Nangia, *Cryst. Growth Des.* 2014, **14**, 5991; (c) A. Nangia, *Acc. Chem. Res.* 2008, **41**, 595.
28. Silverstein, R. M. *Spectrometric Identification of Organic Compounds*, 6th Ed., John Wiley, New York, 2002.
29. (a) P. M. Dewick, *Essentials of Organic Chemistry: For Students of Pharmacy and Medical Chemistry and Biological Chemistry*, John Wiley, 2006; (<https://books.google.co.in/books?isbn=1118681967>).
- (b) M. Paul, A.J. Cruz-Cabeza, *CrystEngComm*, 2012, **14**, 6362;
- (c) http://research.chem.psu.edu/brpgroup/pKa_compilation.pdf.
30. B. Sarma, N. K. Nath, B. R. Bholgala, A. Nangia, *Cryst. Growth Des.*, 2009, **9**, 1546;
31. (a) T. L. Threlfall, *Org. Proc. Res. Dev.*, 2009, **13**, 1224; (b) S. Cherukuvada, R. Thakuria, A. Nangia, *Cryst. Growth Des.*, 2010, **10**, 3931.
32. X. L. Yu, A. S. Carlin, G. L. Amidon, A. S. Hussain, *Int. J. Pharm.*, 2004, **270**, 221.
33. A.T. Florence, D. Attwood, *Physicochemical Principles of Pharmacy*. 2006, 393.
34. (a) G. L. Miessler, D. A. Tarr, *Inorganic Chemistry, Third Edition*, Pearson Education., 2004, 167. (b) R.P. Bell, *The Proton in Chemistry, Second Edition*, 1973, 86.
35. J. M. Williams, J. Ferraro, R. R. J. Thorn, K. Carlson, D. U. Geiser, H. H. Wang, A. M. Kini, M-H. Whangbo, *Organic Superconductors*, Prentice Hall, Englewood Cliffs, NJ, 1992.
36. (a) X-AREA and X-RED, Stoe&Cie GmbH, Darmstadt, Germany, 2007; (b) G. M. Sheldrick, *Program for Refinement of Crystal Structures*, University of Göttingen, Germany, 1997; (c) G. M. Sheldrick, *Acta Crystallogr., Sect. A.* 2008, **64**, 112; (d) G. M. Sheldrick, *Acta Cryst., Sect. C: Struct. Chem.* 2015, **71**, 3; (e) X-STEP32, Stoe&Cie GmbH, Darmstadt, Germany, 2000.
37. T. Higuchi, K. A. Connors, *Adv. Anal. Chem. Instrum.* 1965, **4**, 117.

CHAPTER FOUR

Polymorphism, Isostructurality and Structure-Property Relations: Glibenclamide Salts



Three salts of anti-diabetic drug Glibenclamide are reported along with their hydrates and polymorphs. Glibenclamide-sodium (GBA-Na) salt shown geometrical and packing polymorphism and 3D packing similarity in molecular arrangements of Na^+ ion in the GBA-Na form II/ K^+ ion in the GBA-K form I are interchanged with simple NH_4^+ ion present in GBA-NH₄ and retain the and yet retain isostructurality. All the salts forms were exhibited better solubility in water, among these, GBA-K salt forms I and II, higher solubility than all other solids.

4.1 Introduction

Polymorphism¹⁻³ and isostructurality^{4,5} are inversely related phenomena, and both demonstrated great deal of impact in crystal engineering and material science. Polymorphism can be stated as the ability of the chemical substance that exist in different crystalline packing arrangements in a crystal and isostructurality referred as identical or a nearly identical packing arrangements of chemically distinct and/or related substances in a crystal. Polymorphism is well established in pharmaceuticals and it is considered as a prime method during drug development and formulation. There are numerous reports highlighted the significance of polymorphism in APIs.^{6,7} It offers to tune the properties such as physical (solubility, stability)^{8,9} and mechanical¹⁰⁻¹³ including hygroscopicity, particle size and shape, density, flowability, compactibility, and further bioavailability which leads to the better therapeutic efficacy. On the downside, polymorphs of the API may pose problems during bulk production, stability, formulation and storage. Because polymorphism outcomes from the interplay of thermodynamic functions (free energy, enthalpy and entropy) and kinetic factors (activation energy, temperature, supersaturation, rate of evaporation etc.) that guides the crystallization process. Due to these particulars, there is an increasing interest in understanding the polymorphism phenomenon. Moreover, it is a fundamental task to understand the nucleation of crystal forms, controlling the selective growth of required form, phase transformations between polymorphs, and high-throughput screening crystallization of APIs and their salts/cocrystals.¹⁴ On the other hand, isostructurality in organic molecules is unusual and it can be observed in closely related structures nevertheless, deals with multicomponent systems which is likely to be expected or to occur (by virtue of changing only one of the components). Frequently isostructurality can form a continuous series of solid solutions or alloys, but it is less explored in organic materials and pharmaceuticals as well as the study of their structure-property relations. In this chapter, we identified and demonstrated the novel polymorphs and how isostructurality in classical drug molecule Glibenclamide salts by exchanging the counter ion of simple NH_4^+ ion (simple cation) with Na^+/K^+ ion (metal cation). Further, solubility and stability of salts were discussed.

4.2 Literature reports on Glibenclamide and CSD analysis of $-\text{SO}_2-\text{N}-\text{CO}-\text{N}-$ group

The sulfonyl urea ($-\text{SO}_2-\text{N}-\text{CO}-\text{N}-$) group acts as a weak acid and occupies a prominence place in drug molecules, being a common functional moiety of Chlorpropamide, Tolbutamide, Gliclazide, Glimepiride, Tolazamide, Chlorpropamide, Torsemide etc. A CSD search for molecules with $-\text{SO}_2-\text{N}-\text{CO}-\text{N}-$ (sulfonyl urea)

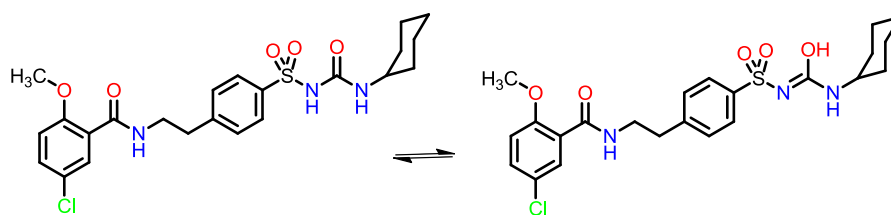
skeleton showed 237 hits. Among them 191 single components and 46 multi-components were present. In single components, only six components (refcodes: BEDMIG, QAXSUD, TOHBUL, TORSEM, ZZZPUS, and CABCU) shown polymorphism and there is no polymorphism reports in multi-components. As well as only three salts structures were available with ref codes: BENVIP¹⁵, KETNIH¹⁶ and PIJCUI.¹⁷ Thus, exploring the structural outcome of single and multicomponent via polymorphism is prominently required to understand the diversity of their packing and geometry. This would enable us to have a better understanding of the molecular interactions associated with physicochemical properties such as solubility, stability and melting point. In this regard, we have chosen the anti-diabetic drug, Glibenclamide with $-\text{SO}_2-\text{N}-\text{CO}-\text{N}-$ skeleton for our study.

Glibenclamide (GBA) or Glyburide belongs to the class of sulfonylurea drugs and has been used to treat the type-II diabetes (non-insulin-dependent diabetes mellitus, NIDDM) to bring down the blood glucose levels by increasing the amount of insulin production from beta cell located in the pancreas.¹⁸ According to Biopharmaceutical Classification System (BCS), GBA belongs to class-II drug with high permeability and low aqueous solubility ($\sim 18\text{mg/L}$ at 37°C).¹⁹ In order to improve the aqueous solubility of GBA, several physical modification strategies have been reported in the literature such as solid dispersion,²⁰ micronization,²¹ incorporation of surfactants,²² cyclodextrin complexation etc.²³ Along with, the synthesis and structural characterization of its metal complexes with magnesium, chromium, cobalt, nickel, zinc and cadmium were reported.²⁴ A CSD search on GBA, only guest free form GBA crystal structure without any hydrogens (disordered, Refcode: DUNXAL) reported ²⁵ and no polymorphs, solvates/hydrates, cocrystals or salts were reported.

4.3 Results and Discussion

GBA exists in amide tautomer in its solid state; however, there is a possibility that the other imide tautomer may exist (scheme 4.1). It acts as a weak organic acid ($-\text{SO}_2-\text{NH}-\text{CO}-\text{N}-$ Sulfonyl urea H, pK_a is 5) and thus it was screened with strong alkali metal hydroxides such as sodium hydroxide, NaOH; potassium hydroxide, KOH; (to remove sulfonyl urea proton) and ammonia, NH_3 (to transfer the proton from sulfonyl urea to give NH_4^+) to form salts. Predominately the selection of the pertinent salt form of a potential drug candidate to enhance/modify the physicochemical properties is the major essence of the drug development.²⁶ Conventionally, salt formation is a green synthesis and quiet simple, but on average there are more consequences like hydrates, solvates, polymorphs

and amorphous solids. Most of the alkali metal salts of drugs revealed greater importance, especially for sodium as a counter ion which is more superior cation for the salt formation to enhance the solubility.²⁷ According the orange book database list, various drug salts were approved by US-FDA, the occupation of alkali metal complexes with Na (75.3%) or K (6.3%) as a counter ion drug was at an elevation.²⁷⁻³⁰ The present work we obtained different crystalline salts of the GBA with NaOH (Glibenclamide-sodium salt, GBA-Na) KOH (Glibenclamide-potassium salt, GBA-K) and NH_3 (Glibenclamide-ammonium salt, GBA- NH_4). Among these, GBA-Na salt exist as dimorphic (GBA-Na form I and II) and one hydrate (GBA-Na form III). GBA-K salt exists as anhydrate (form I) and hydrate (form II) and GBA- NH_4 salt exists as anhydrate. All these salt forms were synthesised via the slurry method (A summary of the experimental methods and crystallization conditions are given in experimental section) and characterized by various spectroscopic, thermal and powder X-ray diffraction techniques. We unable reproduce GBA-Na form II and its single crystals obtained by solution crystallization (crystallization procedure in Experimental section). Further crystal structures were confirmed by single crystal X-ray diffraction technique except for GBA-K form II (hydrate) we unable to grow suitable single crystals. Selected crystal data, data collection and refinement parameters are summarized in Table 4.1 hydrogen bonds are listed in Table 4.2. A kinetic stability study through dynamic vapor sorption (DVS) analysis, solubility and dissolution rate measurements are also explored for all GBA salts except GBA-Na form II.



Scheme 4.1 Schematic representation of tautomerism in Glibenclamid

Table 4.1 Crystallographic parameters of GBA and its salts

	GBA	GBA-Na form I	GBA-Na form II	GBA-Na form III	GBA-K form I	GBA-NH4
Mol. form.	C ₂₃ H ₂₈ ClN ₃ O ₅ S	C ₂₃ H ₂₇ ClN ₃ NaO ₅ S	C ₂₃ H ₂₇ ClN ₃ NaO ₅ S	C ₂₃ H ₂₉ ClN ₃ NaO ₆ S	C ₂₃ H ₂₇ ClKN ₃ O ₅ S	C ₂₃ H ₃₁ ClN ₄ O ₅ S
Form. Wt.	493.99	515.98	515.98	533.99	532.09	511.03
Cryst. syst.	Monoclinic	Monoclinic	Monoclinic	Monoclinic	Monoclinic	Monoclinic
Sp. gr.	<i>P</i> ₂₁ / <i>n</i>	<i>P</i> ₂₁	<i>P</i> ₂₁ / <i>c</i>	<i>P</i> ₂₁ / <i>c</i>	<i>P</i> ₂₁ / <i>c</i>	<i>P</i> ₂₁ / <i>c</i>
<i>T</i> (K)	298(2)	298(2)	298(2)	298(2)	298(2)	298(2)
<i>a</i> (Å)	9.45444(13)	10.9425(10)	19.7594(13)	19.5991(16)	19.819(4)	19.718(4)
<i>b</i> (Å)	17.6795(3)	10.1583(7)	6.1759(3)	5.8086(3)	6.2006(9)	6.1475(11)
<i>c</i> (Å)	14.4839(2)	11.5023(11)	21.5560(15)	23.4722(17)	21.636(5)	21.732(5)
<i>α</i> (°)	90	90	90	90	90	90
<i>β</i> (°)	93.4373(13)	91.164(9)	109.627(7)	108.746(8)	109.69(2)	109.69(2)
<i>γ</i> (°)	90	90	90	90	90	90
<i>Z</i>	4	2	4	4	4	4
<i>V</i> (Å³)	2416.63(6)	1278.31(19)	2477.7(3)	2530.4(3)	2503.3(8)	2503.3(8)
Rflns. collect	4732	5086	5063	4984	5110	4241
Unique rflns.	4613	4011	5057	4906	5104	4237
Obsd. Rflns.	4082	2956	3454	3105	2515	1284
Parameters	311	308	308	325	312	324
<i>R</i>1	0.0505	0.0617	0.0834	0.0816	0.0832	0.0644
w<i>R</i>2	0.1476	0.1566	0.2495	0.2667	0.2564	0.0980
GOF	1.007	1.072	1.042	1.032	0.986	0.769
Diffractionmeter	Oxford Xcalibur Gemini	Oxford Xcalibur Gemini	Oxford Xcalibur Gemini	Oxford Xcalibur Gemini	Oxford Xcalibur Gemini	Oxford Xcalibur Gemini

Table 4.2 Hydrogen bonds in GBA and its salts

D–H...A	D...A (Å)	H...A (Å)	D–H...A (°)	symmetry code
GBA				
N1–H1A...O2	2.665(2)	1.97	137	intramolecular
N1–H1A...O5	2.948(2)	2.29	134	-1/2+x,1/2-y,-1/2+z
N2–H2A...O1	2.815(2)	2.05	154	-1/2+x,1/2-y,1/2+z
GBA-Na form I				
N1–H1A...O2	2.658(7)	1.97	136	intramolecular
C23–H23C...O5	3.468(8)	2.54	163	intramolecular
GBA-Na form II				
N3–H3A...O1	3.820(6)	2.988	163	x,-y+1/2+1,+z-1/2
C9–H9B...O1	3.525(7)	2.56	174	x,-1+y,z
C23–H23B...O4	3.532(8)	2.57	177	x,1+y,z
GBA-Na form III				
N1–H1A...O2	2.641(6)	1.99	132	intramolecular
N3–H3A...O6	3.292(12)	2.65	131	x,y,z
O6–H6A...O5	3.293(.009)	2.66	123	x,+y-1,+z
C23–H23C...O5	3.094(8)	2.39	130	intramolecular
GBA-K form I				
C23–H23A...O5	3.544(.007)	2.589	173	x,+y-1,+z
GBA-NH₄				
N1–H1A...O5	2.615(6)	1.99	129	intramolecular
N3–H3A...O1	3.661(5)	2.83	161	x,-y+1/2,+z-1/2
N4–H4A...O3	2.831(7)	1.87	164	-x,1-y,-z
N4–H4B...O1	2.871(7)	1.93	164	x,1/2-y,-1/2+z
N4–H4C...O2	2.780(7)	1.92	148	x,-1+y,z
N4–H4D...N2	2.823(7)	1.85	175	x,y,z
C23–H23A...O4	3.396(7)	2.49	158	x,-1+y,z

4.3.1 Crystal Structure Analysis

GBA: The X-ray crystal structure of GBA was earlier reported²⁵ by S. R. Byrn *et. al.* without proton positions. For a better understanding of hydrogen bonding interactions, reflections on a crystal of the GBA were collected to give the complete crystal structure. It crystallized in the monoclinic space group $P2_1/n$. In the crystal structure, adjacent GBA molecules connected along the N–H...O (N3–H3A...O1, 2.34 Å, 144° and N2–H2A...O1, 2.05 Å, 154°) hydrogen bonds in a $R_2^1(6)$ ring motif between sulfonyl NH and amide C=O group of GBA. Such $R_2^1(6)$ ring motifs extend in a layered structure through N–H...O (N1–H1A...O5, 2.29 Å, 134°) interaction (Figure 4.2). Additionally the amide N–H forms an intramolecular hydrogen bond with methoxy (–OCH₃) group via

N–H \cdots O (N1–H1A \cdots O2, 1.97 Å, 137°) in an energetically favorable six membered ring geometry (*S*(6) graph set pattern) hinders conformational flexibility.

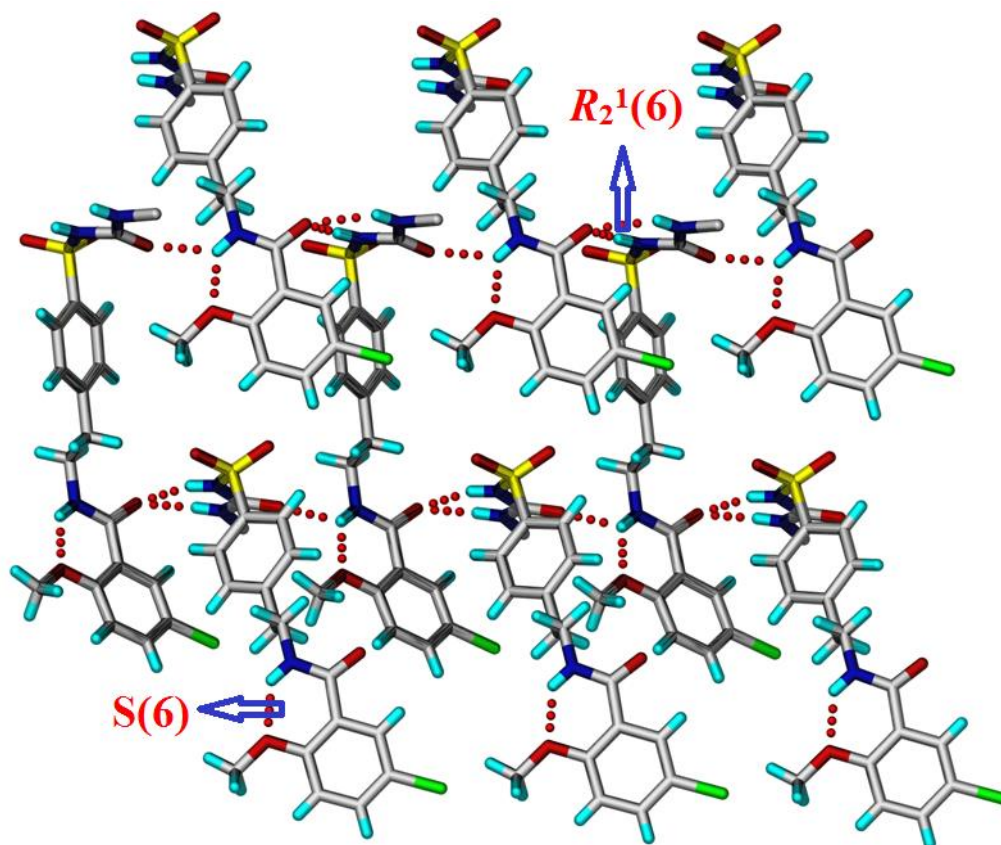


Figure 4.2: Crystal structure of GBA; adjacent GBA molecules interacted through N–H \cdots O hydrogen bonding in crystal lattice (Cyclohexyl group is removed for clarity).

Glibenclamide-Sodium (GBA-Na) salt forms

All three forms of GBA-Na (I, II and III) were established by single crystal X-ray diffraction technique along with other techniques; however, we are unable to reproduce the GBA-Na form II for further characterization and property studies.

GBA-Na Form I: The GBA-Na form I was crystallized in the monoclinic space group $P2_1$ with 1:1 stoichiometric ratio. In the crystal structure, the central sodium ion which is coordinated by four O-bonded and one N-bonded ligands come from the GBA anion through Na–O (Na1–O1, 2.247(5) Å; Na1–O3; 2.480(4) Å; Na1–O4 2.377(4) Å; Na1–O5, 2.270(4) Å) and Na–N (Na1–N2, 2.439(5) Å) coordination bonds within a square

pyramid geometry. The adjacent molecules propagated into a 1D sinusoidal wave through two Na–O coordination bonds along *c*-axis (Figure 4.3).

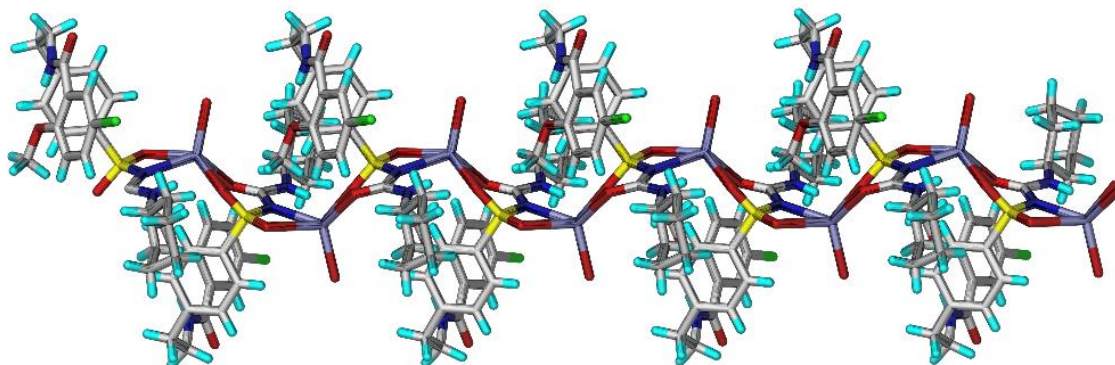


Figure 4.3: Square pyramid geometry of GBA-Na form I 1D polymeric sinusoidal wave in crystal lattice.

GBA-Na form II: It crystallized in the monoclinic space group $P2_1/c$ and the asymmetric unit contains 1:1 stoichiometric ratio of Na^+ cation and GBA anion. In the crystal structure, central six coordinated sodium cation is bound to five oxygen atoms (three from sulfonyl and two from amide carbonyl of the GBA) and one nitrogen atom from different distinct ligands of GBA and displays the distorted octahedral geometry. The five Na–O bond lengths are Na1–O1, 2.857(4) Å; Na1–O3, 2.658(4) Å; Na1–O4, 2.951(4) Å; Na1–O5, 3.030(4) Å and one Na1–N2 bond length is 2.822(4) respectively. Remarkably SO_2 group oxygen atom binds to two adjacent sodium cation centers to join the coordination complex into a 1D polymeric chain in a parallel mode (Figure 4.4) with a nonbonded $\text{Na}\cdots\text{Na}$ metal ion interaction. The packing and geometry of form II is entirely different compared with GBA-Na form I.

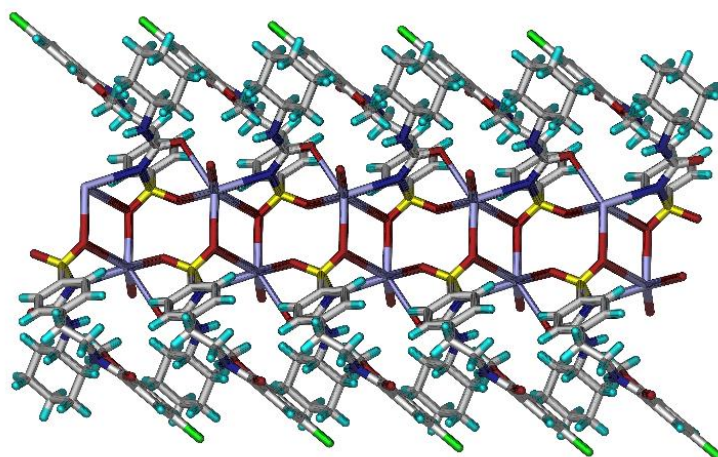


Figure 4.4: Distorted octahedron geometry of GBA-Na form I complex 1D polymeric chain in crystal lattice.

GBA-Na Form III: The X-ray crystal structure of GBA-Na form III was solved and refined in space group $P2_1/c$ with 1:1:1 stoichiometric ratio of GBA anion, Na^+ cation and water molecule in the asymmetric unit. In the crystal structure, the central Na^+ ion coordinated by four O- and one N-bonded ligands from the GBA anion and one water molecule through Na–O (Na1–O3, 2.693(4) Å; Na1–O4, 2.401(4) Å; Na1–O4 2.411(4) Å; Na1–O5, 2.380(4) Å; Na1–O6, 2.367(7) Å) and Na–N (Na1–N2, 2.487(4) Å) coordination bond in a distorted octahedron geometry. The 1D propagation of the polymeric chain of this structure is similar to GBA-Na form II through bridged sulfonyl group oxygen atoms between two Na^+ cations in a parallel mode along c -axis (Figure 4.5).

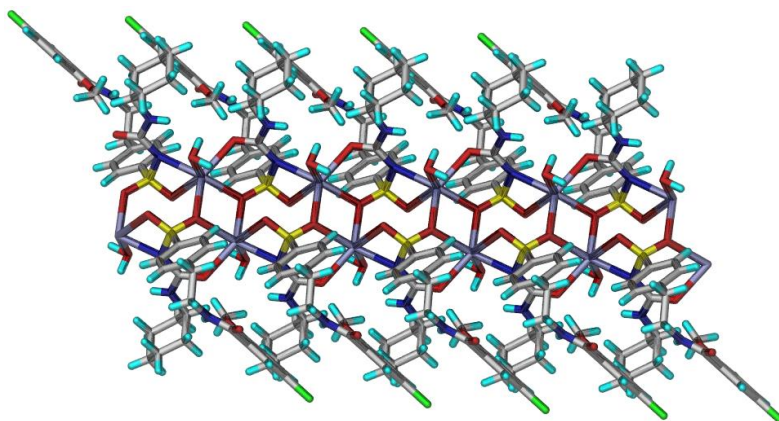


Figure 4.5: Distorted octahedron geometry of GBA-Na form III complex 1D polymeric chain in crystal lattice.

From the above crystal structures of GBA-Na salt forms, we found that they are arranged in different geometric and packing of the (ligands bonded and number) central alkali metal Na^+ ion in the crystal lattice. GBA-Na form I have a square pyramidal geometry (five coordinated complex) while in other two forms GBA-Na form II and III exhibited distorted octahedral geometry (six coordination complexes). In detail analysis, comparison of GBA-Na form II and III were varied by one water molecule and it is directly coordinated to the central metal ion in form III instead of carbonyl oxygen bonded in GBA-Na form II. Especially when comparison of GBA-Na I and II polymorphs, which are different in geometry and coordination number on central metal ion and this type polymorphism is uncommon in literature. The central metal sodium ion coordination geometry of all three forms of GBA-Na salt is shown in Figure 4.6.

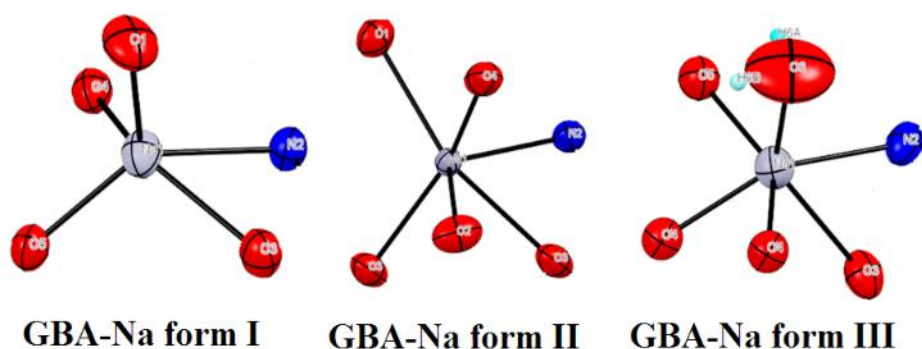


Figure 4.6: Coordination geometry differences of GBA-Na form I, II, and III.

Glibenclamide-Potassium (GBA-K) salt forms

The resulted two forms of GBA-K, form I was established by single crystal x-ray diffraction technique and form II which did not yield suitable single crystals for structure elucidation by single X-ray diffraction technique.

GBA-K form I: The X-ray analysis of GBA-K form I was solved and refined in monoclinic space group $P2_1/c$ with 1:1 stoichiometric ratio of GBA anion and K^+ cation. Similar to GBA-Na form II, this complex central K^+ cation which is coordinated by six ligands come from the GBA anion. Out of six ligands, five are O- bonded and one is N- bonded ligands through K–O (K1–O1, 2.856(5) Å; K1–O2 2.661(5) Å; K1–O3, 2.952(4) Å; K1–O3, 2.776(3) Å; K1–O4, 3.025(4) Å) and K–N (K1–N2 2.826(4) Å) coordination bonds. In the crystal lattice, SO_2 oxygen atom binds to two adjacent potassium cation

centers to connect the coordination complex into a 1D polymeric chain in parallel mode (Figure 4.7) with a nonbonded $K \cdots K$ metal ion interaction.

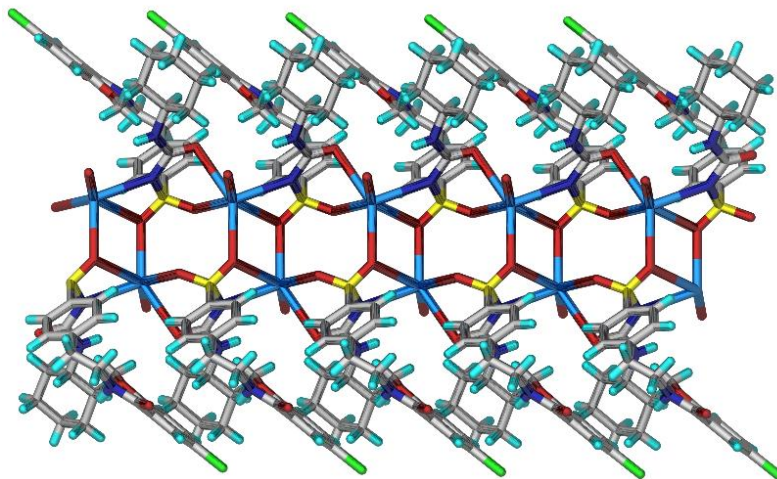


Figure 4.7: Distorted Octahedron geometry of GBA-K form I complex 1D polymeric chain in crystal lattice.

Glibenclamide-Ammonium (GBA- NH_4) salt: It crystallizes in the monoclinic space group $P2_1/c$ and the asymmetric unit contains NH_4^+ cation and GBA anion with 1:1 stoichiometric ratio. The NH_4^+ ion forms intermolecular ionic hydrogen bonds with sulfonyl urea N anion via $N-H \cdots N$ ($N4-H4D \cdots N2$ 1.85 Å, 175°) and on the other side it forms $N-H \cdots O$ ($N4-H4A \cdots O3$ 1.87 Å, 164°) with adjacent GBA anion in a $R_4^4(8)$ motif. Such motifs are associated through $N-H \cdots O$ ($N4-H4C \cdots O2$, 1.92 Å, 148°) interaction in a $R_4^4(8)$ ring motifs within the 1D lattice (Figure 4.8).

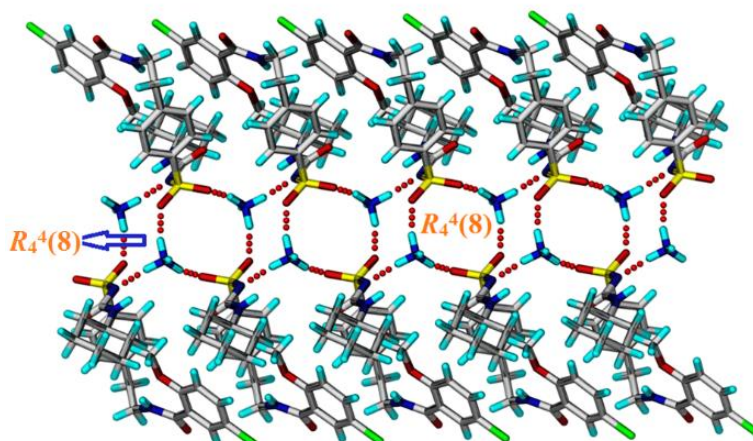


Figure 4.8: $N-H \cdots O$ hydrogen bond ring motifs in the crystal structure of GBA- NH_4 salt.

4.3.2 Unit Similarity index equation and X-Pac analysis

In the above all salts, GBA-Na form II, GBA-Na form III, GBA-K form I and GBA-NH₄ exhibit near identical cell parameters indicating them to be an isostructural. Isostructurality, traditionally interpreted by using the Kàlmàn unit similarity index (Π) equation³¹ and it is based on the unit cell parameters of two structures. If this Π value is close to zero indicates the identical length of the unit cell axes and that pair should be an isostructural. Utilization of this Π equation to GBA-Na form II & GBA-K form I, GBA-Na form II & GBA-NH₄ and GBA-K form I & GBA-NH₄ pairs resulted Π index score is zero. It indicates all these pairs are isostructural to each other (Equation and Π values are listed in Table 4.3). On the other hand GBA-Na form III with other forms (GBA-Na form II/GBA-K form I/ GBA-NH₄) resulted Π index score is 0.02 due to large anisotropic shift in a and b axes which are also isostructural to each other according to Kàlmàn equation.

Table 4.3: Unit Cell similarity indices of all combinations of GBA salts

$$\Pi = \left| \frac{a+b+c}{a'+b'+c'} \right| - 1 \cong 0$$

Salt combination	Unit cell similarity index
GBA-Na form II & GBA-K form I	0.0034
GBA-Na form II & GBA-NH ₄	0.0022
GBA-K form I & GBA-NH ₄	0.0012
GBA-K form I & GBA-NH ₄	0.0012
GBA-Na HYD form III & GBA-NH ₄	0.0269
GBA-Na form II & GBA-Na HYD form III	0.0292
GBA-K form I & GBA-Na form III	0.0256

In addition to the Π parameter which gives the identity of the crystallographic unit cell for the isostructurality, the internal molecular arrangement was compared by the XPac software.³²⁻³⁴ Generally, the analysis of the two structures/pair is based on comparing the angular, planar and distance relationships between the coordination spheres of neighboring molecules around a central molecule in each structure. Depending on the number of matches, the dimensionality (1D/2D/3D) and the similarity of the structures are derived. Usage of XPac software to the above pairs, only GBA-K form I & GBA-NH₄ and GBA-Na form II & GBA-NH₄ pairs showed 3D supramolecular construct. This

means that two pairs exhibited 3D similarity in molecular arrangements and Na^+ ion in the GBA-Na form II/ K^+ ion GBA-K form I, can be interchanged with simple NH_4^+ ion present in GBA- NH_4 and yet retain isostructurality. The 3D supramolecular constructs of GBA-K form I & GBA- NH_4 and GBA-Na form II& GBA- NH_4 pairs along with their dissimilarity index plots were shown in Figure 4.9. In addition to this, the other combinations of GBA-Na form III with any one of GBA-Na form II/GBA-K form I/ GBA- NH_4 and GBA-Na form II & GBA-K form I, did not result, to supramolecular construct in 1D/2D/3D.

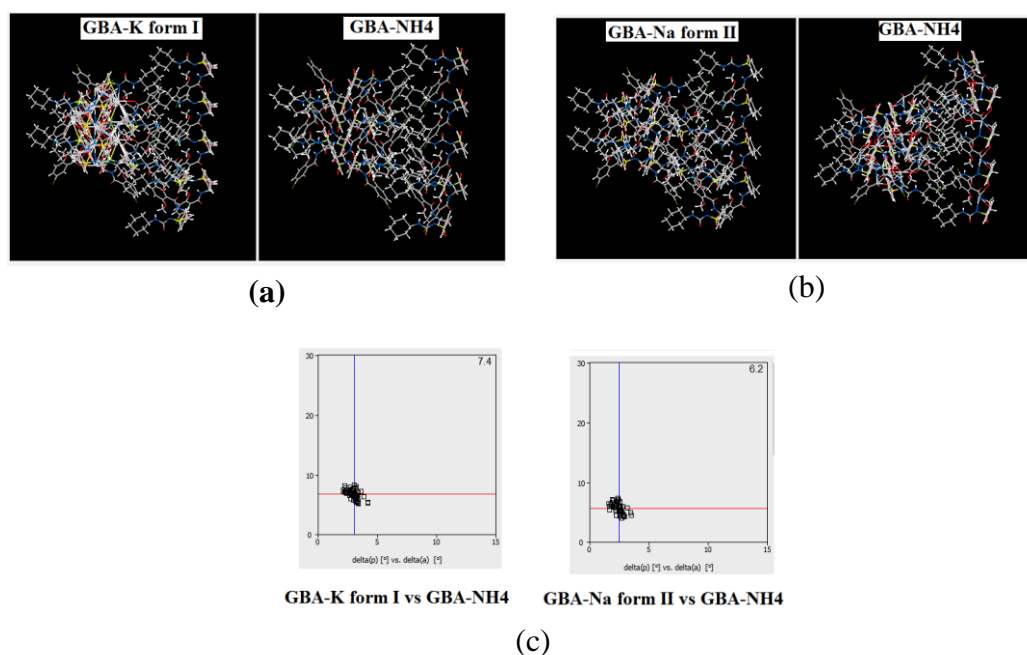


Figure 4.9: (a) 3D supramolecular construct of GBA- K form I and GBA- NH_4 (b) 3D supramolecular construct of GBA- Na form II and GBA- NH_4 (c) the plot of the interplanar angular deviation vs. angular deviation (u) in XPac with a dissimilarity index of 7.4 for the GBA- K form I vs. GBA- NH_4 and 6.2 for the GBA- Na form II and GBA- NH_4 .

4.3.3 Packing and Powder Pattern Similarity Analysis (Crystal packing in the Mercury software)

Furthermore we analyzed packing and powder similarity of the above all isostructural pairs (according Π equation) by the packing similarity tool in the Mercury program, which can facilitate 3D structural analysis basing on the packing of common molecules. For this analysis, isostructural pairs of 20 molecules were used by keeping the default

values to 30% for intermolecular atomic distance and 30° for intermolecular atomic angles to compensate the larger gaps.³⁵ The results obtained from this analysis rationalize into all isostructural pairs, the pairs of GBA-K form I & GBA-NH₄ and GBA-Na form II & GBA-NH₄ are displayed 20 out of 20 molecules, and GBA-Na form III & GBA-NH₄ pair shown 3 out of 20 molecules are isostructural (Figure 4.10 and Table 4.4). In addition to packing similarity, simulated powder pattern similarity also obtained for the above mentioned pairs³⁶ (Mercury powder patterns simulated from the 3D atomic coordinates with Cu-K α X-radiation, wavelength 1.540056 Å from 0-50Å 2 θ which corresponds to the resolution of 1.8 Å). The resulted PXRD similarity index score is > 0.99 for both pairs of GBA-K form I & GBA-NH₄ (0.992463) and GBA-Na form II & GBA-NH₄ (0.994815) whereas for GBA-Na form III & GBA-NH₄^{pair} index score is < 0.99 (0.963229). As a point of comparison, according to Van De Streek & Motherwell,³⁶ among these three pairs, two pairs have a PXRD similarity index score > 0.99. This indicating that, two pairs exhibited genuine isostructurality with highest PXRD similarity is depicted in Figure 4.11. However, on the other side, same applications were also subjected to determine similarity in packing and powder lines of other pairs (GBA-Na form II & GBA-K form I, GBA-Na form II & GBA-Na form III and GBA-K form I & GBA-Na form III), where we haven't observed any similarity either in the packing or powder patterns.

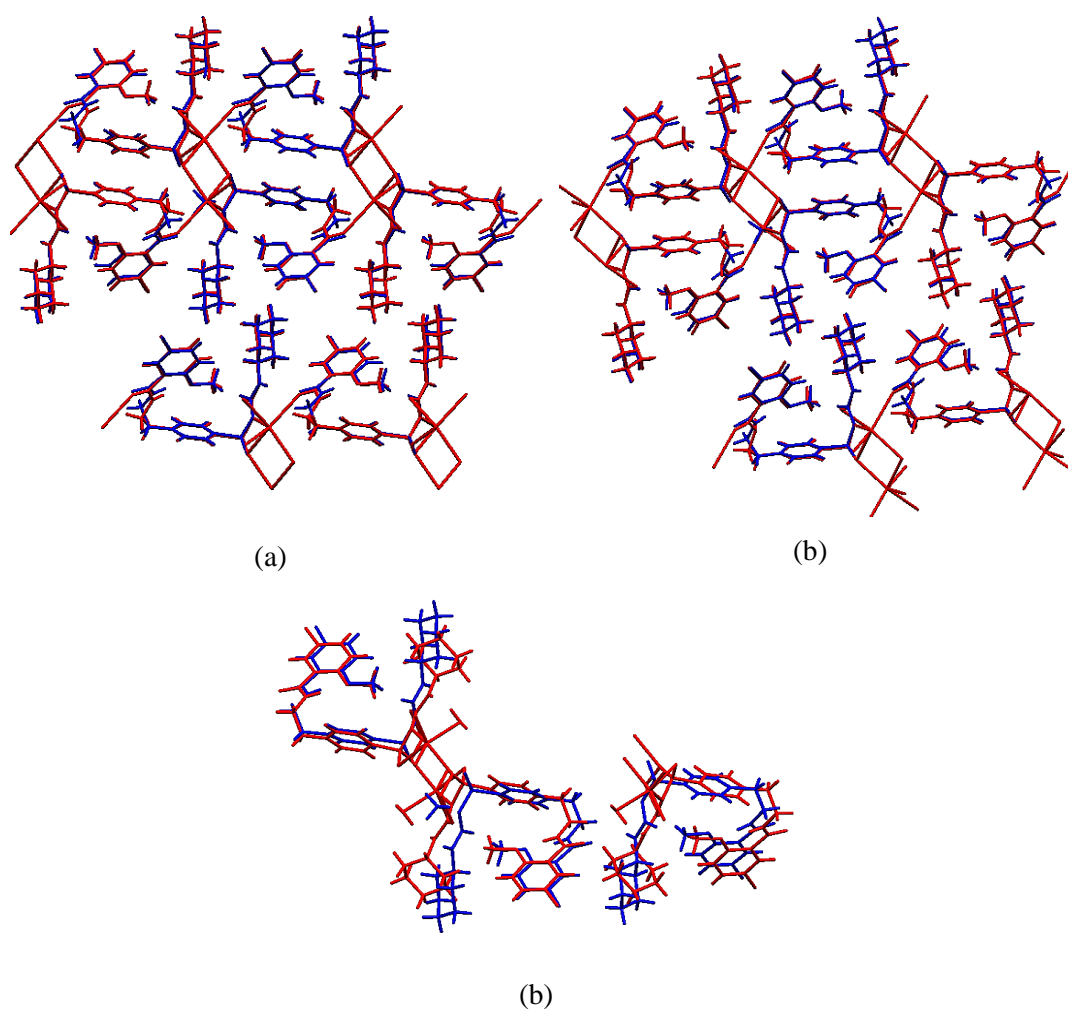


Figure 4.10: (a) packing overlays for GBA-Na form II & GBA-NH₄ (b) packing overlays for GBA-K form I & GBA-NH₄ (c) packing overlays for GBA-Na form III & GBA-NH₄.

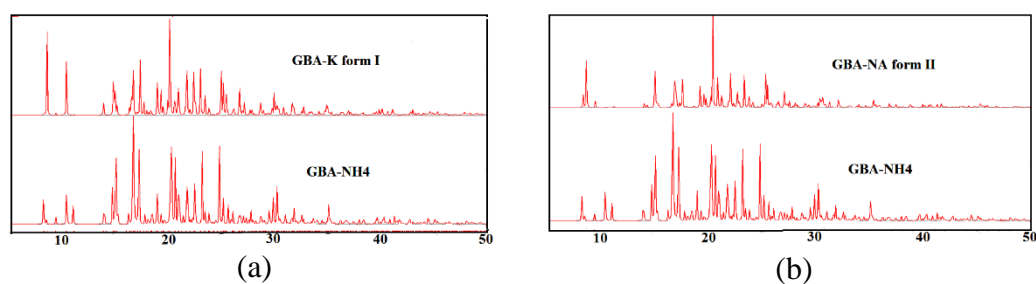


Figure 4.11: (a) and (b) Simulated PXRD patterns of isostructural pairs GBA-K form I & GBA-NH₄ and GBA-Na form II & GBA-NH₄ were showed >99 powder similarity.

Table 4.4 Summary of PXRD and packing similarity results for the GBA-Na form II & GBA-NH₄, GBA-K form I & GBA-NH₄ and GBA-Na form III & GBA-NH₄ pairs.

Compound	PXRD similarity	No. of molecules in common	RMSD (Å)
GBA-Na form II & GBA-NH ₄	0.994815	20 out of 20	0.379116
GBA-K form I & GBA-NH ₄	0.992463	20 out of 20	0.398447
GBA-Na form III & GBA-NH ₄	0.963229	3 out of 20	1.21044

4.3.4 Conformational Analysis

GBA is a conformationally flexible molecule because it adapts different orientations/conformations on salt formed by the influence of steric effect, hydrogen bonding and packing effects in the solid state.³⁷ Conformational changes in GBA are mainly due to phenyl ethyl group rotation, which exists between the 5-chloromethoxybenzamide and cyclohexyl carbomylsulfomyl groups. GBA exhibits different conformations represented in Figure 4.12 and torsion angles are listed in Table 4.5). The comparison of GBA-Na forms, those also exhibited different conformations.

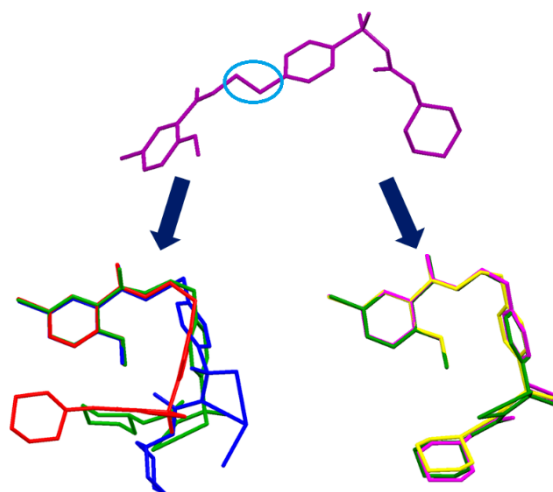
**Figure 4.12** Overlay of GBA molecule extracted from the crystal structure of the guest free form and its salts. Purple = GBA, Green = GBA-Na form I, Red = GBA-Na form II, Blue = GBA-Na form III, Magenta = GBA-K form I and yellow= GBA-NH₄.

Table 4.5 Torsion angles in GBA molecule in different salt crystal structures.

τ_1 C1-N2-C3-C4, τ_2 N2-C3-C4-C5, τ_3 C6-S7-N8-C9, τ_4 S7-N8-C9-N10, τ_5 N8-C9-N10-C11					
	τ_1	τ_2	τ_3	τ_4	τ_5
GBA	-84.26	178.92	70.10	178.14	178.63
GBA-Na form I	174.84	-47.82	74.19	179.22	172.36
GBA-Na form II	177.75	-47.75	68.35	-172.25	173.28
GBA-Na form III	106.44	57.68	-69.60	-172.57	177.64
GBA-K form I	179.99	47.98	-68.50	171.93	-172.85
GBA-NH ₄	-108.62	-40.56	-68.29	172.88	175.25

4.3.5 PXRD Analysis

The bulk materials phase purity (obtained from slurry) of GBA-Na form I and III, GBA-K form I and GBA-NH₄ were confirmed by using PXRD. PXRD patterns of these salt forms were exhibited excellent match with simulated powder lines obtained from X-ray crystal structure. The peculiar GBA-K form II, PXRD pattern showed differences in diffraction peaks at 2θ values from that of the GBA and GBA-K form I (Figure 4.13). And this pattern is similar to GBA-Na form III PXRD pattern.

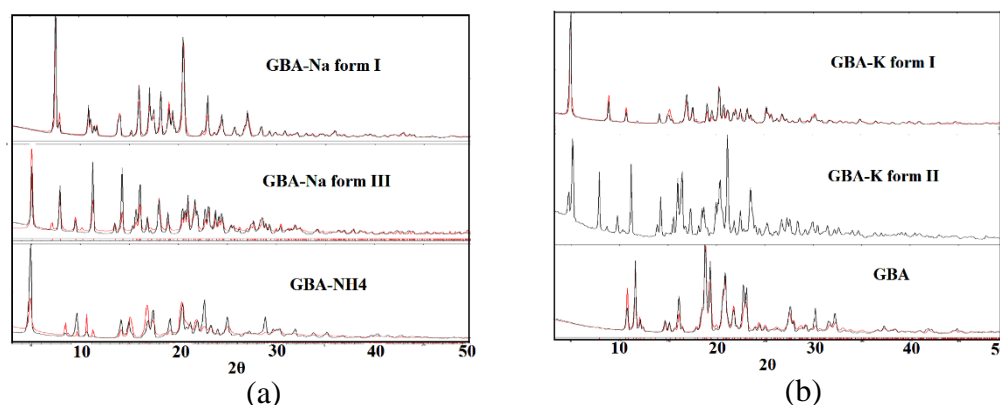


Figure 4.13 (a) Overlay of the experimental PXRD (black) of GBA-Na form I, GBA-Na form III and GBA-NH₄ with the calculated lines from the X-ray crystal structure (red) confirm the bulk purity and homogeneity of each phase (b) Overlay of the experimental PXRD (black) of GBA-K form I and GBA with the calculated lines from the X-ray

crystal structure (red) and experimental PXRD plot of GBA-K form II was compared to GBA-K form I and GBA to contrast 2θ values in the new crystalline phase.

4.3.6 FT-IR Spectroscopy

All GBA salts were analyzed using FT-IR spectroscopy.^{38a} to observe the molecular level interactions.^{38b} Generally it provides the information about the changes occur in the vibrational modes associated with the functional groups, when we obtain a salt/cocrystal.³⁹

The GBA of urea carbonyl and amide carbonyls (C=O) stretching frequencies were appeared at 1715cm^{-1} and 1618cm^{-1} respectively. And the stretching bands at 3315cm^{-1} and 3367cm^{-1} belongs urea and amide of N-H functional groups. These functional groups stretching bands showed significant changes in their vibrational mode regions while forming a salt. Almost all GBA salts were displayed blue shift in their stretching vibrational frequencies, especially in case of N-H and C=O stretching frequencies due to the salt formation. (All frequency changes are listed in Table 4.6 and spectra shown in Figure 4.14). Related to this, other functional group vibrational modes are also red/blue shifted.

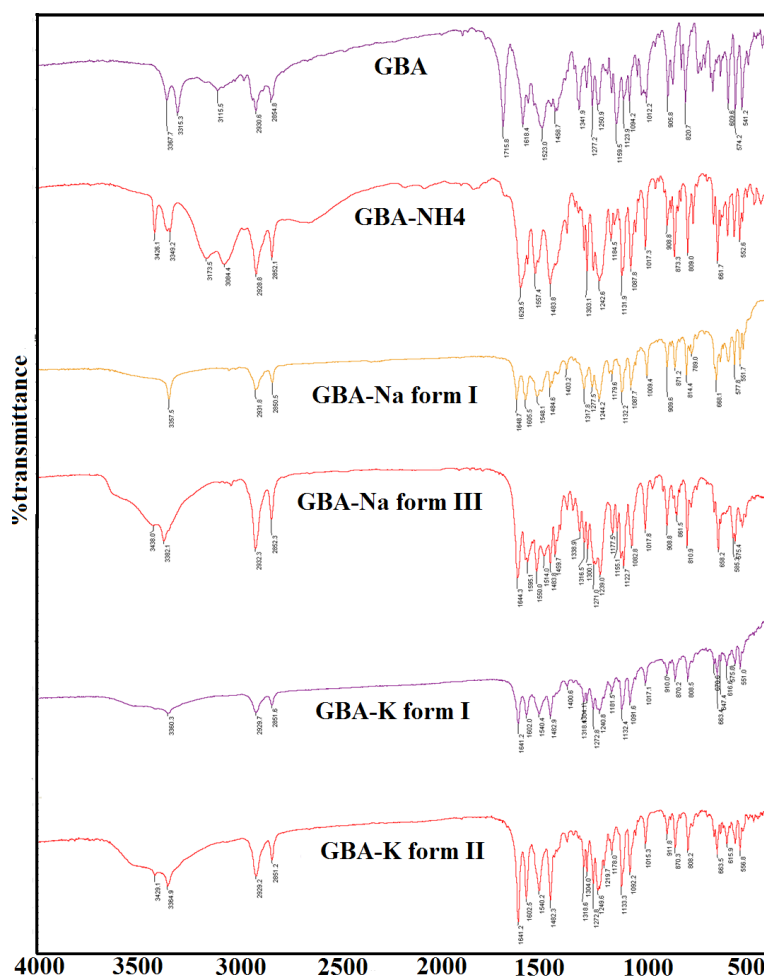


Figure 4.14: FT-IR spectra of GBA and its salt forms

Table 4.6 IR stretching frequencies of GBA urea (NHCONH) and amide (CONH) functional groups in the solid state.

S.No	Solid form	NHCONH ($\nu_{C=O}$ in cm^{-1})	CONH ($\nu_{C=O}$ in cm^{-1})	NHCONH/CONH/H ₂ O ($\nu_{NH/OH}$ in cm^{-1})
1	GBA	1715	1618	3315, 3367
2	GBA-Na form I	1648	1605	3357
3	GBA-Na form III	1644	1595	3382, 3438
4	GBA-K form I	1641	1602	3360
5	GBA-K form II	1641	1602	3364, 3429
6	GBA-NH ₄	1629	1598	3349, 3426

4.3.7 Thermal Analysis

DSC analysis of GBA salts exhibited unique thermal behavior in comparison to their starting materials (Figure 4.15). GBA-Na form I and GBA-K form I were showed single and higher melting endotherm compared to the GBA. While GBA-NH₄ exhibited single broad melting endotherm which is lower than the GBA. It represents that there are charge-assisted N-H \cdots O and N-H \cdots N hydrogen bonds lessens the strength in GBA-NH₄ compared with GBA which does not show any charge assisted N-H \cdots O hydrogen bonds. GBA-Na form III (hydrate) material displayed typical thermal behavior. It exhibited that broad endothermic transition at 80 °C followed by melting endotherm at 167 °C and further it shows an exotherm (crystallization) at 213 °C then again melts at 242 °C. Corresponding material dehydration in TGA, water loss showed (experimental 3.35% and calculated 3.37% for 1 mole of water) between 80 °C to 167 °C temperatures. It indicates that the dehydration and melting occur simultaneously (Figure 4.16a). Dehydration is known result in new polymorphs³⁹ and accordingly GBA-Na form III was subjected to controlled heating experiments of dehydration at 90 °C and 167°C for 1h and resultant powder material characterized by PXRD. At 90 °C no change in PXRD lines, but its shown semi crystalline and at 167 °C it was melted and given fully amorphous PXRD pattern. This amorphous form further transformed to the stable crystalline GBA-Na form I at room temperature. This result signifies that the transition occurred to GBA-Na form III \rightarrow I via amorphonization (Figure 4.17a). While GBA-K form II (hydrate) exhibited broad endotherm at 54 °C prior to melting endotherm (238 °C) which is due to dehydration of water as observed from the weight loss of the material in TGA at the corresponding temperature (experimental 3.27% and calculated 3.27% for 1 mole of water, Figure 4.16b). Further controlled heating experiment at 85°C for dehydration, results the GBA-K form I, was confirmed by PXRD (Figure 4.17b).

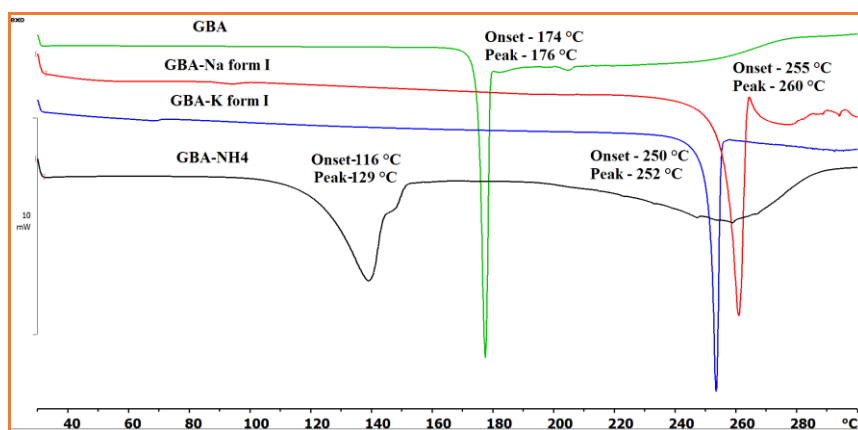
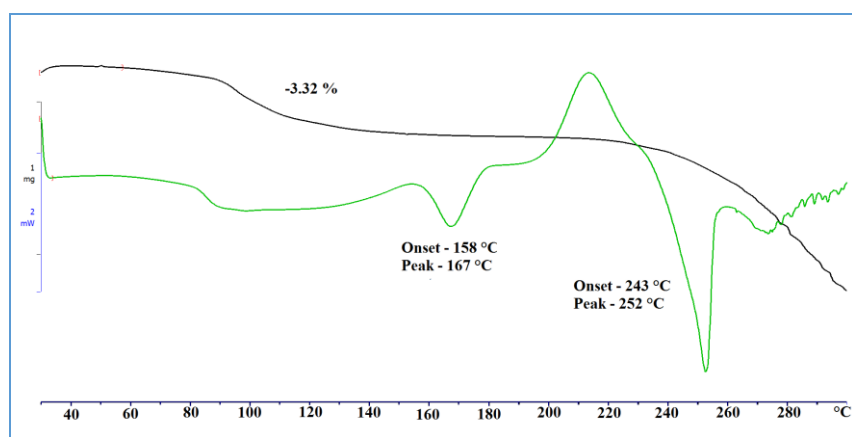
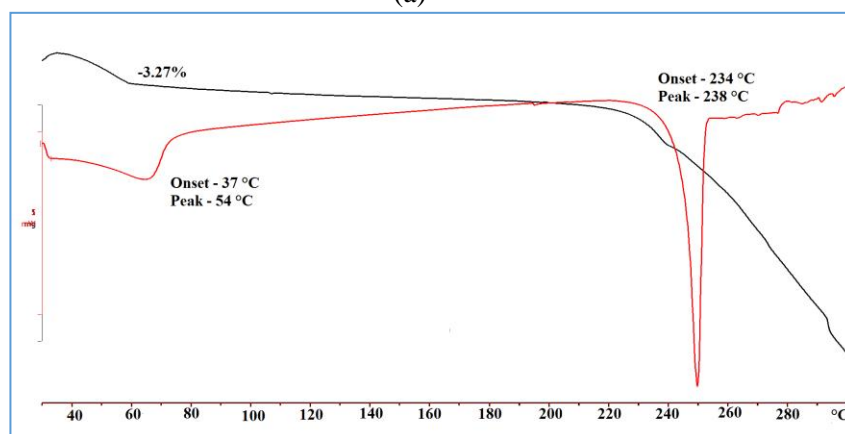


Figure 4.15 DSC heating curves of GBA, GBA-Na form I, GBA-K form I and GBA-NH₄.



(a)



(b)

Figure 4.16: (a) DSC (green) and TGA (black) of GBA-Na form III (b) DSC (red) and TGA (black) of GBA-K form II

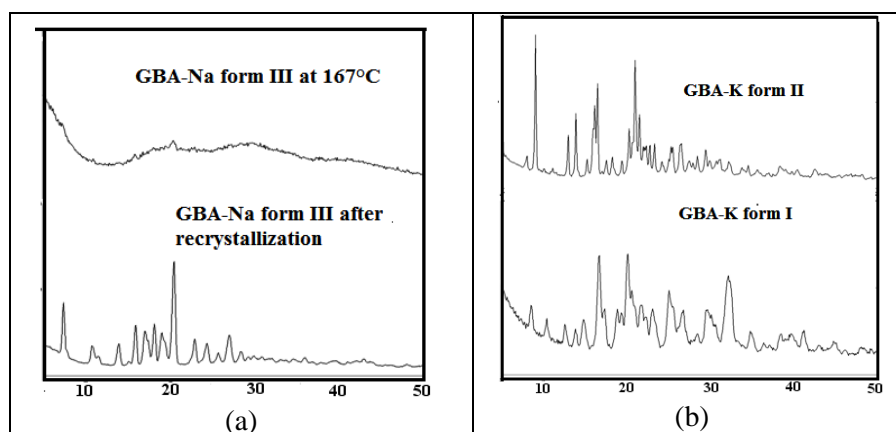


Figure 4.17 (a) GBA-Na form III transformed to form I via amorphonization (b) GBA-K form II transformation to form I upon heating at 85°C.

4.3.8 Solubility Studies

Solubility measures the “how much” amount of solute dissolves in a given solvent system and it is a thermodynamic function. It is mainly depends on the solubility of the counter ion, melting point, hydrogen bonding, and efficient crystal packing.⁴⁰ Equilibrium solubility was carried in pH 7 phosphate buffer and water media. The observed solubility of GBA and its salts showed more in water than pH 7 phosphate buffer and all salt exhibited higher solubility than the GBA. Among all the salts, GBA-K form I and II exhibited 77 folds higher solubility (6.94mg/mL for form I and 6.95 mg/mL for form II) in water media and 33 folds (1.35mg/mL) for form I and 34 folds (1.37mg/mL) for form II in buffer media in comparison with the parent drug GBA (0.09 mg/mL). As well as GBA-Na form I and III also showed 41 (3.74mg/mL for form I) and 47 (4.28mg/mL for form III) folds improvement in water media and 15(0.61mg/mL for form I) and 16 (0.67mg/mL for form III) folds improvement in buffer media. We are assuming that the greater ionic radius of K^+ ion exhibiting lower lattice enthalpy which may favor the solubility enhancement than sodium salts. In contrast to the isostructurality, GBA-K form I & GBA-NH₄ pair have shown no similarity in the solubility properties. The equilibrium solubility order in both media is GBA-K form I> GBA-K form II>GBA-Na form III>GBA-Na form I>GBA-NH₄>GBA. The solubility concentrations were displayed in Figure 4.18, and values listed in Table 4.7. Further solid residues of all salt forms were analyzed by PXRD to know phase dissociation/transformation during dissolution equilibrium solubility experiments (Figure 4.19). PXRD analysis is suggested that the GBA-Na form III and GBA-K form II are

stable in both media during the solubility studies. Whereas GBA-Na form I and GBA-K form II were transformed in to their corresponding hydrates (GBA-Na form III and GBA-K form II) in both water or phosphate buffer media. Also GBA-NH₄ salt was dissociated to give GBA in both media. To summarize the solubility by making the salts, we have achieved the solubility enhancement of GBA which is essential for the better formulations.

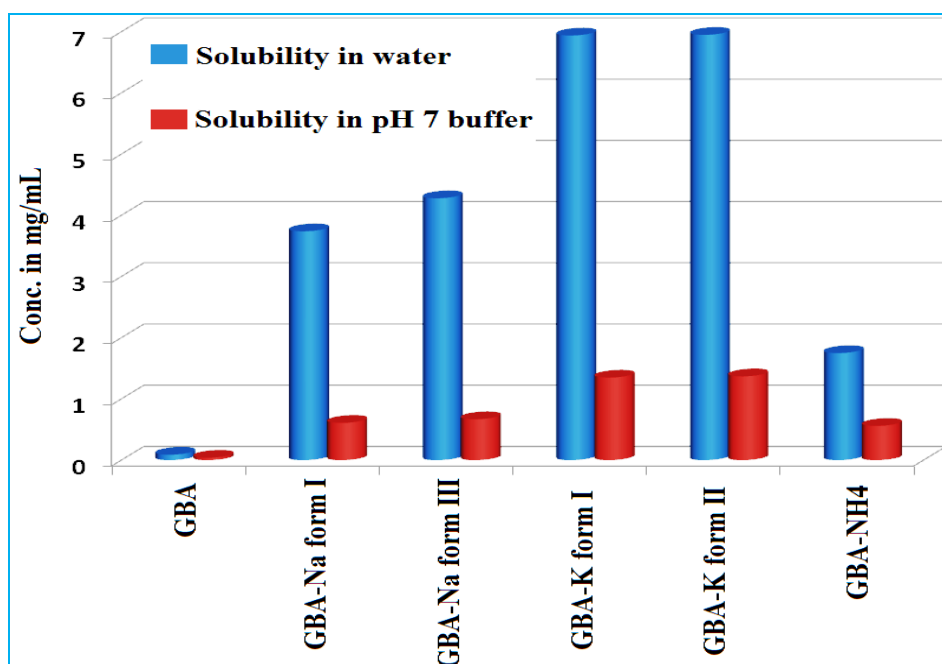


Figure 4.18: Solubility concentrations of GBA salts in water and pH7 buffer

Table 4.7: solubility concentrations of salts were listed below.

S.No	Compound	Solubility in water (mg/mL)	Solubility in pH7 buffer (mg/mL)
1	GBA	0.09	0.04
2	GBA-Na form I	3.74(x41.5)	0.61 (x15.2)
3	GBA-Na form III	4.28(x47.5)	0.67 (x 16.7)
4	GBA-K form I	6.94(x77.1)	1.35 (x33.7)
5	GBA-K form II	6.95(x77.2)	1.37 (x34.2)
6	GBA-NH4	1.75(x19.4)	0.56 (x14.0)

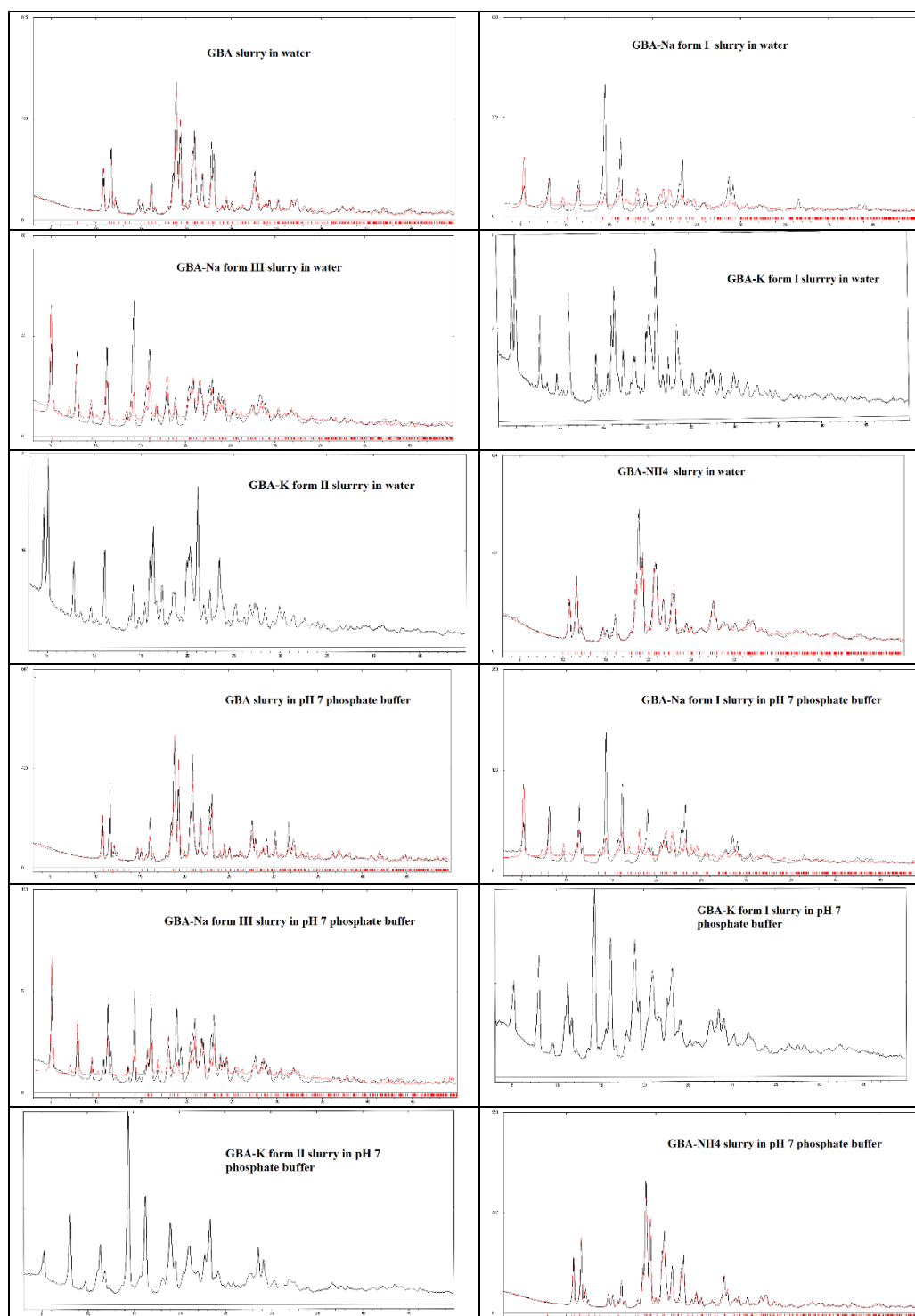
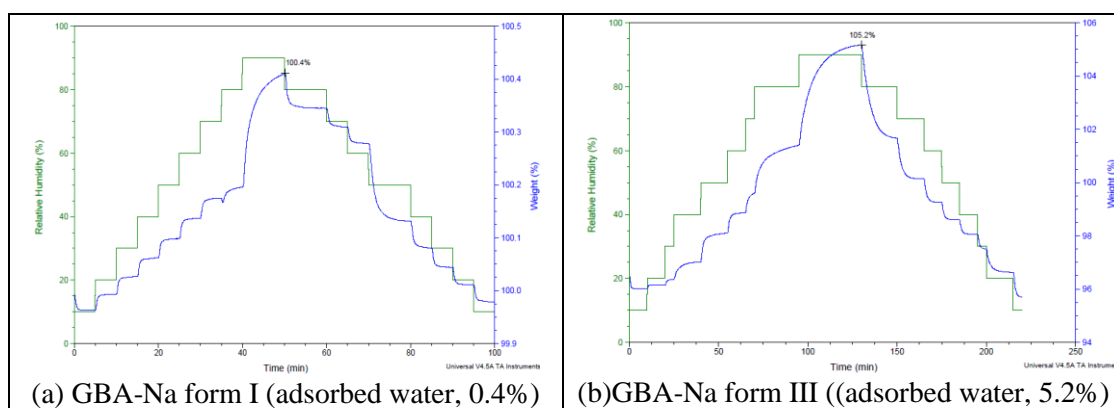


Figure 4.19 PXRD plots of GBA and its salt forms at the end of equilibrium solubility experiment in pH 7 phosphate buffer and water media.

4.3.9 Stability study by Dynamic Vapor Sorption (DVS) Analysis

DVS is a method to measure the kinetics of water adsorption and desorption. It quantifies “how quickly” and “how much” of water is absorbed by the sample.^{40,41} It also gives the information about phase stability/transformations in the presence of high/low humidity range at a particular temperature. The vapor studies on GBA-Na form I and III showed gradual adsorption of water to 0.4% for form I and 5.2% for form III respectively at 90% of RH and upon desorption the materials showed water weight loss. On the other side GBA-K form I and II showed water gain of 6.2 % for form I and 4.9% for form II at 90% RH and upon desorption the materials were releases the adsorbed water. At the same time there is no significant water gain/loss were observed in GBA-NH₄. All of these DVS plots were depicted in Figure 4.20.

Throughout these experiments, all salt forms (except GBA-K form II) are found to be stable confirmed by PXRD. It is a good case study of simple water sorption rather than lattice absorption. Adsorption-desorption cycles of all forms were reversible without having any hysteresis. Though there is an interesting observation in the GBA-K form II, it underwent into transition, from form II to form I (II → I). The dehydration suggests that the bounded water molecule in form II may be loosely bonded to this complex (Figure 4.21). This water loss was also identified in DSC where it starts from 37 °C to 85 °C.



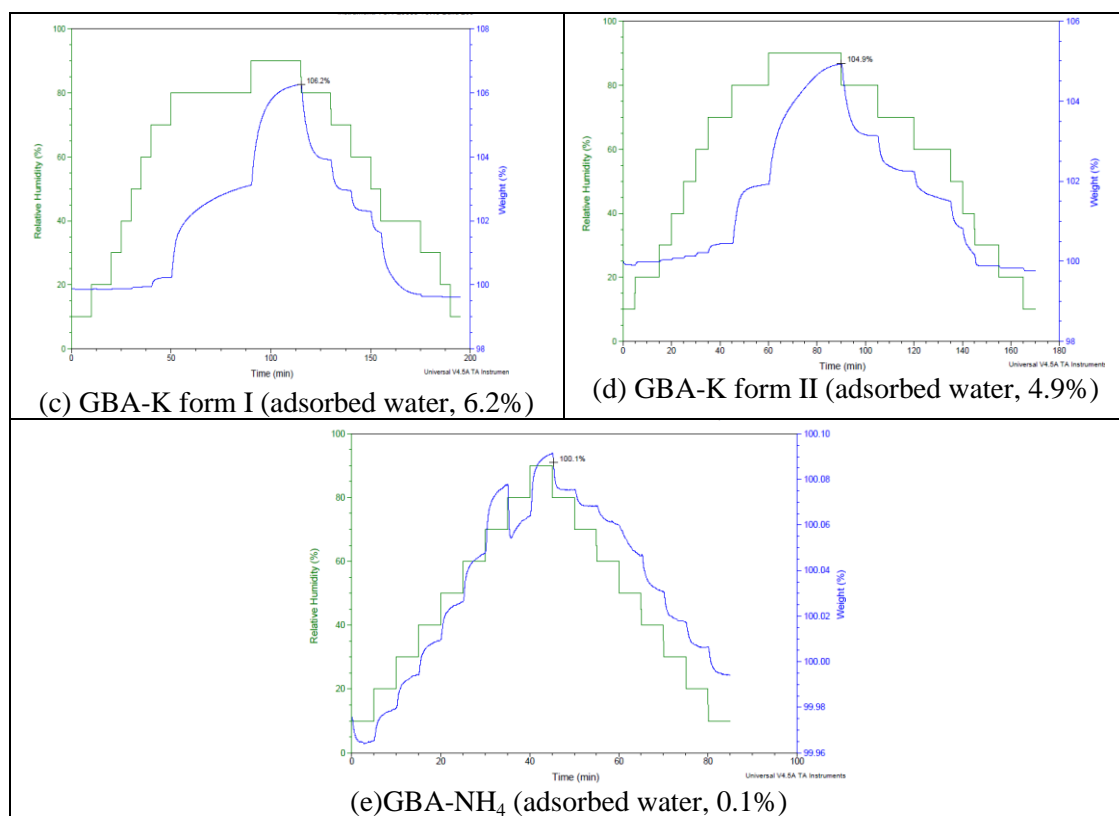
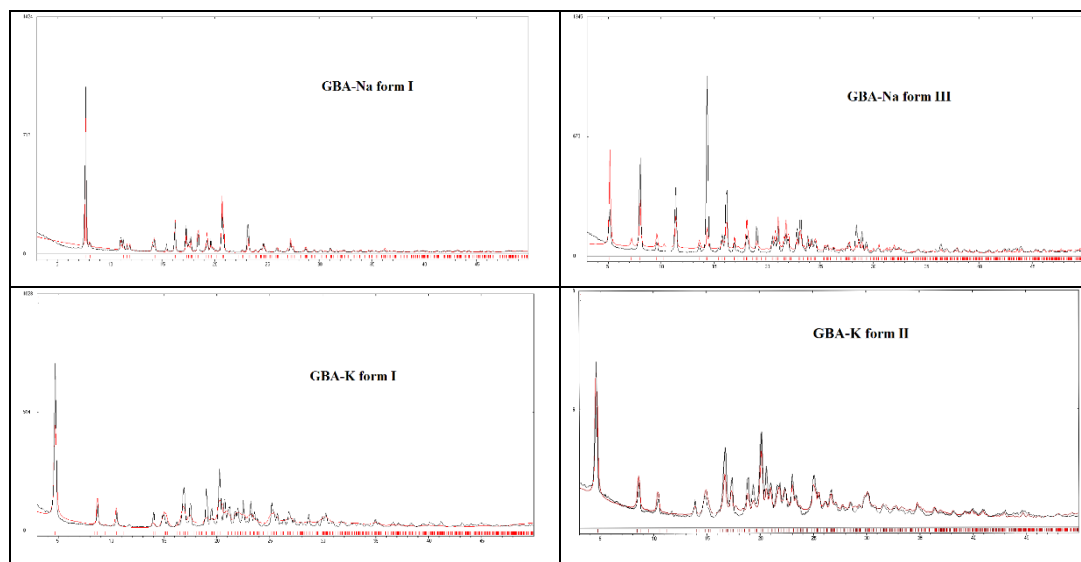


Figure 4.20: DVS plots of GBA-Na and GBA-K forms.



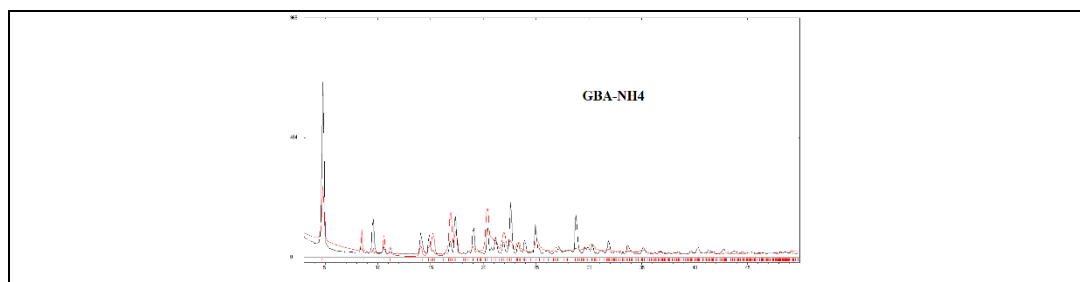


Figure 4.21 PXRD plots of GBA salt forms recorded at the end of DVS analysis.

4.4 Conclusions

We have synthesized novel GBA salts and corresponding hydrates using NaOH, KOH and NH_3 . We found that the GBA-Na salt exists in dimorphic and one hydrate (form I, II and III) and GBA-K exists as an anhydrate and hydrate (form I and II). All these new solid forms (except GBA-Na form II) were characterized by various spectroscopic, thermal and diffraction techniques. As well as crystal structures were established by SXRD except GBA-K form II. Crystal structures of GBA-Na forms, GBA-Na form I shown a square pyramidal geometry and GBA-form II and III were showed distorted octahedral geometry and all these forms different in packing arrangements. We also identified that, GBA-Na form I & GBA- NH_4 and GBA-K form I and GBA- NH_4 were isostructural pairs which are having packing and powder XRD similarities by interchanged of simple NH_4^+ ion present in GBA- NH_4 with Na^+ ion in the GBA-Na form II/ K^+ ion in the GBA-K form I. Solubility studies shown that all the obtained GBA salts were having a very good solubility in water and pH 7 buffer media. Moreover, all these forms were absorbed significant amount of water (0.4 to 6.2% range for all salts) during adsorption and at the same time loses the adsorbed water during desorption cycle. It indicates the all these solid forms were reversible without any hysteresis. To summarize the solubility and stability, significant increases in the solubility with stability of GBA-K form I or II optimum solid for pharmaceutical development.

4.5 Experimental Section

GBA (purity >99.8%) was purchased from Yarrow Chem Products (Mumbai, India) and salts formers were purchased from Aldrich (Hyderabad, India). Solvents (purity >99%) were purchased from Hychem Laboratories (Hyderabad, India).

Preparation of salt

GBA-Na form I: 494mg (0.1mmol, >99.8% purity) of GBA and 39mg (0.1mmol, 97% purity) of NaOH were dissolved in 10ml of ethanol and this mixture was taken into a 25mL round bottom flask. It was stirred at room temperature for one hour and filtered. Material was dried and analyzed using PXRD, DSC and TGA. To get the single crystal, we have taken the 30mg of this material and was dissolved in 5 mL ethanol and left for slow evaporation at room temperature. Good quality single crystals were harvested for SCXRD analysis in 4-5 days.

GBA-Na form II: 15 mg of NaOH was dissolved in 6 ml methanol-ammonia mixture (5:1 ratio) volume and 20mg of GBA was added in 25ml conical flask upon gentle heating. The resulting solution was kept for slow evaporation under ambient conditions. Suitable single crystals obtained for SCXRD after 7 days.

GBA-Na form III: 494mg (0.1mmol, >99.8% purity) of GBA added to 41mg (0.1mmol, 97% purity) of NaOH in 10ml of water and this was taken into a 25mL round bottom flask. This mixture was stirred for one hour at room temperature and filtered. The formation of salt was confirmed by PXRD, DSC and TGA. 30 mg of this material was dissolved in 5 mL methanol and left for slow evaporation at ambient conditions. Suitable single crystals were obtained for SCXRD after 4-5 days.

GBA-K form I: 494mg (0.1mmol, >99.8% purity) of GBA and 65mg (0.1mmol 85%purity) of KOH in 10ml of ethanol taken into a 25mL round bottom flask. The mixture was stirred for one hour at room temperature and filtered. The formation of salt was confirmed by PXRD, DSC and TGA. 30 mg of this material was dissolved in 5 mL methanol and left for slow evaporation at ambient conditions. Good quality single crystals were obtained to get the SCXRD after 4-5 days.

GBA-K form II: 494mg (0.1mmol, >99.8% purity) of GBA and 65mg (0.1mmol 85%purity) of KOH in 10ml of water and was taken into a 25mL round bottom flask. The mixture was stirred for one hour at room temperature and filtered. The formation of salt was confirmed by PXRD, DSC and TGA.

Powder X-ray diffraction

Powder X-ray diffraction was recorded on Bruker D8 Advance diffractometer (Bruker-AXS, Karlsruhe, Germany) using Cu-K α X-radiation ($\lambda = 1.5406 \text{ \AA}$) at 40 kV and 30 mA power. X-ray diffraction patterns were collected over the 2θ range $3\text{--}50^\circ$ at a scan rate of $3.9^\circ/\text{min}$. Powder Cell 2.4⁴² (Federal Institute of Materials Research and Testing, Berlin, Germany) was used for Rietveld refinement of experimental PXRD and calculated lines from the X-ray crystal structure.

Vibrational spectroscopy

Thermo-Nicolet 6700 FT-IR-NIR spectrometer with NXR FT-Raman module (Thermo Scientific, Waltham, MA) was used to record IR spectra. IR spectra were recorded on samples dispersed in KBr pellets. Data were analyzed using the Omnic software (Thermo Scientific, Waltham, MA).

Thermal analysis

DSC was performed on a Mettler Toledo DSC 822e module and TGA on a Mettler Toledo TGA/SDTA 851e module. The typical sample size is 3-5 mg for DSC and 5-12 mg for TGA. Samples were placed in sealed pin-pricked aluminum pans for DSC experiments and alumina pans for TGA experiments. A heating rate of $10 \text{ }^\circ\text{C min}^{-1}$ in the temperature range $30\text{--}300 \text{ }^\circ\text{C}$ was applied. Samples were purged by a stream of dry nitrogen flowing at 80 mL min^{-1} for DSC and 50 mL min^{-1} for TGA.

X-ray crystallography

X-ray reflections were collected on Oxford CCD X-ray diffractometer (Yarnton, Oxford, UK) equipped with Mo-K α radiation ($\lambda = 0.71073 \text{ \AA}$) and Cu-K α X-radiation ($\lambda = 1.5406 \text{ \AA}$) source. Data reduction was performed using CrysAlisPro 171.33.55 software.⁴³ Crystal structures were solved and refined using Olex2-1.0 with anisotropic displacement parameters for non-H atoms.⁴⁴ Hydrogen atoms were experimentally located through the Fourier difference electron density maps in all crystal structures. All O–H and C–H atoms were geometrically fixed using HFIX command in SHELX-TL

program of Bruker-AXS. Crystal parameters (Table 1) and Hydrogen bond distances shown in Table 2 are neutron normalized to fix the D–H distance to its accurate neutron value in the X-ray crystal structures (O–H 0.983 Å, N–H 1.009 Å, and C–H 1.083 Å). X-Seed^{45,46} was used to prepare packing diagrams.

Solubility measurements

Solubility of GBA and its five salts in purified (HPLC grade) water and pH 7 phosphate buffer medium was determined by using equilibrium solubility method. The known concentrations were prepared in 1mL methanol in to 25mL volumetric flask to dissolve the compound and after complete dissolution the flask was to the mark with water/ pH 7 phosphate buffer medium. First, the absorbance of a known concentration of the GBA and GBA salts was measured at the given λ_{max} (GBA 302nm) in purified water medium on Thermo Scientific Evolution 300 UV-vis spectrometer (Thermo Scientific, Waltham, MA). These absorbance values were plotted against several known concentrations to prepare the concentration vs. intensity calibration curve. From the slope of the calibration curves, molar extinction coefficients for GBA and its salts were calculated. An excess amount of the sample (GBA/its salts) was added to 5 mL of purified water/ pH 7 phosphate buffer medium. The supersaturated solution was stirred at 800 rpm using a magnetic stirrer at 30 °C. After 24 h, the suspension was filtered through Whatmann 0.45µm syringe filter. Remaining residue of GBA and its salts were characterized by PXRD.

Dynamic Vapor Sorption (DVS) analysis

DVS measurements were performed using a Q5000SA vapor sorption analyzer (TA Instruments, Delaware, and USA) at 40 °C. About 5 mg of the sample was placed in a metallic quartz sample pan and subjected to relative humidity flux from 10 to 90% and back to 10% RH with a step size of 10% change in humidity. A dwell time of 60 min was set for a weight change of >0.1% in the adsorption/desorption phase at a particular RH (5 min dwell time for a weight change of <0.1%). Thus, if the weight loss/gain is >0.1% at a particular RH, the instrument maintains the same RH for 60 min and then automatically sets at the next higher/lower value. If the weight gain/loss is <0.1%, the DVS cycle (10–90–10%) will be completed within 2 hours, otherwise it will take a longer duration.

4.6 References

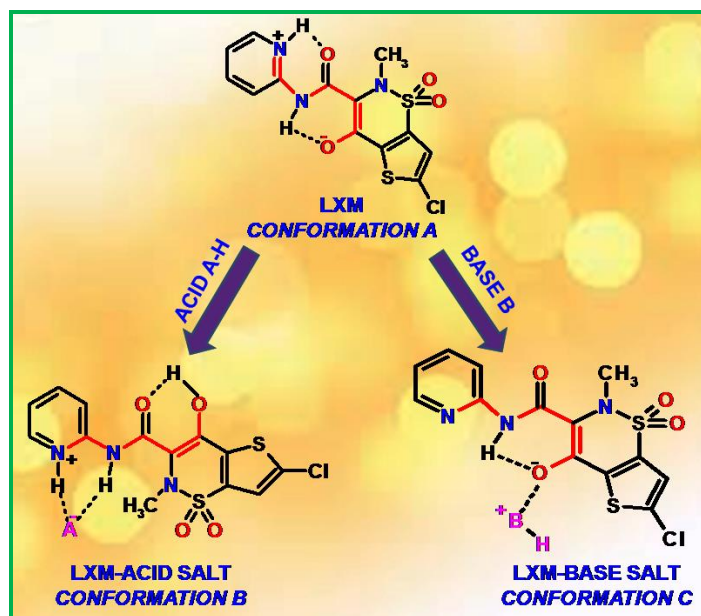
1. J. Bernstein, *Polymorphism in Molecular Crystals*; Clarendon, Oxford, U. K., 2002.
2. J. Halebian, W. McCrone, *J. Pharm. Sci.*, 1969, **58**, 911.
3. A. Nangia, *Acc. Chem. Res.* 2008, **41**, 595–604.
4. A. I. Kitaigorodskii, *Organic Chemical Crystallography*, Consultants Bureau, 1961, 222.
5. D. Cinčić, T. Frišćić and W. Jones, *Chem.–Eur. J.*, 2008, **14**, 747.
6. [H. G. Brittain](#), *Polymorphism in Pharmaceutical Solids, Second Edition*, 2009.
7. D. Singhal, W. Curatolo. *Adv. Drug. Deliv. Rev.* 2004, **56**, 335.
8. S. S. Kumar, S. Rana, A. Nangia. *Chem. Asian J.* 2013, **8**, 1551.
9. S. Mondal, G. Muges. *Angew. Chem. Int. Ed.* 2015, **54**, 10833.
10. C. Kulkarni, A. Kelly, J. Kendrick, T. Gough, A. Paradkar. *Cryst. Growth Des.* 2013, **13**, 5157.
11. M. K. Mishra, P. Sanphui, U. Ramamurty, G.R. Desiraju. *Cryst. Growth Des.* 2014, **14**, 3054.
12. M. K. Mishra, S. Varughese, U. Ramamurty, G. R. Desiraju, *J. Am. Chem. Soc.* 2013, **135**, 8121.
13. S. C. Sahoo, S. B. Sinha, M. S. R. N. Kiran, U. Ramamurty, A. F. Dericioglu, C. M. Reddy, P. Naumov, *J. Am. Chem. Soc.* 2013, **135**, 13843.
14. R. Hilfiker, *Polymorphism in the Pharmaceutical Industry*, Wiley: Weinheim, 2006.
15. T. N. Drebuschak, N.A. Pankrushina, A. N. Mikheev, M. K. A. Thumm, *CrystEngComm.* 2013, **15**, 3582.
16. K. Jun-Jie, L. Zheng-Ming, S. Hai-Bin, *Chin. J. Struct. Chem.* 2006, **25**, 1414.
17. E. Conterposito, G. Croce, L. Palin, C. Pagano, L. Perioli, D. Viterbo, E. Boccaleri, G. Paul, M. Milanese, *Phys.Chem.Chem.Phys.* 2013, **15**, 13418.
18. S. Mutalik, N. Udupa, *J. Pharm. Sci.*, 2004, **93**, 1577.
19. K. Hartke, *Ed. Comments to the European Pharmacopoeia*, 14th ed.; WVG mbH: Stuttgart, 2001.
20. J. A. Ganley, J. McEven, R. T. Calvert, C. J. Barker, *J. Pharm. Pharmacol.* 1984, **36**, 734.

21. W. Rupp, M. Badian, W. Heptner, V. Malerczyk. *Biopharm. Pharmacokinet., Eur. Congr.*, 2nd. 1984, **1**, 413.
22. J. Singh, *Drug. Dev. Ind. Pharm.* 1986, **12**, 851.
23. A. Mitrevej, N. Sinchaipanid, V. Junyaprasert, L. Warintornuwat. *Drug Dev. Ind. Pharm.* 1996, **22**, 1237.
24. M. K. Zaman, M. S. Arayne, N. sultana, A. Farooq. *Pak. J. Pharm. Sci.*, 2006, **19**, 114.
25. S. R. Byrn, A. T. McKenzie, M. M. A. Hassan, A. A. Al-Badr. *J. Pharm. Sci.*, 1986, **75**, 596.
26. S. M. Berge, L. D. Bighley, D. C. Monkhouse. *J. Pharm. Sci.* 1977, **66**, 1.
27. G. S. Paulekuhn, J. B. Dressman, C. Saal, *J. Med. Chem.*, 2007, **50**, 6665.
28. L. R. Chen, V. G. Y. Jr, D. Lechuga-Ballesteros, D. J. Grant, *J. Pharm. Sci.*, 1999, **88**, 1191.
29. R. Khankari, L. Chen, D. J. Grant, *J. Pharm. Sci.*, 1998, **87**, 1052.
30. G. C. Wermuth, P.H. Stahl. Eds. *Pharmaceutical Salts: A Hand Book*, Strasbourg and Freiburg, January 2002.
31. A. Kálmán, L. Párkányi, G. Argay. *Acta Crystallogr. Sect. B:* 1993, **49**, 1039.
32. T. Gelbrich, T. L. Threlfall, M. B. Hursthouse, *CrystEngComm*, 2012, **14**, 5454.
33. T. Gelbrich, M. B. Hursthouse, *CrystEngComm*, 2006, **8**, 448.
34. T. Gelbrich, M. B. Hursthouse, *CrystEngComm*, 2005, **7**, 324.
35. P. A. Wood, M.A. Oliveira, A. Zink, M. B. Hickey. *CrystEngComm*, 2012, **14**, 2413.
36. J. Van de Streek and W. D. S. Motherwell, *Acta Crystallogr., Sect. B: Struct. Sci.*, 2005, **61**, 504.
37. K. Suresh. A. Nangia. *Cryst. Growth Des.* 2014, **14**, 2945.
38. (a) S. Chakraborty, S. Ganguly, G.R. Desiraju, *CrystEngComm*, 2014, **16**, 4732.
(b) R. M. Silverstein, *Spectrometric Identification of Organic Compounds*, 6th Ed., John Wiley, New York, 2002.
39. (a) D. Martins, M. Sanselme, O. Houssin, V. Dupray, M. N. Petit, D. Pasquier, C. Diolez and G. Coquerel, *CrystEngComm*, 2012, **14**, 2507 (b) B. Samas, C. Seadeek, A. M. Campeta and B. P. Chekal, *J. Pharm. Sci.*, 2011, **100**, 186 (c) B. Nicolaï, P. Espeau, R. Céolin, M. -A. Perrin, L. Zaske, J. Giovannini and F. Leveiller, *J. Ther. Anal. Cal.*, 2007, **90**, 337

40. U. B. R. Khandavilli, S. Gangavaram, N. R. Goud, S. Cherukuvada, S. Raghavender, A. Nangia, S. G. Manjulatha, S. Nambiar, S. Pal. *CrystEngComm*, 2014, **16**, 4842.
41. W. Ong, E. Y. Cheung, K. A. Schultz, C. Smith, J. Bourassa, M. B. Hickey *CrystEngComm*, 2012, **14**, 2428.
42. Powder Cell, a program for structure visualization, powder pattern calculation and profile fitting. Accessed at www.ccp14.ac.uk/tutorial/powdercell.
43. CrysAlis CCD and CrysAlis RED, Versions 1.171.33.55, Oxford Diffraction, Oxford, **2008**.
44. O.V. Dolomanov, L.J. Bourhis, R.J. Gildea, J.A.K. Howard, H. Puschmann, *J. Appl. Crystallogr.* 2009, **42**, 339.
45. L. J. Barbour. *Supramol. Chem.* 2001, **1**, 189.
46. L. J. Barbour. X-Seed, Graphical Interface to SHELX-97 and POV-Ray; University of Missouri-Columbia, Columbus, MO, 1999.

CHAPTER FIVE

Lornoxicom Salts: Crystal Structures, Conformations, and Solubility



Crystal structures of Lornoxicom salts exhibit conformational changes depending on hydrogen bonding and counter ion. Both acidic and basic salt formers may be used with an amphoteric drug molecule. Improved solubility and stability were noted for the methane sulfonate salt.

5.1 Introduction

Salt formation¹ is the traditional and first line approach for solid form development in pharmaceuticals and it provides the modification and optimization of the physicochemical properties of Active Pharmaceutical Ingredients (APIs). Properties such as solubility, dissolution rate, hygroscopicity, physical or chemical stability and crystal habit can be affected by using pharmaceutically acceptable counter ions or salt formers.² Even polymorphism of an API issue can also be addressed in many cases by formation of salts. Owing to these advantages currently 50% of the marketed drugs are administered as salt form either an intravenous or oral route.³ Chemical modification of a 'pharmaceutical salt' is refer to as a newly engineered ionized form construct by fusing two molecules, reaction involving proton transfer or neutralization between an API which is either weakly acidic or basic and a corresponding basic or an acidic counter ion molecule. Typically counter ion molecules or salt formers are small inorganic molecules (e.g., sodium, potassium, calcium, and magnesium and other hydrochloride, and phosphate ions) or small organic molecules (e.g., succinate, fumarate, maleate, tartarate, oxalate citrate from di or tri carboxylic acids and other strong ions such as mesylate).^{1c,4} The selection of counter ion from GRAS list substances,⁵ must be rationally designed during drug discovery and development for the optimum salt form with desirable physicochemical properties. Specifically the solubility enhancement of pharmaceutical salt adjusts the pH of micro environment during drug dissolution and it could be vary for each counter ion. Therefore counter ions play significant role in adjusting the pH to increase the solubility and dissolution rate. Conventionally the solubility of salts at various pH conditions, varies dramatically enhancement about 100-2000 folds.⁶

For example in 1976 Higuchi et. al⁷ reported the hydrochloride salt of a weakly basic anti-malarial agent α -(2-piperidyl)-3,6-bis(trifluoromethyl)-9-phenanthrenemethanol has two folds higher solubility than free base. When organic salts of same drug were synthesized and found that lactate salt shown approximately 200 folds higher solubility than hydrochloride salt. Additional reports, Nangia et. al. improved the solubility olanzapine, antipsychotic drug by forming mono and dimaleate salts with maleic acid cofomer^{6a} and also from same group enhanced the solubility of aceclofenac (NSAID) drug by forming salts with lysine, cytosine, piperazine counter ion molecules.⁸ Likewise several examples were reported where different counter ion molecules altered the

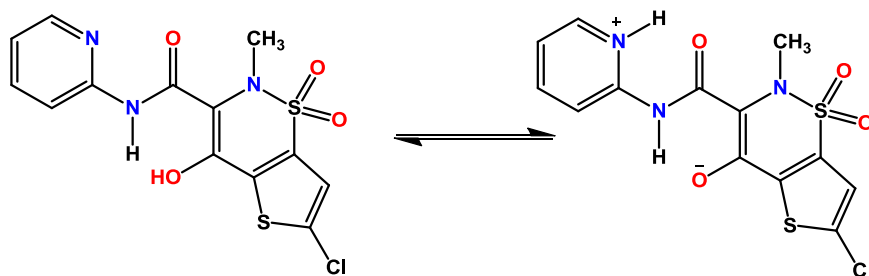
solubility and dissolution rate at varying levels.^{9,1c,4} The differences in solubility was attributed to varying in the pK_a , melting point, and aqueous solubility of counter ions.^{1c,10} These consequences indicate that, salt formation is a not straightforward pick and go exercise to select the counter for high aqueous solubility. Apart from high solubility, other properties such as high degree of crystallinity (it allows the purification and removal of unwanted impurities), chemical stability and less hygroscopicity (at stored or under accelerated ICH conditions) are also required in the salt form of drug for the efficacy. Hence it is an essential task to select the counter ion molecule and more holistically to strike an acceptable balance between solubility and stability. Whilst for the most part, salification¹⁰ (the process of crystallizing a salt of a given substance) improves both chemical and physical properties of an API, there are a few negative aspects associated with this process. The first of these relates to the developing that it is not feasible to prepare the stable salt form for some kind of drugs.^{10b} Furthermore salt may have certain undesirable properties specifically hygroscopicity compared to the parent API.^{10c-h} With this background in this chapter, we highlight solubility, stability of counter ion effect in lornoxicam salts.

Usually the formation of salt or cocrystal between acid and base substances depends on the ΔpK_a of the API and coformer. According to “ ΔpK_a rule” or “rule of three”¹¹ salt formation generally requires a difference of at least three pK_a between conjugate base and acid, i.e. $\Delta pK_a > 3$ results in a salt and if $\Delta pK_a < 0$ then it would result in a cocrystal and if intermediate ΔpK_a range of $0 < \Delta pK_a < 3$ is may result cocrystal-salt continuum. However recently these ΔpK_a values were revised using crystallographic data from the Cambridge Structural Database (CSD) and calculated pK_a in Marvin¹² for over 6000 acid- base adducts to $\Delta pK_a < -1$ for cocrystals, $\Delta pK_a -1$ to 4 for cocrystal/salt, and $\Delta pK_a > 4$ for salts.¹³

5.2 Lornoxicam - Literature Reports

The oxycam (weakly acidic character molecules) family are a class of closely related chemical substances of non-steroidal anti-inflammatory drugs (NSAIDs) associated with analgesic, anti-inflammatory, and antipyretic activities.¹⁴ They are used to treat acute and inflammation by inhibiting the activity of the two cyclooxygenase (COX-1 and COX-2 isoforms) enzymes. Among all oxycam APIs, meloxicam, piroxicam, tenoxicam solid

state structure structural behavior of neutral or zwitterion forms and polymorphism is well studied by using single crystal X-ray diffraction technique.¹⁵ Cocrystals and salts and their property studies such as solubility, stability are also explored.¹⁶ A Cambridge Structural Database search of lornoxicam (LXM) gave no single crystal structure, polymorphs, solvates/hydrates, or cocrystals/salts. It is an amphoteric molecule containing both acidic (β -keto-enol) and basic (pyridine) groups hence there is a possibility to exist in either neutral or zwitterion or dual states in solid state (Scheme 5.1). Amino acids are popular examples of amphoteric molecules and they majorly exist in zwitterion nature in the solid state. Predominantly amphoteric molecules can undergo salt formation at lower (acidic) and higher (basic) pH range. LXM is a BCS class II category drug with low solubility and high permeability (solubility of LXM in water 15 mg/L).¹⁷ Cyclodextrin complexes^{18a} and solid dispersions^{18b} are reported to improve the solubility and bioavailability of LXM. Furthermore polymorphs¹⁷ and cocrystals¹⁹ and its enhanced solubility studies are also reported and characterized by using powder X-ray diffraction and thermal techniques. To improve the solubility and dissolution rate of BCS class-II APIs, having ionizable group, the foremost option is pharmaceutical salt formation.^{1,6a,8}

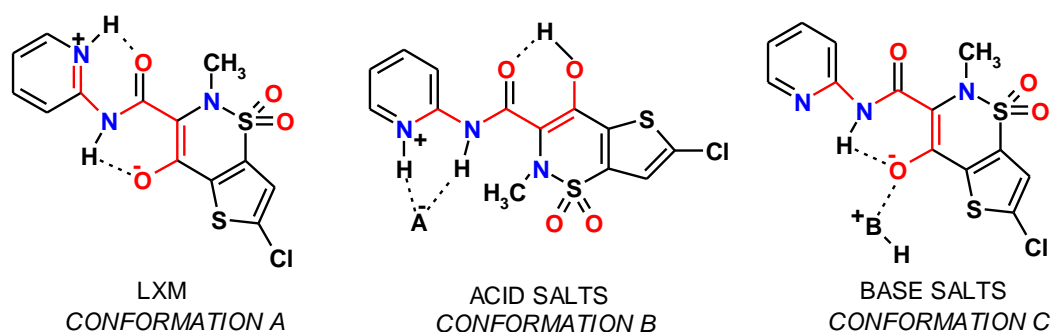


Scheme 5.1 Schematic representation of possible neutral and zwitterion forms of LXM.

5.3 Preparation of Lornoxicam salts

From the above background literature of LXM we planned a systematic study of the counter ion (acid and base salt formers) effect on conformational/structural modulation^{1,5,6a,8} in solid state and its solubility enhancement for better formulation. We selected two strong acids (hydrochloric acid, HCL and methane sulfonic acid MSA) and two strong bases (piperazine, PIP and ammonia, AMM) each and the high ΔpK_a values¹³ (Table 5.1) invariably resulted in salts of LXM by slurry technique. All these adducts were characterized by powder X-ray diffraction, DSC and FT-IR techniques. The powder

materials salt and guest free form were used as seeds in evaporative crystallization (see Experimental Section) to obtain single crystals for single crystal X-ray diffraction. The crystal structures were solved and refined. LXM adopts three conformations (designated as A, B, and C) in crystal structures (see Scheme 5.2).



Scheme 5.2 (a) Different conformations of LXM in salt structures. (Red in color bonds depicted the difference in conformations)

Table 5.1 Salt formers resulting in salts with Lornoxicam and their ΔpK_a values.

	pK_a in water	ΔpK_a	Molecular structure
LXM	1.82, 4.22	2.4	zwitterionic
HCL	-7.00	11.22	1:1 Salt
MSA	-1.61	5.83	1:1 Salt
PIP	9.72	7.9	1:0.5 Salt
AMM	8.86	7.04	1:1 Salt

pK_a 's were calculated using Marvin 5.10.1, 2012, ChemAxon (<http://www.chemaxon.com>)¹².

5.4 Results and Discussion

LXM is an amphiprotic molecule containing a β -keto-enol group on chlorothianothiazine ring, which is connected to a pyridyl ring through the imide group (Scheme 5.1). The LXM guest free structure we solved and refined orthorhombic space group $P2_12_12_1$ and it exists as a zwitterion with proton transfer from the β -keto-enolic OH group to the pyridine N but there is no hydrogen bonding between them as the groups are far apart (Figure 5.3). The competing N–H acceptor of the imide group cannot abstract the proton, though its pK_a is higher than the pyridine N (Table 5.1), because of the electron-withdrawing effect of the flanking C=O (of imide) and pyridyl groups.^{16,20} It forms an intramolecular hydrogen bond with the β -keto-enolate group ($N-H\cdots O^-$, 2.61 Å, 140°), which also eliminates repulsion between the adjacent imide NH, pyridyl NH^+ , imide

C=O and enolic C–O groups. These repelling groups point away from each other with an intramolecular H bond $N^+-H\cdots O$ (2.54 Å, 134°) (Figure 5.3). Therefore LXM adopts conformer A because of internal proton transfer and proximity of hydrogen bond donor-acceptor groups induces intramolecular hydrogen bond, which lock the molecular flexibility. Two intramolecular hydrogen bonds in the energetically favorable six-membered ring geometry (*S*(6) graph set pattern),²¹ and linear tapes of such LXM molecules extend in a sheet structure. In the crystal structure, linear tapes of LXM molecules formed by $C-H\cdots Cl$ interactions extend into a sheet structure through $N^+-H\cdots O=S$, $C-H\cdots O$ and $C-H\cdots S$ interactions.

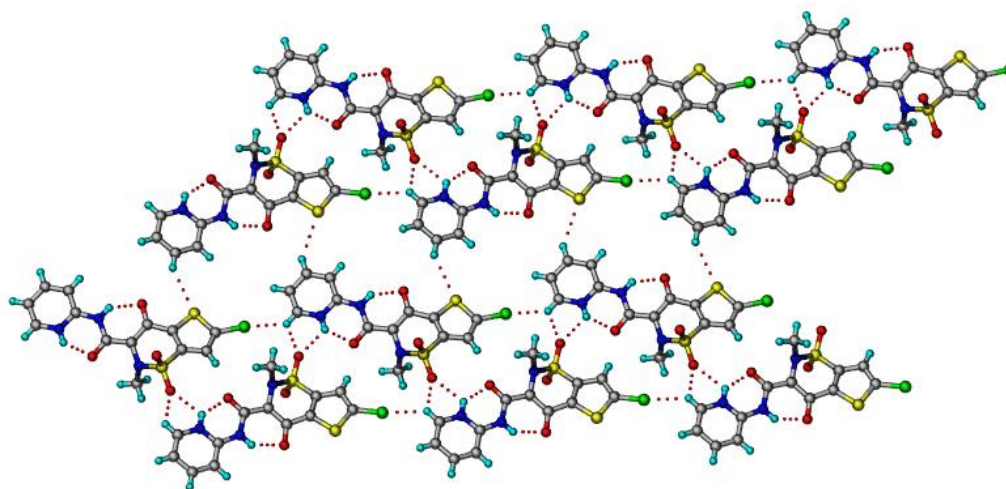


Figure 5.2 Layered section of lornoxicam molecules connected via $N^+-H\cdots O$, $N-H\cdots O^-$ H bonds and weaker $C-H\cdots Cl$, $C-H\cdots O$, $C-H\cdots S$ interactions.

5.4.1 Crystal structures of LXM Acid salts:

The crystal structures of HCL and MSA salts show that the β -keto-enolic proton is intact on the LXM molecule but the pyridyl group is protonated (Figures 5.4 & 5.5). The strong acids donate proton to the pyridyl group compared to the weaker β -keto-enol moiety. Understandably the imide NH cannot be protonated because of electronic and steric effects. In this situation, the H–H repulsion between imide N–H and β -keto-enolic proton and the energetic advantage of intramolecular *S*(6) H-bond in the β -keto-enol group invokes conformational change in LXM molecule. In effect, the imide bond rotates such that imide keto group makes an intramolecular hydrogen bond with unionized β -keto-enol through $O3-H3A\cdots O4$ (2.52 Å, 135°) with *S*(6) $O\cdots H\cdots O$ ring motif and imide NH makes hydrogen bond with the anion (chloride or mesylate). Both the intramolecular $N/N^+-H\cdots O^-/O$ bonds of conformer A in the guest-free structure of

LXM are replaced by a new intramolecular β -keto-enol $O\cdots H\cdots O$ hydrogen bond in the acid salts. The imide NH and pyridyl NH^+ , and imide $C=O$ and enolic OH groups become *syn*-oriented to each other (trans-orientation in conformer A), and form a new conformation B which is same in both salts (Figures 5.4 & 5.5).

Lornoxicamium hydrochloride (LXM-HCL, 1:1) salt: The salt was solved in the orthorhombic space group $P2_12_12_1$. The *syn*-oriented pyridinium NH^+ and imide NH form intermolecular H bonds with a chloride ion ($N1^+-H1\cdots Cl^-$ 2.14 Å, 166°; $N2-H2A\cdots Cl^-$ 2.45 Å, 148°) in a $R_2^1(6)$ motif. Such units are connected as linear tapes via $C-H\cdots Cl^-$ interactions which further extend in a layer through $Cl\cdots Cl^-$ interactions.

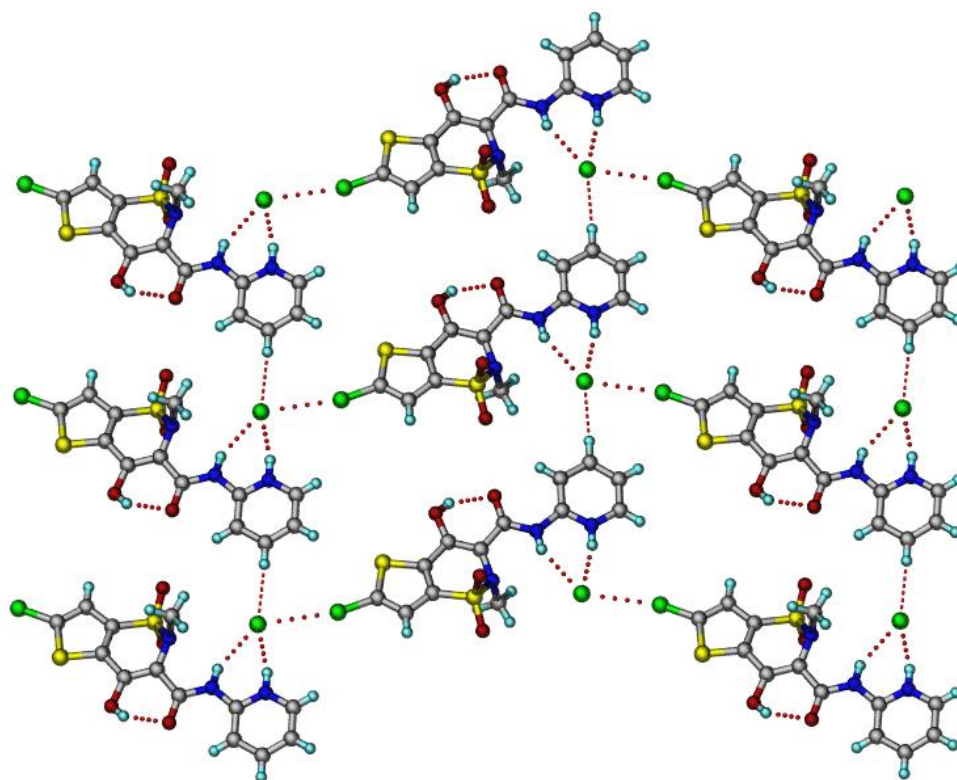


Figure 5.4 Linear tapes are connected via $C-H\cdots Cl^-$ interactions between the $R_2^1(6)$ ring motifs of pyridinium NH^+ and imide NH with a chloride ion and extend through $Cl\cdots Cl^-$ interactions in the structure of LXM-HCL salt.

Lornoxicamium mesylate (LXM-MSA, 1:1) salt: It was solved in the monoclinic space group $P2_1/c$. The *syn*-oriented pyridinium NH^+ and imide NH form intermolecular hydrogen bonds with sulfonate ion ($N1^+-H1\cdots O6^-S3$ 1.830 Å, 109.81°; $N2-H2A\cdots O7-S3$ 2.034 Å, 121.84°) in a $R_2^2(8)$ motif. Such motifs translate as linear tapes via $Cl_{(LXM)}\cdots O_{(MSA)}$ ($C12-Cl\cdots S3-O6$ 3.33 Å, 168.79°) interactions which propagate as

antiparallel tapes through β -keto-enol-sulfonyl ($\text{O3-H3A}\cdots\text{O2-S1}$ 2.213 Å, 123.36°) interactions. Crystal data are summarized in Table 2 and hydrogen bonds are listed in Table 3.

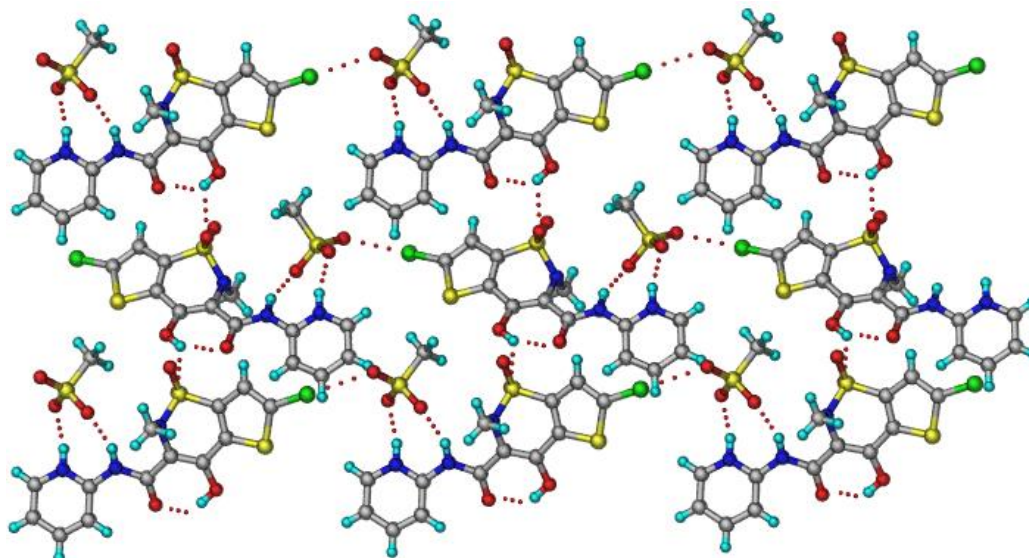


Figure 5.5 Linear tapes formed by $\text{Cl}\cdots\text{O}$ interactions between $R_2^2(8)$ motifs of pyridinium NH^+ and imide NH with mesylate ion propagate as antiparallel tapes in 2D through β -keto-enol-sulfonyl interactions.

5.4.2 Crystal structures of LXM Base salts

The crystal structures of PIP and AMM salts show that the β -keto-enol proton of LXM is transferred to the added base ((Figures 5.6 & 5.7) in competition to the internal pyridyl group which is weaker (see pK_a values in Table 5.1). As a result, the pyridyl group remains unionized; the intramolecular H-bond with the imide keto group of conformer A is absent. Moreover, the repulsion between the pyridine N and imide O atoms results in rotation of the pyridyl ring such that it forms a hydrogen bond with the NH^+ of piperazine or ammonium ion donor (Figures 5.6 & 5.7). This new LXM conformation C has a syn-oriented imide NH and pyridyl N (as in the acid salts) and *trans*-oriented imide $\text{C}=\text{O}$ and enol $\text{C}-\text{O}^-$, whereas the imide NH and enolate are involved in intramolecular hydrogen bonding. The effect of the counter-ions on the conformational changes of LXM is depicted in Scheme 5.2.

Piperazinium- lornoximate (LXM-PIP, 1:0.5) salt: It crystallized as a 1:0.5 salt consistent with the acid-base donor-acceptor ratio. One LXM and half PIP are present in

the asymmetric unit of a monoclinic $P2_1/c$ crystal structure. The PIP dication lies about an inversion centre (protons abstracted each from two lornoxicam molecules) and bridges the molecules through $N^+-H\cdots O^-$ hydrogen bonds (1.75 Å, 167°). Additional $C-H\cdots N$ interaction between the CHs of piperazinium ion and LXM pyridine together with heteroatom $O\cdots Cl$ interactions strengthen the structure.

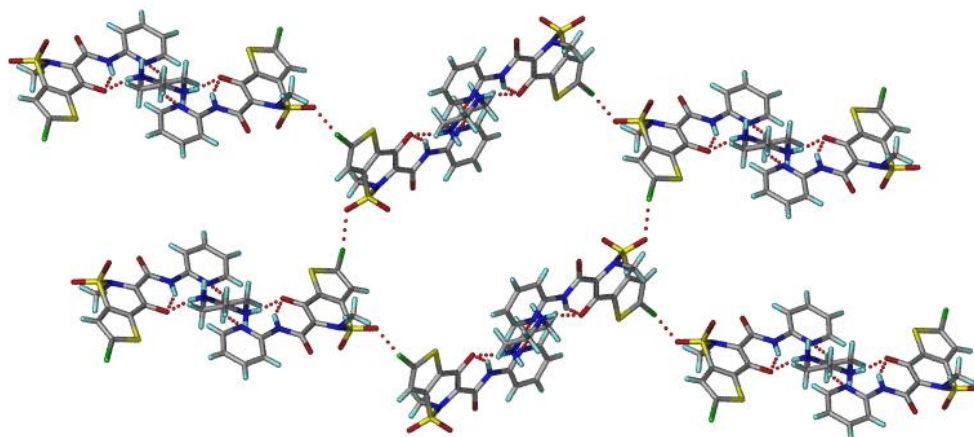


Figure 5.6 LXM –PIP molecules connected through $N^+-H\cdots O^-$ and $C-H\cdots N$ interactions and form inversion centre and linear tapes are formed by $O\cdots Cl$ interactions. ID tapes are propagate as antiparallel tapes in 2D via through $O\cdots Cl$ interactions.

Ammonium lornoxicamate (LXM-AMM, 1:1): It crystallized in $P\bar{1}$ space group with one lornoxicamate anion and ammonium cation each in asymmetric unit. The ammonium ion forms intermolecular ionic hydrogen bonds with enolate anion ($N4^+-H4A\cdots O3^-$ 2.19 Å, 143°; $N4^+-H4B\cdots O3^-$ 1.83 Å, 174°) and pyridine ($N4^+-H4D\cdots N1$ 2.05 Å, 158°) in a $R_4^2(8)$ motif. Such motifs are bonded via $R_3^2(8)$ ring motifs about the inversion center and extend through ammonium cation–sulfonyl interactions.

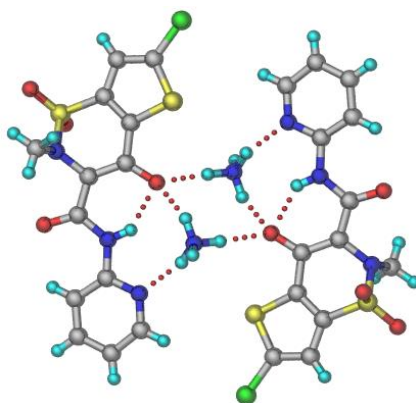


Figure 5.7 N–H···O hydrogen bond ring motifs in the crystal structure of LXM-AMM salt.

Table 5.2 Crystallographic parameters of LXM salts.

	LXM	LXM-HCL	LXM-MSA	LXM-PIP	LXM-AMM
Emp. form.	C ₁₃ H ₁₀ N ₃ O ₄ S ₂ Cl	C ₁₃ H ₁₁ N ₃ O ₄ S ₂ Cl ₂	C ₁₄ H ₁₄ N ₃ O ₇ S ₃ Cl	C ₁₅ H ₁₆ N ₄ O ₄ S ₂ Cl	C ₁₃ H ₁₃ N ₄ O ₄ S ₂ Cl
Form. wt.	371.81	408.29	467.94	414.90	388.86
Cryst. syst.	Orthorhombic	Orthorhombic	Monoclinic	Monoclinic	Triclinic
Sp. gr.	<i>P</i> 2 ₁ 2 ₁ 2 ₁	<i>P</i> 2 ₁ 2 ₁ 2 ₁	<i>P</i> 2 ₁ / <i>c</i>	<i>P</i> 2 ₁ / <i>c</i>	<i>P</i> $\bar{1}$
<i>T</i> (K)	298(2)	298(2)	298(2)	298(2)	298(2)
<i>a</i> (Å)	7.2020(4)	6.8795(5)	13.4730(11)	13.2445(9)	7.5577(7)
<i>b</i> (Å)	13.5420(8)	9.1606(8)	13.2684(8)	13.0698(7)	10.3747(9)
<i>c</i> (Å)	14.9987(7)	26.201(2)	11.2407(8)	11.6414(8)	12.0879(12)
α (°)	90	90	90	90	68.516(9)
β (°)	90	90	111.707(9)	111.547(8)	75.433(8)
γ (°)	90	90	90	90	70.585(8)
<i>Z</i>	4	4	4	4	2
<i>V</i> (Å ³)	1462.82(14)	1651.2(2)	1867.0(3)	1874.3(2)	822.65(15)
Rflns. collect	4334	4783	8057	7900	5347
Unique rflns.	2731	3204	3818	3832	3353
Obsd. rflns.	1976	1699	2030	2377	1908
Parameters	209	219	256	236	269
<i>R</i> ₁	0.0483	0.0707	0.0507	0.0406	0.0692
w <i>R</i> ₂	0.1031	0.1586	0.0828	0.0984	0.1513
GOF	0.960	0.980	0.907	0.905	0.972
Diffractometer	Oxford Xcalibur Gemini	Oxford Xcalibur Gemini	Oxford Xcalibur Gemini	Oxford Xcalibur Gemini	Oxford Xcalibur Gemini

Table 5.3 Hydrogen bonds in LXM salts (N–H, O–H, and C–H distances were neutron-normalized).

D–H...A	D...A (Å)	H...A (Å)	D–H...A (°)	symmetry code
LXM				
N1–H1...O4	2.545(4)	1.87	134	--- ^a
N1–H1...O1	3.008(5)	2.45	124	1/2–x, 1–y, –1/2+z
N2–H2A...O3	2.611(4)	1.89	140	--- ^a
C2–H2...O2	3.295(5)	2.51	142	1–x, –1/2+y, 1/2–z
C4–H4...O2	3.332(4)	2.39	123	–1/2+x, 1/2–y, –z
C5–H5...Cl	3.407(3)	2.67	137	x, y, –1+z
C11–H11...O4	3.227(5)	2.32	165	1/2–x, 1–y, –1/2+z
LXM–HCL				
N1–H1...Cl2	2.976(7)	2.13	166	–1/2+x, 1/2–y, –z
N2–H2A...Cl2	3.217(6)	2.46	148	x, y, z
N2–H2A...N3	2.785(8)	2.39	108	--- ^a
O3–H3A...O4	2.528(7)	1.88	135	--- ^a
C3–H3...Cl2	3.530(8)	2.60	177	x, 1+y, z
C5–H5...O1	3.265(10)	2.38	160	–1/2+x, 1/2–y, –z
LXM–MSA				
N1–H1...O5	2.673(4)	1.83	167	x, y, z
N2–H2A...O7	2.845(4)	2.03	157	x, y, z
N2–H2A...N3	2.727(3)	2.32	109	--- ^a
O3–H3A...O4	2.638(3)	1.95	142	--- ^a
O3–H3A...O2	2.819(4)	2.21	131	–x, –1/2+y, 1/2–z
C14–H14C...O6	3.384(5)	2.45	165	1–x, 1–y, 1–z
LXM–PIP				
N2–H2A...O3	2.649(2)	1.92	142	--- ^a
N4–H4A...O3	2.642(3)	1.76	168	x, 1/2–y, –1/2+z
N4–H4B...O4	2.730(2)	1.90	151	x, 1/2–y, –1/2+z
C2–H2...O4	2.914(3)	2.34	120	--- ^a
C15–H15A...O4	3.215(3)	2.53	128	1–x, –1/2+y, 1/2–z
LXM–AMM				
N2–H2A...O3	2.702(5)	2.06	144	--- ^a
N4–H4A...O1	3.020(6)	2.51	118	–1+x, y, z
N4–H4A...O3	2.945(7)	2.19	143	1–x, –y, 1–z
N4–H4B...O3	2.835(6)	1.83	174	–x, –y, 1–z
N4–H4C...O4	2.849(6)	1.99	162	–1+x, y, z
N4–H4D...N1	2.956(7)	2.05	158	x, y, z
C2–H2...O4	3.218(6)	2.58	133	2–x, 1–y, 1–z
C11–H11...O2	3.285(6)	2.37	155	3–x, –y, –z
C1–H13C...O4	3.213(7)	2.58	128	--- ^a

^a intramolecular hydrogen bond

5.4.3 Powder Analysis

Powder X-ray diffraction²² enables a rapid identification of new crystalline salts. PXRD of experimental and calculated (obtained from the X-ray crystal structure) patterns of the salts showed excellent superposition to confirm phase purity of the bulk samples (Figure 5.8).

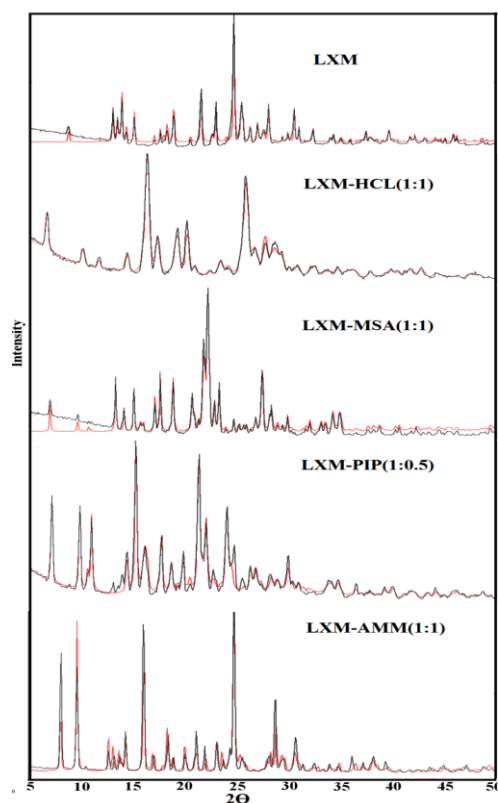


Figure 5.8 Overlay of experimental PXRD patterns of novel solid forms (black) showed good match with their calculated line profile from the X-ray crystal structure (red) indicating bulk purity and phase homogeneity.

5.4.4 FT-IR Spectroscopic Analysis

Infrared spectroscopy²³ provides information about vibrational modes in a molecule due to changes in molecular conformations and hydrogen bonding. LXM exhibits the amide carbonyl stretch at 1646 cm^{-1} , enolate peak at 1623 cm^{-1} and the pyridine $\text{N}^+\text{-H}$ stretch broad peak at 3444 cm^{-1} . These functional groups showed significant changes in their vibrational patterns on salt formation. In LXM-HCL and LXM-MSA the amide carbonyl stretching frequency is blue shifted to 1657 and 1666 cm^{-1} . The β -keto-enol frequency resonates at 1633 and 1631 cm^{-1} , and pyridine $\text{N}^+\text{-H}$ at 3447 and 3441 cm^{-1} .

(broad). In LXM-PIP and LXM-AMM the β -keto-enolate peak is at 1625 and 1612 cm^{-1} . PIP and AMM salts $\text{N}^+\text{-H}$ broad stretching vibration peak at 3414 and 3438 cm^{-1} . FT-IR spectra are displayed in Figure 5.9.

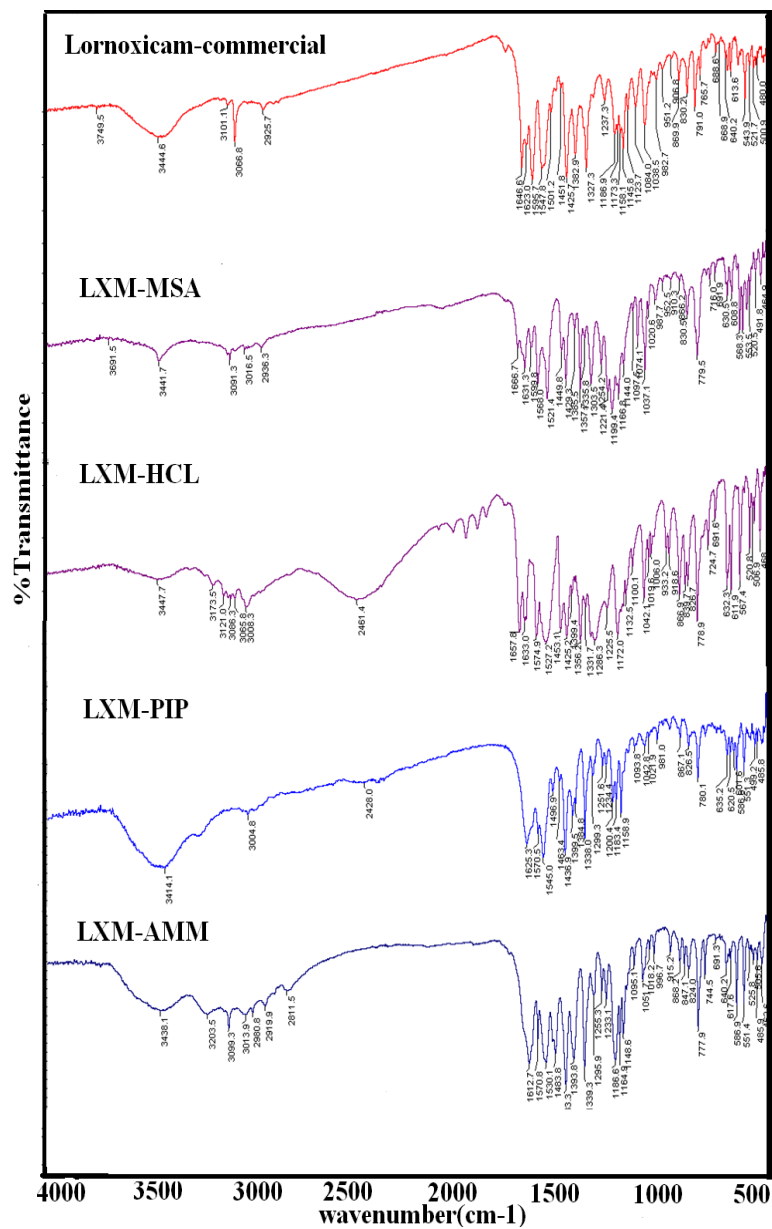


Figure 5.9 FT-IR spectra of LXM salts.

5.4.5 ss-NMR Spectroscopic Analysis

Solid state NMR spectroscopy²⁴ is informative about short range order in the solid-state and complements PXRD. We analyzed of all the compounds and we observed interesting changes in LXM salts ¹³C ss-NMR spectra. The LXM enol group which is deprotonated in the guest-free form and the base salts showed similar chemical shift values (δ LXM 107.8, LXM-PIP 111.47, LXM-AMM 109.13; Figure 5.10 Table 5.4), thus indicating that the chemical environment around the enolate group is similar in these structures (see Scheme 5.2 for conformers A and C which have a trans-oriented enol C–O[−] and imide C=O groups). In acid salts, the LXM enol proton makes an intramolecular H bond (conformer B, δ ~190 ppm) compared to enolic C–O[−] of guest-free LXM and base salts (δ ~109 ppm). The ss-NMR spectra not only characterized the salts but also correlated with the NMR peak positions.

Table 5.4 ss-NMR ¹³C chemical shifts (δ , ppm) of LXM salts.

Carbon No.	LXM	LXM-HCL	LXM-MSA	LXM-PIP	LXM-AMM
1	150.18	156.91	166.31	159.98	167.23
2	107.23	137.17	139.9	112.47	109.13
3	146.68	137.17	139.9	144.13	138.09
4	116.33	119.92	123.89	119.97	117.09
5	140.80	150.37	129.1	152.69	151.60
6	84.5	168.15	173.54	165.79	165.74
7	143.84	111.07	111.07	147.22	145.03
8	107.23	190.07	190.07	111.47	109.13
9	137.74	147.01	150.88	138.41	136.12
10	123.64	111.07	111.07	119.97	121.96
11	120.70	131.24	132.03	119.97	121.96
12	134.04	116.16	117.6	134.74	133.07
13	40.15	42.66	40.5	39.96	40.4
14	-	-	40.5	43.67	-
15	-	-	-	41.96	-

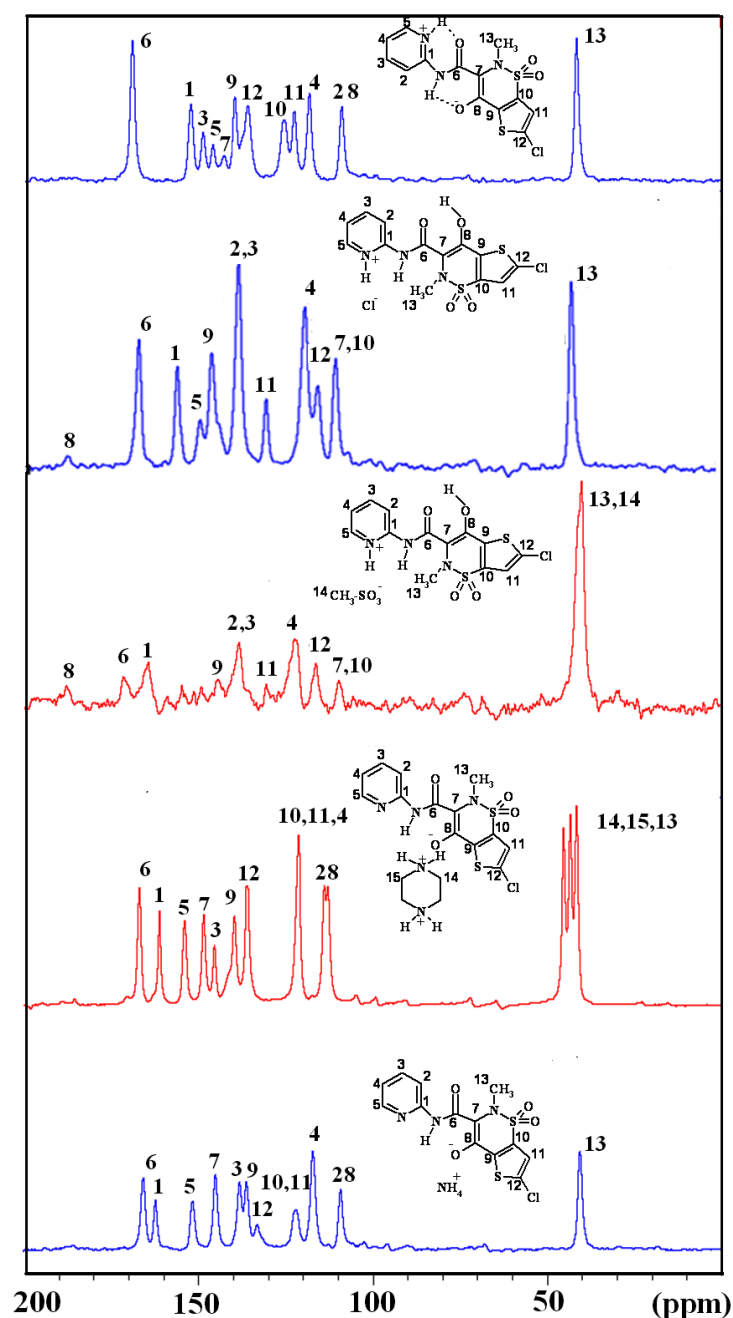


Figure 5.10 ss-NMR spectra of LXM and its salts (δ , ppm).

5.4.6 Thermal Analysis

Differential Scanning calorimetry (DSC)²⁵ is characteristic in establishing the purity of the component and phase changes upon heating. An exotherm peak in LXM at 210 °C (decomposition) as well as its salts (at slightly different temperatures) indicating decomposition of the drug.¹⁹ LXM-HCL, LXM-AMM exhibited a weak endotherm followed by the major exotherm peak (Figure 5.11, Table 5.5).

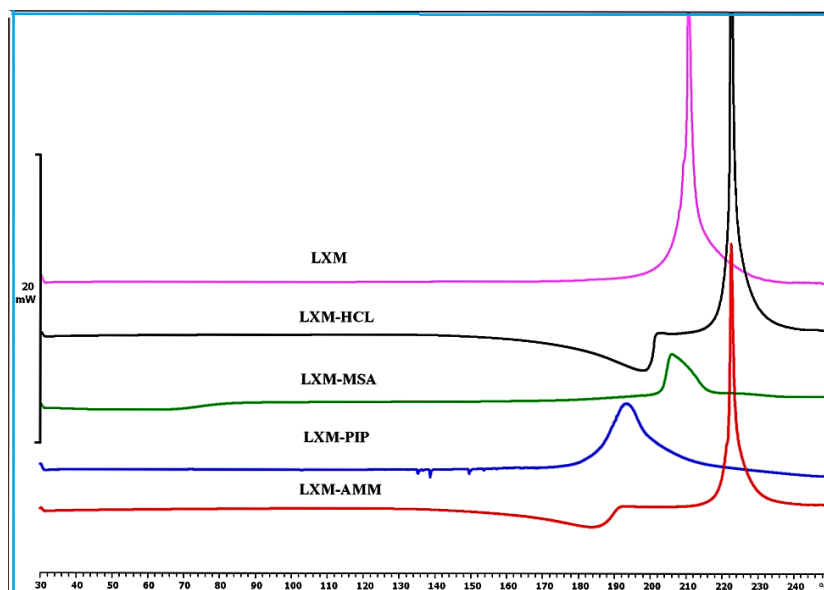


Figure 5.11 heating curves of LXM salts.

Table 5.5 Melting point and decomposition temperature of LXM salts from DSC

S. No.	Sample name	Melting point of salt	Decomposition of salt
1	LXM	-- ^a	210 °C
2	LXM-HCL	175 °C	221 °C
3	LXM-MSA	-- ^a	205 °C
4	LXM-PIP	-- ^a	193 °C
5	LXM-AMM	165 °C	221 °C

^a No endotherm observed

5.4.7 Solubility and Powder Dissolution

The bioavailability and efficacy of a drug largely depends upon its solubility and dissolution rate in the aqueous medium. Solubility and permeability of a drug molecule determine its mode of administration into the body. Modifying the physicochemical properties of a drug can change bioavailability²⁶ and therapeutic action. Solubility and powder dissolution of the new salts was performed in pH 7 phosphate buffer (neutral) medium. Solubility of LXM-HCL and LXM-MSA salts could not be determined as they dissociated to the parent LXM within 24 h. The stable LXM-PIP and LXM-AMM salts exhibited 7.0 and 2.3 times higher solubility than the parent drug. PXRD plots of the undissolved residue at the end of the equilibrium solubility experiment (Figure 5.13a-e) confirm that there is no phase transformation²⁷ or degradation of the base salts during the solubility experiment. Dissolution is a time dependent phenomenon which can estimate

the apparent solubility of compounds and hence this method is preferable for solids which undergo phase transformation during the solubility measurements (see stability PXRD in Figure 5.13f-j). Powder dissolution was carried out on all compounds and the PDRs at 60 min of peak solubility are LXM-MSA 158 mg/L > LXM-HCl 143 mg/L > LXM-AMM 133 mg/L > LXM-PIP 127 mg/L > LXM 100 mg/L. The equilibrium solubility of LXM and its base salts LXM-PIP are 2355 mg/L > LXM-AMM 879 mg/L > LXM 339 mg/L. In summary, the acid salts have higher apparent solubility/ PDR than the basic salts and overall the salts are superior to the reference drug (Figure 5.12, dissolution rates and AUC_{0-60min} are listed in Table 5.6). LXM and its basic salts did not show any form conversion, but the acidic salts converted to LXM after 90 min.

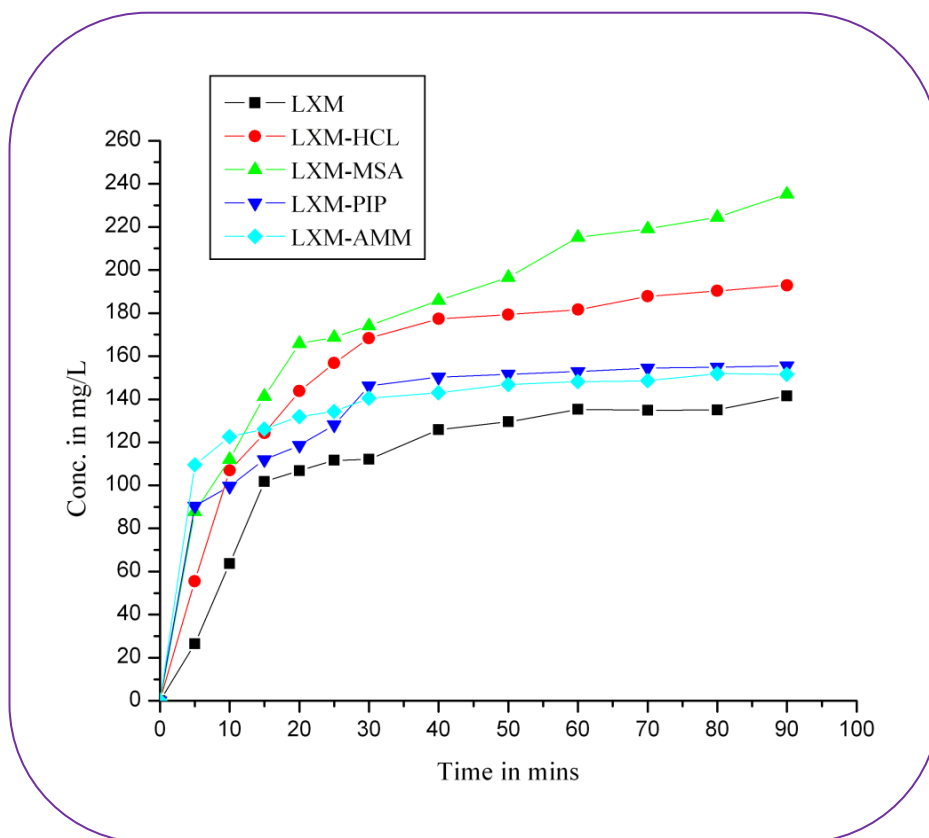
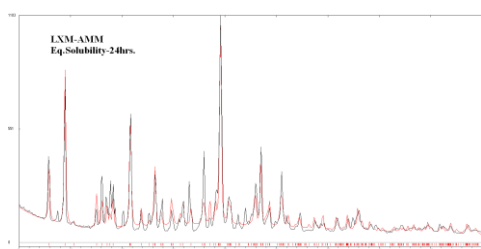


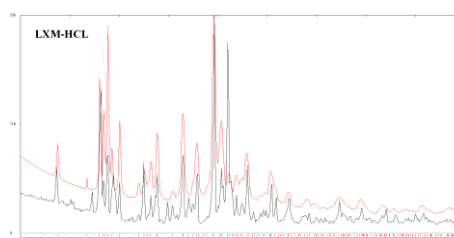
Figure 5.12 Powder dissolution rates of LXM and its salts in pH 7 phosphate buffer medium.

Table 5 Powder dissolution and solubility of LXM salts. The n-fold enhancement compared to LXM is given in parenthesis.

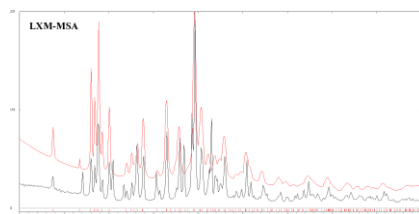
Compound	Molar extinction coefficient, ϵ /mM cm	Equilibrium Solubility (mg/L)	Solution concentration in mg/L (60 min)	Area under the curve, $AUC_{0-60\text{min}}$ (mg h)/L
LXM	17.28	339.0	100.9	105
LXM-HCL	15.96	--	143.7 (x1.43)	128 (x1.21)
LXM-MSA	13.08	--	158.9 (x1.57)	219 (x2.08)
LXM-PIP	16.12	2355.6 (x6.94)	127.1 (x1.26)	109 (x1.03)
LXM-AMM	15.41	879.8 (x2.59)	133.6 (x1.32)	109 (x1.03)



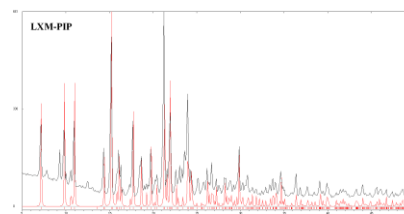
(a)



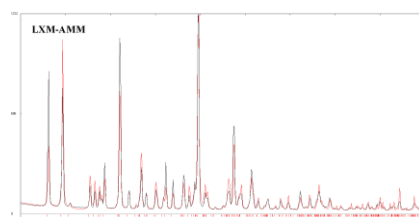
(b)



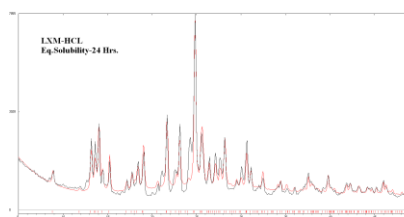
(c)



(d)



(e)



(f)

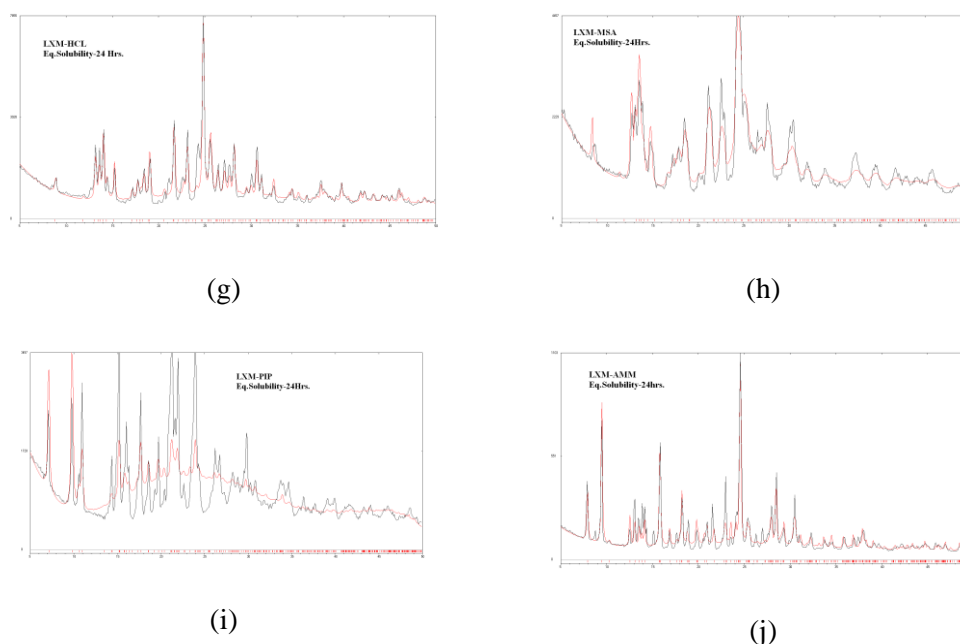


Figure 5.13: PXRD plots of LXM and its salts at the end of equilibrium solubility and IDR experiment in pH 7 buffer medium. All the solid forms were found to be stable in both experiments.

5.5 Conclusions

Lornoxicam (LXM), a non-steroidal anti-inflammatory drug (NSAID), is an amphiprotic molecule which exists as a zwitterion in the solid-state. The formation of two strong intramolecular $N^+-H\cdots O$ and $N-H\cdots O^-$ hydrogen bonds in a stable six-member ring geometry, $S(6)$, renders this otherwise flexible molecule in a rigid conformation (conformer A). A salt screen of LXM gave a better understanding on the effect of counter-ion on conformational changes in the drug molecule. Strong acids and bases changed the conformational flexibility by changes in intramolecular hydrogen bonding LXM to give conformations A, B and C. All the new salts exhibited good solubility and powder dissolution rate than the parent drug LXM. LXM salts with acids exhibited higher solubility than the base salts, e.g. LXM-MSA salt has two times higher AUC compared to PIP and AMM salts. However, the base salts are more stable than the acid salts, in line with the solubility–stability inverse correlation. This is a systematic study of conformational changes in a drug molecule due to counter-ion and partner molecules.

The present study with LXM salts offers acidic and basic counter ions for an amphoteric drug to improve its physicochemical properties.

5.6 Experimental Section:

Lornoxicam was purchased from Mesochem Import & Export Co. Ltd., China. Solvents (purity > 99%) and other coformers were purchased from Hychem Laboratories (Hyderabad, India) and Sigma-Aldrich (Hyderabad, India). Water filtered through a double deionizer purification system (Aqua DM, Bhanu, Hyderabad, India) was used for all experiments.

Preparation of LXM salts

LXM-HCL: To a solution of 250 mg of LXM in ethanol (5 mL), 2 mL conc. HCl (37%) solution was added and the slurry was ground up to 45 min. The solution was filtered through Whatman filter paper and salt formation (93% recovery) was confirmed by PXRD. 40 mg of the salt was dissolved in nitromethane (5 mL) and left for slow evaporation at room temperature. Single crystals were obtained after 4 days.

LXM-MSA: 372 mg of LXM and 96 mg of MSA (1:1 molar ratio) were dissolved in 5 mL of ethanol and the slurry was ground for 1 h. The solid was filtered and confirmed as the salt (96%) by PXRD. 40 mg of the salt was dissolved in EtOH-CH₃CN (3 mL + 2mL) solvent mixture and left for slow evaporation at room temperature. Single crystals were obtained after 4 days.

LXM-PIP: 372 mg of LXM and 43 mg of PIP (1:0.5 molar ratios) were dissolved in 5 mL ethanol and the slurry was ground for 1 h. The solid was filtered (95% recovery) and the material confirmed as the salt by PXRD. 40 mg of this salt was dissolved in nitromethane (5 mL) and left for slow evaporation at room temperature to harvest single crystals after 5 days.

LXM-AMM: To a solution of 250 mg of LXM in ethanol, 2 mL of conc. aqueous ammonia solution (25% conc.) was added and the slurry was ground for 45 min. The solution was filtered through Whatman filter paper and salt product (92%) formation was confirmed by PXRD. 40 mg of the salt was dissolved in ethyl methyl ketone (5mL) solvent mixture and left for slow evaporation at room temperature. Single crystals were obtained after 4 days.

X-ray crystallography

X-ray reflections were collected on Oxford CCD X-ray diffractometer (Yarnton, Oxford, UK) equipped with Mo-K α radiation ($\lambda = 0.71073 \text{ \AA}$) source. Data reduction was performed using CrysAlisPro 171.33.55 software.^{28a} Crystal structures were solved and refined using Olex2-1.0 with anisotropic displacement parameters for non-H atoms.^{28b} Hydrogen atoms were experimentally located through the Fourier difference electron density maps in all crystal structures. All O–H, N–H and C–H atoms were geometrically fixed using HFIX command in SHELX-TL program of Bruker-AXS. A check of the final CIF file using PLATON^{28a,b} did not show any missed symmetry. Hydrogen bond distances shown in Table 2 are neutron normalized to fix the D–H distance to its accurate neutron value in the X-ray crystal structures (O–H 0.983 \AA , N–H 1.009 \AA , and C–H 1.083 \AA). X-Seed^{28c,d} was used to prepare packing diagrams. Crystallographic .cif files (CCDC Nos. 986789–986793) are available at www.ccdc.cam.ac.uk/data or as part of the Supporting Information.

Powder X-ray diffraction

Powder X-ray diffraction was recorded on Bruker D8 Advance diffractometer (Bruker-AXS, Karlsruhe, Germany) using Cu-K α X-radiation ($\lambda = 1.5406 \text{ \AA}$) at 40 kV and 30 mA power. X-ray diffraction patterns were collected over the 2θ range $5\text{--}50^\circ$ at a scan rate of $5^\circ/\text{min}$.

Vibrational spectroscopy

Nicolet 6700 FT-IR spectrometer with a NXR FT-Raman Module was used to record IR spectra of samples dispersed in KBr pellets.

Solid-state NMR spectroscopy

Solid-state ^{13}C NMR spectra were recorded on Bruker Avance 400 MHz spectrometer (Bruker- Biospin, Karlsruhe, Germany). SS-NMR measurements were carried out on Bruker 4-mm double resonance CP-MAS probe in zirconia rotors with a Kel-F cap at 5.0-kHz spinning rate with a cross-polarization contact time of 2.5 ms and a delay of 8 s. ^{13}C NMR spectra were recorded at 100 MHz and referenced to the methylene carbon of glycine, and then recalibrated to the TMS scale ($\delta_{\text{glycine}} = 43.3 \text{ ppm}$)

Thermal Analysis

DSC was performed on a Mettler Toledo DSC 822e module. Samples were placed in crimped but vented aluminum sample pans. The typical sample size is 4-6 mg, temperature range was 30-250 °C @ 5 °C/min. Samples were purged by a stream of nitrogen flowing at 150 mL/min. HSM was performed on a PolythermA hot stage and Heitzsch microscope supplied by Wagner & Munz. A Moticam1000 (1.3 MP) camera supported by software Motic Image Plus 2.0ML was used to record crystal images.

Dissolution and solubility measurements

The solubility curves of LXM salts were measured using the Higuchi and Connor method²⁹ in pH7 phosphate buffer medium at 30 °C. First, the absorbance of a known concentration of the salt was measured at the given λ_{max} (LXM 374 nm) in pH7 phosphate buffer medium on Thermo Scientific Evolution 300 UV-vis spectrometer (Thermo Scientific, Waltham, MA). These absorbance values were plotted against several known concentrations to prepare the concentration vs. intensity calibration curve. From the slope of the calibration curves, molar extinction coefficients for LXM salts were calculated (The respective molar extinction coefficients (LXM 17.28, LXM-HCL 15.96, LXM-MSA 13.09, LXM-PIP16.12, and LXM-AMM 15.41 mL mg⁻¹ cm⁻¹ respectively are used to determine the powder dissolution). An excess amount of the sample was added to 6 mL of pH7 phosphate buffer medium. The supersaturated solution was stirred at 300 rpm using a magnetic stirrer at 30 °C. After 24 h, the suspension was filtered through Whatman 0.45 µm syringe filter. The filtered aliquots were diluted sufficiently, and the absorbance was measured at the given λ_{max} . The powder dissolution studies of LXM salts was done using LXM 300 mg, LXM-HCL 329 mg, LXM-MSA 377 mg, LXM-PIP 369 mg, and LXM-AMM 313 mg, (0.8 mmol of each compound) which was directly poured into 500 mL of pH 7 phosphate buffer dissolution medium. The paddle rotation was fixed at 100 rpm and dissolution experiments were continued up to 90 min at 37 °C. At regular intervals, 5 mL of the dissolution medium was withdrawn and replaced by an equal volume of fresh medium to maintain a constant volume. The AUC was calculated using the linear trapezoidal rule of drug solubility.³⁰ The nature of the solid samples after solubility/dissolution measurements was verified by PXRD to know if there is any phase transformation.

5.7 References

1. (a) S. M. Berge, L. D. Bighley, and D. C. Monkhouse, *J. Pharm. Sci.*, 1977, **66**, 1; (b) P. L. Gould, Salt selection for basic drugs. *Int. J. Pharm.*, 1986, **33**, 201; (c) G. C. Wermuth and P. H. Stahl. Eds.; *Pharmaceutical Salts: Properties, Seclection, and Use / Intrenational Union of Pure and Applied Chemistry (IUPAC)*,Strasbourg and Freiburg , 2002; (d) A. T. M. Serajuddin, *Adv. Drug Delivery Rev.*, 2007, **59**, 603; (e) B. Sarma, R. Thakuria, N. K. Nath and A. Nangia, *CrystEngComm*, 2011, **13**, 3232; (f) J. B. Nanubolu, B. Sridhar, K. Ravikumar and S. Cherukuvada, *CrystEngComm*, 2013, **15**, 4321; (g) W. Ong, E. Y. Cheung, K. A. Schultz, C. Smith, J. Bourassa and M. B. Hickey, *CrystEngComm*, 2012, **14**, 2428.
2. (a) J. Galcera and E. Molins, *Cryst. Growth Des.*, 2009, **9**, 327; (b) A. Portell, R. Barbas, M. Font-Bardia, P. Dalmases, R. Prohens and C. Puigjaner, *CrystEngComm*, 2009, **11**, 791; (c) M. L. Cheney, N. Shan, E. R. Healey, M. Hanna, L. Wojtas, M. J. Zaworotko, V. Sava, S. Song and J. R. Sanchez-Ramos, *Cryst. Growth Des.*, 2010, **10**, 395; (d) S. Li, S. M. Wong, S. Sethia, H. Almoazen, Y. M Joshi, and A. T. M Serajuddin, *Pharm. Res.* 2005, **22**, 628; (e) K. M. OConnor, and O. I. Corrigan, *Int. J. Pharm.* 2001, **222**, 281.
3. S. Sweetana and M. J. Akers, *J. Pharm. Sci. Tech.*, 1996, **50**, 330.
4. (a) G. S. Paulekuhn, J. B. Dressman and C. Saal, *J. Med. Chem.*, 2007, **50**, 6665; (b) P. L. Gould. . *Int. J. Pharm.*, 1986, **33**, 201.
5. GRAS chemicals list may be accessed at www.fda.gov/Food/FoodIngredientsPackaging/GenerallyRecognizedasSafeGRAS/GRASSubstancesSCOGSDatabase/default.htm (accessed 20 January 2014).
6. (a) R. Thakuria and A. Nangia, *CrystEngComm*, 2011, **13**, 1759; (b) R. Banargee, P.M. Bhatt, N. V. Ravindra, G. R. Desiraju, *Cryst. Growth. Des.*, 2005, **5**, 2299.
7. Agharkar, S.; Lindenbaum, S.; Higuchi, T. *J. Pharm. Sci.*, 1976, **65**, 747.
8. Goud, N. R.; Suresh, K.; Nangia, A. *Cryst. Growth Des.*, 2013, **13**, 1590.
9. (a) K. R. Morris, M. G. Fakes, A. B. Thakur, A. W. Newman, A. K. Singh, J. J. Venit, C. J. Spagnuolo, A. T. M. Serajuddin, *Int. J. Pharm.*, 1994, **105**, 209; (b) R. J. Bastin, M. J. Bowker, B. J. Slater, *Org. Process.Res. Dev.*, 2000, **4**, 435.

10. (a) Haleblan, J. K. *J. Pharm. Sci.*, 1975, **64**, 1269. (b) G. A. Stephenson, A. Aburub, T. A. Woods, *J. Pharm. Sci.*, 2011, **100**, 747. (c) P. L. Gould, *Int. J. Pharm.*, 1986, **33**, 201; (d) T. Vasconcelos, B. Sarmento and P. Costa, *Drug Disc. Today*, 2007, **12**, 1068; (e) S. Janssens, C. Roberts, E. F. Smith and G. V. Mooter, *Int. J. Pharm.*, 2008, **355**, 100; (f) A. Fahr and X. Liu, *Expert Opin. Drug Deliv.*, 2007, **4**, 403; (g) H. Bhutani, S. Singh, K. C. Jindal and A. K. Chakraborti, *J. Pharm. Biomed. Anal.*, 2005, **39**, 892; (h) S. Singh and B. Mohan, *Int. J. Tuberc. Lung Dis.*, 2003, **7**, 298.
11. (a) C. B. Akeroy, M. E. Fasulo, J. Desper, *Mol. Pharm.* 2007, **4**, 317; (b) S. L. Childs, G. P. Stahly, A. Park, *Mol. Pharm.* 2007, **4**, 323; (c) B. Sarma, N. K. Nath, B. R. Bhogala and A. Nangia *Cryst. Growth Des.*, 2007, **9**, 1607.
12. Marvin 5.10.1, 2012, ChemAxon (<http://www.chemaxon.com>).
13. A. J. Cruz-Cabeza, *CrystEngComm*, 2012, **14**, 6362.
14. (a) L. L. Brunton, J. S. Lazo, K. L. Parker, Eds., *Goodman & Gilman's: The Pharmacological Basis of Therapeutics*, 11th Ed., McGraw Hill Medical Publishing, New York, **2006**, 700; (b) E. Atzpadien, N. Mehdi, D. Clarke, *J. Food Anal. Chem. Toxicol.*, 1997, **35**, 465; (c) J. R. Vane, R. M. Botting, *Int. J. Tissue React.*, 1998, **20**, 3. (d) R. N. Rao, S. Meena, A. R. Rao, *J. Pharm. Biomed. Anal.* 2005, **39**, 349; (e) Vippagunta, S. R.; Brittain, H. G.; Grant, D. J. W. *Adv. Drug Del. Rev.* 2001, **48**, 3.
15. (a) F. Vrečer, M. Vrbinc, A. Meden, *Int. J. Pharm.* 2003, **256**, 3; (b) A. L. Lehninger, D. L. Nelson, M. M. Cox, *Principles of Biochemistry*, 2nd ed.; Worth Publishers; New York, **1993**, 81. (c) K. Y. Tam, A. Avdeef, O. Tsinman, N. Sun, *J. Med. Chem.* 2010, **53**, 392.
16. (a) J. R. Patel, R. A. Carlton, T. E. Needham, C. O. Chichester, F. G. Vogt *Int. J. Pharm. Sci.*, 2011, **405**, 142; (b) G. Bolla, P. Sanphui, A. Nangia *Cryst. Growth Des.*, 2013, **13**, 1988; (c) M. L. Cheney, D. R. Weyna, N. Shan, M. Hanna, L. Wojtas, M. J. Zaworotko *Cryst. Growth Des.*, **2010**, **10**, 4401; (d) D. R. Weyna, M. L. Cheney, N. Shan, M. Hanna, M. J. Zaworotko, V. Sava, S. Song, J. R. Sanchez-Ramos, *Mol. Pharm.*, 2012, **9**, 2094.
17. J. Zhang, X. Tan, J. Gao, W. Fan, Y. Gao, S. Qian, *J. Pharm. Pharmacol.*, 2013, **65**, 44.

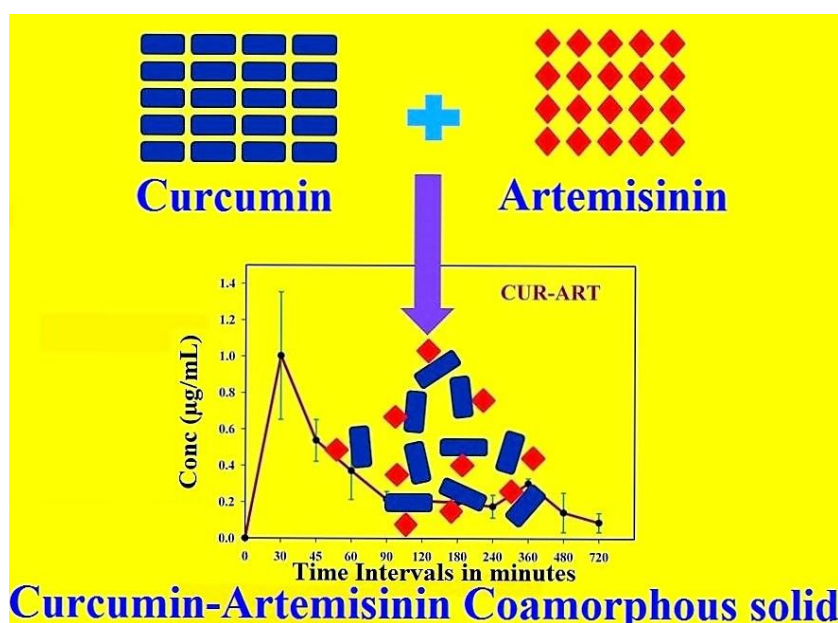
18. (a) P. B. Anjankumar, M. Najmuddin, K. Upendhra, R. C. Hariprasanna, *Int. J. Res. Pharm.* 2011, **2**, 130. (b) A. L. Patil, S. S. Patil, *Int. J. Pharm. Tech. Res.*, 2012, **4**, 201.
19. M. Nijhawan, A. Santhosh, P. R. Babu, C. V. Subrahmanyam, *Drug Dev. Ind. Pharm.* 2014, **40**, 1163.
20. (a) N. K. Nath, S. S. Kumar; A. Nangia, *Cryst. Growth Des.* 2011, **11**, 4594.
21. (a) J. Bernstein, R. E. Davis, L. Shimon, N. L. Chang, *Angew. Chem., Int. Ed. Engl.* 1995, **34**, 1555. (b) M. C. Etter, *Acc. Chem. Res.*, 1990, **23**, 120. (c) M. C. Etter, *J. Phys. Chem.*, 1991, **95**, 4601.
22. (a) V. André, A. Fernandes, P. P. Santos, M. T. Duarte, *Cryst. Growth Des.*, 2011, **11**, 2325; (b) S. Karki, T. Friščić, L. Fábián, W. Jones, *CrystEngComm*, 2010, **12**, 4038.
23. R. M. Silverstein, *Spectrometric Identification of Organic Compounds*, 6th Ed.; John Wiley & Sons, New York, 2002.
24. F. G. Vogt, J. S. Clawson, M. Strohmeier, A. J. Edwards, T. N. Pham, S. A. Watson, *Cryst. Growth Des.*, 2009, **9**, 921.
25. (a) M. K. Stanton, A. Bak, *Cryst. Growth Des.*, 2008, **8**, 3856. (b) A. Bak, A. Gore, E. Yanez, M. Stanton, S. Tufekcic, R. Syed, A. Akrami, M. Rose, S. Surapaneni, T. Bostick, A. King, S. Neervannan, D. Ostovic, A. Koparkar, *J. Pharm. Sci.*, 2008, **97**, 3942.
26. (a) T. Takagi, C. Ramachandran, M. Bermejo, S. Yamashita, X. L. Yu, G. L. Amidon, *Mol. Pharm.*, 2006, **3**, 631; (b) C. A. Lipinski, R. T. Borchardt, E. H. Kerns, D. R. Thakker, B. Wang, *Solubility in water and DMSO issues and potential solutions. In Pharmaceutical profiling in Drug discovery for lead selection*. AAPS Press, Arlington, VA, 2004, 93.
27. J. B. Dressman, G. L. Amidon, C. Reppas, V. P. Shah, *Pharm. Res.* 1998, **15**, 11.
28. (a) CrysAlis CCD and CrysAlis RED, Versions 1.171.33.55, Oxford Diffraction, Oxford, 2008. (b) O. V. Dolomanov, L. J. Bourhis, R. J. Gildea, J. A. K. Howard, H. Puschmann, *J. Appl. Crystallogr.*, 2009, **42**, 339; (c) S. M. Berge, L. D. Bighley, D. C. Monkhouse, *J. Pharm. Sci.*, 1977, **66**, 1.
29. (a) A. L. Spek, *PLATON: A Multipurpose Crystallographic Tool*; Utrecht University, Utrecht, The Netherlands, 2002; (b) A. L. Spek, *J. Appl. Crystallogr.* 2003, **36**, 7; (c) L. J. Barbour, *Supramol. Chem.*, 2001, **1**, 189; (d) L. J. Barbour,

X-Seed, Graphical Interface to SHELX-97 and POV-Ray; University of Missouri-Columbia, Columbus, MO, 1999.

30. Higuchi, T.; Connors, K. A. *Adv. Anal. Chem. Instrum.*, 1965, **4**, 117.

CHAPTER SIX

A Novel Curcumin-Artemisinin Coamorphous Solid: Physical Properties and Pharmacokinetic Profile



Here we describe Curcumin-Artemisinin (1:1) coamorphous solid prepared by rotavaporization and dramatic increase in the pharmacokinetic profile of curcumin (AUC_{0-12} 2.6 $\mu\text{g}\cdot\text{h}/\text{mL}$, C_{max} 1 $\mu\text{g}/\text{mL}$) administered as CUR-ART to SD rats. PXRD and FESEM analysis explain the molecular basis for the solubility enhancement of coamorphous CUR-ART.

6.1 Introduction

Naturally occurring compounds from traditional herbal medicines represent a rich source of therapeutic molecules to treat human diseases with minimal side effects.¹ The major drawbacks of bioactive herbal drugs are low aqueous solubility, poor bioavailability and stability issues (typically short half-life).^{1b,c} For these reasons many bioactive molecules fail to reach the market as drugs, a common example being Curcumin.² Salt formation³ is the first-choice method to enhance the solubility and bioavailability of Active Pharmaceutical Ingredients (APIs) and bioactive molecules, but this traditional approach is ruled out for compounds which lack an ionizable functional group, as is the case for curcumin. Other strategies such as polymorphs,^{4a} cocrystals,^{4b} eutectics,^{4c} solid dispersions,^{4d} cyclodextrin complexes,^{4e} nanoparticles,^{4f} etc. are also used depending on the nature of the drug and the specific problem to be addressed. Amorphization of the drug to a high free energy state can result in solubility enhancement due to particle size reduction (nanoparticles).⁵ The advantages of amorphous materials in terms of solubility and scalability makes this a preferred choice, particularly for those APIs which lack ionizable functional groups. However the rapid conversion of amorphous to crystalline state is a major concern. The addition of polymers to stabilize amorphous formulations gives plasticizing effect, compressibility and incompatibility problems.⁶ Therefore, a strategy that incorporates synergism of the drug and the additive is a desirable goal in molecular pharmaceuticals. Development of the optimal solid formulation with high bioavailability and good stability is the final goal.

In this regard several strategies have been developed. Among these, coamorphous system is a relatively new approach in which the positive effects of the drug combination (coformer effect)⁷ and high thermodynamic functions of the amorphous phase (which confer solubility and dissolution advantage) are synergized to result in an improved pharmaceutical product. A coamorphous system is a multicomponent (two or more low molecular weight components) single phase amorphous solid system which lacks periodic arrangement in the crystal lattice and is associated by weak and discrete intermolecular interactions between the components. They can have short range ordering such as hydrogen bonding of carboxylic acids, carboxamides, phenols/alcohols,⁸ similar to amorphous solids of single component systems. A coamorphous solid may be contrasted with a cocrystal, salt or eutectic primarily by its amorphous nature in that it

exhibits a broad hump ('amorphous halo')⁹ when subjected to powder X-ray diffraction. The identity and integrity of the components of coamorphous systems can be established by spectroscopy. Together with the more well-known counterparts such as salts, eutectics and cocrystals, coamorphous solids are a new entry to pharmaceutical solid form space. Several applications in pharmaceutical field to improve the solubility and bioavailability of marketed drugs, drug candidates and bioactive molecules because of its excess thermodynamic such as free energy, enthalpy and entropy, can confer solubility and dissolution advantage similar to the more popular amorphous solids and solid dispersion.¹⁰ T. Rades and coworkers¹¹ improved the physical stability and solubility of the drug-drug combination of naproxen and indomethacin coamorphous compared to individual crystalline components (Figure 6.1). Moreover they investigated the molecular level interactions between them as the acid-acid dimer by FT-IR spectroscopy. These interactions are stabilize the coamorphous nature of the binary drug-drug system. R. Laitinen and coworkers¹² reported the amorphous phase stability of simvastatin and glibenclamide by formation of coamorphous with amino acids cofomers such as aspartic acid, lysine, threonine and serine. In this work they found that simvastatin-lysine (1:1) coamorphous exhibited 3 months and glibenclamide-serine (1:1) coamorphous shown 6 months stability at 40°C and 0% RH conditions. Thus, the coamorphous system has gained considerable attension in the academic and pharma industry because of their potential utility to improve the drug dissolution rate, stability consequently oral bioavailability. In this chapter we highlited the Curcumin-Artemisinin coamorphous solid utility in terms of enhancement of solubility, stability and oral bioavailblity of curcumin.

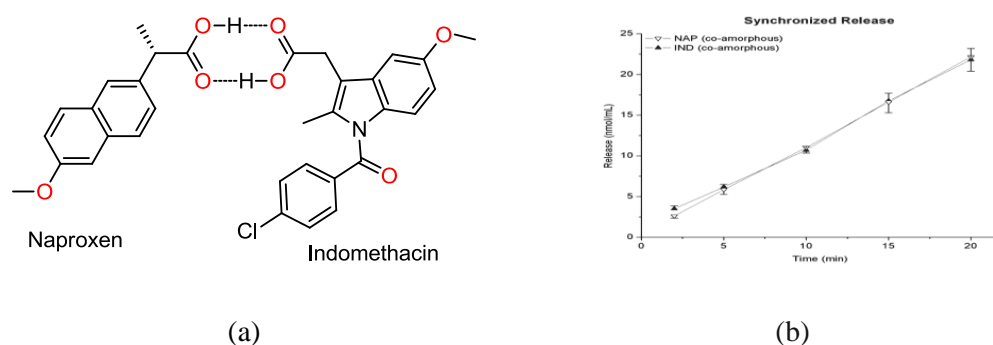


Figure 6.1: (a) Predicted H-bonding between two drugs in coamorphous (b) IDR of the coamorphous demonstrates a synchronized drug release. (Reference 11)

6.2 Literature Reports on Curcumin and Artemisinin

Curcumin (diferuloylmethane, CUR) is a hydrophobic polyphenol derived from the rhizome of the herb *Curcuma longa*, the dietary Indian spice turmeric.¹³ Artemisinin (ART), an antimalarial drug (10-25 mg/kg/day) was first identified by Chinese researchers in the plant of *Artemisia annua*.¹⁴ CUR and ART exhibit anticancer activity by suppressing multiple signaling pathways and inhibit cell proliferation, invasion, metastasis and angiogenesis. Further, these two natural compounds possess activity against bacteria, fungi, and protozoa. Cytotoxic and parasitocidal effects of protozoan parasites have been demonstrated in cultures against *Plasmodium falciparum*.¹⁵ Myocardial infarction protective, hypoglycaemic,¹⁶ and antirheumatic¹⁷ effects are well established with curcumin. Despite safety levels of up to 12 g/ day^{3b,18} in humans, the efficacy of curcumin as a drug is limited by low aqueous solubility (7.8 µg/L) and poor bioavailability (0.051 µg/mL), mainly due to its rapid metabolism.^{3,4} CUR decomposes in neutral and alkaline medium with >90% decomposition occurring within 30 min in pH 7.4 buffer medium.¹⁹ The salt formation approach⁵ is ruled out for curcumin and artemisinin due to the lack of ionizable functional groups in these molecules. The available methodologies for solid form modification and improvement of curcumin are polymorphs,^{20a} cocrystals,^{20b} eutectics,^{20c} solid dispersions,^{21a} cyclodextrin complexes,^{21b} nanoparticles,^{21c} etc. have been reported. Similarly, structural studies such as cocrystallization²² and polymorphism²³ are reported for artemisinin. With this background literature and utility of CUR-ART in combination for anticancer and antimalarial activities, we investigated the possible synergism via cocrystal or eutectic between curcumin and artemisinin (they have phenol and lactone carbonyl complementary functional groups) for both physical and biological property enhancement. We obtained a 1:1 coamorphous solid form, CUR-ART.

6.3 Results and Discussion

Salt formation is the first choice for any drug but in this case it is not possible due to the lack of ionizable sites in both CUR and ART and these two are sensitive (endoperoxide moiety of ART and CUR keto-enol moiety) to strongly acid or basic conditions. Hence the obvious choice was cocrystallization and eutectic formation to improve the solubility and dissolution of the API. Thus, with the intent of exploring a possible synergism between curcumin and artemisinin for both physical and biological property enhancements (they have phenol and lactone carbonyl complementary functional groups), we performed cocrystallization to obtain their solid combination product as a cocrystal or eutectic, mediated by O–H...O=C hydrogen bonds.^{4a,b,c 20b,20c} Therefore cocrystallization by grinding (neat, liquid-assisted and mechanical) and slurry crystallization methods were attempted to obtain a novel solid combination of CUR and ART. Due to the bulky shape, lack of robust supramolecular synthon (except a single hydrogen bond), a eutectic was expected as the product.¹³ Grinding and crystallization experiments afforded a material that appeared to be crystalline by PXRD (Figure 6.2a). The material was subjected to DSC since it can distinguish between physical mixture vs. eutectic composition. The material displayed thermal behavior typical of an amorphous form (Figure 6.3c). This could be due to heat-induced molecular mobility and randomization of the crystalline mixture such that an amorphous/ rubbery phase is formed. The product lacks strong interactions to form a crystalline supramolecular assembly but sufficient to form a coamorphous system. Such weak, but discrete interactions to give a coamorphous phase is possible using conventional techniques in which crystallization is rapid, such as melt-quenching, wet granulation, milling, etc.⁸ Melt-quenching cannot be done for CUR-ART combination since it decomposes at high temperature (see Figure 6.2c); ball-mill grinding gave a semi-crystalline/ amorphous material (see Figure 6.2b). Rotavaporization is a recent technique to obtain metastable forms,²⁴ which involve dissolving the components in a solvent and then fast evaporation under vacuum. The use of ethanol resulted in coamorphous CUR-ART of 1:1 stoichiometry (see experimental section). Solution ¹H NMR confirmed the chemical purity and equimolar stoichiometry of the product. Further the coamorphous was characterized by PXRD, DSC, FT-IR and ssNMR spectroscopy techniques.

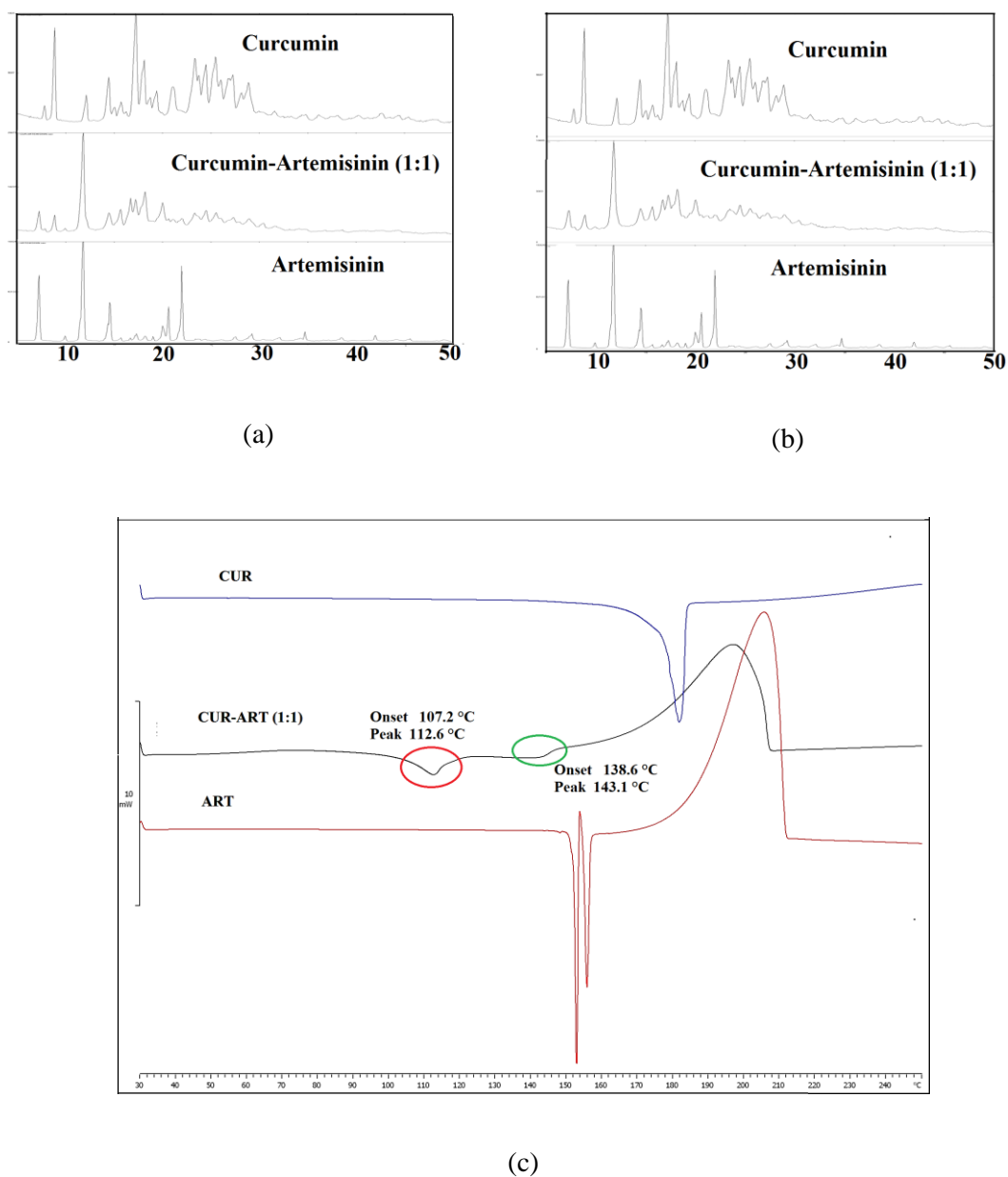


Figure 6.2 (a) CUR-ART (1:1) solvent (EtOH) assisted grinding PXRD pattern comparison with starting materials. (b) CUR-ART (1:1) ball mill grinding PXRD pattern comparison with starting materials. (c) DSC heating curve of CUR-ART (1:1) solid (obtained from grinding) comparison with starting materials.

6.3.1 PXRD Analysis

Powder X-ray diffraction²⁵ technique enabled rapid preliminary identification of crystalline and amorphous phases produced in the coamorphous experiments. The novel solid form of CUR-ART (1:1) by rotavaporization, confirms the bulk phase purity and homogeneity of coamorphous phase (Figure 6.3) where it did not show a regular diffraction pattern of physical mixture of CUR-ART (1:1). In the case of curcumin, amorphous form is reported, but there is no report of ART amorphous form. With rotavaporization to get an individual amorphous form for CUR^{3b} and ART, we reproduced the reported amorphous (Figure 6.4a) form, but ART we obtained a polymorphic mixture of ART (Figure 6.4b). These results are indicate that CUR is inducing to get amorphous nature for ART in coamorphous system of CUR-ART through particle-particle interaction and feeble hydrogen bonding interaction.¹⁶

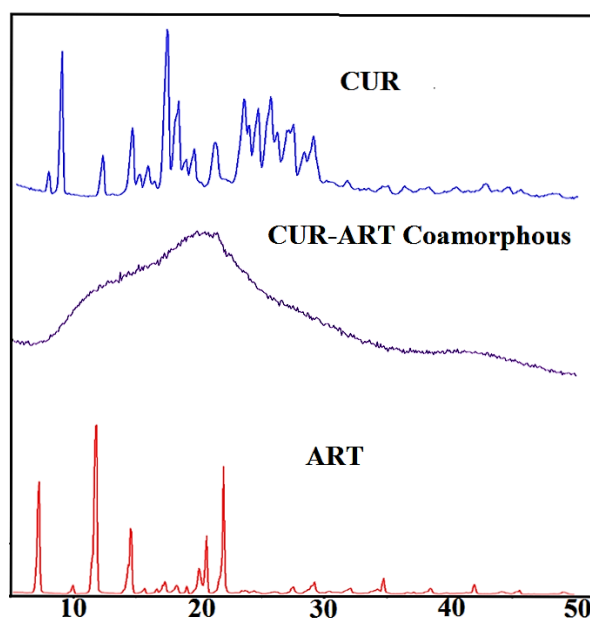


Figure 6.2 (a) Comparison of coamorphous CUR-ART (1:1) with starting materials CUR and ART Form 1. The coamorphous product is lacking the sharp diffraction lines characteristic of the crystalline starting materials.

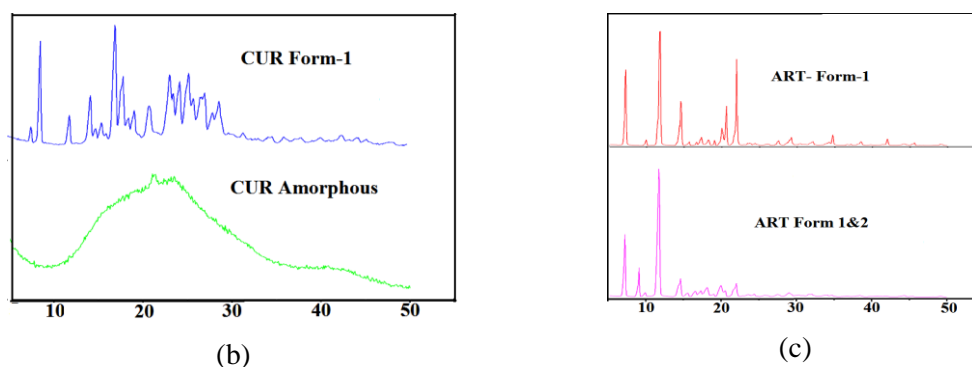


Figure 6.4 (a) PXRD pattern CUR crystalline and CUR amorphous forms obtained by rotavaporization (b) PXRD pattern of ART Form 1 and mixture of ART Form 1 and 2 obtained by rotavaporization.

6.3.2 Thermal Analysis

Differential scanning calorimetry (DSC)²⁶ of an amorphous solid will show a glass transition temperature (T_g), the temperature at which the glassy phase converts to a rubbery phase with properties akin to a liquid phase (Figure 6.5). DSC of a coamorphous material should show a single glass transition event, indicating that one compound is completely miscible in the second component to form a homogenous phase. The melting point of curcumin is 181 °C (Table 6.1) and ART shows two melting endotherms for the two polymorphs.²³ The amorphous form of CUR was reproduced by rotavap technique, and its DSC showed a single exotherm followed by a melting endotherm that matched with reported form.^{20a} In case of ART we did not observe any amorphous form from rotavap technique confirmed by PXRD. The DSC thermogram of coamorphous CUR-ART shows a single glass transition T_g (broad exotherm peak) at 67.58 °C (Figure 6.5) followed by decomposition at 192.67 °C. The single exotherm peak and no major endotherms indicate that the two compounds are freely miscible with each other to form a homogenous phase CUR-ART and that there is no dissociation to the crystalline components upon heating.

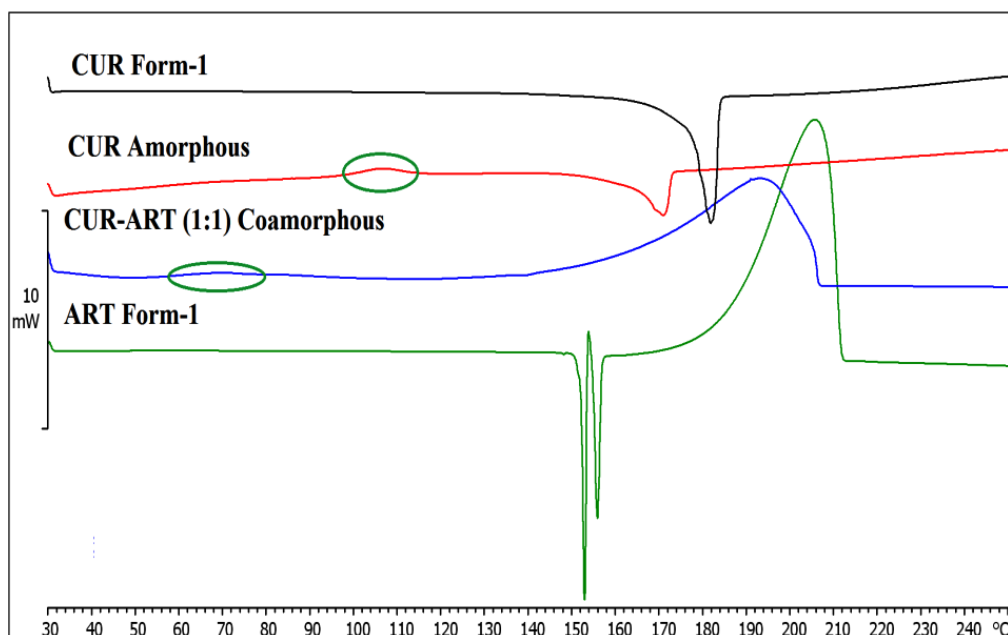


Figure 6.5 DSC thermogram of CUR-ART coamorphous (prepared by rotovaporization) form compared with the starting materials. The circles indicate glass transition of CUR amorphous (98.9 °C) and CUR-ART coamorphous (67.6 °C).

Table 6.1 Melting point, decomposition temperature, and phase transition point for CUR-ART coamorphous and their individual components (in °C).

Sample name	Phase transition	Melting point	Decomposition point
CUR	--	181.42	--
CUR Amorphous	98.90	170.93	--
ART	--	151.89 154.58	185.23
CUR-ART	67.58	--	192.67

6.3.3 FT-IR Spectroscopy Analysis

Spectroscopic techniques have certain threshold limits below which they are not sensitive enough to quantify the strength of interactions and differences in structures for chemical interpretation.²⁷ ss-NMR is sensitive to changes in short-range near-neighbor environment of the molecule. IR spectroscopy responds to changes in vibrational modes of covalent bonds as a result of changes in intermolecular interactions. In fact amorphous or coamorphous forms lacking the long range order, but these materials have some short range ordering such as formation of hydrogen bonds between functional groups like

carboxylic acid dimers or catemers.¹¹ To find out the short range ordering of amorphous or coamorphous materials FT-IR spectra were used to detect any intermolecular interactions.²⁸ When the IR spectra of CUR and ART is compared to that of the coamorphous system CUR-ART, small 1-2 cm^{-1} shift differences were observed in coamorphous form compared to starting materials (Figure 6.6). The carbonyl region for CUR and ART in coamorphous mixture, CUR carbonyl ($\text{C}=\text{O}$) stretching frequency showed at 1627 cm^{-1} and in coamorphous shifted to 1625 cm^{-1} ; while in ART, ester carbonyl($\text{C}=\text{O}$) stretching frequency showed at 1736 cm^{-1} and in coamorphous shifted to 1735 cm^{-1} . The broad hydroxyl or alcoholic region found large differences in OH stretching frequency shift 3434 cm^{-1} in coamorphous of CUR-ART, where as pure CUR, OH stretching frequency at 3510 cm^{-1} . From these IR analyses it may be inferred that, this coamorphous system contains weak hydrogen bonding intermolecular interaction between OH of CUR and ester carbonyl of ART (Scheme 6.7).

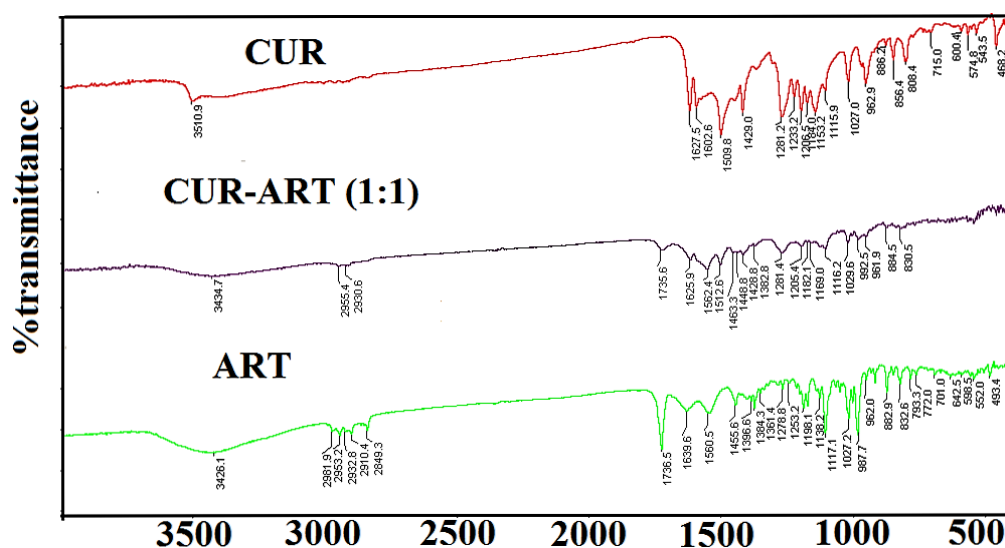
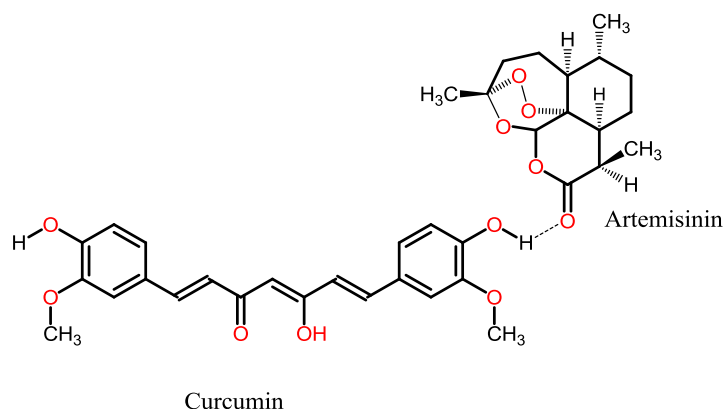


Figure 6.6 Overlay of FT-IR spectra of CUR-ART coamorphous compared to the individual components



Scheme 6.7 Molecular structure of curcumin (CUR)–Artemisinin (ART) and intermolecular O–H···O=C hydrogen bond.

6.3.4 Solid state NMR (ss-NMR) Spectroscopy

^{13}C ss-NMR provides detailed information about the differences in hydrogen bonding, molecular environment, and short range order in crystalline and amorphous solids.³⁴ The spectrum of CUR-ART obtained by rotavaporization (Figure 6.8) matches closely with the individual components in terms of chemical shifts but there is an overall peak broadening indicative of amorphization.

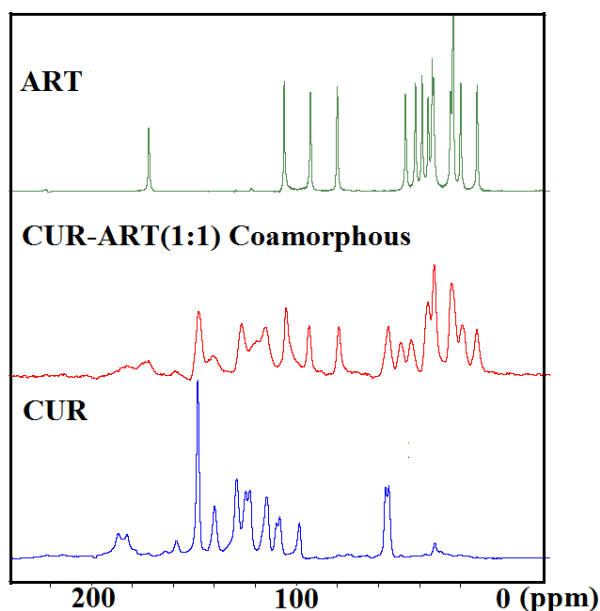


Figure 6.8 Overlay of ^{13}C ss-NMR spectra of CUR-ART coamorphous compared to the individual components.

6.3.5 Stability of CUR-ART Coamorphous Solid

The coamorphous solid was kept in accelerated ICH (International conference on Harmonization)²⁹ conditions of 40 °C temperature and 75% relative humidity stability station. PXRDs were recorded on the material at regular intervals up to 45 days to assess the sample stability. CUR-ART coamorphous was stable for a brief period of 15 days, and thereafter it showed conversion to a crystalline phase. This dissociative transformation could be due to molecular mobility facilitated by moisture and temperature. The PXRD of the semi-crystalline material at 45 days matched with the individual diffraction peaks of CUR and ART (Figure 6.9).

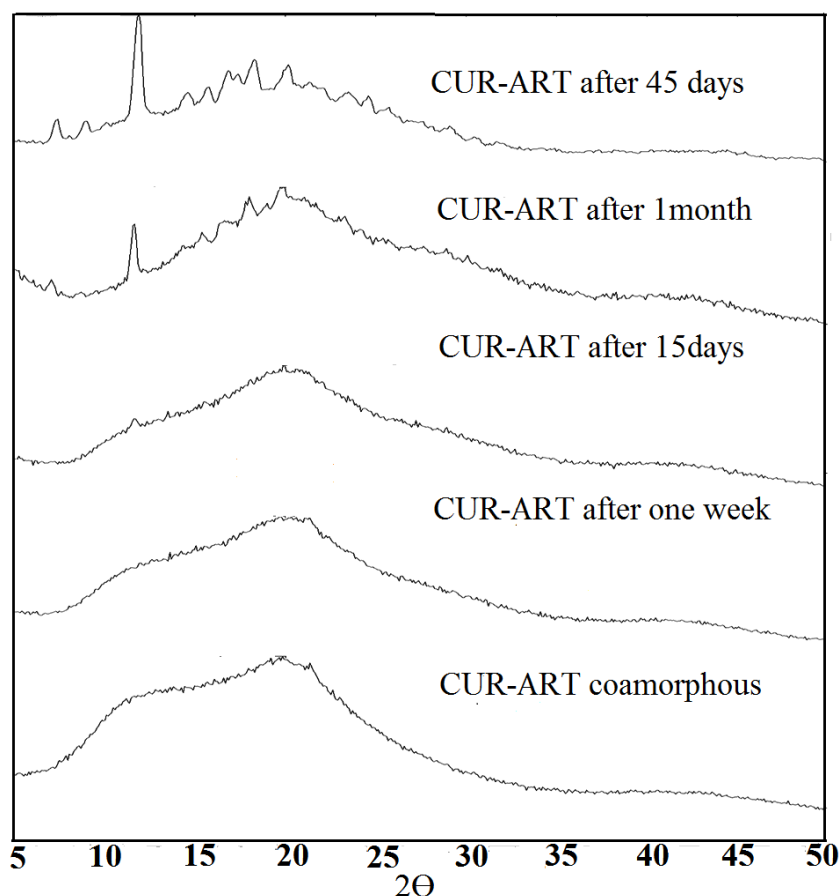


Figure 6.9 PXRD plots CUR-ART kept in the stability chamber at 40 °C and 75% RH for 45 days.

6.3.6 Solubility and Dissolution

Intrinsic Dissolution Rate (IDR) is a kinetic or time-dependent measurement. IDR gives an idea of the time required for drug onset to reach peak concentration (C_{\max}), the amount of drug dissolved (AUC), and the time taken for dissolution before phase transformation/ drug cocrystal dissociation occurs. Faster dissolution rate and high oral drug delivery³⁰ are the goal in pharmaceutical development. The solubility, stability, bioavailability and efficacy of an API or bioactive molecule predominantly depend upon its solubility and dissolution rate in the biological medium. Dissolution was carried in 60% EtOH-H₂O medium for CUR-ART because the components are not soluble in pure water. It was not possible to obtain equilibrium solubility of CUR-ART because the coamorphous form converted to the stable crystalline forms. IDR experiments were performed over 2 h by the rotating disk intrinsic dissolution rate (DIDR) method³¹ at 37 °C. The dissolution rate of CUR-ART is 2.6 faster than curcumin (Figure 6.10, Table 6.2), but there was no change relative to ART. PXRD of the residue remaining at the end of dissolution experiment matched with that of curcumin Form-1 (Figure 6.11). To summarize, the solubility of curcumin is increased in CUR-ART coamorphous compared to pure CUR. Thus, the novel CUR-ART combination is a promising candidate for solubility enhancement of bioactive herbal ingredient curcumin.

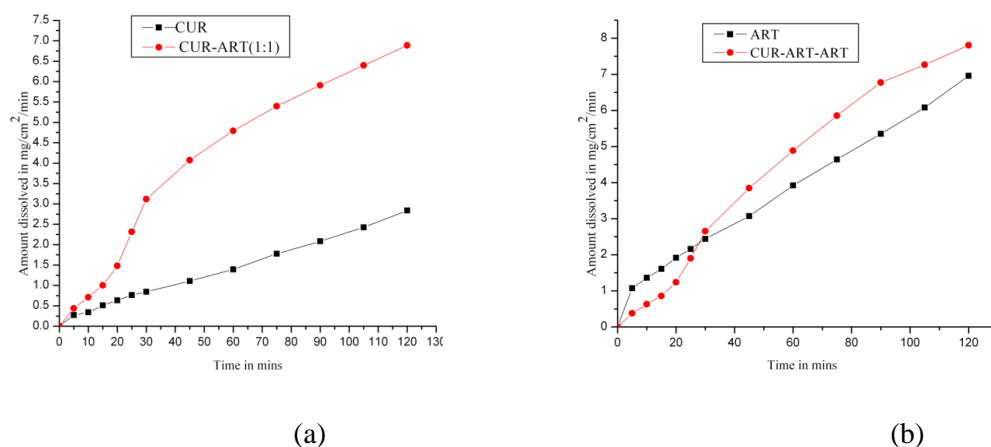


Figure 6.10 Intrinsic dissolution rate curves of (a) CUR and CUR-ART and (b) ART and CUR-ART in 60% EtOH-H₂O.

Table 6.2 Intrinsic dissolution rates of CUR-ART coamorphous system in 60% EtOH–H₂O.^a

Compound	Molar Extinction coefficient (mM ⁻¹ cm ⁻¹) (x10 ⁶)	Intrinsic dissolution rate, IDR (mg/cm ²)/min (x10 ⁻³)	Cumulative amount dissolved per unit area (mg/L)
CUR	100	0.177	17.01
CUR-ART(1:1) Curcumin conc.	200	0.461 (x2.6)	41.31 (x2.4)
ART	1	0.054	41.75
CUR-ART(1:1) Artemisinin conc.	2	0.043 (x1.2)	46.84 (x1.1)

^a Curcumin and Artemisinin concentrations were determined by HPLC analysis

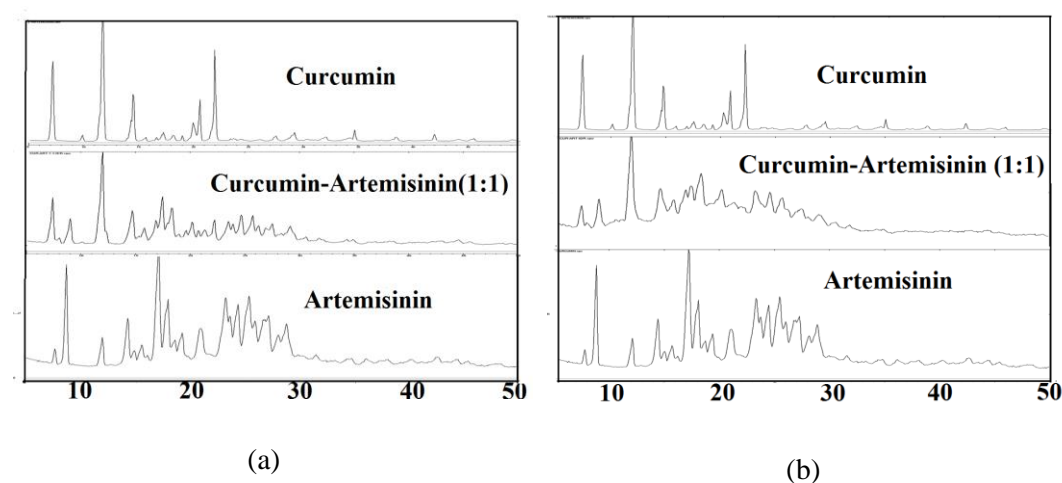


Figure 6.11 (a) PXRD of CUR-ART coamorphous at the end of equilibrium solubility experiment matches with starting materials as a physical mixture of CUR and ART. (b) PXRD of CUR-ART coamorphous at the end of IDR experiment matches with starting materials like physical mixture of CUR-ART.

6.3.7 Pharmacokinetics

Oral bioavailability is one of the most important parameters in drug pharmacology. A majority of drugs marketed worldwide is oral formulations. Oral bioavailability is the fraction of the solid dose administered which reaches systemic circulation in blood/plasma. The physicochemical properties of an API or bioactive molecule can be enhanced to give higher solubility and faster dissolution rate through salts, amorphous, cocrystal or coamorphous forms with better absorption and bioavailability.^{30,32} CUR-ART coamorphous and pure curcumin were administered orally (200 mg/kg) to Sprague Dawley male rats (200±50 g, n = 6 for each drug). Oral bioavailability can be estimated by measuring the AUC (area under the concentration curve) and C_{max} (peak plasma

concentration). Administration of pure curcumin did not show any detectable levels in plasma due to its very low solubility and short half-life. This observation is consistent with recent reports wherein pure curcumin could not be detected by HPLC.³³ Oral administration of CUR-ART coamorphous (corrected for the same molar amount of curcumin as the previous experiment), a C_{\max} value of was 1.003 $\mu\text{g/mL}$ was recorded for curcumin at T_{\max} of 30 min; thereafter, the concentration dropped with a $T_{1/2}$ of 6.4 h and $\text{AUC}_{0-\infty} = 24.7 \mu\text{g.h /mL}$ (Figure 6.12 and Table 6.3). It was not possible to detect ART bioavailability due to limit of quantification in HPLC being too low (20 $\mu\text{g/mL}$) by photodiode array detector since it lacks a chromophore group.

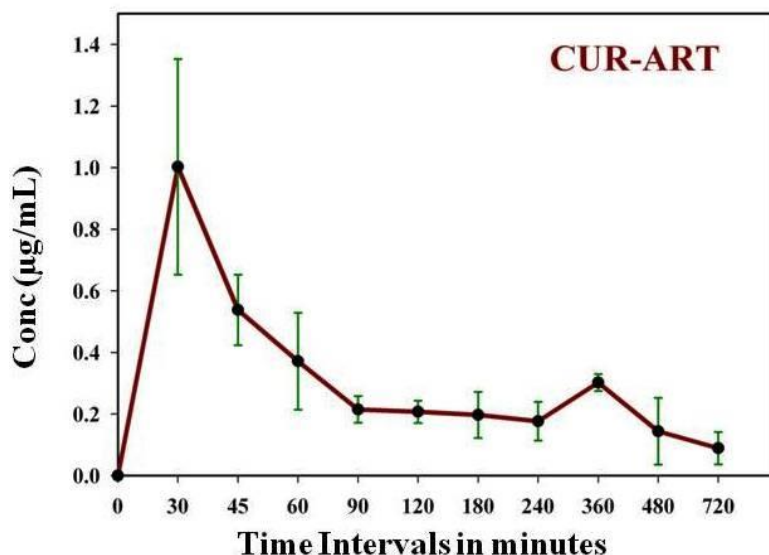


Figure 6.12 Mean Plasma concentration (of Curcumin) vs. Time profile of CUR-ART coamorphous.

Table 6.3 Pharmacokinetic parameters of CUR-ART coamorphous.

Parameter	CUR-ART
C_{\max} ($\mu\text{g/mL}$)	1.003±0.350
T_{\max} (min)	30
Half life (h)	6.4±2.2
$\text{AUC}_{0-\infty}$ ($\mu\text{g. h /mL}$)	24.7±7.4
AUC_{0-12} ($\mu\text{g. h /mL}$)	2.59±0.60
Half-life (h)	6.4±2.2

A high bioavailability C_{\max} value of 1 $\mu\text{g/mL}$ at short T_{\max} of 30 min is very remarkable for curcumin in a solid form (see reported values in Table 6.4).

Table 2 C_{\max}, T_{\max}, AUC for soluble curcumin oral forms.						
Curcumin form	C_{\max} (ng/mL)	T_{\max} (min)	Dose (mg/kg)	$AUC_{0-\infty}$ ($\mu\text{g} \cdot \text{h} / \text{mL}$)	Relative performance ^b C_{\max} , AUC	Ref.
CUR-ART coamorph.	1003	30	200	24.7	100, 2.5	This work
CUR liposome	43	30	100	0.1	8, 0.02	34a
CUR crystalline	35	80	100	11.0	7, 2.2	35a
CUR cryst. disp.	194	55	20	36.2	194, 36	35a
CUR amorph. disp.	147	60	20	27.1	147, 27	35a
Nano CUR	451	9	20	20.0	451, 20	35a
CUR powder	37	120	300	0.1 ^a	2.5, 0.006	35b
Thera CUR	1697	120	300	9.3 ^a	113, 0.62	35b
^a Estimated for 24 h from Fig. 3 of ref. 35b.						
^b Based on a dose of 20 mg/kg and assuming linear profile. This comparison is qualitative because different additives and solubilizers and polymers are added to each formulation.						

6.3.8 FESEM analysis:

The underlying basis for the fast dissolution and enhanced pharmacokinetic profile for CUR-ART was understood by FESEM analysis (Figure 6.13). Not only there is amorphization of CUR-ART (halo in Figure 1) but even at the microscopic level the coamorphous solid has smaller grains of irregular shaped 2-8 μm and mini rods of <1 μm width (Figure 6.13c). In contrast, the individual components and the physical mixture (Figure 6.13a, b, d) are several microns in size. Overall, there is micronization upon amorphization even as the particles composition is somewhat heterogeneous in size and shape distribution. Thus, coamorphization offers a simple approach to not only combine multiple drugs but also enhance their pharmaceuticals for oral delivery.

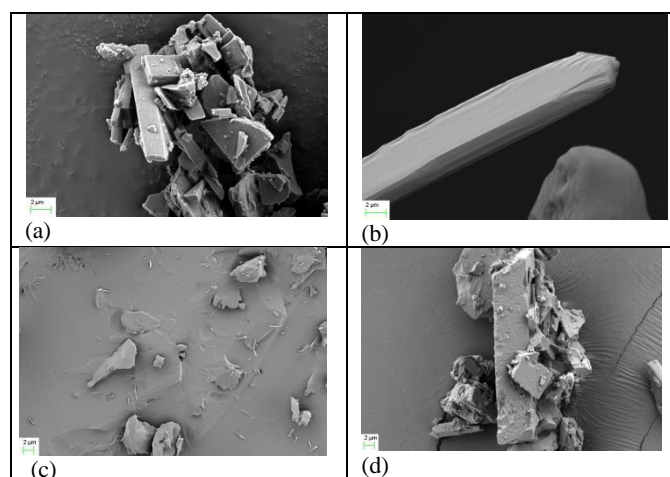


Figure 6.13 FESEM images at 2 μm resolution. (a) Curcumin shows 2 x 10 μm particle size, (b) ART is rod-like morphology of 2 x 25 μm , (c) CUR-ART coamorphous has much smaller grains of about 2-8 μm irregular shape and tiny rods of <1 μm width, and (d) particles of CUR + ART physical mixture resemble those of pure curcumin and artemisinin (large irregular morphology and long rods). The scale bar on the left hand corner is 2 μm .

6.4 Conclusions

Rotavaporization of 1:1 stoichiometric ratio of CUR and ART resulted in a coamorphous solid CUR-ART, which was characterized by powder X-ray diffraction, DSC, FT-IR and ss-NMR. The novel CUR-ART coamorphous is stable solid in accelerated ICH conditions of 40 °C and 75% RH for a brief period of 15 days. Efforts to stabilize amorphous drug forms by solid dispersion and mesoporous silica system^{4d,36} could be used in this case. To summarize the dissolution of the low solubility of curcumin is enhanced 2.6 times in coamorphous CUR-ART and 2.4 times higher drug release. Pharmacokinetic study of coamorphous CUR-ART in SD rats exhibited high curcumin concentration of 1 $\mu\text{g/mL}$ at 30 min, and bioavailability AUC of 2.6 $\mu\text{g.h/mL}$. Our result is significant in light of the fact that curcumin has low bioavailability due to short half life of 30-120 min in vivo. This study opens the potential to combine other artemisinin derivatives, such as dihydroartemisinin artemether, arteether, artesunate and artesunic acid, etc. with wonder herbal ingredient curcumin. The application of coamorphous systems is a promising strategy to enhance the physicochemical properties of drugs. Further, they add to the category of supramolecular solid state assemblies, apart from eutectics, that can be formed when the attributes of geometric compatibility and/or strong heteromolecular interactions are not favorable for a given combination of

materials. The methodology appears to be general enough to exploit the wonder molecule curcumin for solubility and pharmacokinetic profile enhancement with other herbal and synthetic bioactive molecules.

6.5 Experimental Section

Materials

Curcumin (purity > 99.8%) was obtained from Sigma-Aldrich (USA) and Artemisinin was obtained as a gift from Cipla (Mumbai, India). Solvents (purity > 99%) were purchased from Merck (India). Water filtered through a double deionized purification system (Aqua DM, Bhanu, Hyderabad, India) was used for all experiments.

Preparation of CUR-ART coamorphous

Curcumin and the Artemisinin were taken in an equimolar stoichiometric ratio and dissolved in 100 mL ethanol and rotavaporized at 50-55 °C in a Büchi rotavap. The solid residue product was characterized as a coamorphous solid and used in the next experiments.

¹H NMR spectroscopy

The coamorphous CUR-ART product was characterized by ¹H NMR to confirm the stoichiometry (Figure S3, SI). Proton NMR spectra were recorded on Bruker Avance 400 MHz spectrometer (Bruker-Biospin, Karlsruhe, Germany). Chemical shifts are quoted in δ scale and J coupling in Hz.

CUR. ¹H NMR (DMSO-d₆): 3.82 (6H, s), 6.04 (1H, s), 6.76 (2H, d, J 16), 6.82 (2H, d, J 8), 7.15 (2H, d, J 8), 7.31 (2H, s), 7.51 (2H, d, J 16), 9.66 (2H, s). OHs (CUR) exchange in solvent.

CUR-ART (1:1). ¹H NMR (DMSO-d₆): 0.91 (3H, d, J 6), 1.15 (5H, m), 1.34 (5H, m), 1.52 (1H, d, J 4.4), 1.63 (1H, d, J 12), 1.78 (2H, dd, J 5, 4), 1.90 (1H, d, J 3), 2.04 (1H, d, J 13), 2.28 (1H, t, J 12.4), 3.15 (1H, t, J 12), 3.87 (6H, s), 6.04 (1H, s), 6.10 (1H, s), 6.76 (2H, d, J 16), 6.82 (2H, d, J 8), 7.15 (2H, d, J 8), 7.31 (2H, s), 7.55 (2H, d, J 15), 9.64 (2H, s). OHs (CUR) exchange in solvent.

ART. ^1H NMR (DMSO-d_6): 0.91 (3H, d, J 6), 1.15 (5H, m), 1.34 (5H, m), 1.52 (1H, d, J 4.4), 1.63 (1H, d, J 12), 1.79 (2H, dd, J 4, 4) 1.91(1H, d, J 3), 2.05 (1H, d, J 13), 2.48 (1H, t, J 1.6), 3.14 (1H, t, J 13), 6.11(1H, s).

Powder X-ray diffraction

Powder X-ray diffraction was recorded on Bruker D8 Advance diffractometer (Bruker-AXS, Karlsruhe, Germany) using $\text{Cu-K}\alpha$ X-radiation ($\lambda = 1.5406 \text{ \AA}$) at 40 kV and 30 mA power. X-ray diffraction patterns were collected over the 2θ range $5\text{--}50^\circ$ at a scan rate of $5^\circ/\text{min}$.

FT-IR Spectroscopy

Nicolet 6700 FT-IR spectrometer with a NXR FT-Raman Module was used to record IR, NIR and Raman spectra. IR and NIR spectra were recorded on samples dispersed in KBr pellets.

Solid-state NMR spectroscopy

Solid-state ^{13}C NMR spectra were recorded on Bruker Avance 400 MHz spectrometer (Bruker- Biospin, Karlsruhe, Germany). ss-NMR spectra were carried out on a Bruker 4-mm double resonance CP-MAS probe in zirconia rotors with a Kel-F cap at 5.0-kHz spinning rate with a cross-polarization contact time of 2.5 ms and a delay of 8 s. ^{13}C NMR spectra were recorded at 100 MHz and referenced to the methylene carbon of glycine, and then recalibrated to the TMS scale ($\delta_{\text{glycine}} = 43.3 \text{ ppm}$).

Thermal analysis

Differential scanning calorimetry was performed on Mettler-Toledo DSC 822e module, (Mettler-Toledo, Columbus, OH). Samples were placed in crimped but vented aluminum pans for DSC experiments. The typical sample size was 3-5 mg for DSC. The temperature range for the thermogram was $30\text{--}300^\circ\text{C}$, and the sample was heated at a rate of $5^\circ\text{C}/\text{min}$. Samples were purged in a stream of dry nitrogen flowing at $80 \text{ mL}/\text{min}$.

Dissolution and solubility measurements

The calculated molar extinction coefficients were used to determine the IDR values. For IDR measurements, 300 mg of the compound was taken in the intrinsic attachment and compressed to 0.5-cm² disk using a hydraulic press 4.0 ton/ in² pressure for 5 min. The intrinsic attachment was placed in a jar of 500 mL medium preheated to 37 °C and rotated at 150 rpm. 5 mL of the aliquot was collected at specific time intervals, and the concentration of the aliquots was determined with appropriate dilutions from the predetermined standard curves of the respective compounds. The IDR of the compound was calculated in the linear region of the dissolution curve (which is the slope of the curve or amount of drug dissolved/surface area of the disk) per unit time. The identity of the undissolved material after the dissolution experiment was ascertained by PXRD. The nature of the solid samples after disk compression and solubility and dissolution measurements were verified by PXRD.

Chromatographic conditions

The HPLC analyses were performed using a Shimadzu Prominence model LC-20AD equipped with 20 mL injection loop, and a photodiode array detector. CUR detected at 420nm and ART detected at 210nm. Data acquisition and analysis was carried out using LC solution software. A C18 reversed-phase column (250 mm × 4.6 mm, particle size 5 µm) preceded by a C18 guard column (33 mm × 4.6 mm) was used for analysis. In case of samples from in vivo experiments, the mobile phase consisted of acetonitrile-5% acetic acid (75:25, v/v) and for IDR the mobile phase was acetonitrile-water (65:35 v/v). The mobile phase was run through the column at a flow rate of 1.0 mL/min.

Animal study

Sprague-Dawley rats (200±50g) were obtained from Sainath Agencies Limited (Hyderabad, India). Animals were acclimatized for 1 week prior to experimentation in a temperature-controlled, 12/12 h light/dark room, and were allowed standard laboratory food and water. The rats were fasted overnight (~18 hr) with free access to water before the experiment. The study was conducted in compliance with standard animal use practices at Virchow Biotech Private Limited, Department of Preclinical Toxicology, Hyderabad, India (Registration No. 546/02/A/CPSCEA) and supervised by Dr. Durga Bhavani. This study was approved by Animal Ethics Committee meeting dated 6th January 2014.

Liquid-Liquid extraction

Coamorphous CUR-ART and CUR were extracted from plasma by deproteinization. For each time-point, 0.4 mL of whole blood was collected from Retro orbital vein of rat eye into pre-chilled (4°C) lithium heparin tube and placed on ice. Within 10 min of collection, blood samples were centrifuged at 2000g for 15 min at 4 °C. The resulting plasma was frozen at –80 °C until analysis. 0.2 mL of plasma samples are combined with 0.2 mL CH₃CN solvent. The solutions were cyclomixed and sonicated in a bath sonicator for 10 min each followed by centrifugation for 15 min at 2000g. The supernatants were transferred into fresh eppendorf tubes and injected into the HPLC system.

Pharmacokinetics study

Pharmacokinetic studies of CUR-ART coamorphous and CUR were conducted in Sprague Dawley rats weighing (200±50 g) (n = 6) in cross-over design. Coamorphous CUR-ART and CUR (200 mg curcumin drug / kg of rat body weight) was suspended in 1% sodium carboxymethylcellulose and administered through oral gavage. Blood (0.4 mL) was withdrawn from retro-orbital plexus into lithium heparin tube at the following times after drug administration: 30, 45, 60, 90, 120, 180, 240, 360, 480 and 720 min. After centrifugation for 2000g for 15 min, an aliquot of 0.2 mL plasma was collected and analyzed by HPLC. Areas under the curve concentration (AUC in serum) vs. Time plots were calculated by the linear trapezoidal rule. The maximum plasma concentration, C_{max}, and the time T_{max} required to reach C_{max} were obtained from the plasma concentration curve.

FESEM analysis

Morphology and size of the micro structures of CUR, ART, CUR-ART coamorphous and CUR-ART physical mixture solid samples were examined by using a Carl Zeiss Field Emission Scanning Electron Microscopy model no.6027 with MERLIN compact using a beam voltage of 5 kV.

6.7 References

1. (a) G. Williamson, C. Morand, A. Scalbert and C. Rémésy, *Am. J. Clin. Nutr.* 2005, **81**, 230S; (b) R. Cohen, B. Schwartz, I. Peri and E. Shimoni, *J. Agric. Food Chem.*, 2011, **59**, 7932; (c) L. Ye, T. Wang, L. Tang, W. Liu, Z. Yang, J. Zhou, Z. Zheng, Z. Cai, M. Hu and Z. Liu, *J. Pharm. Sci.* 2011, **100**, 5007.
2. (a) P. Anand, A. B. Kunnumakkara, R. A. Newman and B. B. Aggarwal, *Mol. Pharmaceutics*, 2007, **4**, 807; (b) S. Qureshi, A. H. Shah and A. M. Ageel, *Planta Med.* 1992, **58**, 124.
3. G. C. Wermuth and P. H. Stahl, Eds. *Pharmaceutical Salts: A Hand Book*, Strasbourg and Freiburg, January 2002.
4. (a) M. Kennedy, J. Hu, P. Gao, Li. Lan, A. Ali-Reynolds, B. Chal, V. Gupta, C. Ma, N. Mahajan, A. Akrami and S. Surapaneni, *Mol. Pharmaceutics*, 2008, **5**, 981; (b) A. T. M. Serajuddin, *J. Pharm. Sci.* 1999, **88**, 1058; (c) N. R. Goud, K. Suresh, P. Sanphui and A. Nangia, *Int. J. Pharm. Sci.* 2012, **439**, 63; (d) A. Newman, G. G. Knipp and G. Zografi, *J. Pharm. Sci.* 2012, **101**, 1355; (e) A. K. Bhattacharjee, B. W. Koser, K. Carvalho and J. E. V. Hamont, *J. Pharm. Sci.*, 2004, **93**, 2076; (f) A. Kumari, S. K. Yadav and S. C. Yadav, *Colloids and Surfaces B: Biointerfaces*. 2010, **75**, 1.
5. (a) L. Yu, *Adv. Drug Delivery Rev.* 2001, **48**, 27; (b) K. A. Graeser, C. J. Strachan, J. E. Patterson, K. C. Gordon and T. Rades, *Cryst. Growth Des.* 2008, **8**, 128.
6. (a) Chang-Sik. Ha, and Jr. J. A. Gardella, *Chem. Rev.* 2005, **105**, 4205; (b) P. Kallinteri, S. Higgins, G. A. Hutcheon, C. B. St. Pourçain, and M. C Garnett, *Biomacromolecules*. **2005**, **6**, 1885; (c) S. R. Bhatia. *J. Am. Chem. Soc.*, 2003, **125**, 3400.
7. D. J. Good and N. Rodríguez-Hornedo, *Cryst. Growth Des.*, 2010, **10**, 1028; (b) N. Schultheiss and A. Newman, *Cryst. Growth Des.*, 2009, **9**, 2950.
8. (a) K. Löbmann, R. Laitinen, H. Grohgan, C. J. Strachan and T. Rades, *Mol. Pharmaceutics* 2011, **8**, 1919; (b) K. Löbmann, C. J. Strachan, H. Grohgan, T. Rades, O. Korhonen and R. Laitinen, *Eur. J. Pharm. Biopharm.* 2012, **81**, 159; (c) M. Allesø, N. Chieng, S. Rehder, J. Rantanen, T. Rades and J. Aaltonen. *J. Control. Release* 2009, **136**, 45.
9. L. R. Hilden and K. R. Morris, *J. Pharm. Sci.* 2004, **93**, 3.

10. (a) R. Laitinen, K. Löbmann, C.J. Strachan, H. Grohgan, and T. Rades, *Int. J. Pharm. Sci.* 2013, **453**, 65; (b) S. J. Dengale, H. Grohgan, T. Rades and K. Löbmann *Adv. Drug Delivery Rev.* 2016, **100**,116.
11. (a)K. Löbmann, R. Laitinen, H. Grohgan, C. J. Strachan, T. Rades. *Mol. Pharmaceutics* **2011**, 8, 1919; (b) K. Löbmann, C. Strachan, H. Grohgan, T. Rades, O. Korhonen, R. Laitinen, *Eur. J. Pharm. Biopharm.* 2012, **81**, 159.
12. R. Laitinen, K. Löbmann, H. Grohgan, C. Strachan, and T. Rades. *Mol. Pharmaceutics.* 2014, **11**, 2381.
13. H. Hatcher, R. Planalp, J. Cho, F.M. Torti, and S.V. Torti, *Cell Mol. Life Sci.* 2008, **65**, 1631.
14. (a)Artemisinin dose <https://www.cimsasia.com/India/drug/info/artemisinin/?type=full&mtype=generic#Dosage>. (b) N. J. White. *Science*, 2008, **320**, 330. (c) D. L. Klayman, *Science*,1985, **228**, 1049. (c) D. Chaturvedi, A. Goswami, P. P. Saikia, N. C. Barua, and P. G. Rao. *Chem. Soc. Rev.*, 2010, **39**, 435; (d) M. P. Crespo-Ortiz and M. Q. Wei. *J. Biomed. Biotech.*, 2011, **2012**, 1, doi:10.1155/2012/247597.
15. (a) G. Padmanaban, V. A. Nagaraj and P. N. Rangarajan, *Curr. Sci.* 2012, **102**, 704; (b) D. N. Nandakumar, V. A. Nagaraj, G. P. Vathsala, P. Rangarajan, G. Padmanaban. *Antimicrob. Agents Chemother.* 2012, **51**, 1859. (c) G. L. Firestone, S.N. Sundar *Exp. Rev. Mol. Med.* 2009, **11**, e32. (d) P. J. Rosenthal, S. R. Meshnick, *Mol. Biochem. Parasit.* 1996, **83**, 131. (e) L. Cui, J. Miao, L. Cui, *Antimicrob. Agents Chemother.* 2007, **51**, 488.
16. S. D. Deodhar, R. Sethi, and R. C. Srimal, *Indian J. Med. Res.* 1980, **71**, 632.
17. (a) M. Srinivasan, *Indian J. Med. Sci.* 1972, **26**, 269; (b) P. S. Babu, K. Srinivasan, *Mol. Cell. Biochem.* 1995, **152**, 13; (c) P. S. Babu and K. Srinivasan, *Mol. Cell. Biochem.* 1997, **166**, 169; (d) N. Arun, N. Nalini, *Plant Foods Hum. Nutr.* 2002, **57**, 41.
18. C. D. Lao, M. T. Ruffin, D. Normolle, D. D. Heath, S. I. Murray, J. M. Bailey, M. E. Boggs, J. Crowell, C. L. Rock, and D. E. Brenner, *BMC Complement Altern. Med.* 2006, **6**, 10.
19. Y. J. Wang, M. H. Pan, A. L. Cheng, L. L. Lin, Y. S. Ho, C. Y. Hsieh, and J. K. Lin, *J. Pharm. Biomed Anal.* 1997, **15**, 1867.
20. (a) P. Sanphui, N. R. Goud, U. B. R. Khandavilli, S. Bhanoth and A. Nangia, *Chem. Commun.*, 2011, **47**, 5013; (b) P. Sanphui, N. R. Goud, U. B. R.

- Khandavilli and A. Nangia, *Cryst. Growth Des.*, 2011, **11**, 4135; (c) N. R. Goud, K. Suresh, P. Sanphui and A. Nangia. *Int. J. Pharm. Sci.*, 2012, **439**, 63.
21. (a) S. W. Seo, H. K. Han, and M. K. Chun, *Int. J. Pharm. Sci.*, 2012, **424**, 18;(b) V. R. Yadav, S. Prasad, R. Kannappan, J. Ravindran, M. M. Chaturvedi, L. Vaahtera, J. Parkkinen and B. B. Aggarwal, *Biochem. Pharmacol.*, 2010, **80**, 1021;(c) O. Naksuriya, S. Okonogi, R. M. Schiffelers and W. E. Hennink. *Biomaterials.*, 2014, **35**, 3365.
22. S. Karki, T. Friščić, L. Fábián, and W. Jones. *CrystEngComm*, 2010, **12**, 4038.
23. (a) K. Chan, K. Yuen, H. Takayanagi, S. Janadasa, K. Peh, *Phytochemistry* 1997, **46**, 1209;(b) C. Kulkarni, J. Kendrick, A. Kelly, T. Gough, R. C. Dash, A. Paradkar, *CrystEngComm*, 2013, **15**, 6297;(c) C. Kulkarni, J. Kendrick,; A. Kelly, T. Gough, R. C. Dash, A. Paradkar, *Cryst. Growth Des.*, 2013, **13**, 5157.
24. (a) P. P. Bag and C. M. Reddy, *Cryst. Growth Des.*, 2012, **12**, 2740; (b) S. Cherukuvada and A. Nangia, *CrystEngComm*, 2012, **14**, 7840.
25. (a) V. André, A. Fernandes, P. P. Santos, M. T. Duarte, *Cryst. Growth Des.*, 2011, **11**, 2325.
26. (a) M. K. Stanton and A. Bak, *Cryst. Growth Des.*, 2008, **8**, 3856;(b) A. Bak, A. Gore, E. Yanez, M. Stanton, S. Tufekcic, R. Syed, A. Akrami, M. Rose, S. Surapaneni, T. Bostick, A. King, S. Neervannan, D. Ostovic and A. Koparkar, *J. Pharm. Sci.*, 2008, **97**, 3942.
27. R. M. Silverstein, *Spectrometric Identification of Organic Compounds*, 6th Ed.; John Wiley & Sons, New York, **2002**.
28. Y. Hu, K. Gniado, A. Erxleben and P. McArdle, *Cryst. Growth Des.*, 2014, **14**, 803.
29. Stability testing of Active Pharmaceutical Ingredients and Finished Pharmaceutical Products, WHO Technical Report Series, No. 953, http://www.ich.org/fileadmin/Public_Web_Site/ICH_Products/Guidelines/Quality/Q1F/Stability_Guideline_WHO.pdf.
30. J. B. Dressman, G. L. Amidon, C. Reppas and V. P. Shah, *Pharm. Res.*, 1998, **15**, 11.
31. L. X. Yu, A. S. Carlin, G. L. Amidon and A. S. Hussain, *Int. J. Pharm.*, 2004, **270**, 221.

32. (a) S. L. Childs, P. Kandi and S. R. Lingareddy, *Mol. Pharmaceutics*, 2013, **10**, 3112; (b) G. Engel, *Int. J. Pharm.*, 2000, **198**, 239; (c) G. Paintaud, G. Alvan and O. Ericsson, *Br. J. Clin. Pharmacol.*, 1993, **35**, 305.
33. (a) J. Li, Y. Jiang, J. Wen, G. Fan, Y. Wu and C. Zhang, *Biomed. Chromatogr.*, 2009, **23**, 1201; (b) R. A. Sharma, H. R. McLelland, K. A. Hill, C. R. Ireson, S. A. Euden, M. M. Manson, M. Pirmohamed, L. J. Marnett, A. J. Gescher and W. P. Steward, *Clin. Cancer Res.*, 2001, **7**, 1894.
34. (a) J. Li, Y. Jiang, J. Wen, G. Fan, Y. Wu and C. Zhang, *Biomed. Chromatogr.*, 2009, **23**, 1201; (b) R. A. Sharma, H. R. McLelland, K.A. Hill, C. R. Ireson, S. A. Euden, M. M. Manson, M. Pirmohamed, L. J. Marnett, A. J. Gescher and W. P. Steward, *Clin. Cancer Res.*, 2001, **7**, 1894.
35. (a) S. Onoue, H. Takahashi, Y. Kawabata, Y. Seto, J. Hatanaka,; B. Timmermann and S. Yamada, *J. Pharm. Sci.*, 2010, **99**, 1871; (b) H. Sasaki, Y. Sunagawa, K. Takahashi, A. Imaizumi, H. Fukuda, T. Hashimoto, H. Wada, Y. Katanasaka, H. Kakeya, M. Fujita, K. Hasegawa and T. Morimoto, *Biol. Pharm. Bull.*, 2011, **34**, 660.
36. (a) K. K. Qian and R. H. Bogner, *J. Pharm. Sci.*, 2011, **100**, 2801; (b) K. K. Qian and R. H. Bogner, *J. Pharm. Sci.*, 2012, **101**, 444.

CHAPTER SEVEN

Cocrystals and Alloys of Nitazoxanide: Enhanced Pharmacokinetics



Two isomorphous cocrystals of nitazoxanide (NTZ) with p-aminosalicylic acid (PASA) and p-aminobenzoic acid (PABA) as well as their alloys were prepared by slurry and grinding techniques. The cocrystals exhibit faster dissolution rate and higher pharmacokinetic properties compared to the reference drug, and surprisingly the cocrystal alloy (CA2) NTZ-PABA : NTZ-PASA (0.75 : 0.25) exhibited 4 fold higher bioavailability of NTZ in Sprague Dawley rats.

7.1 Introduction

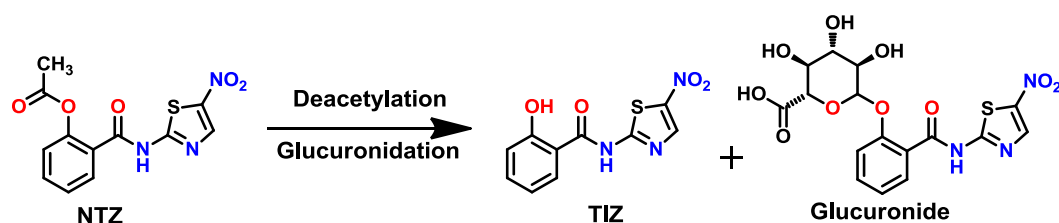
Tuberculosis (TB)¹ is an infectious disease caused by *Mycobacterium tuberculosis* (Mtb) and is still a major global health problem of enormous proportions. It causes ill-health among millions of people each year and death from an infectious disease despite there being extensive research in medicine. Initially BCG (Bacillus Calmette-Guérin) vaccine is the only licensed vaccine used for TB, but its efficacy is reduced after 20 years due to resistance.² Therefore, chemotherapy is an essential mode of treatment for the disease but development of drug resistance warrants sound strategies to contain it. The World health organization (WHO) developed a strategy in 1995 called Directly Observed Treatment (DOT) short course to control TB and drug resistance.³ In accordance, a standard six-month course of four first line drugs namely, Isoniazid, Pyrazinamide, Ethambutol and Rifampicin in a fixed dose combination (FDC) or multidrug therapy (MDT) were administered orally to treat TB comprehensively.³ Later stage drug resistance develops for these first line drugs especially isoniazid and pyrazinamide drugs become relatively inactive against non-replicating Mtb.^{3a,4} In other aspects, FDC drugs have stability issue due to high chemical reactivity of isoniazid and rifampicin.⁵ For this reasons, second generation drugs were developed and those are ciprofloxacin, amikacin, amoxicillin, capreomycin, ethionamide, prothionamide, and cycloserine etc.⁶ though second line drugs predominantly tend to have more adverse effects and limited activity profile compared to first line drugs. Some drugs specifically such as amikacin and capreomycin, have to be given by intravenous route, this leads to an extended duration time to cure TB. As a result, even today TB is not controlled and in 2012 WHO reported, 8.6 million new TB cases and 1.3 million TB deaths, with about 1.0 million among HIV-negative patients and 0.3 million HIV-associated TB cases.^{1a} Thus, there is an urgent need to investigate the right medication for treating the non-replicating and replicating Mtb causing TB. But the time to identify, develop, and eventually advance new drug regimens on the market has been agonizingly slow due to time consuming and cost effective process. On the other side, currently marketed drugs treating for other disease are used for finding the activity against TB is another approach. This is also called as drug repositioning (as using drugs for new purpose) and it is presently an attractive area in pharmaceuticals. Many research groups and pharma industry started to find out correct medication for TB with marketed drugs. Similarly, in a screening program to evaluate the activity of known chemical entities (marketed drugs which has without adverse effects or toxicity and drug

resistance) against both replicating and non-replicating Mtb, Nathan et al. discovered that nitazoxanide (prodrug) as a promising candidate for multi-drug resistant bacteria.⁷ They found that both nitazoxanide and its active metabolite tizoxanide are killing both replicating and non-replicating *M. tuberculosis*. This study suggests that nitazoxanide might offer a therapeutic benefit for patients infected with extensively drug-resistant tuberculosis. However nitazoxanide has poor aqueous solubility^{8a} and limited bioavailability.^{8b} With this background on nitazoxanide and to address the solubility and bioavailability issues, we synthesized pharmaceutical cocrystals and their alloys of nitazoxanide and TB activity studies are pending.

7.2 Literature Reports on Nitazoxanide

Nitazoxanide (NTZ) is a prodrug of nitrothiazolyl-salicylamide derivative used as an anti-protozoal agent and it has broad spectrum activities against many diseases. It was first discovered by Jean-Francois Rossignol research group at the Pasteur institute.⁹ Here they investigated NTZ activity against parasites such as tapeworms. The drug was approved by FDA in 2002, for treating of illness and diarrhoea. It also shows activity against chronic Hepatitis B and chronic Hepatitis C viruses and clinical trials were under the process.¹⁰ In addition to this, apoptosis in colorectal tumor cells activity of NTZ are also reported.¹¹ Because of the wide spectrum activity, lack of toxicity and absence of microbial resistance, Carl Nathan *et. al.* Studied the against mycobacteria species. They found that NTZ and its active metabolite tizoxanide (TIZ) are killing the both replicating and non-replicating *M. tuberculosis* at low 16µg/mL levels.⁷ This study suggests that NTZ might offer a therapeutic benefit for patients infected with extensively drug-resistant tuberculosis. However NTZ has poor aqueous solubility (7.55×10^{-3} mg/mL in water)^{8a} and limited bioavailability (258 ng/mL, 7.5 mg/kg dose in rats)^{8b} due to the inactive metabolism (formation of inactive metabolite glucuronide ether, Scheme 7.1). To improve the solubility of NTZ, with hydrotropic agents¹² and polymeric micelles encapsulation¹³ methods have been reported. A Cambridge Structural Database (CSD) search on NTZ, no polymorphs, solvates/hydrates, or salts, only one guest free form crystal structure¹⁴ and three cocrystals.¹⁵ The development of pharmaceutical cocrystal is an important physicochemical modification of the drug. Cocrystal applications are well studied in pharmaceuticals to improve the properties such as solubility, stability, and bioavailability, liquid drug to solid, tabletability and preservatives parameters.¹⁶ In

addition to cocrystals, very few examples exist in the literature on cocrystals forming alloys/solid solutions¹⁷ and to our knowledge there is no report on the pharmaceutical utility of such cocrystal alloys. Cocrystal alloy is a single phase mixture of two or more isomorphous/isostructural cocrystals is also called as multivariate cocrystals. Both cocrystals and cocrystal alloys can also be significant for making drug-drug combinations and/or fixed dose combinations (FDC) for combination therapy for a specific disease and also useful alternative strategies for repurposing or repositioning of known drugs. In this work we highlight, pharmaceutical solids of both cocrystals and cocrystal alloys with classical drug molecule NTZ to enhance its solubility and pharmacokinetics.



Scheme 7.1 Biochemical transformation of NTZ prodrug to the active metabolite TIZ and TIZ glucuronide (inactive metabolite).

7.3 Preparation of Nitazoxanide cocrystals and their alloys

The selection of coformers for the supramolecular modifications of a drug is primarily based on the functional groups involved in hydrogen bonding/ $\pi\cdots\pi$ stacking/halogen bonding, so as to maximize the strong and robust synthons.¹⁸ NTZ consists functional groups such as carboxamide (CONH_2), ester (OCOCH_3), thiazole ring N and nitro (NO_2) group's forming hydrogen bonds tend to form cocrystals. Because of its rich functionalities here we used mainly COOH , NH_2 , OH and CONH_2 functional groups containing GRAS status coformers which were capable to form cocrystals. Cocrystallization experiments were carried out by slurry grinding of starting materials in definite molar ratio provided two pharmaceutical cocrystals, with *para*-aminosalicylic acid (PASA) and *para*-aminobenzoic acid (PABA) coformers (Scheme 7.2). As well as solid solutions of cocrystal alloys (CA) NTZ-PABA : NTZ-PASA of 0.75 : 0.25 (CA1) and 0.67 : 0.33 (CA2) compositions were obtained by mechanochemical grinding. All of these pharmaceutical solids were characterized by X-ray diffraction, thermal analysis (DSC), and (FT-IR) spectroscopic techniques.



Scheme 7.2: Chemical structure of cofomers successful in forming cocrystals with NTZ and abbreviations are used entire chapter.

7.4 Results and Discussion

NTZ is a functionally rich molecule (five acceptors: amide carbonyl O, thiazolidine N, ester C=O, nitro O atoms; one donor: amide NH) capable to form cocrystals with COOH, NH₂, and OH functional group-containing cofomers of GRAS status.¹⁹ The cocrystal structures of NTZ-PASA and NTZ-PABA in a 1:1 molar ratio were established by single crystal X-ray diffraction (see crystallographic data in Table 7.1 and hydrogen bonds in Table 7.2) and their unit cell parameters has resemblance. Thus the similarity in unit cell parameters, isostructurality index of both cocrystals determined by using two parameters which are unit cell similarity (II) index equation²⁰ and XPac analysis.²¹ The unit cell similarity (II) index resulted zero (0.001) and application of XPac analysis, they shown that 3D supramolecular constructs (3D similarity which is at the highest level of comparison, Figure 7.3) with a dissimilarity index of 11. This results suggests that these cocrystals are isomorphous and isostructural to each other. Based on the near identity of the two chemical structures, which differ by an OH/H group only in cofomer of PASA/PABA and isomorphous a behavior of their cocrystals the possibility of pharmaceutical cocrystal alloys for NTZ-PASA and NTZ-PABA cocrystals was explored in different stoichiometric ratios and The supramolecular approach (Scheme 7.4) shows that binary isomorphous cocrystals may be ground in multivariate stoichiometric ratio to give cocrystal alloys. Hence we prepared single crystals of cocrystal alloys (CA) and further solved and refined. The integrity of the cocrystal alloy was established by a low *R* factor achieved upon assigning the O atom of PASA variable occupancy in the least squares refinement cycles. The product cocrystal alloys (CA) have the stoichiometry 0.67 : 0.33 for CA1 and 0.75 : 0.25 for CA2 of NTZ-PABA : NTZ-PASA by X-ray diffraction (see crystallographic data in Table 7.1 and hydrogen bonds in Table 7.2). The preparation and characterization of cocrystals and alloys is described in experimental section.

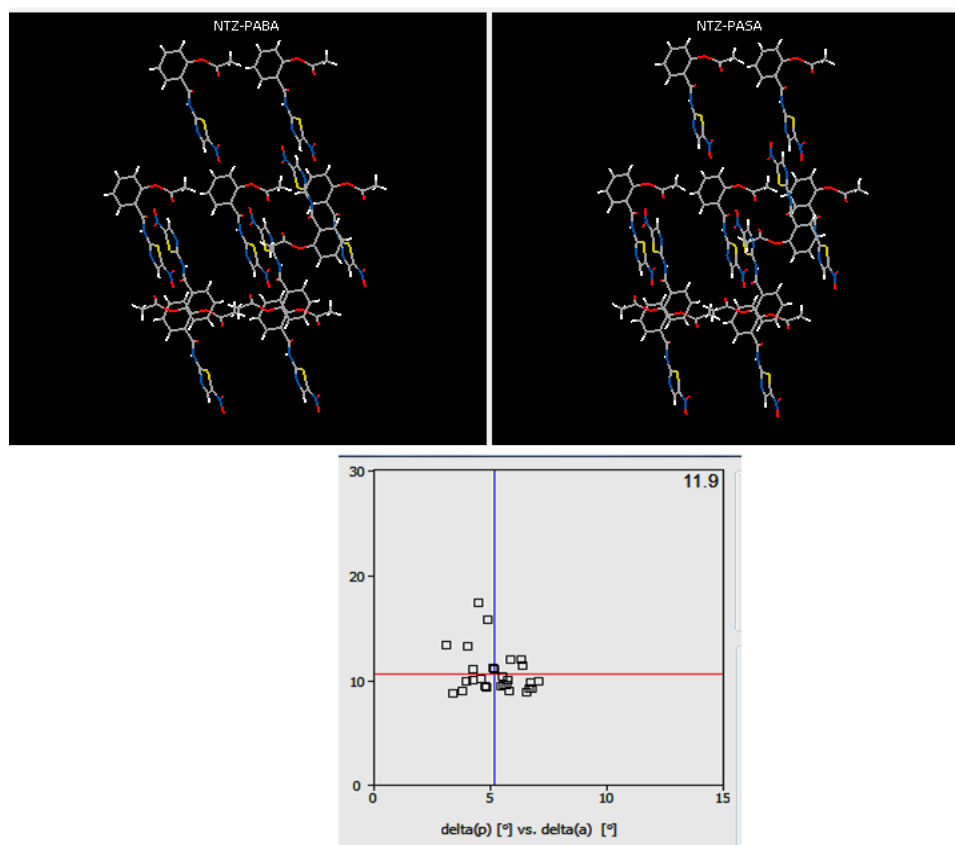
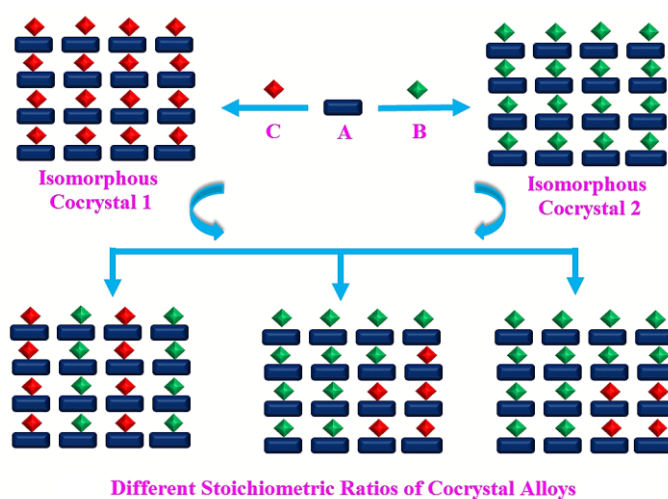


Figure 7.3 3D supramolecular construct of NTZ-PASA and NTZ-PABA cocrystals and the plot of the interplanar angular deviation vs. angular deviation (u) in XPac with a dissimilarity index of 11.



Scheme 7.4 Schematic representation of isomorphous cocrystals and both cocrystals 1 and 2 can result in cocrystal alloys.

Table 7.1 Crystallographic parameters table

	NTZ-PABA	NTZ-PASA	CA1(0.67 : 0.33)	CA2(0.75 : 0.25)
Emp. form.	C ₁₂ H ₉ N ₃ O ₅ S- C ₇ H ₇ NO ₂	C ₁₂ H ₉ N ₃ O ₅ S- C ₇ H ₇ NO ₃	C ₁₂ H ₉ N ₃ O ₅ S- C ₇ H ₇ NO _{2.33}	C ₁₂ H ₉ N ₃ O ₅ S- C ₇ H _{6.25} NO _{2.25}
Form. wt.	443.42	460.42	449.62	447.66
Cryst. syst.	Triclinic	Triclinic	Triclinic	Triclinic
Sp. gr.	<i>P</i> $\bar{1}$	<i>P</i> $\bar{1}$	<i>P</i> $\bar{1}$	<i>P</i> $\bar{1}$
<i>T</i> (K)	298(2)	298(2)	298(2)	100(2)
<i>a</i> (Å)	7.4607(6)	7.2396(4)	7.3750(8)	7.377(2)
<i>b</i> (Å)	11.3799(12)	11.6008(9)	11.4414(12)	11.371(5)
<i>c</i> (Å)	13.9457(15)	13.8909(12)	13.8757(12)	13.888(5)
α (°)	66.488(10)	109.021(7)	108.729(8)	108.933(13)
β (°)	83.048(8)	97.558(6)	97.485(8)	97.742(13)
γ (°)	71.106(9)	104.385(6)	107.618(10)	108.643(19)
<i>Z</i>	2	2	2	2
<i>V</i> (Å ³)	1027.2(2)	1039.19(15)	1022.72(19)	1006.5(6)
Rflns. collect	3343	6589	7161	11091
Unique rflns.	2551	2950	4006	3044
Obsd. rflns.	1930	3974	1880	1224
Parameters	209	298	289	295
<i>R</i> ₁	0.0478	0.0487	0.0593	0.0781
w <i>R</i> ₂	0.1310	0.1428	0.1070	0.1857
GOF	1.008	1.025	0.870	0.842
Diffractomete r	Oxford Xcalibur Gemini	Oxford Xcalibur Gemini	Oxford Xcalibur Gemini	Bruker D8 Quest

Table 7.2 Selected geometric parameters characterizing hydrogen bonds in NTZ cocrystals and cocrystal alloys

D–H...A	D...A (Å)	H...A (Å)	D–H...A (°)	symmetry code
NTZ-PABA				
N1–H1A...O6	2.850(4)	2.00	168	intra
N4–H4A...O3	3.133(4)	2.30	162	x,y,-1+z
N4–H4B...O4	3.075(5)	2.23	169	-1+x,1+y,-1+z
O7–H7A...N2	2.747(4)	1.93	174	intra
C3–H3...O2	3.229(5)	2.59	127	-x,1-y,1-z
C15–H15...O2	3.502(5)	2.60	164	1-x,-y,1-z
NTZ-PASA				
N1–H1A...O6	2.833(3)	2.00	162	1-x,1-y,-z
N4–H4A...O3	3.184(4)	2.33	168	1-x,1-y,1-z
N4–H4B...O5	3.098(4)	2.20	162	1-x,2-y,1-z
O7–H7A...N2	2.722(3)	1.88	169	1-x,1-y,-z
O8–H8A...O6	2.591(6)	1.90	146	intra
C6–H6...O8	3.464(3)	2.57	161	-1+x,-1+y,z
C18–H18...O2	3.421(8)	2.52	164	1+x,y,z
CA1(0.67 : 0.33)				

N1–H1A...O6	2.832(3)	1.94	174	1-x,1-y,1-z
N4–H4B...O3	3.145(4)	2.37	150	1-x,1-y,-z
N4–H5A...O4	3.056(4)	2.44	129	1-x,-y,-z
O7–H7A...N2	2.724(3)	1.91	175	1-x,1-y,1-z
C5–H5...O2	3.258(5)	2.60	129	2-x,2-y,1-z
C18–H18...O2	3.464(5)	2.56	164	-1+x,y,z
CA2(0.75 : 0.25)				
O7–H017...N2	2.724(4)	1.89	174	1-x,1-y,1-z
N1–H1A...O6	2.805(4)	1.94	169	1-x,1-y,1-z
N4–H4A...O4	3.0576(13)	2.33	140	1-x,-y,-z
N4–H4B...O3	3.091(4)	2.41	134	1-x,1-y,-z
C5–H5...O2	3.187(7)	2.54	128	1-x,1-y,1-z
C18–H18...O2	3.424(5)	2.49	166	1-x,1-y,-z

7.4.1 Crystal Structure Analysis

Nitazoxanide (NTZ): The reported crystal structure¹⁴ of NTZ (in space group $Pna2_1$) shows two symmetry-independent molecules constrained in a rigid conformation by intramolecular N–H...O hydrogen bond (2.03 Å, 132° and 2.01 Å, 131°; $S(6)$ graph set) and chalcogen S...O interactions (2.61 Å, 160° and 2.64 Å, 159°; $S(5)$ graph set). Two molecules are connected by C–H...N dimer $R_2^2(6)$ motif (2.74 Å, 142°; Figure 7.5). The overall structure of this nearly planar (except the acetyl group) molecule is layered stacking.

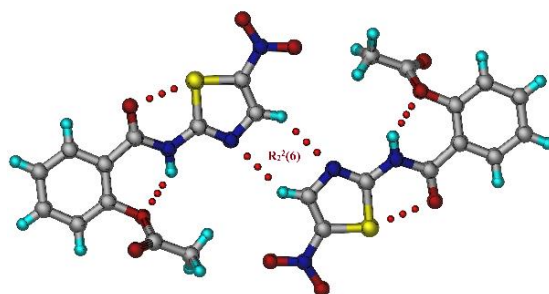


Figure 7.5 Two adjacent non-equivalent NTZ molecules are connected via C–H...N interaction in a dimeric $R_2^2(6)$ ring motif.

Nitazoxanide-*p*-aminobenzoic acid (NTZ-PABA, 1:1): The crystal structure of NTZ-PABA (1:1 in space group $P\bar{1}$) is sustained by the robust heterodimer of amidothiazole-acid groups via N–H...O and O–H...N hydrogen bonds (2.00 Å, 168°; 1.93 Å, 174°) in $R_2^2(8)$ ring (Figure 7.6). Such dimeric ring motifs are arranged in a 1D tape via amino N–H...O to nitro acceptor hydrogen bond (2.22 Å, 169°).

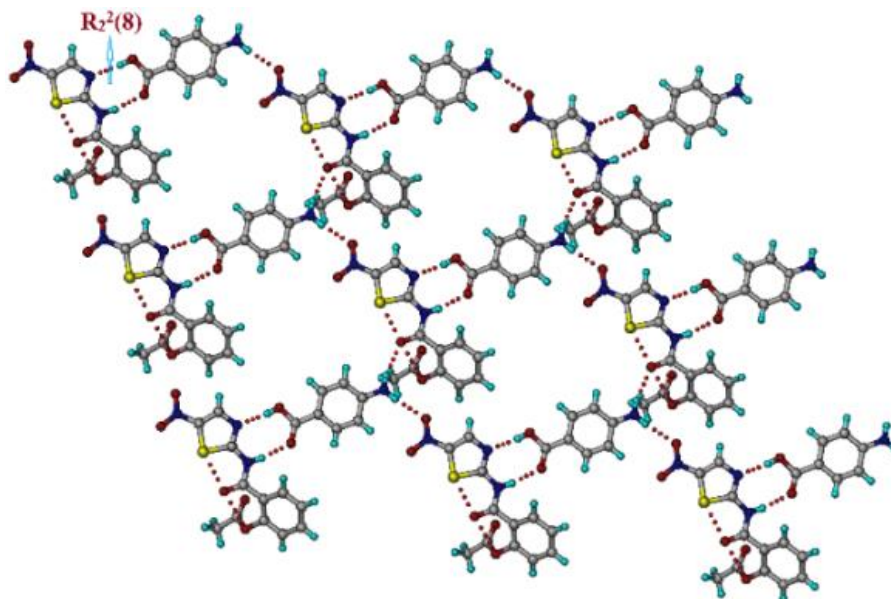


Figure 7.6 Sheet structure of NTZ-PABA is sustained by $R_2^2(8)$ dimer synthon and N–H···O hydrogen bonds.

Nitazoxanide-*p*-aminosalicyclic acid (NTZ-PASA, 1:1): The crystal structure of NTZ-PASA (1:1 in space group $P\bar{1}$ with similar unit cell parameters to those of NTZ-PABA) contains the heterodimer of N–H···O and O–H···N hydrogen bonds (2.00 Å, 162°; 1.88 Å, 169°) in a $R_2^2(8)$ ring motif, which are connected via amino-nitro H bond (2.19 Å, 162°) (Figure 7.7). A reason for the isostructurality between the two cocrystal structures by exchange of H/ OH groups²² is the intramolecular H bond in PASA, which in effect makes the OH donor engaged in a $S(6)$ motif (1.90 Å), and buried inside the hydrogen boned network.

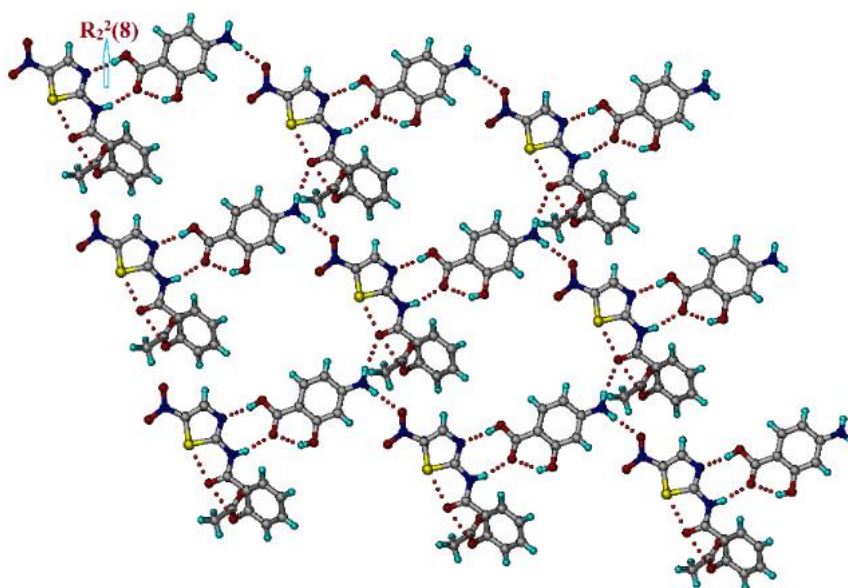


Figure 7.7 Sheet structure of NTZ-PASA is sustained by $R_2^2(8)$ dimer synthon and N–H \cdots O hydrogen bonds.

Isostructurality and isomorphous nature between the binary pharmaceutical cocrystals encouraged us to make combinations in variable stoichiometry with the idea that (1) this will lead to novel multi-component systems with a different stoichiometry of NTZ and coformers, and (2) that both coformers being present in the same crystalline solid could lead to unusual properties for NTZ. We were guided by recent reports wherein organic alloys exhibit advanced functional behavior in solar cells and semiconductors.^{23,24} Because the H atom is smaller than an OH group, a solid solution or alloy of two cocrystals NTZ-PABA and NTZ-PASA will have a higher molar ratio of PABA cocrystal than that of PASA cocrystal. The stoichiometry of CA1 and CA2 obtained by refining the occupancy of electron density at the H/ OH site in the crystal structure gave the lowest *R*-factor for NTZ-PABA : NTZ-PASA composition as 0.67 : 0.33 (CA1, R_f = 0.0593) and 0.75 : 0.25 (CA2, R = 0.0781); the cocrystal structures *R*-factor is 0.0478, 0.0487. The crystal structures of CA1 and CA2 are similar to those of the individual cocrystals (Figure 7.8, Table 7.1 and 7.2). Additionally, in both cocrystals and cocrystal alloy structures, slight conformational changes were observed due to reorganization of the homomeric interactions of NTZ discussed in coming part of conformational analysis.

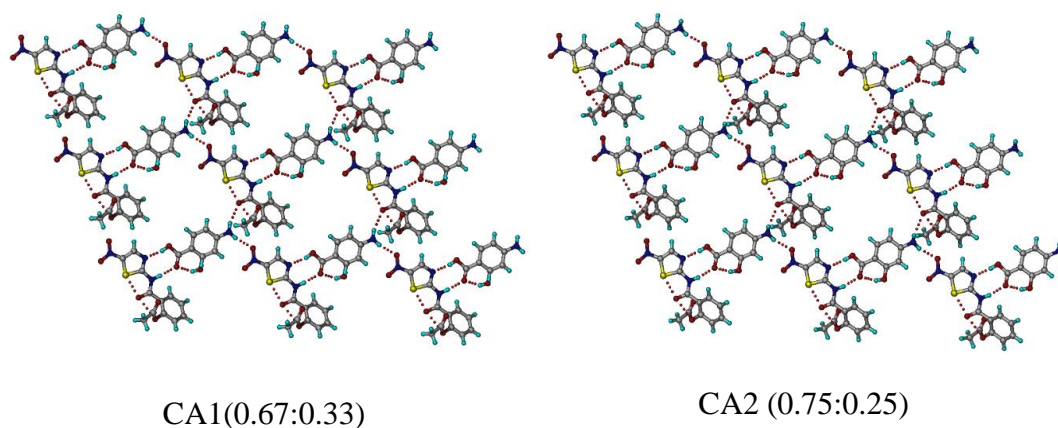


Figure 7.8 The sheet structure of CA1 and CA2 cocrystal alloys extends through N–H···O and O–H···N hydrogen bonds.

7.4.2 Conformational analysis

The main conformational change that occurs in the cocrystals compared to the pure NTZ drug is that the ester group is oriented anti to the amide C=O in NTZ while the phenyl ring rotates about the C–C bond and the ester group is on *syn* side of the amide C=O in the other four cocrystal/ alloy structures. There are other minor torsion angle changes, but they are more in the way of adjustments to fit the overall crystal packing in each case (see Figure 7.9 and Table 7.3).

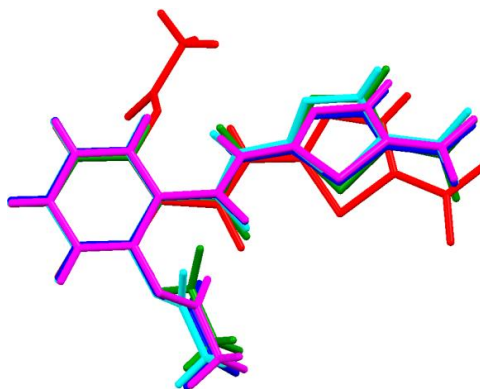
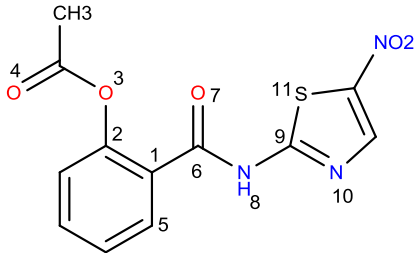


Figure 7.9 Overlay of NTZ molecules extracted from cocrystal crystal structures with guest free form NTZ. NTZ: Red, NTZ-PABA: Green, NTZ-PASA: Cyan, CA1: Blue and CA2: Magenta.

Table 7.3 Torsion angles in NTZ crystal structures.

 <p style="text-align: center;">NTZ</p> <p>τ_1 O4-O3-C1-C2, τ_2 O3-C2-C1-C6, τ_3 C2-C1-C6-O7, τ_4 C2-C1-C6-N8, τ_5 O7-C6-N8-C9, τ_6 O7-C6-N8-N10, τ_7 O7-C6-N8-S15</p>							
	τ_1	τ_2	τ_3	τ_4	τ_5	τ_6	τ_7
NTZ 1	122.53	2.29	164.46	-15.38	-1.48	-170.84	8.57
NTZ 2	117.46	-3.81	-164.73	15.25	1.62	171.02	-9.37
NTZ-PABA	58.92	-0.07	41.19	-139.81	0.47	178.79	0.55
NTZ-PASA	65.78	1.23	36.35	-144.32	3.29	170.60	-1.71
CA1	60.13	0.67	38.91	-142.00	1.61	179.27	-0.33
CA2	-58.83	-0.60	-40.00	140.54	-2.11	179.44	0.88

7.4.3 PXRD Analysis

The PXRD patterns of the two isomorphous cocrystals and cocrystal alloys prepared in this work was confirmed the bulk phase purity and homogeneity of each crystalline phase which shown an excellent overlay of the experimental powder pattern with the calculated lines from the X-ray crystal structure (Figure 7.10). Since these solids forms were isomorphous and isostructural, their PXRD patterns are also similar with subtle changes at 2θ peaks positions shifted in towards higher 2θ which is common observation in solid solutions/cocrystal alloys when compare to parent components.²⁵

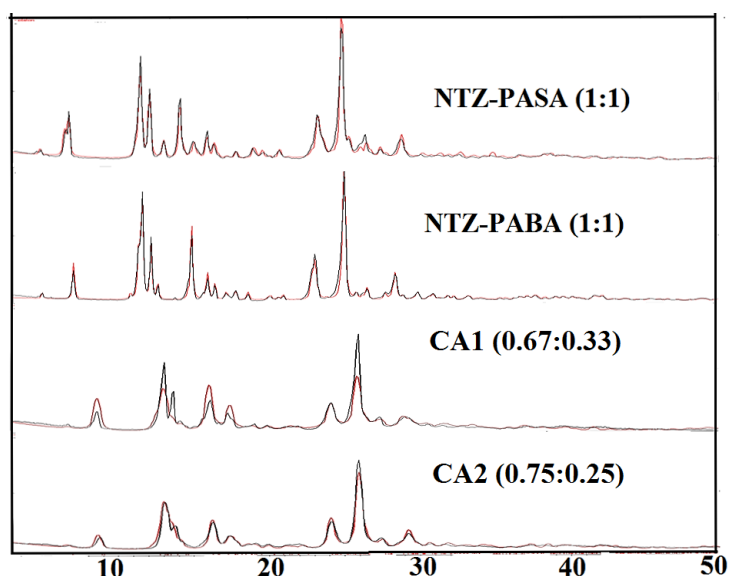


Figure 7.10 Refinement of experimental PXRD pattern of NTZ cocrystals and cocrystal alloys (black) showed good match with their calculated line profile from the X-ray crystal structure (red) indicating bulk purity and phase homogeneity.

7.4.4 FT-IR Spectroscopy

In the IR spectrum of NTZ, the ester carbonyl stretching frequency band appears at 1772 cm^{-1} and the stretching band at 3358 cm^{-1} belongs to the vibrations of the amide NH functional group. The carbonyl group of amide, stretching frequency band appears at 1661 cm^{-1} . All of these stretching frequencies were red or blue shifted in the cocrystals and cocrystal alloys compared to their starting materials. In the NTZ-PASA cocrystal IR spectrum stretching frequency bands at 3475 cm^{-1} and 3383 cm^{-1} assigned for PASA contains COOH and NH_2 were blue shifted when compared PASA that shows at 3495 cm^{-1} and 3387 cm^{-1} . Similarly stretching band at 1675 cm^{-1} refers to the COOH carbonyl group of PASA is red shifted in cocrystal. As well the stretching band appears at 3258 cm^{-1} belongs to the NTZ amide NH group is blue shift when compared to parent NTZ (3252 cm^{-1}). Like NTZ-PASA, a similar change was resembled in NTZ-PABA and also in other two cocrystal alloys (CA1 & CA2). The ester carbonyl stretching band at 1772 cm^{-1} was blue shifted in cocrystals and cocrystal alloys due to rotation of this group by 118° along C-C bond. Changes in FT-IR bands spectra were in Figure 7.11 and changes values listed in table 7.4.

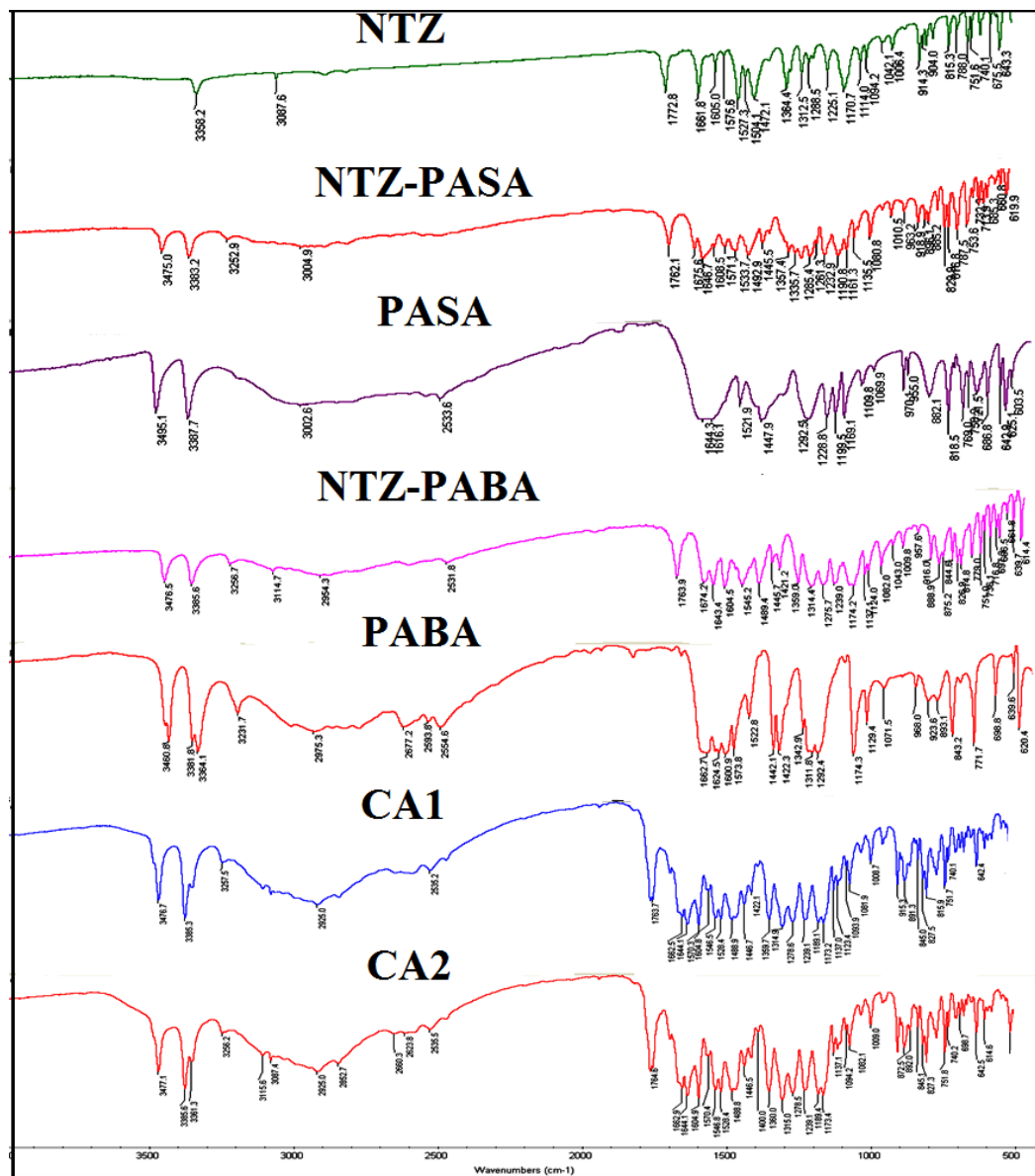


Figure 7.11 FT-IR spectra of NTZ cocrystal / alloy compared with the starting materials.

Table 7.4 IR stretching frequencies of NTZ CONH/OCOCH₃ and coformer COOH/NH₂ functional groups in the solid state (see Figure 7.10 for spectra).

Solid form	N-H/O-H stretch of acid/amide/amine	C=O stretch in amide	C=O stretch in ester	C=O stretch in acid
NTZ	3358	1661	1772	-
NTZ-PASA	3475, 3383, 3252	1646	1762	1675
PASA	3495, 3387	-	-	1644
NTZ-PABA	3476, 3385, 3258	1643	1764	1674
PABA	3460, 3381, 3363	-	-	1666
CA1	3476, 3385, 3257	1644	1763	1662
CA2	3477, 3383, 3256	1644	1764	1662

7.4.5 Thermal Analysis

Thermal analysis of two isomorphous cocrystals and cocrystal alloys were compared with NTZ shown in Figure 7.12 and Table 7.5. The data shows that two isomorphous cocrystals were exhibited sharp melting endotherm followed by decomposition. NTZ-PABA has lower melting point than individual melting points of NTZ and PABA and NTZ-PASA cocrystal exhibited intermediate melting point with respect to NTZ and PASA. Both cocrystals thermal behavior is nearly similar due to ubiquity packing in crystal structure. Interestingly cocrystals alloys CA1 and CA2 were displayed lower melting endotherms compared to parent cocrystals. It validates that these two solid forms were distinctive and different from cocrystals.

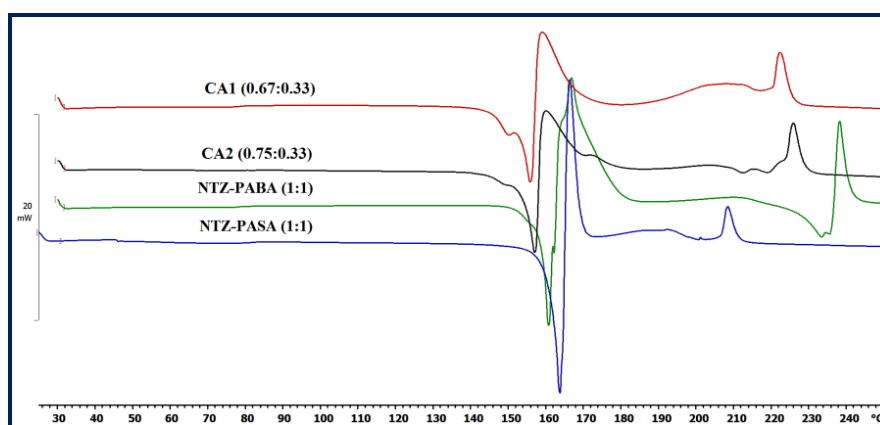


Figure 7.12 DSC thermograms of NTZ cocrystals and alloys exhibit single endotherm melting behavior. The exotherm above 200 °C is due to decomposition of coformer.

Table 7.5 Melting point of NTZ cocrystals, cocrystal alloys and coformers

S.No	Cocrystal/Cocrystal alloy	Melting Point (°C)	Coformer	Melting Point (°C)
1	NTZ-PABA	158-160	PABA	187-189
2	NTZ-PASA	159-163	PASA	150-151
3	CA1	153-155	--	--
4	CA2	152-156	--	--

Melting point of SMT-200-202 °C

7.4.6 Dissolution Studies

Given the purpose of kinetic enhancement in drug solubility (or apparent solubility) for metastable phases such as polymorphs, cocrystals and eutectics,^{26,5c} intrinsic dissolution rate (IDR) measurements were performed in 3% CTAB (cetyltrimethyl ammonium bromide) phosphate buffer (pH 7) medium for 240 minutes by the rotating disk intrinsic dissolution rate (DIDR) method at 37 °C for all these pharmaceutical solids. Interestingly, the cocrystals exhibit higher IDR than pure NTZ (which is common) but surprisingly the cocrystal alloys are even superior to the cocrystals (this is unexpected). The dissolution rate order is CA2 > CA1 > NTZ-PABA > NTZ-PASA (Figure 7.13, Table 7.6). The general observation that the higher solubility coformer (PABA, 6.1 mg/mL) gives higher dissolution rate for the cocrystal is followed in this system. Secondly, the melting point of the alloys is lower than those for the cocrystals, and this is another reason for higher solubility. Predominantly, for crystal forms of the same composition, or nearly the same composition, the lower melting solid has higher solubility. Even though the cocrystals and alloys are isomorphous/ isostructural, their dissolution rate is remarkably different. There is a similar report for isostructural cocrystals exhibiting different thermodynamic stability as explosives.²⁷

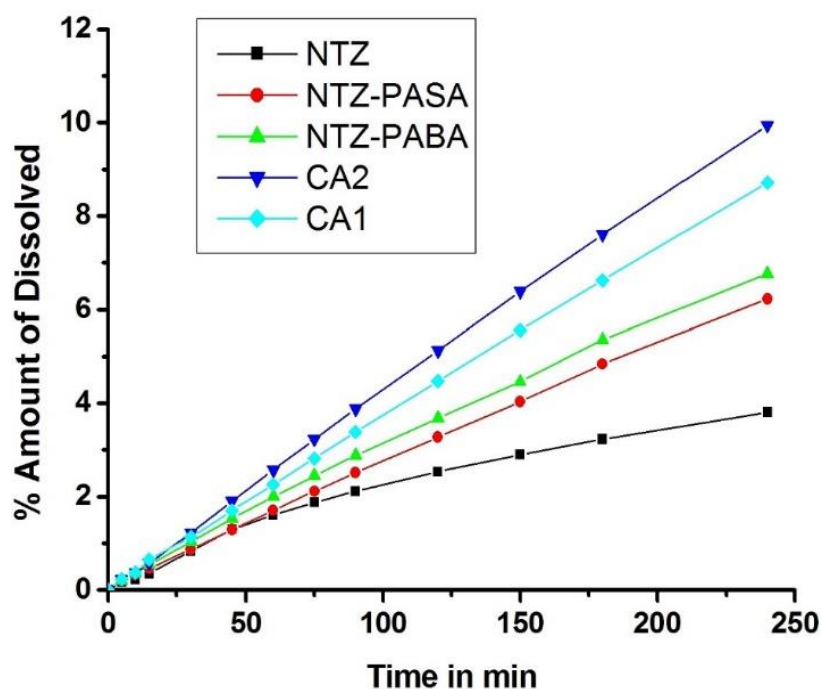


Figure 7.13 Intrinsic dissolution rates of NTZ cocrystals and cocrystal alloys in 3%CTAB (pH7) buffer medium.

Table 7.6 Intrinsic dissolution of NTZ cocrystals and its cocrystal alloys and n-fold enhancement compared to NTZ is given in parenthesis.

Compound	Solubility of coformer in water (mg/mL)	Molar Extinction coefficient ($\text{mM}^{-1} \text{cm}^{-1}$)	Intrinsic dissolution rate, IDR ($\text{mg}/\text{cm}^2/\text{min}$) ($\times 10^{-3}$) (\times) ^a
NTZ	0.007	27.9	0.073
NTZ-PASA	1.690	27.2	0.087 (x1.19)
NTZ-PABA	6.100	23.9	0.099 (x 1.35)
CA1	--	21.7	0.114 (x1.56)
CA2	--	21.5	0.125 (x1.71)

7.4.7 Pharmacokinetics

Next the pharmacokinetics of all solids was measured by oral administration of NTZ (45mg/kg, which is equivalent 500 mg human dosage) on Sprague Dwaley rats. The pharmacokinetic parameter C_{max} of cocrystals of NTZ-PABA and NTZ-PASA were quantified 2.2 and 1.9 fold increase and cocrystal alloys exhibited CA1 (1.9) and CA2 (4) folds improvement in C_{max} as soon compared to NTZ (Figure 7.14, Table 7.7). Despite the fact that there is significant increased bioavailability especially for $\text{AUC}_{(0-12)}$ and $\text{AUC}_{(0-\infty)}$ for CA2 with 3.26 and 2.47 fold and for NTZ-PABA cocrystal with 2.2 fold and 2.5 fold increased respectively once compared all to NTZ alone. The $\text{AUC}_{(0-12)}$ (total

drug delivered in 12 h) is 24.2 $\mu\text{g}\cdot\text{hr}/\text{mL}$ for CA2 compared to 7.5 $\mu\text{g}\cdot\text{hr}/\text{mL}$ for NTZ (it transforms to TIZ in vivo) and which is best and optimized lead to carry out further toxicology and human clinical trials as a repurposed and reposition of anti TB drug

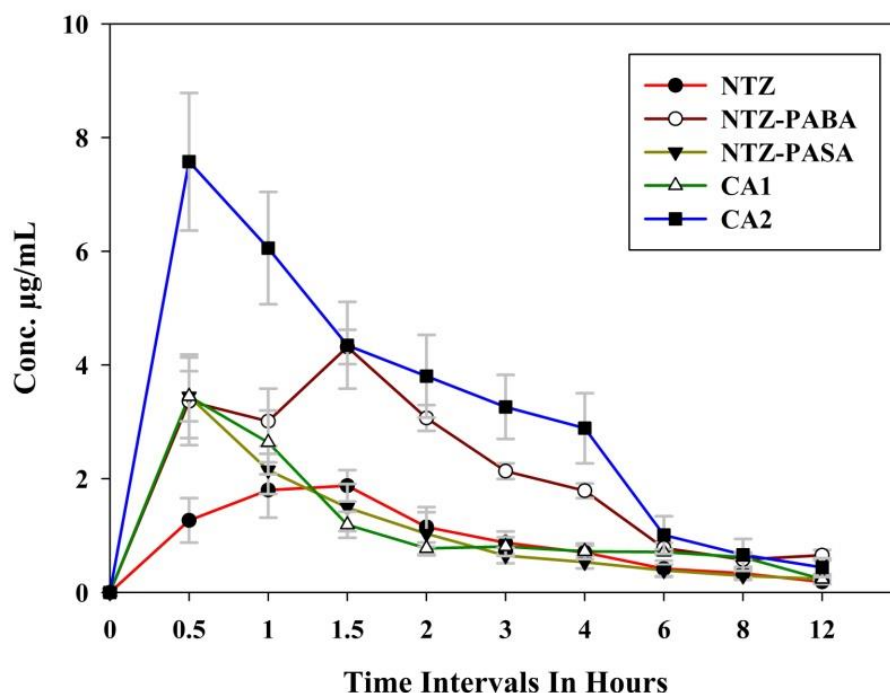


Figure 7.14 Mean Plasma concentration of TIZ vs. Time profile NTZ, cocrystals and cocrystal alloys.

Table 7.7 Pharmacokinetic parameters of NTZ cocrystals and alloys. SD for 6 readings is given in parenthesis.

Solid form	NTZ	NTZ-PABA	NTZ-PASA	CA1(0.67-0.33)	CA2(0.75-0.25)
Parameter	n = 6	n = 6	n = 6	n = 6	n = 6
T_{\max} (min)	90 (0.42)	90 (0.55)	30 (0.20)	30 (0.26)	30 (0.00)
C_{\max} ($\mu\text{g}/\text{mL}$)	1.88 (0.91)	4.32 (0.30)	3.45 (0.74)	3.45 (0.44)	7.58 (1.21)
$T_{1/2}$ (h)	3.85 (0.29)	4.20 (0.90)	3.68 (0.95)	4.57 (0.60)	2.96 (0.67)
$AUC_{(0-12)}$ ($\mu\text{g}\cdot\text{h}/\text{mL}$)	7.47 (1.07)	17.06 (3.80)	7.89 (1.13)	10.01 (2.58)	24.18 (2.14)
$AUC_{(0-\infty)}$ ($\mu\text{g}\cdot\text{h}/\text{mL}$)	42.50 (6.89)	107.2 (22.15)	43.17 (9.66)	67.62 (21.95)	105.27 (36.80)

7.5 Conclusions

In summary, the NTZ cocrystal investigation resulted isomorphous cocrystals and cocrystal alloys. In all of these, drug and coformer associated via N–H···O and O–H···N heterodimer interactions between amidothiazole-acid functional groups in crystal structure. Further, all pharmaceutical solids were exhibited enhanced dissolution rates and pharmacokinetics than NTZ. Among them cocrystal alloy CA2 is shown four folds enhancement in bioavailability and 1.7 times higher dissolution rate than pure NTZ. However, similarity in crystal structures has not translated into the properties. The present study shows that non-stoichiometric multicomponent solid forms present yet another opportunity for oral drug bioavailability alongside the stoichiometric cocrystals and salts. These results open opportunities for the repositioning of nitazoxanide as a multi-strain resistant, anti-TB drug with improved bioavailability.

7.6 Experimental Section

Nitazoxanide was extracted from Nizonide tablets (500 mg) using chloroform solvent. The pure drug was crystallized from methanol. This crystalline powder was used for all experiments (PXRD match of extracted and purified nitazoxanide with the reported X-ray crystal structure of Refcode QUZWOY and purity is confirmed by HPLC 98.6%. The other compounds PABA ($\geq 99\%$), PASA (99%), CTAB ($\geq 99\%$) were purchased from Sigma-Aldrich (Hyderabad, India). Solvents (purity $>99\%$) were purchased from Hychem Laboratories (Hyderabad, India). Water filtered through a double deionized purification system (Aqua DM, Bhanu, Hyderabad, India) was used in all experiments.

Preparation of cocrystals and cocrystal alloys

NTZ-PABA cocrystal: NTZ (307.2 mg) and PABA (137.1 mg) in 1:1 molar ratio were ground in slurry of 5 mL chloroform for 8 h ($n=6$). The formation of cocrystal was confirmed by PXRD and DSC. 30 mg of this material was dissolved in 5 mL chloroform and left for slow evaporation at ambient conditions. Single crystals suitable for X-ray diffraction were obtained after 4-5 days.

NTZ-PASA cocrystal: NTZ (307.2 mg) and PASA (153.1mg) in 1:1 molar ratio were ground in slurry of 5 mL acetone for 2 h ($n=6$). The formation of cocrystal was confirmed by PXRD and DSC. 30 mg of this material was dissolved in 5 mL chloroform

and left for slow evaporation at ambient conditions. Single crystals suitable for X-ray diffraction were obtained after 4-5 days.

Physical mixtures of NTZ-PABA and NTZ-PASA in an equivalent ratio (1:1) were dissolved in 5 mL chloroform and left for slow evaporation at ambient conditions. Single crystals suitable for X-ray diffraction were obtained after 4-5 days. Two crystals were solved and refined as CA1 (0.67:0.33) and CA2 (0.75:0.25) with the composition NTZ-PABA : NTZ-PASA. The presence of other stoichiometry alloys in the crystals harvest is being explored.

CA1 (0.67 : 0.33): The cocrystal alloy bulk material was obtained by grinding NTZ-PABA and NTZ-PASA in 0.67:0.33 stoichiometry with a few drops of n-hexane added in a liquid-assisted method for 30 min (n=6).

CA2 (0.75 : 0.25): The cocrystal alloy bulk material was obtained by grinding NTZ-PABA and NTZ-PASA in 0.75:0.25 stoichiometry with a few drops of n-hexane added in a liquid-assisted method for 30 min (n=6).

Powder X-ray diffraction

Powder X-ray diffraction was recorded on Bruker D8 Advance diffractometer (Bruker-AXS, Karlsruhe, Germany) using Cu-K α X-radiation ($\lambda = 1.5406 \text{ \AA}$) at 40 kV and 30 mA power. X-ray diffraction patterns were collected over the 2θ range $5\text{--}50^\circ$ at a scan rate of $5^\circ/\text{min}$. Powder Cell 2.4(Federal Institute of Materials Research and Testing, Berlin, Germany) was used for Rietveld refinement of experimental PXRD and calculated lines from the X-ray crystal structure.²⁸

Vibrational spectroscopy

Thermo-Nicolet 6700 FT-IR-NIR spectrometer with NXR FT-Raman module (Thermo Scientific, Waltham, MA) was used to record IR spectra. IR spectra were recorded on samples dispersed in KBr pellets. Data were analyzed using the Omnic software (Thermo Scientific, Waltham, MA).

Thermal analysis

Differential scanning calorimetry was performed on Mettler-Toledo DSC 822e module, (Mettler-Toledo, Columbus, OH). Samples were placed in crimped but vented aluminum pans for DSC experiments. The typical sample size is 3-5 mg for DSC. The temperature range for the heating curves was 30-250°C, and the sample was heated at a rate of 5 °C/min. Samples were purged in a stream of dry nitrogen flowing at 80 mL/min.

X-ray crystallography

X-ray reflections were collected on Oxford CCD X-ray diffractometer (Yarnton, Oxford, UK) equipped with Mo-K α radiation ($\lambda = 0.71073 \text{ \AA}$) and Cu-K α X-radiation ($\lambda = 1.5406 \text{ \AA}$) source. Data reduction was performed using CrysAlisPro 171.33.55 software.^{29a} Crystal structures were solved and refined using Olex2-1.0 with anisotropic displacement parameters for non-H atoms.^{29b} Hydrogen atoms were experimentally located through the Fourier difference electron density maps in all crystal structures. All O-H and C-H atoms were geometrically fixed using HFIX command in SHELX-TL program of Bruker-AXS. X-ray reflections for Syringic acidurea Cocrystal was collected on Bruker D8 Quest diffractometer equipped with a graphite mono chromator and Mo-K α fine-focus sealed tube ($\lambda = 0.71073 \text{ \AA}$). Data reduction was performed using Bruker SAINTS Software. Intensities were corrected for absorption using SADABS, and the structure was solved and refined using SHELX-97. All non-hydrogen atoms were refined anisotropically. Hydrogen atoms on hetero atoms were located from difference electron density maps and all C-H hydrogens were fixed geometrically. Hydrogen bond geometries were determined in Platon. X-Seed was used to prepare packing diagrams. X-Seed^{29c,d} was used to prepare packing diagrams.

Dissolution and solubility measurements

The solubility curves of NTZ and binary solids were measured using the Higuchi and Connor method in 3% CTAB (cetyltrimethyl ammonium bromide) phosphate buffer (pH 7) medium at 30 °C. First, the absorbance of a known concentration of the salt was measured at the given λ_{max} (NTZ 435 nm) on Thermo Scientific Evolution 300 UV-vis spectrometer (Thermo Scientific, Waltham, MA). These absorbance values were plotted against several known concentrations to prepare the concentration vs. intensity calibration curve. From the slope of the calibration curves, molar extinction coefficients for NTZ, cocrystals, and cocrystal alloys were calculated. Intrinsic dissolution rate

experiments were carried out on a USP certified Electrolab TDT-08L Dissolution Tester (Mumbai, MH). Dissolution experiments were performed for 240min in 3% CTAB buffer medium at 37 °C.³⁰ Prior to IDR estimation, standard curves for all the compounds were obtained spectrophotometrically at their respective λ_{\max} . The respective molar extinction coefficients were used to determine the IDR values. For IDR measurements, 150 mg of the compound was taken in the intrinsic attachment and compressed to a 0.5 cm² disc using a hydraulic press at pressure of 4.0 ton/inch² for 5 min. The intrinsic attachment was placed in a jar of 500 mL medium preheated to 37 °C and rotated at 100 rpm. 5 mL aliquots were collected at specific time intervals and concentration of the aliquots were determined with appropriate dilutions from the predetermined standard curves of the respective compounds. This experiment was done by single time.

Animal protocol

This pharmacokinetic study was carried in strict compliance of the Committee for the Purpose of Control and Supervision of Experimentation on Animals (546/02/A/CPSCEA), Government of India. The animal handling procedures were reviewed and approved by the Institutional Animal Ethical Committee of Virchow Biotech Private Limited, Department of Preclinical Toxicology, Hyderabad, India. Adult male Sprague Dawley rats (about 200±50g) were purchased from Sainath Agency Limited, Hyderabad, India. The rats were maintained on a 12 h light/dark cycle in a specific free pathogen facility. The rats had free accesses to food and water throughout the study unless rats were fasted overnight with free access to water before the experiment.

Pharmacokinetic profile

To assess the pharmacokinetic profile, 12 rats are selected randomly and divided equally in to two groups (n=6). Each group received single oral dosage of NTZ, cocrystals, and cocrystal alloys through oral gavage at the dose of 45 mg/kg (equivalent to human dosage of 500 mg/kg) for rat body weight. Serial blood (400 µL) samples were collected from retro-orbital plexus into lithium heparin tube of two groups before dosing and at 30, 60, 90, 120, 150, 180, 240, 360, 480 and 720 min. Blood samples were centrifuged at 2,000 g (4 °C) for 15 min, the harvested plasma was collected and stored at -80 °C until HPLC analysis. The plasma exposure was calculated by linear trapezoidal method (area

under the plasma concentration-time plots from 0 to 12 h ($AUC_{0 \rightarrow 12h}$) in all rats receiving oral NTZ and its cocrystal or alloy.

HPLC assay

HPLC was carried out on a Shimadzu LC-20AD liquid chromatography, Diode Array SPD-M20A detector, degasser DGU-20A3 with a RP HPLC column C18G (250 x 4.6 mm, 5 μ m particle size), which was protected by a guard column of 33 mm x 4.6 mm. UV absorbance at 350nm was used to quantify the drug. For liquid extraction, 200 μ L acetonitrile solution was added to 200 μ L plasma. After vigorous vortex, the sample was centrifuged at 8000g at 4 °C for 15 min. Finally, the supernatant liquid was placed in a glass insert, and injected into HPLC. The calibration curve was obtained by TIZ (linearity $R^2 > 0.999$). The mobile phase consists of 5% acetic acid–acetonitrile (40:60), which was filtered through 0.45 μ m membrane filter, degassed by sonicator, and delivered at a rate of 1.5 mL/min. The supernatant plasma of 20 μ L was injected into HPLC with a run time of 12 min.

7.7 References

1. (a) WHO global tuberculosis report 2013.
http://apps.who.int/iris/bitstream/10665/91355/1/9789241564656_eng.pdf
(b) V. Kumar, A. K. Abbas, N. Fausto, M. R. Robbins. Basic Pathology (8th Ed.) Saunders Elsevier. 2007, 516–522; (c) F. Wang. R. Langley, G. Gulten, L. G. Dover, G. S. Besra, J. W. R. Jacobs, J. C. Sacchetti, *J. Exp. Med.* 2007, **204**, 73.
2. (a) P. Andersen and T. M. Doherty, *Nat. Rev. Microbiol.*, 2005, **3**, 656; (b) Y. Hiraishi, S. Nandakumar, S. -O. Choi, J. W. Lee, Y.-C. Kim, J. E. Posey, S. B. Sable and M. R. Prausnitz, *Vaccine*, 2011, **29**, 2626.
3. (a) <http://www.who.int/mediacentre/factsheets/fs104/en/>.
(b) http://whqlibdoc.who.int/publications/2010/9789241547833_eng.pdf.
4. M. D. Iseman, *New Engl. J. Med.*, 1993, **329**, 784.
5. (a) H. Bhutani, S. Singh, K. C. Jindal and A. K. Chakraborti, *J. Pharm. Biomed. Anal.*, 2005, **39**, 892; (b) S. Singh and B. Mohan, *Int. J. Tuberc. Lung Dis.*, 2003, **7**, 298. (c) S. Cherukuvada, A. Nangia *Chem. Commun.*, 2014, **50**, 906.

6. (a) N. R. Gandhi, A. Moll, A. W. Sturm, R. Pawinski, T Govender, U. Laloo, K. Zeller, J Andrews, and G. Friedland. *Lancet*. 2006, **368**, 1575;(b) A. H. Diacon, R. F. Patientia, A. Venter, P. D. van Helden, P. J. Smith, H. McIlleron, J. S. Maritz, and P. R. Donald . *Antimicrob Agents Chemother*. 2007, **51**, 2994.
7. (a) L. Pedro S. D. Carvalho, G. Lin, X. Jiang and C. Nathan, *J. Med. Chem.*, 2009, **52**, 5789; (b) L. Pedro S. D Carvalho, C. M. Darby, K. Y. Rhee, and C. Nathan *ACS Med. Chem. Lett*. 2011, **2**, 849; (c) K. Shigyo, O. Ocheretina, Y.M. Merveille, W.D. Johnson, J.W. Pape, C. F. Nathan, D. W. Fitzgerald *Antimicrob Agents Chemother*. 2013, **57**, 2834.
8. (a) <http://www.drugbank.ca/drugs/DB00507> (b) M. I. Ruiz-Olmedo, J. L. Gallegos-Perez, K. G. Calderon-Gonzalez, J. Franco-Perez, H. Jung-Cook, *Pharmazie*, 2009, **64**, 419.
9. J.F. Rossignol and R. Cavier, *United States Patent* No 3,950,351, April 13, 1976; (b) J.F. Rossignol, H. Maisonneuve. *Am. J. Trop. Med. & Hyg.* 1984, **33**, 511.
10. J. F. Rossignol *Antiviral Res.* 2014, **110**, 94.
11. H. Fan-Minogue, S. Bodapati, D. Solow-Cordero , A. Fan , R. Paulmurugan, T. F. Massoud, D.W. Felsher , and S. S. Gambhir. *Mol Cancer Ther* 2013, **12**, 1896.
12. (a) M. A. Sajid , V. Choudhary *J. Drug Deliv.& Ther.* 2012, **2**, 96; (b) A. P. Sherje, A. Rahigude, S. Warma, S. D. Vanshiv, *Int. J. Chem. Tech. Res.* 2010, **2**, 1965.
13. R. J. Glisoni , A. Sosnik. *J. Nanosci. Nanotechnol.* 2014, **14**, 4670.
14. F. P. Bruno, M. R. Caira, G. A. Monti, D. E. Kassuha, N. R. Sperandeo, *J. Mol. Str.*, 2010, **984**, 51.
15. B. C. Félix-Sonda, J. Rivera-Islas, D. Herrera-Ruiz, H. Morales-Rojas, and H. Höpfl, *Cryst. Growth Des.*, 2014, **14**, 1086.
16. (a) N. K. Duggirala, M. L. Perry, Ö. Almarsson and M. J. Zaworotko, *Chem. Commun.*, 2016, **52**, 640; (b) S. Aitipamula, P. S. Chow and R. B. H. Tan, *CrystEngComm*, 2014, **16**, 3451; (c) J. W. Steed, *Trends Pharmacol Sci.*, 2013, **34**, 185.
17. (a) S. P. Thomas, R. Sathishkumar and T. N. G. Row *Chem. Commun.*, 2015, **51**, 14255; (b) T. Frišćić, A.V. Trask, W.Jones and W. D. S. Motherwell, *Angew.*

- Chem. Int. Ed.*, 2006, **45**, 7546; (c) A. A. Bredikhin, Z. A. Bredikhina, D. V. Zakharychev, A. T. Gubaidullin and R. R. Fayzullin *CrystEngComm*, 2012, **14**, 648; (d) K. D. Prasad, S. Cherukuvada, L. D. Stephen and T.N. Guru Row. *CrystEngComm*, 2014, **16**, 9930.
18. (a) P. Vishweshwar, A. Nangia and V. M. Lynch, *J.Org. Chem.*, 2002, **67**, 556; (b) T. R. Shattock, K. K. Arora, P. Vishweshwar and M. J. Zaworotko, *Cryst. Growth Des.*, 2008, **8**, 4533; (c) R. Santra, N. Ghosh and K. Biradha, *New J. Chem.*, 2008, **32**, 1673.
- (d) B. R. Bhogala, S. Basavoju and A. Nangia, *CrystEngComm*, 2005, **7**, 551; (e) B. R. Bhogala, S. Basavoju and A. Nangia, *Cryst. Growth Des.*, 2005, **5**, 1683; (f) B. R. Bhogala and A. Nangia, *Cryst. Growth Des.*, 2003, **3**, 547; (g) C. B. Aakeröy and D. J. Salmon, *CrystEngComm*, 2005, **7**, 439; (h) C. B. Aakeröy, A. M. Beatty and B. A. Helfrich, *J. Am. Chem. Soc.*, 2002, **124**, 14425; (i) C. B. Aakeröy, A. M. Beatty and B. A. Helfrich, *Angew. Chem., Int. Ed.*, 2001, **40**, 3240; (j) R. D. B. Walsh, M. W. Bradner, S. Fleishman, L. A. Morales, B. Moulton, N. Rodríguez-Hornedo and M. J. Zaworotko, *Chem. Commun.*, 2003, 186.
19. Generally Regarded as Safe chemicals by the US-FDA.
<http://www.fda.gov/Food/IngredientsPackagingLabeling/FoodAdditivesIngredients/ucm091048.htm>
20. (a) D. Cinčić, T. Friščić, W. Jones, *New J. Chem.*, 2008, **32**, 1776; (b) S. Ebenezer, P. T. Muthiah, R. J. Butcher, *Cryst. Growth Des.*, 2011, **11**, 3579; (c) N. K. Nath, B. K. Saha, A. Nangia. *New J. Chem.*, 2008, **32**, 1693; (d) A. Kálmán, L. Párkányi, G. Argay, *Acta Crystallogr.*, 1993, **B49**, 1039.
21. (a) T. Gelbrich, T. L. Threlfall, M. B. Hursthouse, *CrystEngComm*, 2012, **14**, 5454; (b) T. Gelbrich, M. B. Hursthouse, *CrystEngComm*, 2006, **8**, 448; (c) T. Gelbrich, M. B. Hursthouse, *CrystEngComm*, 2005, **7**, 324.
22. A, Anthony, M. Jaskólski, A. Nangia and G. R. Desiraju *Chem. Commun.*, 1998, 2537.
23. J. Zhang, Y. Zhang, J. Fang, K. Lu, Z. Wang, W. Ma, and Z. Wei. *J. Am. Chem. Soc.*, 2015, **137**, 8176.
24. J. B. Sherman, K. Moncino, T. Baruah, G. Wu, S. R. Parkin, B. Purushothaman, R. Zope, J. Anthony and M. L. Chabiny. *J. Phys. Chem. C*, 2015, **119**, 20823.
25. M. A. Oliveira, M. L. Peterson and D. Klein. *Cryst. Growth Des.*, 2008, **8**, 4487

26. N. J. Babu and A. Nangia, *Cryst. Growth Des.*, 2011, **11**, 2662.
27. K. B. Landenberger, O. Bolton and A. J. Matzger, *Angew. Chem. Int. Ed.*, 2013, **52**, 6468.
28. Powder Cell, a program for structure visualization, powder pattern calculation and profile fitting. Accessed at www.ccp14.ac.uk/tutorial/powdercell.
29. (a) CrysAlis CCD and CrysAlis RED, Versions 1.171.33.55, Oxford Diffraction, Oxford, 2008; (b) O. V. Dolomanov, L. J. Bourhis, R. J. Gildea, J. A. K. Howard, H. Puschmann, *J. Appl. Crystallogr.* 2009, **42**, 339; (c) L. J. Barbour, *Supramol. Chem.* 2001, **1**, 189; (d) L. J. Barbour, X-Seed, Graphical Interface to SHELX-97 and POV-Ray; University of Missouri-Columbia, Columbus, MO, 1999.
30. X. L. Yu, A. S. Carlin, G. L. Amidon, A. S. Hussain, *Int. J. Pharm.* 2004, **270**, 221.

CHAPTER EIGHT

Conclusions and Future Prospects

This thesis deals with the supramolecular design, screening, identification, characterization and application of various multi-component solid forms of Active pharmaceutical Ingredients (APIs) and bioactive molecules. Extensive studies on various solid forms such as polymorphs (Chapter 4), salts (Chapter 4 and 5), cocrystals (Chapter 2, 3 and 7), coamorphous (Chapter 6) and alloys (Chapter 7) of several APIs and bioactive molecules were carried out with the intent of understanding the phenomena that govern the physicochemical behavior of pharmaceuticals which leads to improved medicines and aid to pharmaceutical form development, intellectual property management and also avoid pit-falls in during commercialization.

Chapter 1 deliberates about the introduction of crystal engineering, supramolecular synthons and hydrogen bonding rules. In addition, the discovery, design, synthesis and pharmaceutical utility several pharmaceutical solids were discussed.

Screening of the new binary solids (cocrystals) to andrographolide has been carried out in chapter 2. It is a bioactive molecule with diverse pharmacological actions. Despite being safe at high doses of 17 g/kg per day in humans, the efficacy of AP is limits in clinical application by poor aqueous solubility (46 mg/L) and oral bioavailability of 2.67% (reported in rats). A significant drop in the bioavailability of AP is due to an inactive metabolism, as a result four inactive metabolites isolated from humans and rats. Three of the AP metabolites are isomers/diastereomers of 14-deoxy-12-sulfo-andrographolide, and the fourth product is the S-conjugate (sulfated derivative) of AP. Among these, the main inactive metabolite of AP was identified as 14-deoxy-12-(*R*)-sulfo-andrographolide. In order to inhibit this chemical transformation and improves the solubility of AP, we explored the structural landscape via cocrystallization using liquid assisted grinding and isothermal crystallization techniques, where we screened AP with various GRAS coformers of phenols and carboxylic acids which resulted in cocrystals with Vanillin (VAN), Vanillic acid (VLA), Salicylic acid (SLA), Resorcinol (RES), and Guaiacol (GUL). These cocrystals were characterized by various thermal,

spectroscopic and diffraction methods. Among the novel cocrystals of AP, with the objective to inhibit/stop the undesired transformation of sulfation which reduces the activity of andrographolide as a drug, AP–SLA cocrystal showed the best result and there is no secondary chemical reactions. The acidic nature of the ortho-hydroxy acid in SLA and lower pK_a were reasoned as the cause for this inhibitory effect. The 12 fold improvement in solubility and 3 times faster dissolution rate of AP–SLA is an added benefit for oral formulation.

In chapter 3, Sulfamethizole (SMT) is a sulfonamide class antibiotic drug that acts through the competitive inhibition of folate synthesis in microorganisms. Even though SMT has better solubility, (1.05 g/L at 37 °C in water) but it has short half-life (2.1 h) due to rapid metabolism, leads to fast elimination. Cocrystallization of SMT with various GRAS coformers was performed with the intention that the resulting cocrystals would have the appropriate hydrogen bonding interactions to lower the solubility of SMT which in turn might improve its residence time at the site of action and increase its therapeutic efficacy. The cocrystals were produced by co-grinding and tested by powder X-ray diffraction, DSC and IR. The powder samples were used as seeds in evaporative crystallization to obtain single crystals for X-ray diffraction. Cocrystals with adipic acid (ADP), *p*-aminobenzoic acid (PABA), vanillic acid (VLA), *p*-aminobenzamide (ABA), suberic acid (SBA), 4,4'-bipyridine (BIP), and a salt with oxalic acid (OA) were obtained. In the crystal structures, three aliphatic dicarboxylic acids coformers interact with SMT via different hydrogen bonding synthons. SMT-ADP has strong acid-amine synthon, SMT-SBA cocrystal has weak C–H...O hydrogen bonds together with homomeric interactions, and in SMT-OA structure the proton is transferred from OA to SMT. The uncommon chalcogen-oxygen (S...O) interaction was observed in SMT-ADP S...N interaction in SMT-BIP. Further dissolution and equilibrium solubility experiments on these cocrystals and salt exhibited reduced dissolution and solubility profiles than reference drug which is ascribed to efficient molecular packing and stronger interactions through strong homomeric and heteromeric N–H...N and N–H...O interactions in the crystal lattice of salt/cocrystal. Based on this low solubility and good stability of SMT cocrystals/salt, they can be useful in addressing the poor residence time and faster elimination issues associated with SMT drug. IDR and equilibrium solubility of adducts were reduced compared to SMT.

In chapter 4, we identified and demonstrated the novel polymorphs of Glibenclamide salts, and explained how isostructurality by exchanging the counter ion

of simple NH_4^+ ion (simple cation) with Na^+/K^+ ion (metal cation). Initially we synthesized novel GBA salts and corresponding hydrates using NaOH, KOH and NH_3 . We found that the GBA-Na salt exists in dimorphic and one hydrate (form I, II and III) and GBA-K exist as an anhydrate and hydrate (form I and II). We observed an interesting fact that the GBA-Na form I has square pyramidal geometry and GBA-form II and III were shown distorted octahedral geometry and all these forms has different packing arrangements. We also found GBA-Na form I & GBA- NH_4 and GBA-K form I and GBA- NH_4 are isostructural pairs which are having packing and powder XRD similarities. Solubility studies shown that all the obtained GBA salts having very good solubility in water and pH 7 buffer media. All these forms are adsorbed significant amount of water (0.4 to 6.2% range for all salts) during adsorption and at the same time loses the water during desorption cycle. It indicates the all these five solid forms were reversible without any hysteresis. However, with significant increase in the solubility and stability of GBA-K form I optimum solid for pharmaceutical development.

Chapter 5 explains about the Lornoxicam (LXM), is a BCS class II category drug with low solubility and high permeability (solubility of LXM in water 15 mg/L). To improve the solubility or dissolution rate of BCS class-II APIs, having ionizable group, the foremost option is pharmaceutical salt formation. Therefore intended for LXM we planned a systematic study of the counter ion (acid and base salt formers) effect on conformational/structural modulation in solid state and its solubility enhancement for better formulation discussed in this chapter. We selected two strong acids (hydrochloric acid, HCL and methane sulfonic acid MSA) and two strong bases (piperazine, PIP and ammonia, AMM) each and the high ΔpK_a values invariably resulted in salts of LXM by slurry technique. All these adducts were characterized by powder X-ray diffraction, DSC and IR. The powder materials salt and guest free form were used as seeds in evaporative crystallization to obtain single crystals for single crystal X-ray diffraction. The crystal structures were solved and refined. In crystal structures of LXM and its salts, adopts three conformations (designated as *A*, *B*, and *C*) and all these salts exhibited good solubility and powder dissolution rate than the parent drug LXM. LXM salts with acids exhibited higher solubility than the base salts, e.g. LXM-MSA salt has two times higher AUC compared to PIP and AMM salts. However, the base salts are more stable than the acid salts, in line with the solubility-stability inverse correlation. This is a systematic study of conformational changes in a drug molecule due to counter-ion and partner molecules.

The present study with LXM salts offers acidic and basic counter ions for an amphoteric drug to improve its physicochemical properties.

In Chapter 6, novel coamorphous of curcumin-artemisinin was discovered using rotavaporization technique. Although the initial interest is to develop novel cocrystal/eutectic between them for addressing poor solubility and bioavailability of curcumin. Rotavaporization of curcumin and artemisinin (1:1) were dissolved in ethanol solution, resulted coamorphous solid. The coamorphous nature was confirmed by PXRD (broad halo) and DSC (single glass transition). The excess thermodynamic functions of this coamorphous solid was exploited by performing dissolution and Pharmacokinetic studies. The intrinsic dissolution rate of this coamorphous solid was 2.6 times faster than pure curcumin. Pharmacokinetic study of coamorphous CUR-ART in SD rats exhibited high curcumin concentration of 1 µg/mL at 30 min, and bioavailability AUC of 2.6 µg.h/mL. Our result is significant in light of the fact that curcumin has low bioavailability due to short half-life of 30-120 min in vivo.

In chapter 7, novel cocrystals and alloys of Nitazoxanide were discovered by using slurry and liquid assisted grinding techniques. Nitazoxanide (NTZ) is a prodrug of nitrothiazolyl-salicylamide derivative used as an anti-protozoal agent and it has broad spectrum activities against many diseases. However, NTZ has poor aqueous solubility (7.55×10^{-3} mg/mL in water) and limited bioavailability (258 ng/mL, 7.5 mg/kg dose in rats) due to the inactive metabolism. To improve the solubility and bioavailability of NTZ, here we prepared two cocrystals with para-aminosalicylic acid (PASA) and para-aminobenzoic acid (PABA) coformers (Scheme 7.2). As well as solid solutions of cocrystal alloys (CA) NTZ-PABA : NTZ-PASA of 0.75 : 0.25 (CA1) and 0.67 : 0.33 (CA2) compositions. All of these pharmaceutical solids were characterized by X-ray diffraction, thermal analysis (DSC), and (FT-IR) spectroscopic techniques. Moreover, all these pharmaceutical solids were exhibited enhanced dissolution rates and pharmacokinetics than NTZ. Among them cocrystal alloy CA2 (0.67 : 0.33 of NTZ-PABA : NTZ-PASA) is showed four folds enhancement in bioavailability and 1.7 times higher dissolution rate than pure NTZ. The present study shows that non-stoichiometric multi-component solid forms present yet another opportunity for oral drug bioavailability alongside the stoichiometric cocrystals and salts. These results open opportunities for the repositioning of nitazoxanide as a multi-strain resistant anti-TB drug with improved

bioavailability. To conclude, physicochemical properties and bioavailability of some important drugs and bioactive molecules were improved by new solid form modifications.

Future prospects

Andrographolide-Salicylic acid cocrystal (chapter 2) and Sulfamethazole cocrystal and salt (chapter 3) can be further attempted for pharmacokinetics study. It would be an interesting to see the effect of cocrystallization on the bioavailability of both the cocrystals in terms of biotransformation and extended release. Further high solubility of Glibenclamide-potassium and Lornoxicam-mesylate salts in chapter 4 and 5 used as an alternative formulations in future, provided their bioavailability is expected to be better than the parent drugs. In chapter 6 discussion of curcumin-artemisinin high bioavailability it can be further evaluated for anti-malarial activity and in chapter 7, because of nitazoxanide anti tuberculosis activity, cocrystal and alloys can be further tested for activity on live culture.

Coamorphous and eutectics of novel pharmaceutical solids were reported in literature. Though coamorphous is an aperiodic structure (discussed in chapter 6) and eutectic full characterization at molecular packing level is a current challenge to dissect and analyze the local domain structure of these compounds. Techniques like atomic pair distribution function (PDF) approach and extended X-ray absorption fine-structure spectroscopy (EXAFS) are used to understand local structure of materials and may be useful in understanding the internal crystal lattice of eutectic compositions.

LIST OF PUBLICATIONS

1. Novel Furosemide Cocrystals and Selection of High Solubility Drug Forms.
N. Rajesh Goud, Swarupa Gangavaram, **Kuthuru Suresh**, Sharmistha Pal,
Sulur G. Manjunatha, Sudhir Nambiar, and Ashwini Nangia.
J. Pharm Sci. **2012**, *101*, 664–680.
2. Fast Dissolving Eutectic Compositions of Curcumin.
N. Rajesh Goud, **Kuthuru Suresh**, Palash Sanphui and Ashwini Nangia
Int. J. Pharm. **2012**, *439*, 63–72.
3. Solubility and Stability Advantage of Aceclofenac Salts.
N. Rajesh Goud, **Kuthuru Suresh** and Ashwini Nangia
Cryst. Growth Des. **2013**, *13*, 1590–1601.
4. Solid State Forms of Andrographolide,
Kuthuru Suresh, N. Rajesh Goud and Ashwini Nangia
Indian patent, **2013**, Application no. No. 3328/CHE/2013.
5. Andrographolide: Solving Chemical Instability and Poor Solubility by
Means of cocrystals.
Kuthuru Suresh, N. Rajesh Goud and Ashwini Nangia
Chem. Asian J. **2013**, *8*, 3032–3041.
6. Lornoxicam Salts: Crystal Structures, Conformations, and Solubility.
Kuthuru Suresh and Ashwini Nangia
Cryst. Growth Des. **2014**, *14*, 2945–2953.
7. Novel Solid State Forms of Curcumin.
Kuthuru Suresh, M. K. Chaitanya Mannava, and Ashwini Nangia
Indian patent, **2014**, Application No. 4931/CHE/2014.

8. A Novel Curcumin–Artemisinin Coamorphous Solid: Physical properties and Pharmacokinetic profile.
Kuthuru Suresh, M. K. Chaitanya Mannava and Ashwini Nangia
RSC Adv., **2014**, 4, 58357–58361.

9. Preclinical Bioavailability-Bioequivalence and Toxicokinetic Profile of Stable Succinic Acid Cocrystal of Temozolomide.
Edula Sravani, M. K. Chaitanya Mannava, Damandeep Kaur, B. R. Annapurna, Ronaq Ali Khan, **Kuthuru Suresh**, Sudhir Mittapalli, Ashwini Nangia, and B. Dinesh Kumar.
Curr.Sci. **2015**, 108, 1097–1106.

10. Novel Synthons in Sulfamethizole Cocrystals: Structure-Property relations and Solubility studies.
Kuthuru Suresh, Vasily S. Minkov, Kranthi Kumar Namila, Elizaveta Derevyannikova, Ashwini Nangia and Elena V. Boldyreva.
Cryst. Growth Des. **2015**, 15, 3498–3510.

11. A Furosemide-Isonicotinamide Cocrystal: An Investigation of Properties and Extensive Structural disorder
Hannah E. Kerr, Lorna K. Softley, **Kuthuru Suresh**, Ashwini Nangia, Paul Hodgkinson and Ivana Radosavljevic Evans
CrystEngComm. **2015**, 17, 6707–6715.

12. Enhanced Bioavailability in the Oxalate Salt of Anti-TB Drug Ethionamide
M. K. Chaitanya Mannava, **Kuthuru Suresh** and Ashwini Nangia
Cryst. Growth Des. **2016**, 16, 1591–1598.

13. Color Polymorphs of Aldose Reductase Inhibitor Epalrestat: Configurational, Conformational and Synthon differences
Battini Swapna, **Kuthuru Suresh** and Ashwini Nangia
Chem. Commun., **2016**, 52, 4037–4040.

14. Cocrystals and Alloys of Nitazoxanide: Enhanced Pharmacokinetics
Kuthuru Suresh, M. K. Chaitanya Mannava and Ashwini Nangia
Chem. Commun., **2016**, 52, 4223–4226.
15. Structural Characterization and Physicochemical Property Evolution of
Naproxen-Picolinamide Cocrystal
Hannah Kerr, Lorna K. Softley, **Kuthuru Suresh**, Paul Hodgkinson and
Ivana Radosavljevic Evans
(Manuscript to be communicated)
16. Polymorphism, Isostructurality and Structure-Property Relations:
Glibenclamide Salts
Kuthuru Suresh, U.B.Rao Khandavilli, Anilkumar Gunnam and Ashwini
Nangia
(Manuscript under preparation)
17. Cocrystallization Methodology for Transformation of Zwitterion to Neutral
in solid state: A Case Study of Sparfloxacin
Anilkumar Gunnam, **Kuthuru Suresh**, Ramesh Ganduri and Ashwini
Nangia
(Manuscript under preparation)

PARTICIPATION IN SYMPOSIA & CONFERENCES

1. Participated in **“Bruker Symposium on Pharmaceutical Solids”** at Hyderabad, by Bruker AXS GmbH, Germany and Bruker AXS, India, May 10, 2012.
2. Participated in the **“2nd UK-India MedChem Congress”** held at IICT, Hyderabad, Telangana State, India, during March 22-23, 2013.
3. Presented a poster entitled **“Andrographolide: Solving Chemical Instability and Poor Solubility By means of Cocrystal”** in **“8th CRSI-RSC Joint Symposium in Chemistry and 16th CRSI National Symposium in Chemistry”** at IIT Bombay, Bombay, February 6-9, 2014.
4. Delivered an oral presentation entitled **“Cocrystal Applications in Pharmaceutical Industry to Improve the Chemical Stability and Solubility of APIs/Bioactive agents”** in the **Dr. K. V. Rao Scientific Society Annual Science Awards – 2014-15** held on May 23, 2015 at IICT auditorium, Hyderabad, India.
5. Presented a poster entitled **“A Novel Curcumin–Artemisinin Coamorphous Solid: Physical Properties and Pharmacokinetic Profile”** in the Conference on **DRILS Young Scholars’ Science Café Meet-2015** held on 10 August 2015 at Dr. Reddy’s Institute of Life sciences, Hyderabad, India.
6. Presented a poster entitled **“Pharmaceutical Cocrystals of Nitazoxanide: Solubility, Stability and Bioavailability studies”** in **13th Asian Crystallographic Association** held in Science City, Kolkata, India, during December 5-8, 2015.
7. Delivered an oral presentation entitled **“Cocrystals and Alloys of Nitazoxanide: Enhanced Pharmacokinetics”** at the **Chemfest 2016** held at University of Hyderabad, Hyderabad, India, during March 18-19, 2016.

ABOUT THE AUTHOR

Kuthuru Suresh, son of Mr. Kuthuru Sayanna and Mrs. Kuthuru Laxmi, was born at Komanpally, Nizamabad District, Telangana state, India. He received primary education at Upper Primary School (UPS), Komanpally, and secondary education at Andhra Pradesh Social Welfare Residential School (APSWRS), Armoor. He completed Intermediate (B.P.C.) at Dr. BRACSWR Jr. College for boys, Hatnoora, Medak. He pursued Bachelor of Science (B.Sc., Microbiology, Genetics and Chemistry) at Nizam College, Hyderabad and Master of Science (M. Sc., Organic Chemistry) from Prathibha P.G. College, Kukatpally, Hyderabad affiliated to Osmania University. He qualified CSIR-UGC-JRF National Eligibility test for 'Junior Research Fellowship' (JRF) held in June 2010 and was awarded research fellowship by University Grant Commission (UGC). He then joined (in 2011) Prof. Ashwini Nangia's Research Group, School of Chemistry, University of Hyderabad, as a PhD Student and was upgraded as a 'Senior Research Fellow' (SRF) in 2013.